

2

AD-A255 563

3



DTIC
ELECTE
AUG 28 1992
S C D

FIRST ANNUAL REPORT

**SYNTHESIS AND EVALUATION
OF
POLYMERIC MATERIALS**

GC-TR-92-2303

Prepared for
Naval Research Laboratory
4555 Overlook Avenue, SW
Washington, D.C. 20375-5000

As Required By
Contract Number
N00014-90-C-2269

Prepared by
GEO-CENTERS, INC.
7 Wells Avenue
Newton Centre, MA 02159

July 1992



GEO-CENTERS, INC.

92-23887



2584K
4/10/92

92 8 27 040

REPORT DOCUMENTATION PAGE

Form Approved
OMB No. 0704-0188

Public reporting burden for this collection of information is estimated to average 1 hour per response, including the time for reviewing instructions, searching existing data sources, gathering and maintaining the data needed, and completing and reviewing the collection of information. Send comments regarding this burden estimate or any other aspect of this collection of information, including suggestions for reducing this burden, to Washington Headquarters Services, Directorate for Information Operations and Reports, 1215 Jefferson Davis Highway, Suite 1204, Arlington, VA 22202-4302, and to the Office of Management and Budget, Paperwork Reduction Project (0704-0188), Washington, DC 20503.

1. AGENCY USE ONLY (Leave blank)	2. REPORT DATE 30 June 1992	3. REPORT TYPE AND DATES COVERED Interim, 30 Sept 90 - 30 April 92
----------------------------------	--------------------------------	---

4. TITLE AND SUBTITLE Synthesis and Evaluation of Polymeric Materials First Annual Report	5. FUNDING NUMBERS C N00014-90-C-2269
---	--

6. AUTHOR(S) E. Greenawald, J. Nagode, H.Hu, L. Levenberry, R. Newbegin, H. Schrader, K. Groot, S. Kate	
---	--

7. PERFORMING ORGANIZATION NAME(S) AND ADDRESS(ES) GEO-CENTERS, INC. 7 Wells Avenue Newton Centre, MA 02159	8. PERFORMING ORGANIZATION REPORT NUMBER GC-TR-92-2303
--	--

9. SPONSORING/MONITORING AGENCY NAME(S) AND ADDRESS(ES) Naval Research Laboratory Code 6120 4555 Overlook Avenue, S.W. Washington, D.C. 20375-5000	10. SPONSORING/MONITORING AGENCY REPORT NUMBER
--	---

11. SUPPLEMENTARY NOTES

12a. DISTRIBUTION/AVAILABILITY STATEMENT Approved for public release Distribution unlimited	12b. DISTRIBUTION CODE
---	------------------------

13. ABSTRACT (Maximum 200 words)

GEO-CENTERS, INC. has been supporting the research efforts at the Naval Research Laboratory including novel fluoropolymers, conductive polymers, epoxies, and modified nylons. Major efforts were conducted in radiographic analysis development and use in evaluation of Sonar Rubber Domes (SRD) and Sonar Dome Rubber Windows (SDRW). This report is a summary of accomplishments for Year One of the contract period of performance.

14. SUBJECT TERMS Polymer, Sonar dome, radiograph, synthesis, SDRW, SRD, nondestructive evaluation, fluoropolymer, conductive polymer.	15. NUMBER OF PAGES 257
	16. PRICE CODE

17. SECURITY CLASSIFICATION OF REPORT Unclassified	18. SECURITY CLASSIFICATION OF THIS PAGE Unclassified	19. SECURITY CLASSIFICATION OF ABSTRACT Unclassified	20. LIMITATION OF ABSTRACT UL
--	---	--	----------------------------------

GENERAL INSTRUCTIONS FOR COMPLETING SF 298

The Report Documentation Page (RDP) is used in announcing and cataloging reports. It is important that this information be consistent with the rest of the report, particularly the cover and title page. Instructions for filling in each block of the form follow. It is important to stay *within the lines* to meet optical scanning requirements.

Block 1. Agency Use Only (Leave blank).

Block 2. Report Date. Full publication date including day, month, and year, if available (e.g. 1 Jan 88). Must cite at least the year.

Block 3. Type of Report and Dates Covered. State whether report is interim, final, etc. If applicable, enter inclusive report dates (e.g. 10 Jun 87 - 30 Jun 88).

Block 4. Title and Subtitle. A title is taken from the part of the report that provides the most meaningful and complete information. When a report is prepared in more than one volume, repeat the primary title, add volume number, and include subtitle for the specific volume. On classified documents enter the title classification in parentheses.

Block 5. Funding Numbers. To include contract and grant numbers; may include program element number(s), project number(s), task number(s), and work unit number(s). Use the following labels:

C - Contract	PR - Project
G - Grant	TA - Task
PE - Program Element	WU - Work Unit Accession No.

Block 6. Author(s). Name(s) of person(s) responsible for writing the report, performing the research, or credited with the content of the report. If editor or compiler, this should follow the name(s).

Block 7. Performing Organization Name(s) and Address(es). Self-explanatory.

Block 8. Performing Organization Report Number. Enter the unique alphanumeric report number(s) assigned by the organization performing the report.

Block 9. Sponsoring/Monitoring Agency Name(s) and Address(es). Self-explanatory.

Block 10. Sponsoring/Monitoring Agency Report Number. (If known)

Block 11. Supplementary Notes. Enter information not included elsewhere such as: Prepared in cooperation with...; Trans. of...; To be published in.... When a report is revised, include a statement whether the new report supersedes or supplements the older report.

Block 12a. Distribution/Availability Statement. Denotes public availability or limitations. Cite any availability to the public. Enter additional limitations or special markings in all capitals (e.g. NOFORN, REL, ITAR).

DOD - See DoDD 5230.24, "Distribution Statements on Technical Documents."

DOE - See authorities.

NASA - See Handbook NHB 2200.2.

NTIS - Leave blank.

Block 12b. Distribution Code.

DOD - Leave blank.

DOE - Enter DOE distribution categories from the Standard Distribution for Unclassified Scientific and Technical Reports.

NASA - Leave blank.

NTIS - Leave blank.

Block 13. Abstract. Include a brief (Maximum 200 words) factual summary of the most significant information contained in the report.

Block 14. Subject Terms. Keywords or phrases identifying major subjects in the report.

Block 15. Number of Pages. Enter the total number of pages.

Block 16. Price Code. Enter appropriate price code (NTIS only).

Blocks 17. - 19. Security Classifications. Self-explanatory. Enter U.S. Security Classification in accordance with U.S. Security Regulations (i.e., UNCLASSIFIED). If form contains classified information, stamp classification on the top and bottom of the page.

Block 20. Limitation of Abstract. This block must be completed to assign a limitation to the abstract. Enter either UL (unlimited) or SAR (same as report). An entry in this block is necessary if the abstract is to be limited. If blank, the abstract is assumed to be unlimited.

TABLE OF CONTENTS

INTRODUCTION 1

TECHNICAL REPORT 2

 1.0 EVALUATION OF SONAR DOME DAMAGE 2

 1.1 Background 2

 1.2 Radiographic Inspection 3

 1.2.1 Inspection results 3

 1.3 Improved Nondestructive Evaluation Methods 3

 1.3.1 X-ray Backscatter Tomography 3

 1.3.2 Image Processing 4

 1.3.3 Direct Stiffness Measurement 4

 1.4 Database Management 4

 1.5 Failure Analysis 5

 1.6 Improved SDRWs 5

 1.7 Cord Load Measurement of the Monolithic SDRW 5

 1.8 SRD Corrective Action Program 5

 1.9 SDRW Technical Package for NWSC 6

 2.0 POLYMER SYNTHESIS AND EVALUATION 6

 2.1 Background 6

 2.2 Conductive Polymers 7

 2.3 Phthalonitrile Resins 7

 2.4 Elastomers 8

 2.5 Fluorinated Polymers 8

 2.6 L-Proline Modified Nylons 9

 2.7 Characterization of Nylon Webbing 9

3.0	OTHER TECHNICAL SUPPORT	10
3.1	Wind Tunnel Sample Collection System	10

APPENDICES

Appendix A	Sonar dome rubber window (SDRW) and sonar rubber dome (SRD) radiographic inspection reports (September-December 1990)
Appendix B	Advancements in x-ray backscatter tomography
Appendix C	Computer simulation of steel cord radiograph profiles
Appendix D	Application of neural networks to radiograph profile analysis
Appendix E	Sonar rubber dome structural damage characterization
Appendix F	An R:BASE database application for an optical disk document storage and retrieval (ODDSAR) system
Appendix G	On-site inspection of the bead neck regions of the AN/SQQ 23 sonar rubber domes (SRDS) installed on the USS Dahlgren, DDG-43, Norfolk, VA, 21 December 1990
Appendix H	Radiographic inspection and subsequent evaluation of the damaged bead neck region on the A063 keel dome, formerly installed on the USS Simpson
Appendix I	Proposed changes to sonar dome rubber window (SDRW) inspection intervals
Appendix J	Mechanical, physical, and thermal properties of an electrically conductive heat resistant polymer
Appendix K	Tensile and fracture properties of a phthalonitrile poly mer

INTRODUCTION

This report is a summary of GEO-CENTERS' research efforts for the Naval Research Laboratory (NRL) under contract number N00014-90-C-2269, entitled "Synthesis and Evaluation of Polymeric Materials". The period of performance was from September 30, 1990, through April 30, 1992, the first contract year. The work was carried out at NRL using Chemistry and Materials Science Division facilities and in collaboration with NRL staff scientists. The work has resulted in several publications in scientific journals, presentations at various scientific meetings, and patent disclosures for products and processes developed under the contract. Copies of the publications are appended to this report. The various research projects in which GEO-CENTERS has been involved under this contract are divisible into two main groups, as follows:

- Evaluation of sonar dome damage
- Polymer synthesis and evaluation

The sonar dome work involved fleet support functions as well as research. We provided interpretation and analysis of radiographic inspection data in support of a routine inspection program. We also conducted failure analyses of individual domes. Research projects have focused upon improved materials and nondestructive evaluation methods. In addition, we provided the engineering needed to support our research and the database management support for the sonar dome effort.

In the area of synthesis and evaluation, we conducted research on the synthesis of novel polymers, such as fluoropolymers, epoxies, conductive polymers, and modified nylons. We have also characterized these and a variety of other materials with respect to their mechanical, rheological, chemical, and electrical properties. Detailed discussions of these areas, and the many sub-tasks within them are provided in the following paragraphs and in the appendices.

TECHNICAL REPORT

1.0 EVALUATION OF SONAR DOME DAMAGE

1.1 Background

Sonar Dome Rubber Windows (SDRW) and Sonar Rubber Domes (SRD) are installed on Navy surface combatants to provide a window for the transmission of sonar signals. These structures provide a hydrodynamic fairing surrounding the sonar transducer arrays for the purpose of eliminating turbulence, and the resulting system self-noise, and hydrodynamic drag. They also protect the sonar system from the action of the sea and collisions with debris. Sonar domes are fabricated of a steel cord reinforced rubber material composite. The SDRW is a large, bow-mounted structure fitted to ten classes of cruisers, destroyers, and frigates. SRDs are of two types, associated with the AN/SQS-56 and AN/SQQ-23 sonar systems. The former is a 273-inch-long keel-mounted dome installed on *Perry* class frigates. The latter is a 400-inch-long keel dome installed on four classes of cruisers and frigates which are currently being phased out of service. The larger keel domes are installed in pairs on some ships. In the following discussion, we will refer to all of these structures as "sonar domes". We will use SDRW or SRD, when specifically applicable.

Sonar domes have a history of rupturing during service. NRL has determined that the SDRW failures are due to corrosion fatigue failure of the steel reinforcement cords in a splice area of the composite structure. SRD failure is less well understood, although corrosion fatigue and other mechanisms have been identified in SRD failure analyses. X-ray radiography is used to detect incipient corrosion fatigue damage. An inspection program has been developed with the goal of maintaining an up-to-date evaluation of the entire antisubmarine warfare fleet's sonar domes. Since replacement domes are subject to the same problems as the originals, the need to inspect, monitor, and repair or replace them has remained. Radiographic inspection is routinely used as a basis for determining these options. In addition, the accumulated radiographic data has contributed to the failure analysis effort by revealing patterns of damage distribution and correlations with other data. The inspection and analysis methods developed in response to the SDRW failure problem have since become applicable to similar problems with the smaller keel domes.

GEO-CENTERS' support of the sonar dome corrective action programs (CAP) has been in the areas of radiographic inspection, database management, failure analysis, materials development, and improved methods of nondestructive evaluation. The following paragraphs discussed these efforts in detail.

1.2 Radiographic Inspection

GEO-CENTERS' support role in the radiographic inspection program involves the interpretation of radiographs provided by the Navy's inspection contractors, and the development and maintenance of standards for the radiographic data and criteria for actions taken.

When sonar dome radiographs arrived for processing they were given the highest priority and read immediately. Any damage or other pertinent features were located, measured, and diagrammed either as a hand sketch or as a computer generated image from the database. The appropriate recommendation was determined according to our standardized criteria. The results were then communicated verbally to the NRL task manager and/or others designated by NRL (typically NAVSEA 06U1B). Then the data were entered into the appropriate database, and a report was written and distributed.

1.2.1 Inspection results

During the period of performance, GEO-CENTERS staff evaluated 127 radiographic inspections of sonar domes. For each inspection a report was created detailing our findings, recording other inspection data (date, location, etc.) and including illustrations of inspection coverage and damage locations, if applicable. Our recommendation for action is determined by a set of well defined and established criteria. The inspection reports were initially transmitted to NAVSEA via modem for immediate use in determining actions to be taken. We later provided accumulations of these reports as appendices to a summary memorandum to NRL. These memoranda were distributed to NAVSEA as NRL letter reports. Seven such letter reports have been generated during the period of performance. To reduce the volume of paper in this report, we will not provide all of the inspection data here. The summary pages of each report have been compiled as Appendix A.

1.3 Improved Nondestructive Evaluation (NDE) Methods

1.3.1 X-ray Backscatter Tomography

Steel cord elements of the steel/rubber composite sonar domes are known to fail by tensile, stress corrosion, and corrosion fatigue mechanisms. The radiographic inspection program has been instrumental in managing the problem for large bow-mounted sonar domes, which have accessible interiors. Inspections are conducted using either dry dock or underwater techniques. We are able to identify and monitor damaged domes with the goal of deferring replacement until a scheduled overhaul. Smaller keel domes, however, are accessible only in dry dock and sometimes must be removed from the ship's hull. A one-sided radiography

technique would make possible an inspection schedule similar to that used for the bow domes. We have investigated x-ray backscatter tomography as such a technique. A summary of our review of x-ray backscatter tomography which was presented at the March 1991 meeting of the American Society for Non-destructive Testing (ASNT) in Oakland, California, is included as Appendix B.

1.3.2 Image Processing

Image processing techniques, and the application of neural networks to the processing of SDRW and SRD radiographic data promise to improve the non-destructive evaluation of these structures in the future. A paper on our effort in the computer simulation of steel cord profiles for development of neural network applications is included as Appendix C. Our work towards the application of neural networks to radiographic profile analysis for the detection of corrosion in steel cords was presented at a poster session of the Gordon Conference on Non Destructive Evaluation in Oxnard, California. See Appendix D.

1.3.3 Direct Stiffness Measurement

As part of the task to investigate one-sided inspection techniques for SRDs, alternative methods were researched. One such method attempts to correlate the SRD's local stiffness with internal structural integrity. Preliminary tests done on a sonar dome with known damage locations revealed that the stiffness gradient of the SRD surface in damaged regions differed from measurements taken in areas without damage. The development of improved instrumentation for these measurements is underway. We plan to inspect additional damaged and undamaged domes to determine whether the observed features are indicative of structural damage. Our preliminary report is included as Appendix E.

1.4 Database Management

Under a previous contract, GEO-CENTERS improved upon existing databases for SDRWs and SRDs and developed new databases for the following: SDRW bead seat survey data, sonar dome publications and reports, and engineering drawings.

Thus far under this contract, we have maintained and improved the existing databases for SDRWs and SRDs to meet the expanding needs of the sonar dome program. In addition, we have developed an R:BASE database application for NAVSEA's Optical Disk Document Storage and Retrieval (ODDSAR) System. A draft of the documentation is included as Appendix F.

1.5 Failure Analysis

Failures of SRDs in the bead neck region have been documented in earlier work. The evaluation of two such failures during the current period of performance prompted a proposal for engineering changes to the mold-ring design, and the fabrication processes of SRDs were modified accordingly. Copies of our evaluations are included as Appendices G and H.

1.6 Improved SDRWs

Radiographic inspection and the analysis of failed SDRWs have resulted in changes to SDRW design and construction methods. These changes were made in an attempt to effect short-term improvements to the structure and thus slow or prevent the process of corrosion fatigue failure. A sub-population of SDRWs known as "6-ply" windows have acquired sufficient numbers and time in service to be evaluated statistically. In collaboration with an NRL reliability statistician we have determined that these SDRWs merit being called "improved". This classification has enabled us to increase our recommended radiographic inspection intervals for new and undamaged 6-ply SDRWs from two to four years. A copy of the NRL Letter Report outlining the proposed changes to the inspection intervals is included as Appendix I.

1.7 Cord Load Measurement of the Monolithic SDRW

Cord load data acquisition is a task that must be accomplished whenever a newly designed sonar dome is produced as a prototype. The first spliceless, or "monolithic", SDRW manufactured will have numerous load-cell type gauges installed during the fabrication process. GEO-CENTERS has provided logistical and technical support in preparation for this task. This involved gauge placement and calibration, cabling, and data processing. We anticipate further involvement in both the hydro test measurements and sea-trials.

1.8 SRD Corrective Action Program

The primary cause of SDRW failure is understood to be corrosion fatigue of the steel cords in the composite dome wall. Corrosion fatigue has been implicated in SRD failure, as well. Although various new design changes have increased the projected service life of SDRWs, the same claim cannot be made for SRDs.

The SRD Corrective Action Program (CAP) includes nondestructive evaluation (NDE), finite element modeling (FEM) and analysis, and an investigation into the potential of a new keel dome design. GEO-CENTERS has provided support to all of these technical areas.

In addition to our research in new NDE methods discussed in section 1.3, we have provided technical support to the acoustic deflection measurement project, which is expected to yield data crucial to developing a dynamic finite element model for the 273" SRD. The system will measure distances relative to a fixed receiver and track the deflection of the SRD in numerous locations while the ship is underway at sea. Initially we collaborated on the design, construction, positioning, and installation of a sonar transducer array mock-up for the project. We also provided logistical and technical support in the measurement, placement, and installation of the numerous ultrasonic transducers to be used in this project. We developed a mapping system for the interior surface of the SRD, which will enable us to translate a given surface location to the standardized x-y-z coordinate system used by the manufacturer and other activities. A ship has been chosen by NAVSEA, and system installation and sea trial are to be scheduled.

1.9 SDRW Technical Package for NWSC

As part of our task to maintain SDRW/SRD engineering data, we have provided technical assistance to the Naval Weapons Support Center (NWSC) in Crane, Indiana. NWSC is in the process of documenting various manufacturing processes, procedures, and material requirements associated with U.S. Navy weapons and defense systems, including sonar domes. Our knowledge of sonar dome construction requirements and procedures has enabled us to review, evaluate, and make the necessary changes to the engineering documentation. When complete, the new documentation, which includes all manufacturing requirements and drawings, will be the basis for future sonar dome manufacturing contracts.

2.0 POLYMER SYNTHESIS AND EVALUATION

2.1 Background

The Materials Chemistry Branch is responsible for the development and characterization of new polymeric materials for Navy applications. GEO-CENTERS' support of the branch's effort has been broad based involving the synthesis and characterization of many varied materials. Characterization has involved the use of such diagnostic methods as differential scanning calorimetry (DSC), thermal analysis, scanning electron microscopy (SEM), transmission electron microscopy (TEM), nuclear magnetic resonance (NMR), electron spin resonance (ESR) and infrared and ultraviolet spectroscopies. In addition we have used mechanical, rheologic, and dielectric tests where appropriate. The specific project areas are discussed in detail below.

2.2 Conductive Polymers

Our approach to developing electrically conducting organic materials that have high stability in aggressive environments is based on the synthesis of polymers with extended π -electron delocalization. The prepolymers are soluble and meltable, and completely conjugated with reactive end groups that are capable of being polymerized into conjugated/aromatic linking groups to form the polymer structure. Because of the extended conjugation, these materials are intrinsically conducting without doping. We have studied the mechanical properties and thermal behavior of such a conducting polymer, demonstrating that the high temperatures used to introduce conductivity have not resulted in charred materials lacking mechanical integrity. To the contrary, we have seen improved tensile strength, as well as high oxidative and thermal stability. Initially, our results on these materials were presented to the International SAMPE Technical Conference, September 1989. Further work during this contractual period has resulted in the acceptance of our paper (included here as Appendix J) for publication in the Journal of Applied Polymer Science.

2.3 Phthalonitrile Resins

Organic polymers that are both thermally and oxidatively stable above 315°C are in demand as matrix materials for advanced composite applications, as adhesives for high temperature materials, and as weight-reducing replacement materials for metals. A new class of phthalonitrile-based polymers with excellent thermoxidative properties has been under investigation for application in these areas. The phthalonitrile monomers are readily converted to crosslinked thermosetting polymers in the presence of thermally stable aromatic diamines. The polymerization reaction occurs through the terminal phthalonitrile units which are interconnected by aromatic dioxy linkages, yielding heterocyclic crosslinked materials. Shaped components are easily processed by heating the polymerization mixture above its melting point or glass transition until gelation occurs. The prepolymers formed from these monomers are soluble in common solvents and indefinitely stable at room temperature.

Current work during this period of performance detailed the tensile failure and fracture properties of the phthalonitrile polymer following exposure to elevated temperature and oxidative conditions. Our paper has been submitted to Polymer Communications and is included here as Appendix K.

2.4 Elastomers

Polymer blends have been much investigated in recent years. Our previous work in the area of rubber blends reported a miscibility due to specific interactions in a polychloroprene/epoxidized polyisoprene mixture. If entropy due to mixing is negligible, the thermodynamics, and therefore the incidence of miscibility, are governed substantially by component interactions. Characterization of these interactions is obviously useful in the study of polymer blends.

Xenon is soluble in many polymers, with the atoms residing in the free volume. Since the chemical shift of ^{129}Xe is proportional to the number of collisions per unit time the xenon experiences, or equivalently to the density of its environment, it provides a measure of free volume in the polymer. Below the glass transition temperature, segmental motion of the polymer chains is suppressed, so that Xe atoms are trapped in different sites. The distribution in local free volume produces variations in chemical shift resulting in an inhomogeneously broadened ^{129}Xe nuclear magnetic resonance (NMR) line. Rapid diffusion of the polymeric components collapses the inhomogeneously broadened resonance into a narrow line; the observed chemical shift is an average over the inhomogeneously broadened line. Since this action is time dependent, ^{129}Xe NMR will yield the diffusion coefficients for the polymer chains through simple calculations. This work was presented at the March 1992 meeting of the American Physical Society in Indianapolis, Indiana. The abstract and summary figures are included as Appendix L.

2.5 Fluorinated Polymers

The highly polar nature of the carbon-fluorine bond has been used to provide improved properties in comparison with their hydrogen-containing or other halogen-containing analogs. Fluorine-containing epoxies or acrylics generally exhibit resistance to water penetration, chemical reaction, and environmental degradation; they also show different degrees of surface tension, friction coefficient, optical clarity, refractive index, vapor transmission rate, and electromagnetic radiation resistance.

Previously, this task included efforts by GEO-CENTERS to maximize the hydrophobicity polymer systems, without compromising the structural characteristics which are necessary in the development of polymeric materials. We have now begun to design and synthesize the heavily fluorinated epoxy and acrylic resins to produce compounds with dielectric constants among the lowest in the literature. This effort has resulted in a major patent disclosure and several publications. The U.S. patent application was filed for "Fluorinated resins with low dielectric constants" on 14 February 1992. A copy of the patent disclosure is included as Appendix M. Three publications outlined a new process for synthesizing heavily fluorinated epoxy resins, and described the structure and preparation of these resins. They are included here as Appendices

N, O, and P. In addition, results of this work were presented at the American Chemical Society meetings in 1991 and 1992, and various invitations have been extended to collaborate on related research and to author chapters in three books. We have also been invited to submit samples of our polymers for publishing in Sadtler Standard Spectra, an infrared (IR) spectra reference book.

2.6 L-Proline Modified Nylons

The conformational constraints that L-proline imposes upon natural polypeptides has been recognized as the most significant factor in the occurrence of β bends and pleats. The amino group of this most unusual natural α -amino acid is secondary and contained in a five-membered ring structure. One consequence of this, the peptide linkage formed with the amine group lacks an available hydrogen atom for hydrogen bonding. The implications for the materials properties, as opposed to the biological properties, of natural and synthetic polyamides containing L-proline are most interesting. Thus we have begun a synthetic effort with a first objective of defining the minimal structure of synthetic polymer for which L-proline will control the elastic properties.

Two publications, the second of which is in revision, are the current results of this work. They are included as Appendices Q and R. In addition, we presented results of this work at the American Chemical Society meeting in 1991.

2.7 Characterization of Nylon Webbing

The synthetic webbings in an air drop parachute system connect the parachute lines with the various pieces of military or industrial equipment involved in the drop. In order to predict the performance of such a system, one must study the interaction of the system with the surrounding air during deployment. A mathematical model was developed by Allied Signal Corporation to predict the system's behavior and estimate the magnitude of strain energy and stresses in the webbing sling.

To assist Allied in evaluating webbings of two types of nylons wound at two separate facilities, we developed a test utilizing NRL facilities. A summary report, prepared by Allied Signal using our data, outlines the results of our efforts. It is included here as Appendix S.

3.0 OTHER TECHNICAL SUPPORT

3.1 Wind Tunnel Sample Collection System

During a previous contract with NRL, we provided hardware and software to support a data acquisition project. The system collected target residues from within a wind tunnel environment. We designed and fabricated a portable computer-based control system for this project.

During field use at White Sands, damage to the electronics was sustained. During this period of performance on the current contract, we have repaired the damaged electronics and upgraded to a more robust design. Our software and the system documentation were also updated to accommodate the changes.

APPENDIX A

**SONAR DOME RUBBER WINDOW (SDRW) AND SONAR RUBBER
DOME (SRD) RADIOGRAPHIC INSPECTION REPORTS
(SEPTEMBER-DECEMBER 1990)**



GEO CENTERS, INC.

MEMORANDUM

December 13, 1990

From: James B. Nagode
To: Chester F. Poranski, Jr.

Subj: SONAR DOME RUBBER WINDOW (SDRW) AND SONAR RUBBER DOME (SRD)
RADIOGRAPHIC INSPECTION REPORTS (SEPTEMBER - DECEMBER 1990)

1. USS RADFORD (SDRW): No corrosion fatigue damage is apparent from the radiographs. Routine inspection scheduling is recommended. See Appendix A.
2. USS WAINWRIGHT (SDRW): The SDRW's first damage site is apparent from the radiographs. Supplemental inspection of a section 90 degrees port revealed an additional damage site. Monitoring of this SDRW is recommended. See Appendixes B, and C, respectively.
3. USS VALDEZ (SDRW): Previously reported damage is unchanged. No new damage is apparent from the radiographs. The continued monitoring of this SDRW is recommended. See Appendix D.
4. USS STUMP (SDRW): No corrosion fatigue damage is apparent from the radiographs. Routine inspection scheduling is recommended. See Appendix E.
5. USS SIMPSON (SRD): Four damage sites are apparent in the forward areas of the dome; two starboard, two port. No damage is apparent in the aft areas. See Appendix F.
6. USS INGERSOLL (SDRW): No corrosion fatigue damage is apparent from the radiographs. Routine inspection scheduling is recommended. See Appendix G.
7. USS CARON (SDRW): Previously reported damage has grown. The continued monitoring of this SDRW is recommended. See Appendix H.
8. USS KIDD (SDRW): Previously reported damage is unchanged. The continued monitoring of this SDRW is recommended. See Appendix I.
9. USS BROWN (SDRW): No corrosion fatigue damage is apparent from the radiographs. Routine inspection scheduling is recommended. See Appendix J.
10. USS KNOX (SDRW): Two new damage sites are seen on this SDRW. A previously reported site has grown. Continued monitoring is recommended. See Appendix K.
11. B.F.GOODRICH SRD (TYPE 56) LAYUP 99: No structural damage is apparent from the radiographs. See Appendix L.

12. B.F.GOODRICH SDRW LAYUPS 238 (TYPE SL), 29 (TYPE 2), AND 239 (TYPE SL): No structural damage is apparent from the radiographs. See Appendixes M, N, and O, respectively.

MEMORANDUM

February 28, 1991

From: James B. Nagode
To: Chester F. Poranski, Jr.

Subj: SONAR DOME RUBBER WINDOW (SDRW) AND SONAR RUBBER DOME (SRD)
RADIOGRAPHIC INSPECTION REPORTS (DECEMBER 1990 - FEBRUARY
1991)

1. USS DAHLGREN (SRD): Pre-existing damage has grown, and new damage sites have emerged on the FORWARD SRD. Two new damage sites have appeared on the AFT SRD as well. See Appendix A.
2. USS MILLER (SDRW): Previously reported damage is unchanged. The continued monitoring of this SDRW is recommended. See Appendix B.
3. USS PATTERSON (patched SDRW): One new damage site is seen outside of the repair area. The continued monitoring of this SDRW is recommended. See Appendix C.
4. USS CAPODANNO (SDRW): A two-ply damage site, as well as indications of bottom damage is apparent from the radiographs. We recommend that this SDRW be repaired or replaced. See Appendix D.
5. USS KNOX (SDRW patch): Inspection is for repair verification only. The recommendation remains MONITOR. See Appendix E.
6. USS BRISCOE (SDRW): No corrosion fatigue damage is apparent from the radiographs. The routine inspection schedule is recommended. See Appendix F.
7. USS HANCOCK (SDRW): Two-ply damage is now present. We recommend that the SDRW be repaired or replaced. See Appendix G.
8. USS VANDEGRIFT (SRD-56): Two-ply damage is apparent on both sides of this SRD. See Appendix H.
9. USS PAUL (SDRW): No corrosion fatigue damage is apparent from the radiographs. The routine inspection schedule is recommended. See Appendix I.
10. USS BEARY (SDRW): No corrosion fatigue damage is apparent from the radiographs. The routine inspection schedule is recommended. See Appendix J.
11. USS MONTEREY (SDRW): No corrosion fatigue damage is apparent from the radiographs. The routine inspection schedule is recommended. See Appendix K.

12. B.F. GOODRICH SDRW-2 LAYUP 30, and SDRW-1 LAYUPS 240 and 241: No structural damage is apparent from the radiographs. See Appendixes L, M, and N, respectively.

13. B.F. GOODRICH SRD-56 LAYUPS 100 and 101: No structural damage is apparent from the radiographs. See Appendixes O, and P, respectively.

MEMORANDUM

June 4, 1991

From: James B. Nagode
To: Chester F. Poranski, Jr.

Subj: SONAR DOME RUBBER WINDOW (SDRW) AND SONAR RUBBER DOME (SRD)
RADIOGRAPHIC INSPECTION REPORTS (FEBRUARY - MAY 1991)

1. USS AINSWORTH (SDRW): No corrosion fatigue damage is apparent from the radiographs. The routine inspection schedule is recommended. See Appendix A.
2. X-USS DAVIDSON (SDRW): Currently on Brazilian Naval vessel Ct Paraiba. No corrosion fatigue damage is apparent from the radiographs. The routine inspection schedule is recommended. See Appendix B.
3. USS ANTIETAM (SDRW): No corrosion fatigue damage is apparent from the radiographs. The routine inspection schedule is recommended. See Appendix C.
4. USS BIDDLE (SDRW): Previously reported damage is unchanged since the last inspection. The continued monitoring of this SDRW is recommended. See Appendix D.
5. USS TAYLOR (SRD-56): Two-ply damage is apparent from the radiographs. See Appendix E.
6. USS BRADLEY (SRD-56): Both forward inspection areas exhibited moderate damage. See Appendix F.
7. USS TRIPPE (SDRW): No corrosion fatigue damage is apparent from the radiographs. The routine inspection schedule is recommended. See Appendix G.
8. USS YORKTOWN (SDRW): Previously reported damage is unchanged since the last inspection. The continued monitoring of this SDRW is recommended. See Appendix H.
9. USS TRUETT (SDRW): Previously reported damage has grown. One new damage site is reported. The continued monitoring of this SDRW is recommended. See Appendix I.
10. USS GLOVER (SDRW-2): A previously reported damage site has grown. The far-port repair area contains no new structural damage. The continued monitoring of this SDRW is recommended. See Appendix J.
11. USS O'BANNON (patched SDRW): No new damage is apparent from the radiographs. The continued monitoring of this SDRW is recommended. See Appendix K.

12. B.F.GOODRICH SDRW-SL LAYUPS 242, 243, 244, AND SDRW-2 LAYUP 31: No structural damage is apparent from the radiographs. See Appendixes L, M, N, and O, respectively.

13. B.F.GOODRICH SRD-56 LAYUPS 102, 103, 104, 105, AND 106: No structural damage is apparent from the radiographs. See Appendixes P, Q, R, S and T, respectively.

MEMORANDUM

August 6, 1991

From: James B. Nagode
To: Chester F. Poranski, Jr.

Subj: SONAR DOME RUBBER WINDOW (SDRW) AND SONAR RUBBER DOME (SRD)
RADIOGRAPHIC INSPECTION REPORTS (JUNE - JULY 1991)

1. USS PETERSON (SDRW): No corrosion fatigue damage is apparent from the radiographs. The routine inspection schedule is recommended. See Appendix A.
2. USS MISSISSIPPI (SDRW): No corrosion fatigue damage is apparent from the radiographs. The routine inspection schedule is recommended. See Appendix B.
3. USS RODGERS (SDRW): No corrosion fatigue damage is apparent from the radiographs. The routine inspection schedule is recommended. See Appendix C.
4. USS HAYLER (SDRW): No corrosion fatigue damage is apparent from the radiographs. The routine inspection schedule is recommended. See Appendix D.
5. USS BUNKER HILL (SDRW): One damage site is apparent from the radiographs. Monitor is recommended for this SDRW. See Appendix E.
6. USS CHOSIN (SDRW): No corrosion fatigue damage is apparent from the radiographs. The routine inspection schedule is recommended. See Appendix F.
7. USS SIMS (SDRW): No corrosion fatigue damage is apparent from the radiographs. The routine inspection schedule is recommended. See Appendix G.
8. USS GETTYSBURG (SDRW): No corrosion fatigue damage is apparent from the radiographs. The routine inspection schedule is recommended. See Appendix H.
9. USS CUSHING (patched SDRW): Two post-repair damage sites are now apparent from the radiographs. The continued monitoring of this SDRW is recommended. See Appendix I.
10. USS SIDES (SRD-56): A two-ply damage site is apparent from the radiographs. See Appendix J.
11. USS CONOLLY (SDRW): Previously reported damage is unchanged. The continued monitoring of this SDRW is recommended. See Appendix K.
12. USS DANIELS (SDRW): Previously reported damage has grown. The continued monitoring of this SDRW is recommended. See Appendix L.
13. USS SOUTH CAROLINA (SDRW): No corrosion fatigue damage is apparent from the radiographs. The routine inspection schedule is recommended. See Appendix M.



GEO-CENTERS, INC.

14. USS SPRAGUE (SRD-56): A two-ply damage site is apparent from the radiographs. See Appendix N.
15. B.F.GOODRICH SDRW-1 LAYUP 245 and SDRW-2 LAYUP 32: No structural damage is apparent from the radiographs. See Appendixes O, and P, respectively.
16. B.F.GOODRICH SRD-56 LAYUPS 107, 108, and 109, and SRD-23 LAYUP 28: No structural damage is apparent from the radiographs. See Appendixes Q, R, S, and T, respectively.



GEO-CENTERS, INC.

MEMORANDUM

October 8, 1991

From: James B. Nagode
To: Chester F. Poranski, Jr.

Subj: SONAR DOME RUBBER WINDOW (SDRW) AND SONAR RUBBER DOME (SRD)
RADIOGRAPHIC INSPECTION REPORTS (AUGUST - SEPTEMBER 1991)

1. USS HART (SDRW): Previously reported damage has grown. The continued monitoring of this SDRW is recommended. See Appendix A.
2. USS OLDENDORF (patched SDRW): One post-repair damage site is apparent from the radiographs. The continued monitoring of this SDRW is recommended. See Appendix B.
3. USS FLATLEY (SRD-56): One and two ply damage sites are apparent from the radiographs. See Appendix C.
4. USS KIDD (SDRW): Previously reported damage has grown. New damage is also apparent. The continued monitoring of this SDRW is recommended. See Appendix D.
5. USS TICONDEROGA (SDRW): No corrosion fatigue damage is apparent from the radiographs. Routine inspection schedule is recommended. See Appendix E.
6. EX-USS DAVID (SDRW): No corrosion fatigue damage is apparent from the radiographs. Routine inspection schedule is recommended. See Appendix F.
7. USS FOSTER (SDRW): Two damage sites are apparent from the radiographs. We recommend that this SDRW be monitored. See Appendix G.
8. USS BELKNAP (SDRW): No corrosion fatigue damage is apparent from the radiographs. Routine inspection schedule is recommended. See Appendix H.
9. USS MOBILE BAY (SDRW): No corrosion fatigue damage is apparent from the radiographs. Routine inspection schedule is recommended. See Appendix I.
10. USS STERETT (SDRW): No corrosion fatigue damage is apparent from the radiographs. Routine inspection schedule is recommended. See Appendix J.
11. USS PHARRIS (SDRW): No corrosion fatigue damage is apparent from the radiographs. Routine inspection schedule is recommended. See Appendix K.

12. USS MCINERNEY (SRD-56): One and two ply damage sites are apparent from the radiographs. See Appendix L.

13. B.F. GOODRICH SDRW-1 LAYUP 246: No structural damage is apparent from the radiographs. See Appendix M.

14. B.F. GOODRICH SRD-23 LAYUP 29, and SRD-56 LAYUP 111: No structural damage is apparent from the radiographs. See Appendixes N, and O, respectively.

MEMORANDUM

From: James B. Nagode
To: Chet Poranski

December 11, 1991

Subj: SONAR DOME RUBBER WINDOW (SDRW) AND SONAR RUBBER DOME (SRD)
RADIOGRAPHIC INSPECTION REPORTS (OCTOBER - NOVEMBER 1991)

1. USS COWPENS (SDRW): No corrosion fatigue damage is apparent from the radiographs. Routine inspection schedule is recommended. See Appendix A.
2. USS FLETCHER (SDRW): Previously reported damage has grown to include both longitudinal plies. One new damage site is apparent. Repair or replacement of this SDRW is recommended. See Appendix B.
3. USS SPRUANCE (SDRW): No corrosion fatigue damage is apparent from the radiographs. Routine inspection schedule is recommended. See Appendix C.
4. USS SAN JACINTO (SDRW): No corrosion fatigue damage is apparent from the radiographs. Routine inspection schedule is recommended. See Appendix D.
5. USS MACDONOUGH (SRD-23 FWD): Forward regions were inspected only. Previously reported damage is unchanged since the last inspection (2/87). See Appendix E.
6. USS MACDONOUGH (SRD-23 AFT): Forward regions were inspected only. Previously reported damage is unchanged since the last inspection (2/87). One new damage site is apparent from the radiographs. See Appendix F.
7. USS ANTRIM (SRD-56): Five damage sites are apparent from the radiographs. One site involves two structural plies. See Appendix G.
8. USS PHILIPPINE SEA (SDRW): No corrosion fatigue damage is apparent from the radiographs. Routine inspection schedule is recommended. See Appendix H.
9. USS CARON (SDRW): Previously reported damage is unchanged since the last inspection (10/90). One new damage site is apparent from the radiographs. See Appendix I.
10. USS SCOTT (SDRW): No corrosion fatigue damage is apparent from the radiographs. Routine inspection schedule is recommended. See Appendix J.
11. USS NICHOLSON (SDRW): No corrosion fatigue damage is apparent from the radiographs. Routine inspection schedule is recommended. See Appendix K.

12. USS GATES (SDRW): The first damage site for this SDRW is reported. Monitor is recommended. See Appendix L.

13. B.F. GOODRICH SDRW-1 LAYUP 247: No structural damage is apparent from the radiographs. See Appendix M.

14. B.F. GOODRICH SRD-23 LAYUPS 30 and 31, and SRD-56 LAYUP 113: No structural damage is apparent from the radiographs. See Appendixes N, O, and P, respectively.

MEMORANDUM

March 24, 1992

From: James B. Nagode
To: Chester F. Poranski, Jr.

Subj: SONAR DOME RUBBER WINDOW (SDRW) AND SONAR RUBBER DOME (SRD)
RADIOGRAPHIC INSPECTION REPORTS (DECEMBER 1991 - MARCH
1992)

1. USS KINKAID (SDRW): No corrosion fatigue damage is apparent from the radiographs. Routine inspection schedule is recommended. See Appendix A.
2. USS MOOSBRUGGER (SDRW): No corrosion fatigue damage is apparent from the radiographs. Routine inspection schedule is recommended. See Appendix B.
3. USS PULLER (SRD-56): No structural damage is apparent from the radiographs. See appendix C.
4. USS BOWEN (SDRW): Initial damage reported 3/88 is unchanged. Two new damage sites are now apparent from the radiographs. The continued monitoring of this SDRW is recommended. See appendix D.
5. USS LEFTWICH (SDRW): One damage site is apparent from the radiographs. We recommend that this SDRW be monitored. See Appendix E.
6. USS FORD (SRD-56): No structural damage is apparent from the radiographs. See Appendix F.
7. USS LEYTE GULF (SDRW): No corrosion fatigue damage is apparent from the radiographs. Routine inspection schedule is recommended. See Appendix G.
8. USS McCANDLESS (SDRW): No corrosion fatigue damage is apparent from the radiographs. Routine inspection schedule is recommended. See Appendix H.
9. USS TISDALE (SRD-56): Seven damage sites are apparent in the forward regions of this SRD, one of which consists of 2-ply damage. See Appendix I.
10. USS COPELAND (SRD-56): Four damage sites are apparent in the forward regions of this SRD, one of which consists of 2-ply damage. See Appendix J.

11. BF GOODRICH SRD-23 LAYUP 32: No structural damage is apparent from the radiographs. See Appendix K.

12. BF GOODRICH SRD-56 LAYUPS 18, 19, and 20: No structural damage is apparent from the radiographs. See Appendixes L, M, and N, respectively.

13. BF GOODRICH SDRW-SL LAYUPS 248 and 249, and SDRW-2 LAYUP 34: No structural damage is apparent from the radiographs. See Appendixes O, P, and Q, respectively.

APPENDIX B

ADVANCEMENTS IN X-RAY BACKSCATTER TOMOGRAPHY



GEO CENTERS, INC.

ADVANCEMENTS IN X-RAY BACKSCATTER TOMOGRAPHY

Edward C. Greenawald
Geo-Centers, Inc.
10903 Indian Head Highway
Fort Washington, MD 20744
(202) 767-3039

Chester F. Poranski, Jr.
Materials Chemistry Branch
Naval Research Laboratory
Washington, DC 20375
(202) 767-2488

INTRODUCTION

Of the several processes which may occur when x-rays interact with matter, Compton scattering is dominant in the range of energies commonly used in radiography. The effect is particularly important in elements with low atomic number, Z , due to the low binding energy of the outer shell electrons. The Compton interaction between an x-ray photon and a free or outer shell electron causes the electron to recoil and the photon to be propagated in a new direction with a reduced energy. As the incident photon energy increases, the mean scatter direction moves toward the incident beam direction. However, even at relatively high energies, some photons are scattered in the backwards direction. High Z materials contribute fluorescent photons as well, due to the photoelectric effect. We will refer to all such secondary radiation effects detectible from the source side of the object as backscatter. We will also not distinguish between backscatter produced by *bremsstrahlung* and γ -ray sources.

The potential for determining material properties by detection of x-ray backscatter has been recognized for some thirty years. Medical applications were demonstrated using the backscatter signal to measure tissue densities. Backscatter imaging techniques were also demonstrated. This work, however, has been eclipsed by the rapid development of computed tomography for medical applications. Research has also been reported on a variety of industrial inspection techniques. Tomographic techniques, which produce images representing planes of interest within the object, are of particular interest to us. We have investigated the use of such techniques for the inspection of steel-reinforced rubber sonar domes on U.S. Navy vessels.

BACKSCATTER IMAGING

Ordinary optical images are scatter images. It provides a useful insight to the backscatter imaging process to consider this analogy. Let us substitute the x-ray radiation in our experiment with light, and substitute the object of our interest with an optically transparent one. We can intuitively appreciate the ease with which a flaw or other discontinuity in the transparency of the object can be detected by illuminating the object. The image so produced can be

projected onto our retina or captured on film by a camera. Similarly, illuminating an object with x-rays should produce an x-ray scatter image. Although high energy x-rays can not be sufficiently refracted by lenses, a pinhole camera can be used to produce an image on film. To produce a tomograph the illuminating beam must be collimated through a slit so as to illuminate only the plane of interest. Unfortunately, the pinhole accepts only a tiny fraction of the scatter produced, requiring hours to expose the film. Recently developed techniques produce digital images by using collimated arrays of detectors and scanning x-ray beams. Such systems create and detect scattered photons in such a way as to record the location and signal level of each volume element, or voxel, in a plane.

Incident x-rays and the backscatter signal are attenuated by the material between the plane of interest and the x-ray source. As a consequence, image artifacts are produced and inspection depth is limited. Tomographs however, are superior to transmission radiographs for the detection of thin planar features such as disbonds, delaminations, and cracks. They also excel at revealing small features otherwise obscured by layers of thick or dense materials. The one-sided nature of the inspection process is an advantage where accessibility or object size is a problem.

TOMOGRAPHY OF SONAR DOME SPECIMENS

Naval sonar domes sometimes rupture unexpectedly at sea. An NDE method is sought which will not require drydocking and removal of the structure, as is currently done. The sonar dome material consists of layers of steel cord reinforced rubber fabric. Each cord has 29 individual wires (7x4+1) and a diameter of 1.48 mm. The cords are initially calendared into the rubber fabric such that they are parallel and spaced 10 per inch. They are known to fail by tensile, stress corrosion, and corrosion fatigue mechanisms.

Three systems were evaluated for NDE of sonar domes: A system developed by American Science and Engineering (AS&E) for the inspection of rocket motors; A "breadboard" apparatus developed to demonstrate an approach of Advanced Research and Applications Corporation (ARACOR); and a production system manufactured by Philips Electronic Instruments.

The AS&E system (ZT) consisted of a source of scanning radiation and a large, efficient collimated detector. A "sidescatter", or tangential geometry had been chosen for the cylindrical rocket motors. We traversed our samples through the focal line of the detector. This work resulted in the successful imaging of a broken ply 14mm deep within the specimen. We also developed some image processing algorithms to compensate for artifacts created by sample curvature.

We also provided our sonar dome sample to ARACOR for demonstration scans using their Backscatter Imaging Tomography (BIT) breadboard scanner. A simple and time consuming technique was used to interrogate each voxel in a plane perpendicular to the sample surface. ARACOR's unique process acquires the overlying voxels first, and uses this data to compensate for the attenuation of signals from deeper levels. Good high resolution images were obtained of steel

cords in the sample. Although the perpendicular image planes were not appropriate for inspection of sonar domes, the acquisition of full volume data by this method promises the display of arbitrary plane orientation by computer methods.

The Philips system (COMSCAN) uses a unique helical-grooved, rotating cylinder to collimate and sweep its x-ray beam. This compact mechanism allows the positioning of both the x-ray tube target and detector arrays very close to the object. The resulting high flux density results in very low voxel measurement times. Arrays of slit-collimated detectors are used to provide 22 independent overlapping tomographs in one pass of the scanner. As with the other systems, we were able to image the broken ply in our sample. Moreover, the multiple tomographs facilitated "browsing" by paging up and down through the 22 planes to follow non-planar features in our curved sample. Two sets of detector apertures were evaluated. One set projected the 22 slices from a thickness of material from 10mm to 20mm from the scanner head. The other set projected from 10mm to 60mm.

CONCLUSION

X-ray backscatter tomography affords a solution to our sonar dome NDE problem. We have demonstrated success in obtaining images of damaged sonar dome plies with three varied systems. We have recommended the development of a system for the inspection of keel mounted sonar domes based upon the COMSCAN instrument. Our primary consideration was that the compact scanner head will facilitate underwater use. Other features of the system design, scan time requirements and system availability were also suitable for our needs.

The proposed system will consist of a COMSCAN system installed in a special shipping/utilization container for use in shipyard environments. The scanning head will be installed in an underwater enclosure. After positioning against the sonar dome inspection area, indexing and scanning will be accomplished remotely through the wall of the underwater enclosure. An umbilical to the surface will contain the high voltage cable, cooling water lines, and data and control cable links to the containerized control racks.

ACKNOWLEDGEMENTS

We were supported by the NAVSEA Naval Surface Ship ASW Group and the NRL Materials Chemistry Branch under NRL contract number N00014-90-C-2269. The AS&E ZT™ system was built for the Air Force Astronautics Laboratory under contract number F04611-88-C-0051. ARACOR BIT scans were supported by the Wright Research and Development Center (WRDC) Materials Lab under contract F33615-87-C-5249 (Ms. C. Kropas, project officer).

APPENDIX C
COMPUTER SIMULATION OF STEEL CORD RADIOGRAPH
PROFILES



GFO CENTERS, INC.

COMPUTER SIMULATION OF STEEL CORD RADIOGRAPH PROFILES

Edward C. Greenawald
Geo-Centers, Inc.
10903 Indian Head Highway
Fort Washington, MD 20744

Chester F. Poranski
Materials Chemistry Branch
Naval Research Laboratory
Washington D.C. 20375

INTRODUCTION

Image processing methods have proven useful as an aid in interpreting radiographs of Naval sonar domes. The flaw of interest in these steel cord reinforced rubber structures is a run of cords broken due to corrosion fatigue. Risk assessment is based upon the number and extent of damage sites. The detection of corrosion, which occurs prior to the breakage of cords, would be a welcome addition to our capability. We have investigated radiograph profile analysis as a method for identifying corrosion in the steel cords.

Flaws in standardized parts are often detected by subtracting the radiographic image of a good part from that of the tested part. Although our composite material does not produce a standard image in the same sense as a simple part, individual cords within the radiographic image can be sampled and compared using one dimensional profiles of the image grey level. Such profiles represent projections of the cord cross section. One could expect, then, that the subtraction of a standard cord profile from test profiles would reveal corrosion. But steel cords are standardized only by conformance to a cord specification. Their profiles are infinitely varied due to superposition of the twisted cord sub-structures. Do cord profiles nonetheless contain an indication of corrosion? If so, how can we access this information?

In this paper we present a computer simulator of steel cord profiles to be used for inquiry into these questions. The quantitative simulation of radiographic imagery, taking into account all of the complex interactions involved, is beyond the scope of our inquiry. We have based our simulation upon a simplified x-ray transmission image model. We describe the model and provide samples of its output. We also present an artificial neural network which we have developed to identify corrosion from the simulated profile data. We discuss plans for future work towards bringing neural network based profile analysis to bear upon real inspection data.

STEEL/RUBBER COMPOSITE

Sonar domes are similar to large tires. They are constructed by manually building up layers of both un-reinforced and steel cord reinforced rubber plies in a mold. The assembly is cured by heating in an autoclave. The wall in the region of interest typically contains 5 or 6 structural plies. Cords within each ply are spaced 2.54 mm apart. The full cord specification [1] is

$(1 \times 4) \times 0.175 + (6 \times 4) \times 0.175 + 1 \times 0.15 \quad 10/20/3.5 \quad \text{SZS}$

which describes seven strands, each of which consists of four 0.175 mm diameter wires twisted together in the left hand direction at a pitch (lay length) of 10 mm per revolution. One strand is in the center and the other six are twisted in the opposite (right hand) direction about the center strand at a pitch of 20 mm per revolution. A single 0.15 mm wrap wire is wound around the cord in the left hand direction at a pitch of 3.5 mm per turn. Figure 1 illustrates this construction. We will use the terms cord, strand, and wire consistent with this description.

RADIOGRAPHS

The Navy inspection parameters were optimized for the detection of broken cords. An x-ray tube operating in the range of 150 to 200 kv and fine grain film (DuPont NDE 45) are used. Resolution is sufficient to identify individual 0.175 mm wire elements protruding from broken cord ends. Although the multiple ply images are superimposed, the 2.5 mm cord spacing allows a number of individual cords to be seen between the images of other plies. Anomalous spacing between cords normal to those being observed also frequently allows unobstructed views as shown in Figure 2. These views present opportunities to measure profiles across single cords.

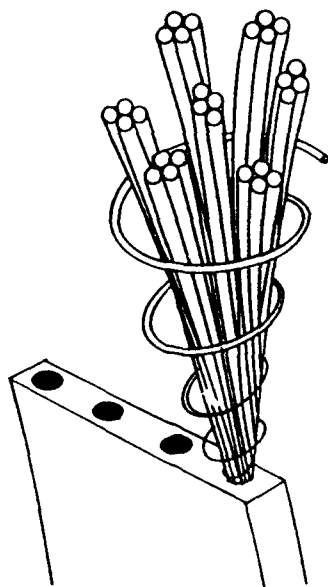


Figure 1. Structure of 1.48 mm $7 \times 4 \times 0.175 + 0.15$ tire cord.

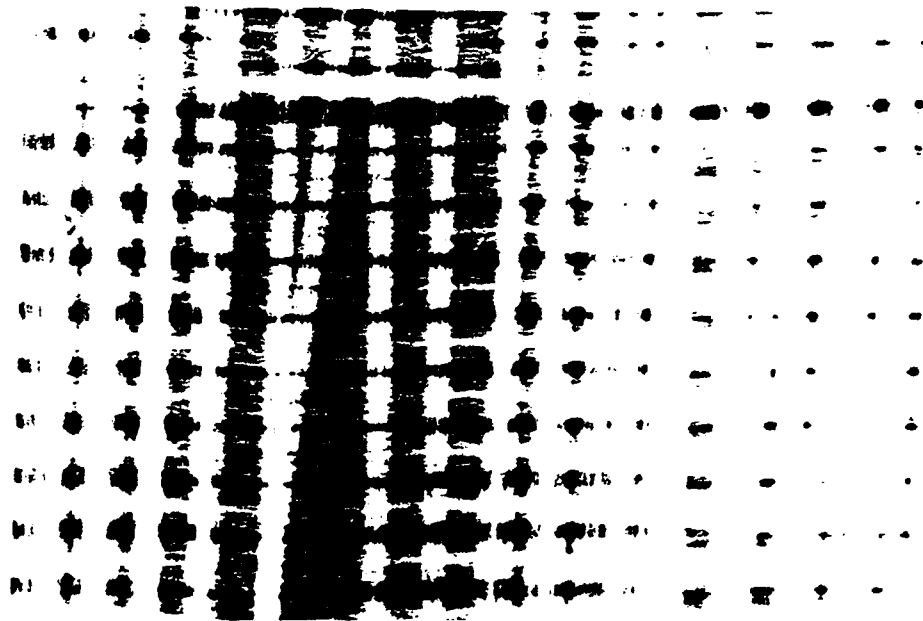


Figure 2. Sonar dome radiograph showing two horizontal (longitudinal) plies seen between three vertical (radial) plies. Cord diameters are 1.48 mm.

CORD PROFILES

We digitized illuminated radiograph images and measured profiles using a Quantex QX-7 image processing system with MTI Series 68 video camera. We wrote programs for the image processor to allow the selection and acquisition of cord profiles using a mouse. The resulting data was saved to disk files for further analysis and plotting. We collected data from radiographs of both new sonar domes, known to be uncontaminated by seawater, and domes which had failed in service soon after inspection and were therefore likely to contain corrosion. Figure 3 shows example profiles of the known good cords and suspected rusty cords. We used a magnification which provided a sampling resolution of 25 pixels per cord width (.059mm / pixel).

A difficulty with this approach is that while the general condition of the dome can be inferred from its status (e.g. new, damaged), the actual condition of a cord at a particular location is unknown. We needed a simulator of cord profiles to provide information about cord structure along with the profile data. An additional benefit is the capability of the simulator to provide the large sets of data needed for artificial neural network training and testing.

SIMULATION

The fundamental relationship between monoenergetic incident and transmitted x-ray intensities and a material's properties is described by the formula

$$I = I_0 e^{-\mu z} \quad (1)$$

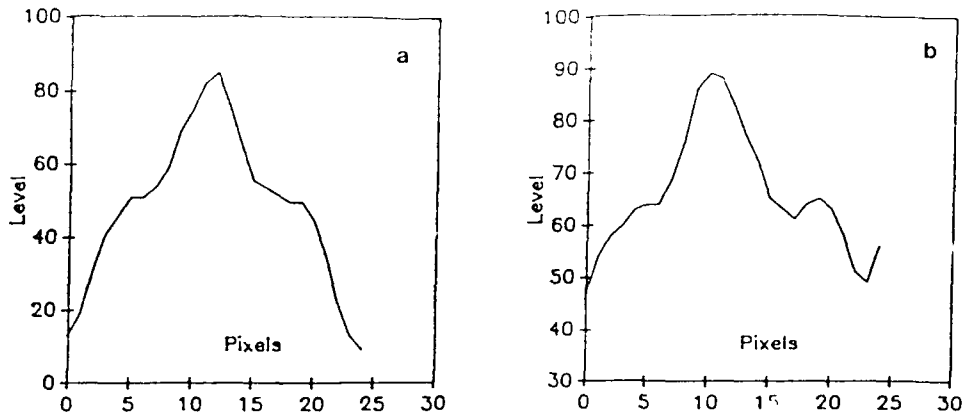


Figure 3. Examples of digitized cord profiles from radiographs of a new sonar dome (a), and a known contaminated dome (b). Each plot represents 25 measurements of the image brightness level.

where I and I_0 are the transmitted and incident intensity, μ is the linear absorption coefficient for the material, and z is the material thickness [2]. The mass absorption coefficient, μ/ρ , is obtained by dividing the linear coefficient by the density of the material, ρ . For homogeneous materials consisting of more than one element,

$$\frac{\mu}{\rho} = \sum_I w_i \left(\frac{\mu}{\rho} \right)_i \quad (2)$$

where w_i and $(\mu/\rho)_i$ are the weight fraction and mass absorption coefficient, respectively, of elemental component i [3]. Using equation (2), we have calculated values of μ/ρ for neoprene (C_4H_5Cl)_x from published tables of elemental mass absorption coefficients for 150 KeV radiation [4]. A similar treatment was applied to the carbon black filled rubber matrix assuming a ratio of 2 parts neoprene to 1 part carbon black [5]. Linear absorption coefficients of 0.206 cm^{-1} and 1.85 cm^{-1} were obtained for the matrix and steel cords, respectively, by multiplying the mass coefficients by published density values.

Radiographic images are produced by the action of the transmitted rays on a film emulsion [6]. We are concerned with the brightness image observable by placing developed x-ray film on an illuminator. The film density D is defined in terms of exposure as

$$D = \gamma \log(It) \quad (3)$$

where γ is a film response characteristic, I is x-ray intensity, and t is exposure time. In terms of the incident and transmitted light intensities, L_0 and L_t ,

$$D = \log\left(\frac{L_0}{L_t}\right) \quad (4)$$

Solving equations (1), (3), and (4) for L_t in terms of material properties, inspection parameters, and film illumination we obtain

$$L_c = \frac{I_0 e^{\gamma \mu z}}{(I_0 t)^\gamma} \quad (5)$$

For non-homogeneous materials, such as our steel/rubber composite, μ becomes a function of position. For a given exposure the inspection and illumination parameters are constant and the image $L(x,y)$ over a small area of interest can be approximated by assuming flat radiation and illumination fields:

$$L(x,y) = ke^{\gamma \int \mu(x,y,z) dz} \quad (6)$$

where k and γ are constants.

We modeled the cord cross sections as arrays of filled (colored) circles on a computer graphics screen. Each wire is represented by an appropriately sized and located circle. Random angle values are used to orient the wires about strand centers, strands about the cord center and the wrap wire about the cord. Sequential cross sections can also be generated by incrementing the angles according to the lay lengths of the three twisted sub-structures. Corrosion was modeled as a random thinning of wires up to 50% of their diameters. We chose a resolution of 200 pixels per millimeter for the simulation. This is a convenient scale for display and printing, and is well above the 10 pixel/mm resolution typically used on our image processor for radiographs. Geometric unsharpness, determined to be on the order of 0.05 mm, [7] was modeled by convolution with a blurring filter mask.

Normalized intensity profiles $P(x)$ were simulated by algorithms implementing a three step process. First the profile $L(x)$ was generated by the discrete form of equation (6) for one dimension

$$L(x) = ke^{\gamma \sum_{z=0}^T \mu(x,z) \Delta z} \quad (7)$$

where T is the cord thickness, $\mu(x,z)$ is the absorption coefficient for steel (colored pixels) or for rubber (black pixels) as determined above, Δz is the thickness represented by one pixel, $k = 1$, and $\gamma = 1$. Blurring of the image due to geometric unsharpness, U_g , was then simulated by convolution:

$$P(x) = \sum_{i=x-m}^{x+m} L(i) \quad (8)$$

where $m = U_g/2$. Lastly, the profiles were normalized over the range 0 to 255, consistent with the 8 bit grey level depth of our digitized radiograph images. Output was in the form of disk files of numeric profile data (406 profile data points and 2 cord condition indicators) and printed graphics showing the cord cross sections and associated profiles. Figure 4 shows examples of the graphics output. Program input variables include the number of profiles to be generated in one run, material attenuation coefficients, wire diameters, lay lengths, scale factors, inter-cord wire spacing, and plot resolution. Menu control is also provided for selecting options.

ARTIFICIAL NEURAL NETWORK

Classification of the simulated profiles was demonstrated using Brainmaker, a feed forward artificial neural network using a back

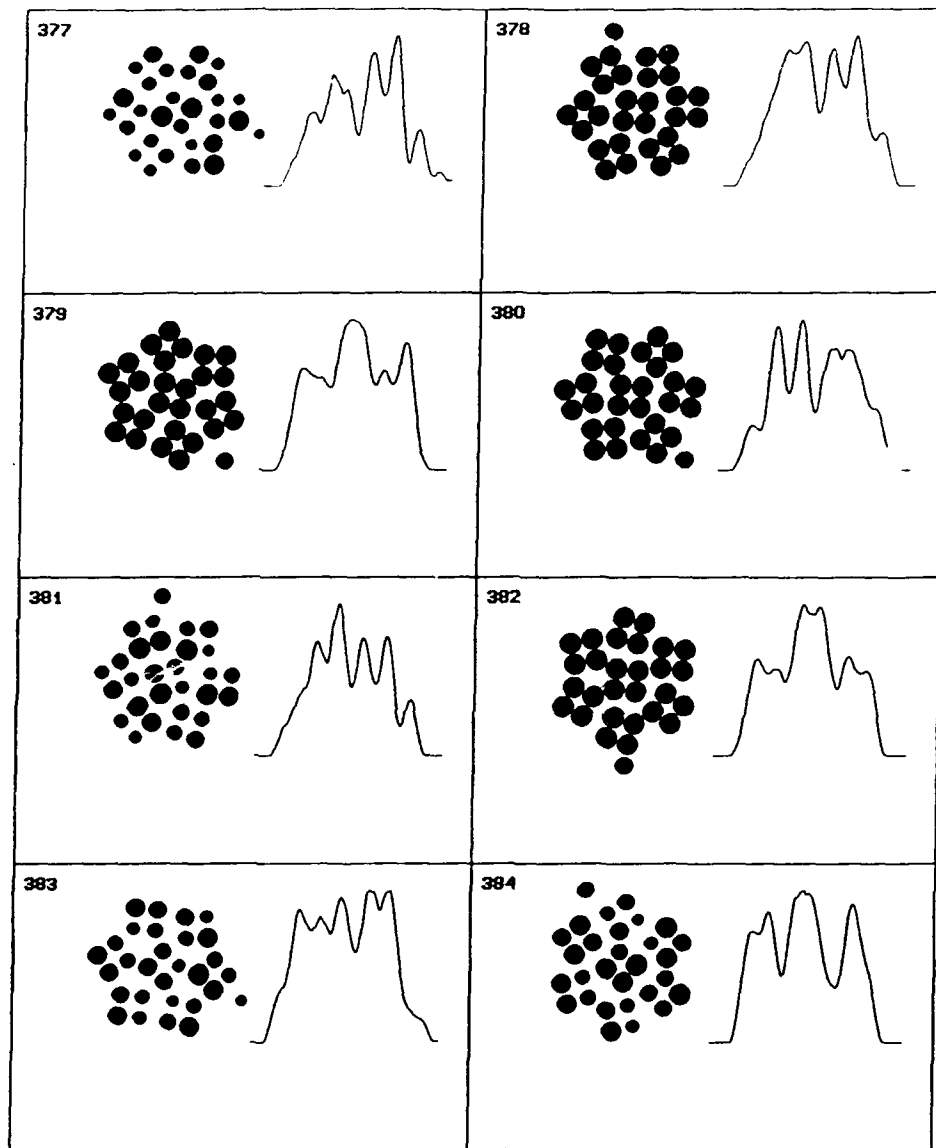


Figure 4. Examples of cord profile simulator output. Simulated cross sections are shown with their respective normalized profiles. Numbers 377, 381, 383, and 384 represent rusty cords. Numbers 378, 379, 380, and 382 represent good cords.

propagation learning algorithm [8]. We used a three layer network topology, with 25 input neurons, 100 hidden neurons, 2 output neurons, and a sigmoid transfer function. Attempts to train a network using 25 and 50 intermediate neurons both failed, an indication of the complexity of our problem.

Inputs to the network consisted of 25 point samplings of the profile data. The two output neurons corresponded to indications that the input profile represented a "good" cord or a rusty one. Two sets of 1000 profiles were generated by the cord profile simulator: one to be used for network training and the other for testing. Half of each set, selected randomly, represented rusty cords. Since mirror images of the profiles are equally valid as profile data, we made use of a Brainmaker feature which takes advantage of such symmetry and presents the data both ways. This resulted in effective training and testing data sets of 2000 profiles each.

Prior to training, neuron connection weights were randomized. During training, the profile data were sequentially presented to the network along with the known desired outputs. During the back propagation process, output error was used to determine corrections to the weights. 196 presentations of the training data set were required for the network to converge upon a solution (100% accuracy) within a training tolerance of 0.1. This tolerance means that either output in the range 0 to 1.0 found to be greater than 0.1 in error constitutes an incorrect characterization. Testing the trained network with the 2000 profiles of the test data set resulted in 118 wrong answers using the same tolerance, but only 71 wrong with a tolerance of 0.4 (An error of 0.4 on one output still provides an unambiguous characterization). This result represents a success rate of 96.5%. The time required for training was 1:34:12 using a Gateway 2000 486/25C computer at 25 MHz.

CONCLUSION

We have developed a cord radiograph model to generate simulated profile data. We have used the simulated data to develop an artificial neural network capable of characterizing cord condition with a high success rate. We conclude that profile analysis by neural network is worthy of further development. It remains to be determined whether our success so far is due to the nature of cord profiles or to an artifact of the simulation.

FUTURE PLANS

Our goal is to train an artificial neural network using simulated data for use in characterizing real profile data. We plan to improve the simulation by taking into account scattered radiation, additional sources of unsharpness, and noise. An experimental determination of the response of the film system and our video camera/image processing system will enable us to quantitatively include these effects in the model. We must also improve our model of corrosion. The random thinning of cords is unrealistically simplistic, although it served to demonstrate the characterization problem. A study of actual rusty cord profiles at higher magnification should lead to a more realistic simulation. The generation of sequential profiles will also enable us to view and compare two dimensional images of simulated cord radiographs as we refine the model.

More work on the neural network configuration could improve its performance. This will be important if, as expected, the improved model results in more difficult characterizations. Various input vectors other than the raw profile data will be considered. Others have used spectral data [9] or various statistics of the input data, such as mean intensity, variance, kurtosis, and skewness [10]. Since most of the wrong characterizations were of rusty cords, more of these can be included in the training data.

ACKNOWLEDGEMENTS

We acknowledge the support of the NAVSEA Naval Surface Ship ASW Group and the NRL Materials Chemistry Branch under NRL contract number N00014-90-C-2269. We also thank Mr. James Nagode of Geo-Centers, Inc. for his assistance with illustrations and calculations.

REFERENCES

1. *Steel Cord Catalogue* (N.V. Bekaert S.A., Zwevegem Belgium, 1987), p. 23.
2. R. Halmshaw, *Physics of Industrial Radiology* (American Elsevier, New York, 1966), p. 132.
3. L.E. Alexander, *X-Ray Diffraction Methods in Polymer Science* (Krieger, New York, 1979), p. 28.
4. *Handbook of Chemistry and Physics*, 52d Edition, Edited by R.C. Weast (Chemical Rubber Co., Cleveland Ohio, 1972).
5. *Compounder's Handbook*, Monsanto Rubber Chem. Div. (Akron, Ohio, 1981).
6. Halmshaw, *op. cit.*, p. 101.
7. R. Falabella, E.C. Greenawald, C.D Beachem, and W.B. Moniz, *Interpretation of SDRW Radiographs*, Naval Research Laboratory MR-5533, 1985.
8. J. Lawrence and M. Lawrence, *Brainmaker User's Guide and Reference Manual* (California Scientific Software, Grass Valley, Ca, 1990).
9. D. Berry, L. Udpa, and S.S. Udpa, "Classification of Ultrasonic Signals Via Neural Networks," *Review of Progress in Quantitative NDE*, Edited by D.O. Thompson and D.E. Chimenti (Plenum Press, New York, 1991), Vol 10A, p. 659.
10. L.M. Brown and R. DeNale, "Classification of Ultrasonic Defect Signatures Using an Artificial Neural Network," *Review of Progress in Quantitative NDE*, *op. cit.*, p. 705.

APPENDIX D

**APPLICATION OF NEURAL NETWORKS TO RADIOGRAPH PROFILE
ANALYSIS**



GEO CENTERS, INC.

**Application of Neural Networks
to Radiograph Profile Analysis**

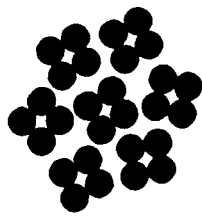
**Edward C. Greenawald
Geo-Centers, Inc.
10903 Indian Head Hwy.
Fort Washington MD 20744
(202) 767-3039**

**Chester F. Poranski
Naval Research Laboratory (6120)
Washington D.C. 20375**

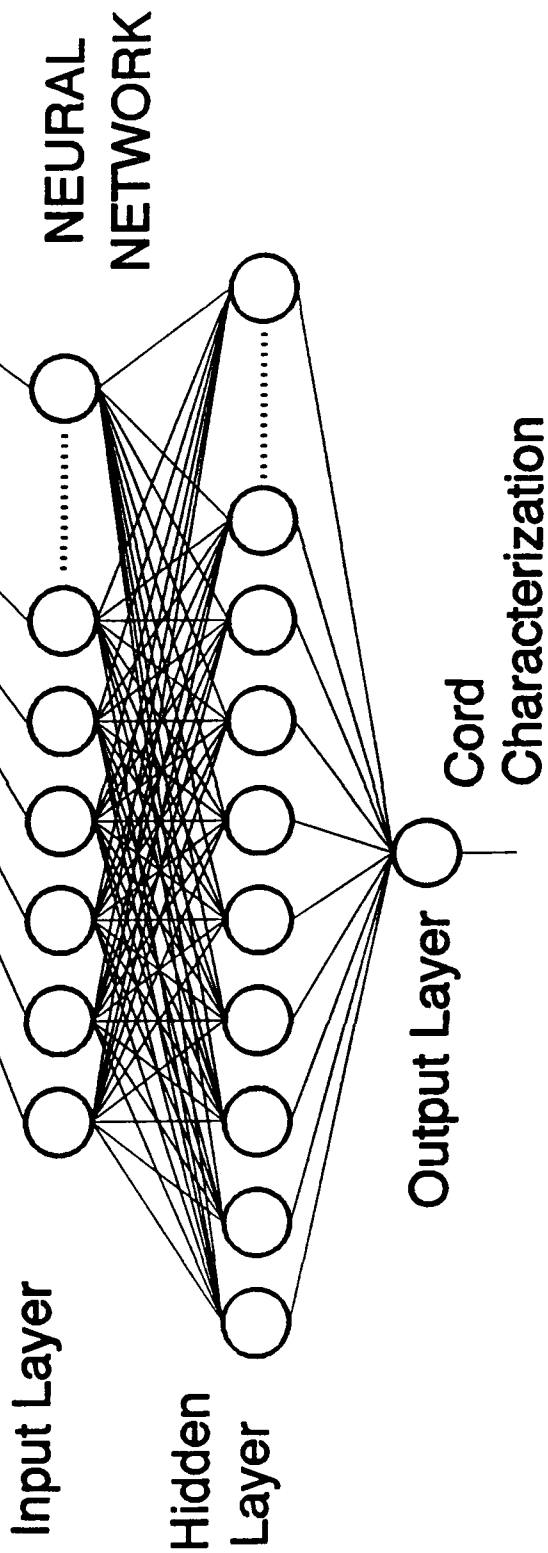
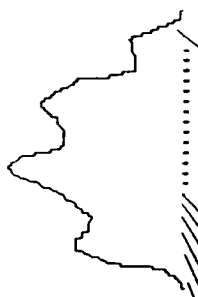
SUMMARY

Our objective is to develop an artificial neural network for the detection of corrosion in steel cord reinforced rubber composites. Our approach is to let a digitized radiograph profile represent the cross section of an individual steel cord and use the network to determine from this single projection whether the cord section is well-formed. We have also developed a computer simulator of cord sections and their profiles to provide data for testing this concept. Results are presented for a feed forward back propagation network configuration and various representations of the profile data. We conclude that further development of this approach is worthwhile.

Cord
Section
Simulation



X-ray
Profile
Simulation



X-RAY IMAGE PROFILE SIMULATION

X-ray attenuation:

$$I = I_0 e^{-\mu z}$$

Mass attenuation coefficient of rubber matrix:

$$\frac{\mu}{\rho} = \sum_i w_i \left(\frac{\mu}{\rho} \right)_i$$

Film density as function of exposure:

$$D = \gamma \log(It)$$

Film density as function of incident/transmitted light:

$$D = \log\left(\frac{L_0}{L_t}\right)$$

Transmitted light as function of x-ray attenuation:

$$L_t = \frac{L_0 e^{\gamma \mu z}}{(I_0 t)^\gamma}$$

Image as integration through non-homogeneous material:

$$L(x, y) = ke^{\gamma \int \mu(x, y, z) dz}$$

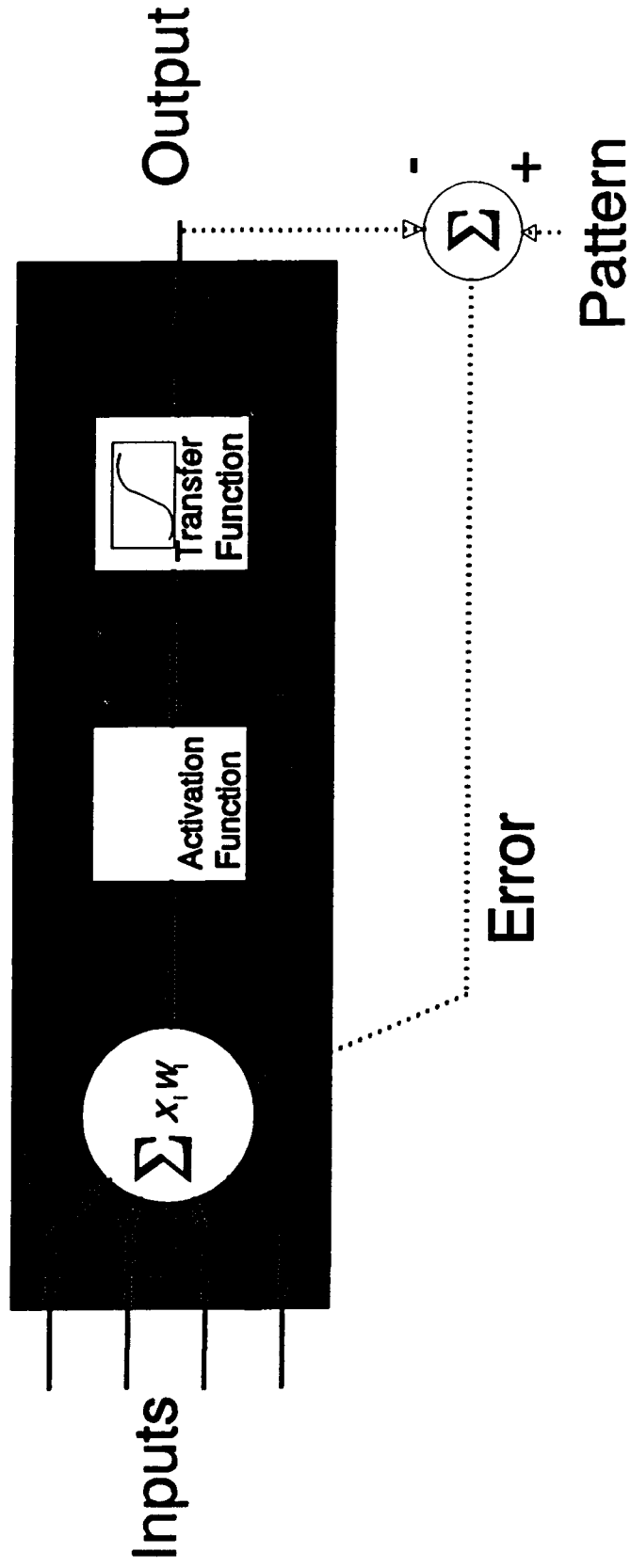
Profile as discrete form in one dimension:

$$L(x) = ke^{\gamma \sum_{z=0}^T \mu(x, z) \Delta z}$$

Unsharpness as averaging (blurring) filter:

$$P(x) = \sum_{i=x-m}^{x+m} L(i)$$

Neuron Schematic



ARTIFICIAL NEURAL NETWORK

Type: Feed Forward - Back Propagation

Software: Brainmaker by California Scientific Software

Host Computer: Gateway 2000 486/25

Network Topography: 25 input neurons
100 intermediate neurons
1 output neuron

Transfer Function: Sigmoid

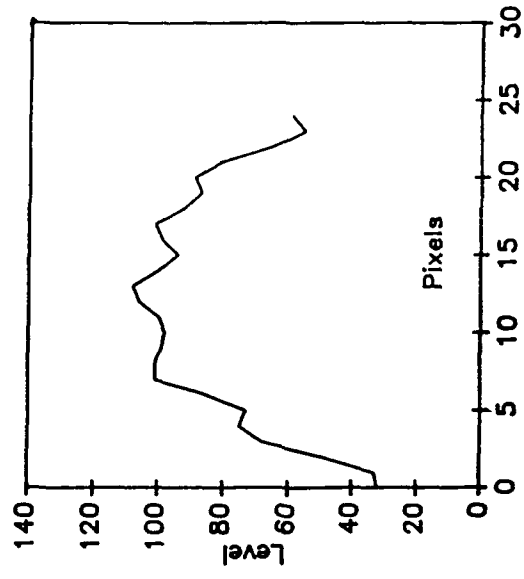
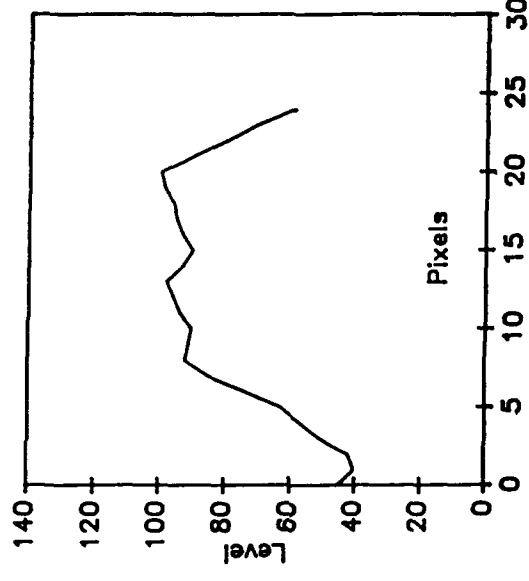
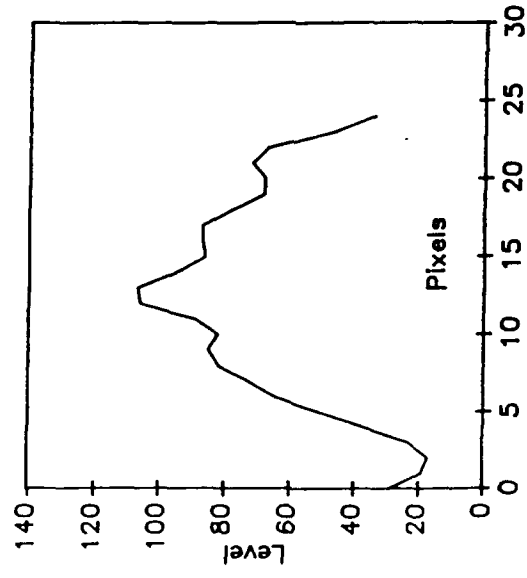
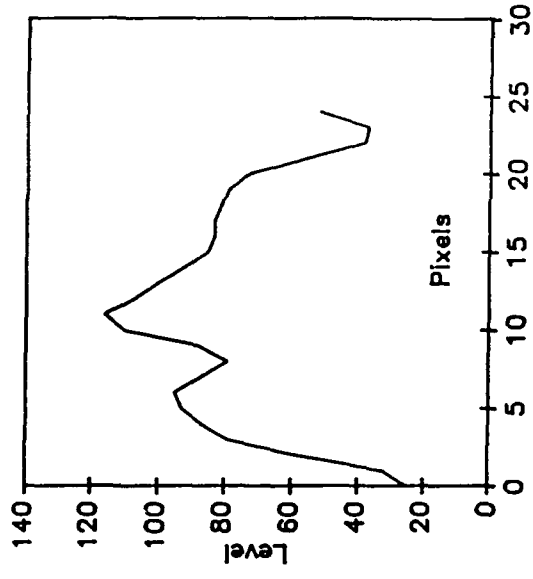
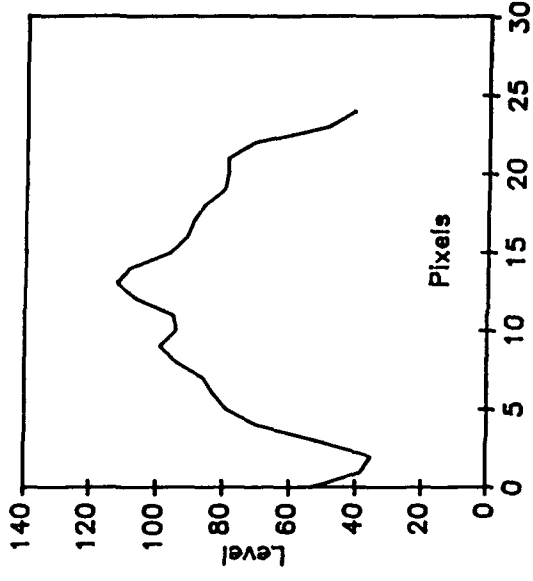
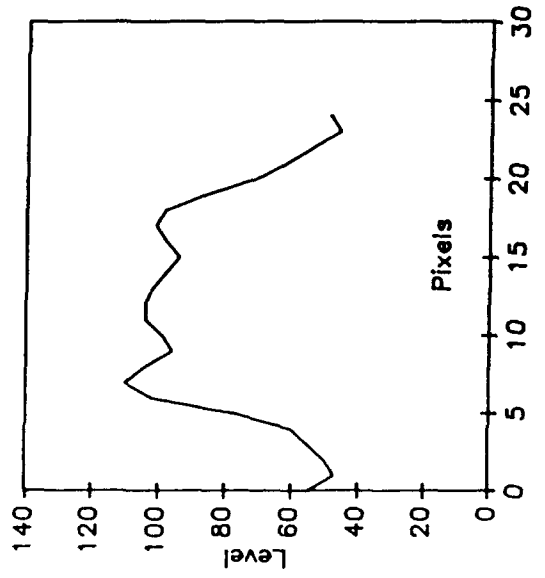
Training Parameters: Learning Rate 1.0 Tolerance 0.1

Training data (facts): 2000 Test data: 2000

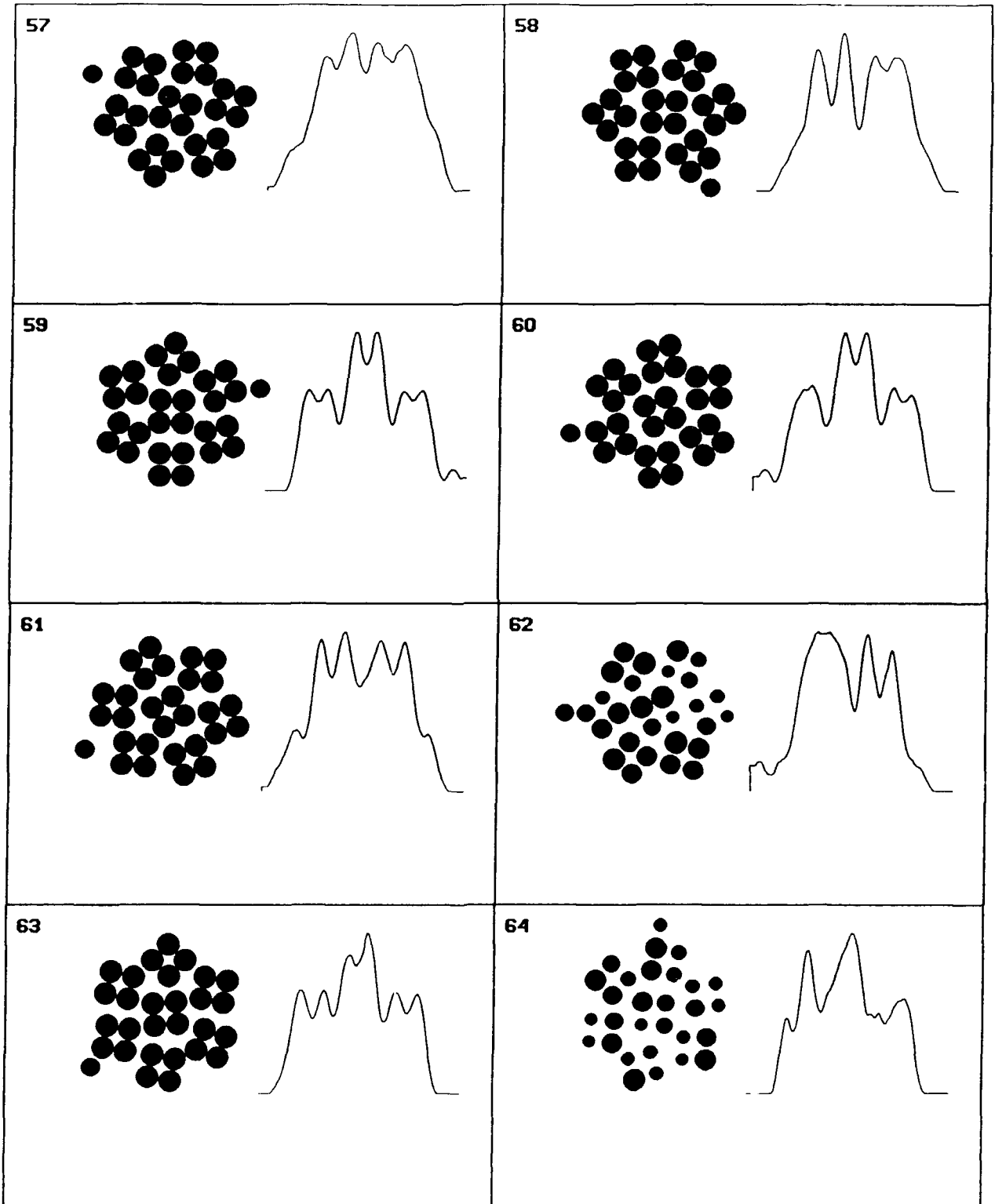
Training Results: Convergence upon solution . Elapsed time 0:31.

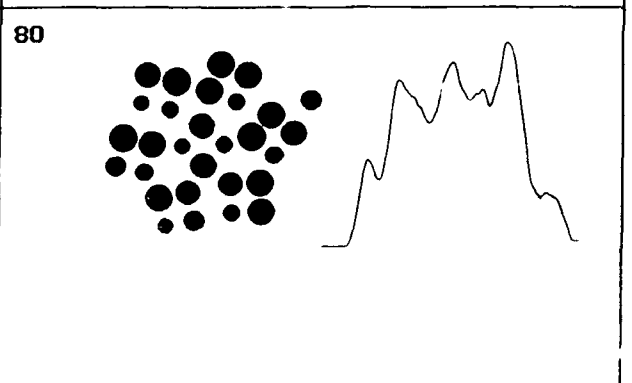
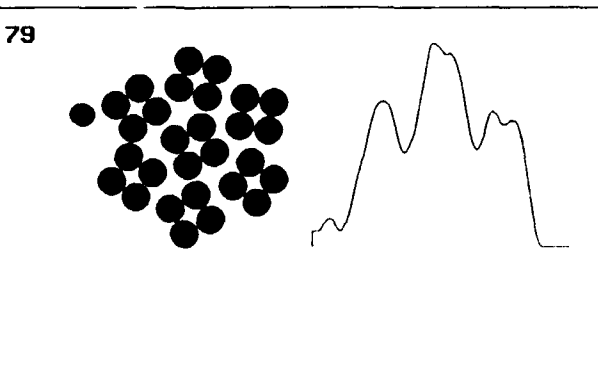
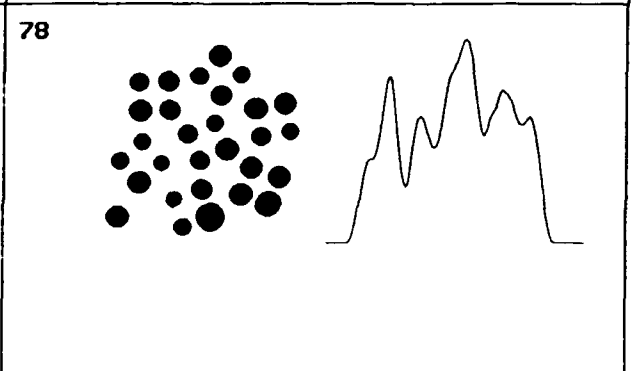
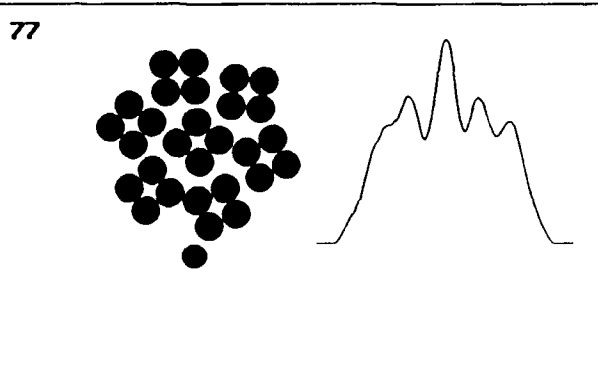
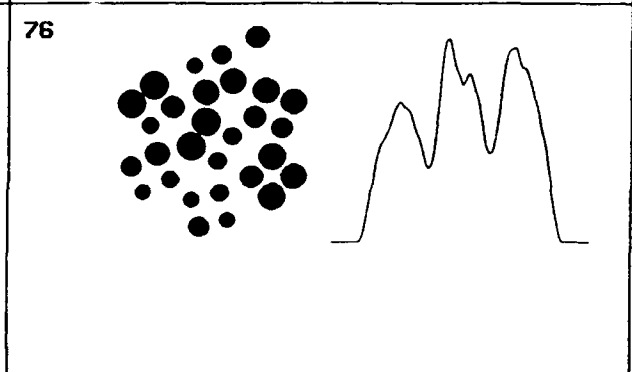
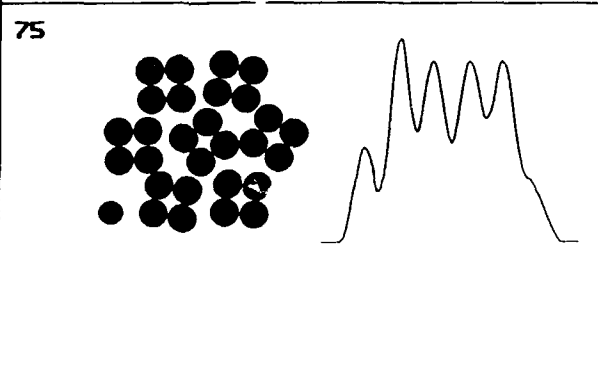
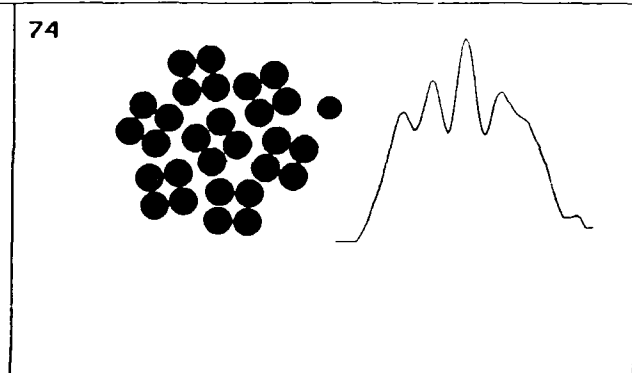
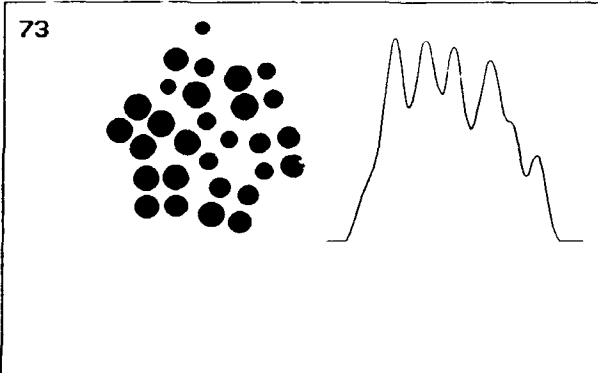
Test Results: 1932 correct out of 2000 profiles with tolerance 0.4
96.6 %

DIGITIZED RADIOGRAPH PROFILES

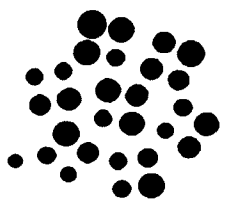


SIMULATED RADIOGRAPH PROFILES

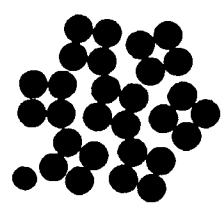




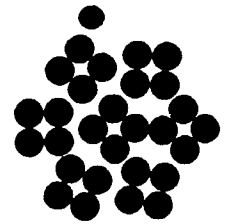
105



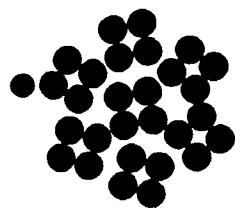
106



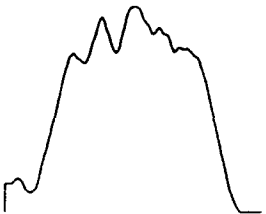
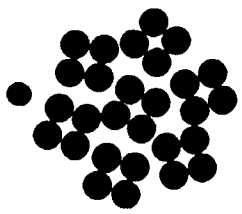
107



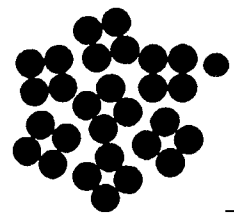
108



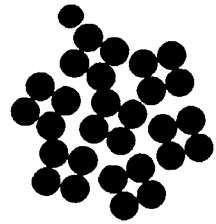
109



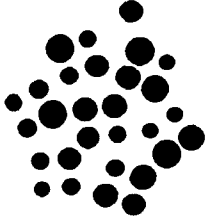
110

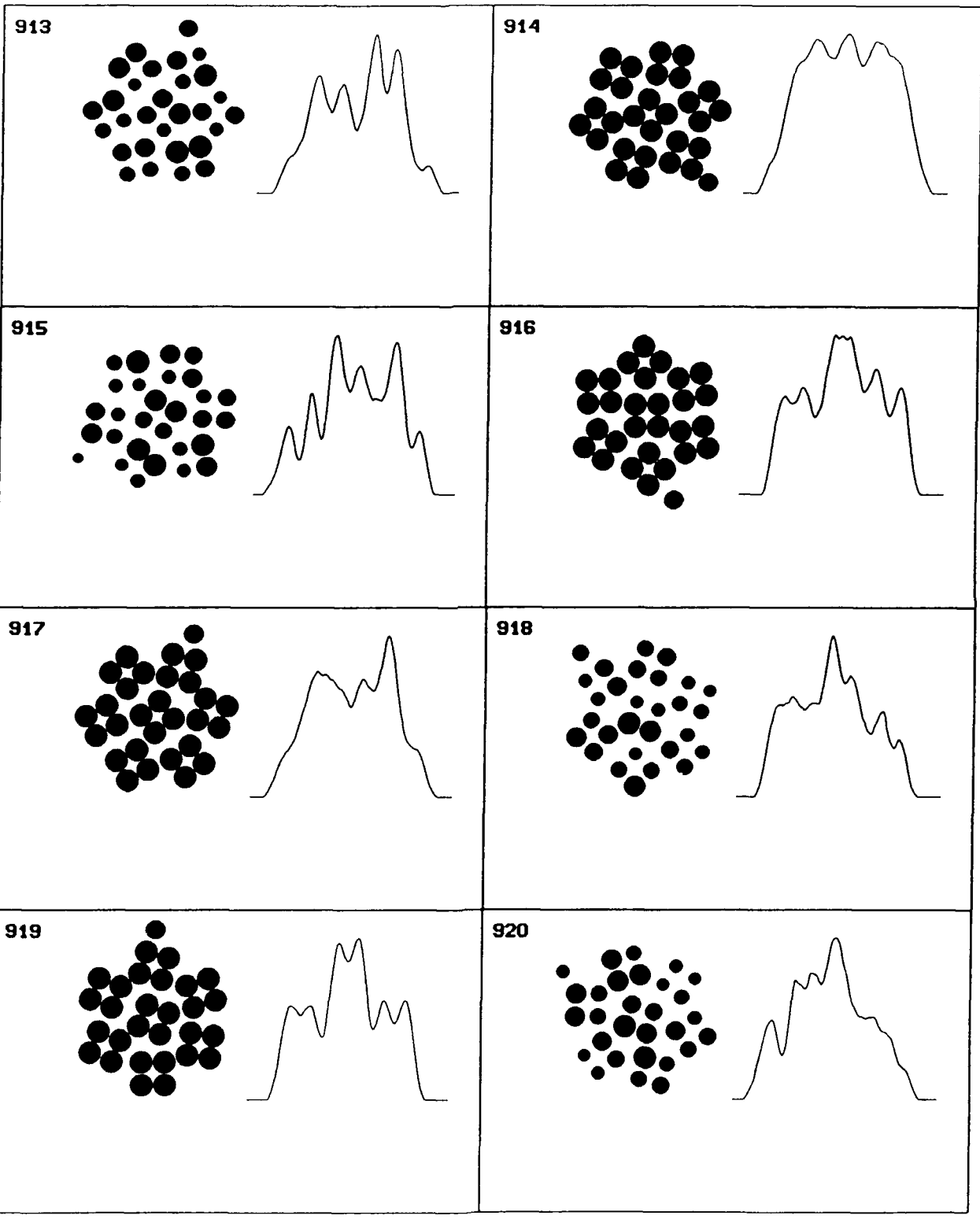


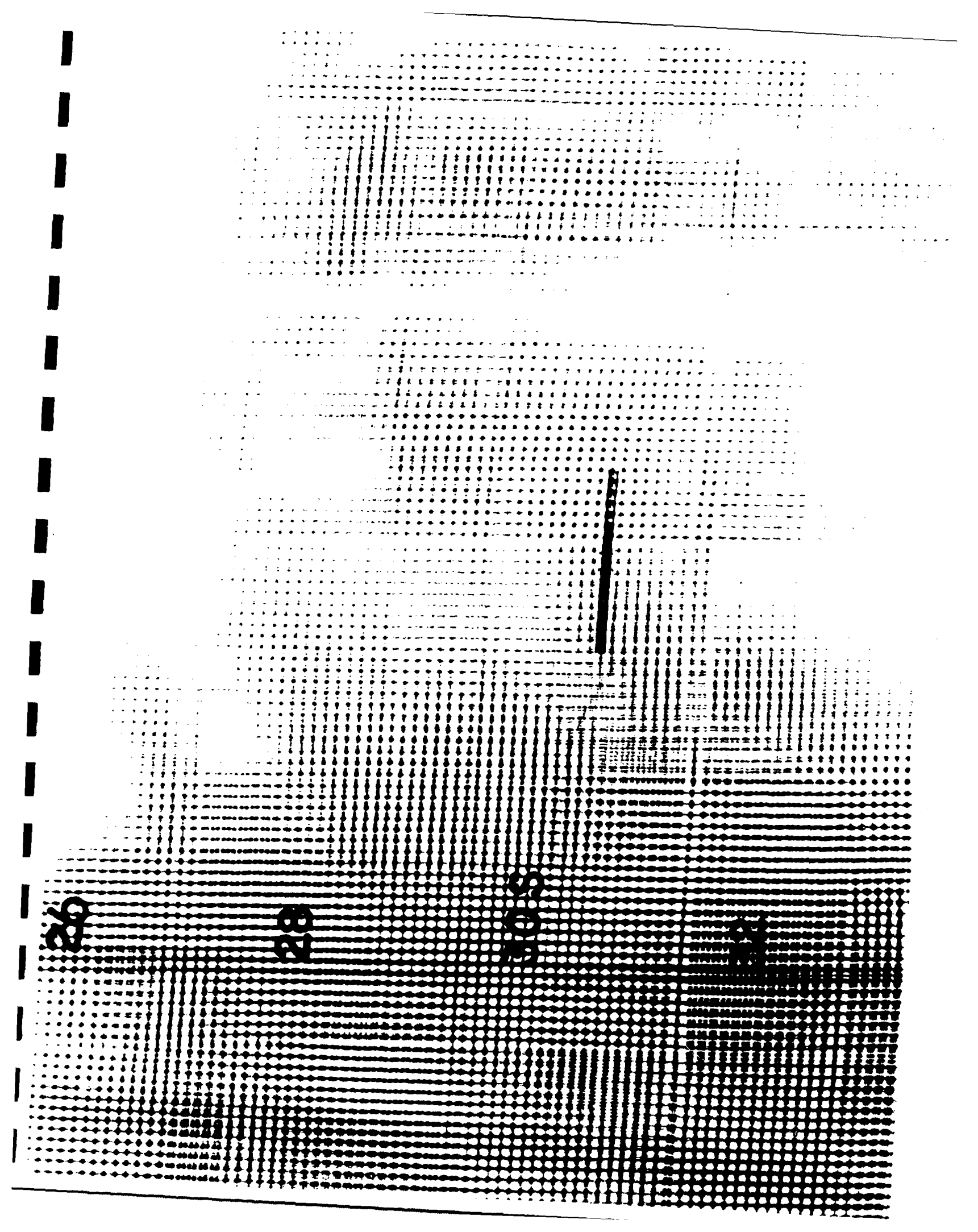
111

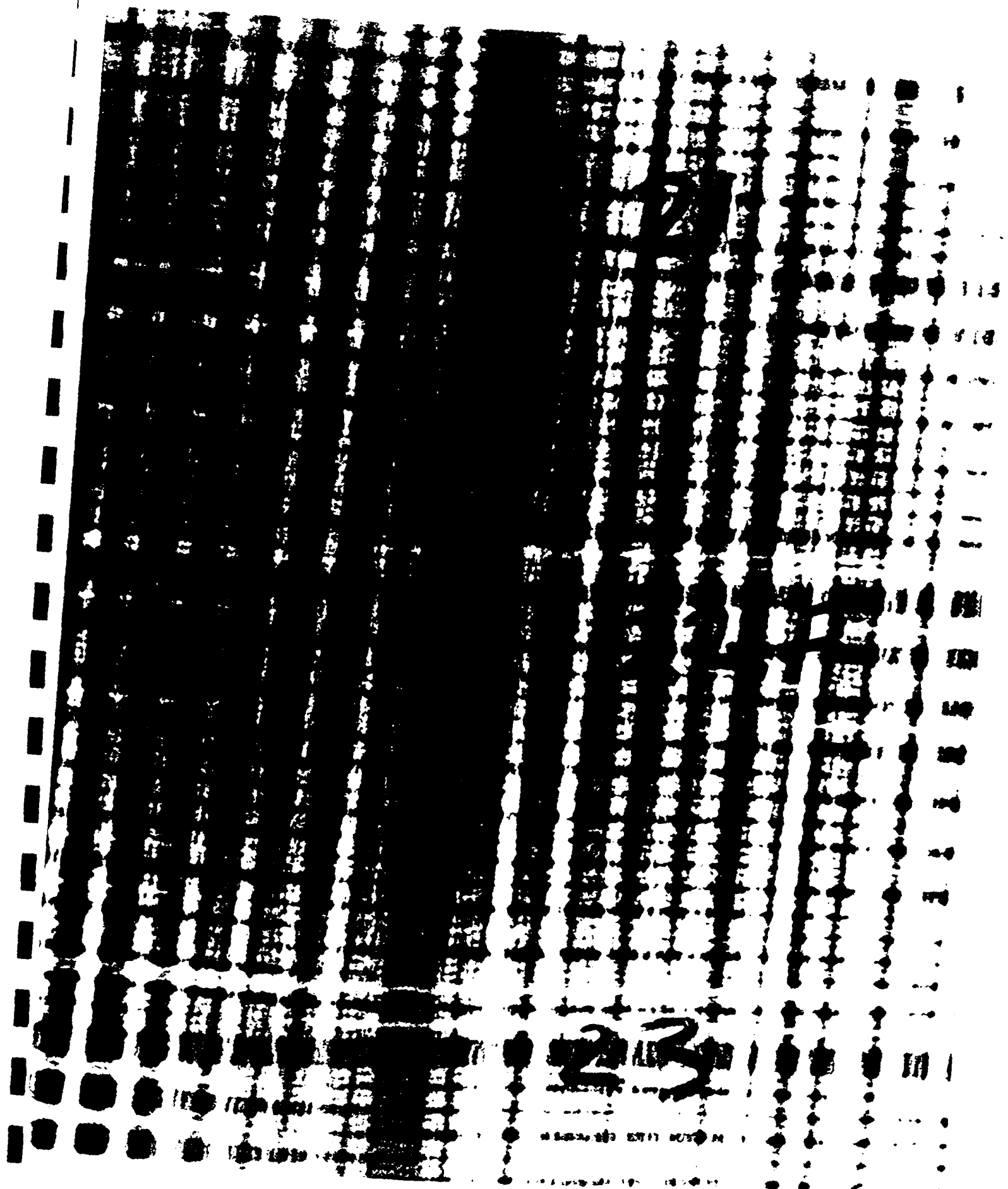


112









© 1997

APPENDIX E
SONAR RUBBER DOME STRUCTURAL DAMAGE
CHARACTERIZATION



GED CENTERS, INC.

Sonar Rubber Dome Structural Damage Characterization

**I. Technical Summary and Analysis of Preliminary
Load/Indentation Results for the AN/SQS-56 Sonar Rubber
Dome (S/N A008) from the USS *Clark*, FFG 11**

M. L. Warzel

*Geo-Centers, Inc.
Ft. Washington, MD 20744*

August 9, 1991

CONTENTS

Introduction	1
Test Apparatus and Procedures	1
Field Test Results	2
Discussion	5
Summary & Conclusions	6
Recommendations	6
References	8
Appendix A — SRD Load/Indentation Data for S/N A008 Removed From the USS <i>Clark</i> (FFG 11)	9
Appendix B — SRD Radiographic Inspection Report — Forward Exposures for the USS <i>Clark</i> (FFG 11), Inspection Date: 6/11/90	16

Sonar Rubber Dome Structural Damage Characterization

I. Technical Summary and Analysis of Preliminary Load/Indentation Results for the AN/SQS-56 Sonar Rubber Dome (S/N A008) from the USS *Clark*, FFG 11

Introduction

Recent investigations into the failure mechanisms of sonar rubber domes (SRDs)^{1,2} have shown that failure is accompanied by structural damage in the plies. Such damage is typically localized to the forward starboard and port regions near the intersection of the keel band and bead band edges. The gradual development of damage in these regions has led to the development of a continuing radiographic inspection program to aid in the early detection of steel cord failure in the plies. However, due to the difficulty of examining SRDs for the AN/SQS-56 sonar, necessitating the removal of the SRD from the ship, a need has arisen for a pierside screening technique to indicate the possibility of structural damage in SRDs.

This report details the results of recent investigations into the deformation characteristics of a sonar rubber dome structure. This work is intended to provide a preliminary basis for further efforts directed toward the ultimate development of a rubber/steel cord damage screening device and test procedure. The basic procedure involves the application of static point loads within the region of an SRD where the forward keel band and bead band edges intersect. Measurement of the deformation of the SRD surface under load, it is hoped, will allow for a determination of the likelihood of structural damage in the affected area. In combination with x ray examinations, or as a tool to determine if an SRD is in need of a detailed x ray examination, such a test should provide a useful composite picture of SRD structural integrity and help to forestall any future in-service failures.

Test Apparatus and Procedures

A simple test apparatus was developed for these investigations consisting of a 1000 lb. tension/compression load cell attached to a 24 in. long, 1.0 in. diameter steel rod. The rod was threaded to accept a 5/8 in. x 18 tpi load cell coupling provided on standard Instron load cells. A load was applied to the SRD exterior surface by the use of three aircraft cable ratchet winches attached to both the load cell and the SRD support frame. One cable was typically attached to the interior metal lip of the bead clamps, thereby supporting most of the weight of the load cell fixture. The remaining two winch cables were spaced at approximately 120° intervals around the load cell and attached to the beams of the SRD support frame.

The load cell was powered by a DC voltage excitation from a Measurements Group model 2310 signal conditioning amplifier. The amplifier was powered by a portable 120 volt AC generator. A custom-wired cable was fabricated to connect the load cell to the amplifier. The load cell was operated at a DC excitation of 3.5 volts. A mechanical calibration of the load cell was performed by loading the cell under compression with a total of 40 lb. in weights. The amplifier gain was typically adjusted to provide a load calibration factor of 50 lb./volt.

A standard XY coordinate system was mapped onto the forward port side of the SRD to simplify the placement of the loading fixture. Due to the difficulty of locating the precise positions of the band and ply structures at the intersection of the keel and bead band edges, the origin of the coordinate system was referenced relative to the keel centerline and the top of the rubber dome ("marriage line" or upper rubber line "URL" between the rubber dome and the bead clamps). The advantage of this coordinate system is the ease with which it may be located on the exterior of any SRD surface without knowing the precise positions of the underlying ply structures. The origin was measured along the SRD surface from the keel centerline to the edge of the 20 in. keel band and 24 in. from the top of the dome to the edge of the bead band. The Y axis line was drawn as a line spaced 20 in. from the keel centerline along the surface of the dome. The X axis line was drawn as a line spaced 24 in. from the upper rubber line along the surface of the dome. Positive X and Y directions were taken as aft and above the origin, respectively; negative X and Y directions were forward and below the origin.

The test procedure consisted of holding the rod to the surface of the dome and applying increasing loads by tightening the three winches. The rod was maintained in a position that was approximately normal to the surface. Several methods were evaluated for measuring the indentation of the surface relative to the original profile; the best procedure is summarized as follows: The original surface curvature was matched by placing an aluminum wire along the Y axis or parallel to this axis for measurements forward of the port side keel band edge. A slight amount of tension was placed on the wire to maintain direct contact with the dome prior to deformation (the level of tension was sufficient to maintain contact without distorting the wire profile shape as the dome was indented). A dial caliper mounted on the loading rod was then used to record the SRD indentation as the difference between the rod length and the distance to the original profile wire. Prior adjustment of the caliper provided a direct measure of the indentation from the original surface profile.

Field Test Results

Results of the load/indentation data obtained from field tests on 8/6/91 are summarized in Figures 1 and 2. Raw data for these figures as well as previous results obtained on 7/31/91 and 8/2/91 are compiled in Appendix A. Figure 1 depicts the data as recorded along vertical (Y axis) lines starting at X=0 (along the edge of the 20 in. keel band) and progressing forward to the keel centerline at 2.0 in. intervals. Due to the single and two-ply damage in this region (see Appendix B), field investigations on 8/6/91 were limited to an area 12.0 in. above and below the X axis, the Y axis, and 6.0 in. forward of the Y axis. Figure 2 depicts these results, arranged to illustrate the effects of loading along the keel band forward of the keel band edge.

Previous investigations on 7/31/91 and 8/2/91 were concerned with load/indentation results along the edge of the 20 in. keel band (Y axis) and the X axis. In addition, preliminary results for the extent of the indentation profile diameter are available in Appendix A. It should be noted that results obtained on 7/31/91 are based on an XY origin that is displaced approximately 3 in. below the origin (on the Y axis) used on 8/2/91 and

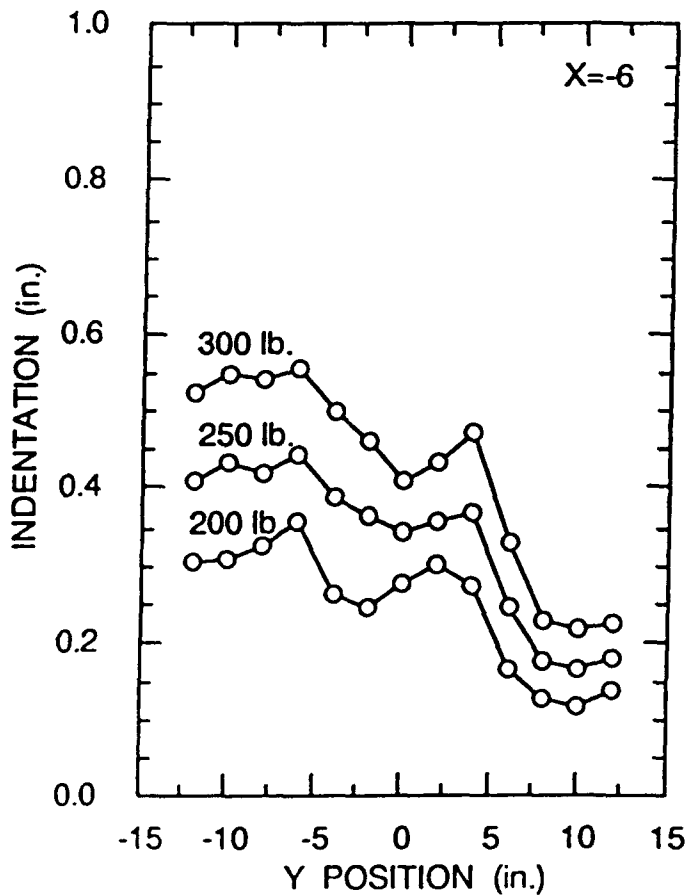
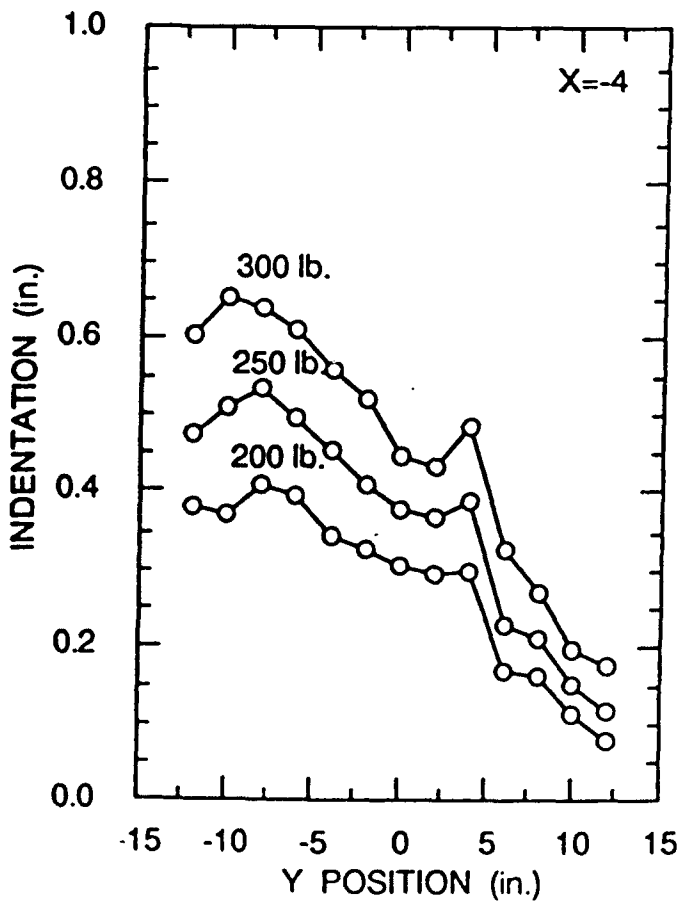
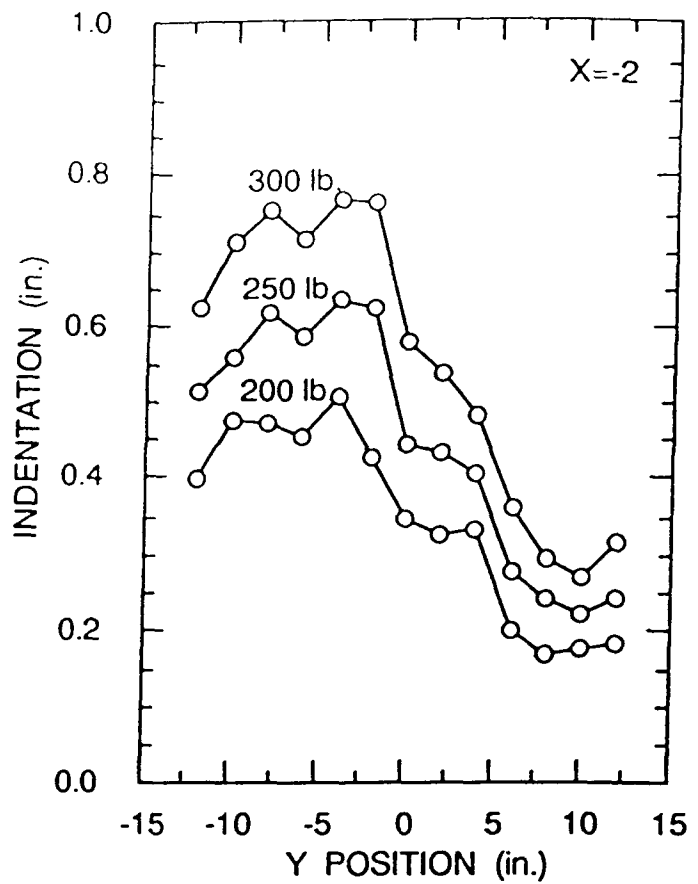
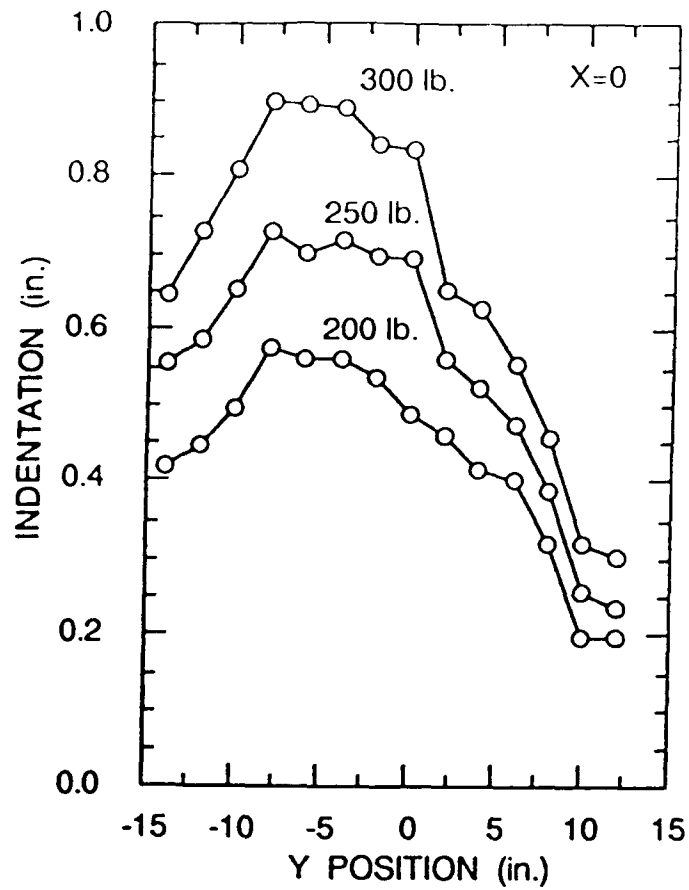


Fig. 1 — Load/indentation results from 8/6/91 for the forward port side of SRD S/N A008 removed from the USS *Clark* (FFG11). Data are shown for vertical lines paralleling the keel band edge.

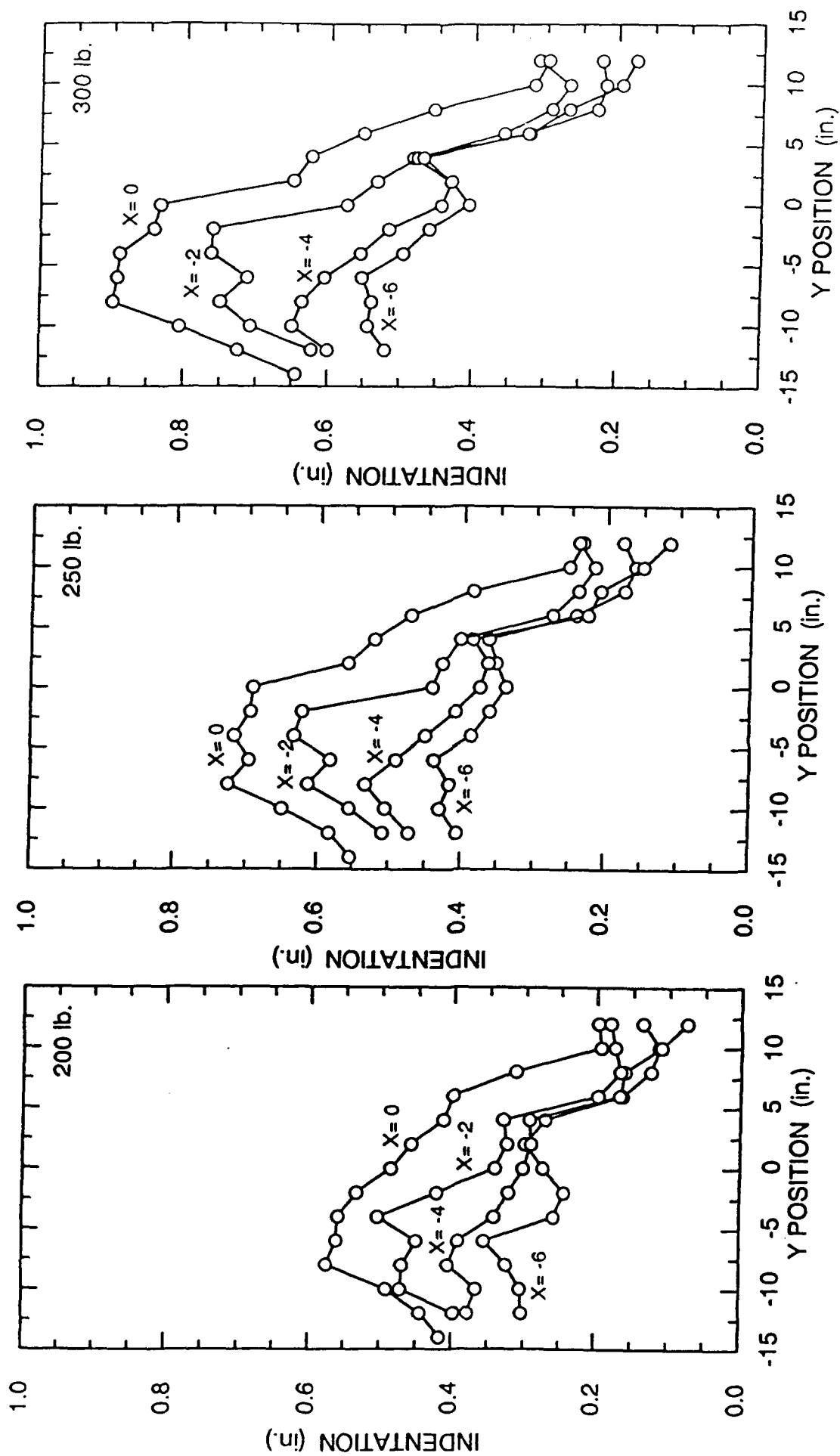


Fig. 2 — Load/indentation results from 8/6/91 for the forward port side of SRD S/N A008 removed from the USS Clark (FFG11). Data are shown at constant load for variations in X and Y position.

8/6/91. Results obtained on 8/2/91 are based on a relative measure of SRD indentation since it was necessary to apply an initial load of 50 lb. to hold the steel rod against the SRD. Indentation results recorded by this procedure do not account for the small indentation that occurs under this load.

The indentation profile diameter was recorded on 7/31/91 as an approximate point where the indented surface matched the original profile of the undistorted surface. Earlier trials had shown that differences in the indentation profile shape are observed for different loads and positions. It was hoped that some characteristic measure of these shapes could provide information that would indicate the presence of a potential damage site. However, due to the large amount of data necessary to develop a picture of the profile shape, these efforts were postponed for possible future investigations.

Discussion

As shown in Fig. 1, a large variation in stiffness is evident within the damage region. Each vertical line (at constant X) paralleling the edge of the port side keel band shows a general trend of relatively low indentation above the X axis, increased indentation through the region immediately above and below the X axis, and decreased indentation at distances well below the X axis. Each line shows similar trends for loads from 200 to 300 lb., although at higher load the accompanying larger deformation generally improves the measurement precision. The evident indentation maxima between $-7 \leq Y \leq 0$ for $X=0$ appear to reduce in both magnitude and range from the edge of the keel band ($X=0$) forward to the keel band centerline. At a 6.0 in. distance forward of the keel band edge ($X=-6$), the maxima between $-7 \leq Y \leq 0$ are no longer clearly evident. The magnitude of the indentation in this area is also reduced by 40-50% compared with values obtained at $X=0$.

The appearance of a second maximum between $+2 \leq Y \leq +6$ as X varies from 0 to -6 in. is also evident. At $X=0$ and $X=-2$ this region shows an increased indentation that is not clearly identified but rather is characterized by a reduced stiffness or "spongy" behavior. At $X=-4$ and $X=-6$, a clear maximum develops in this area. Plotted at constant load for variations in both X and Y positions, Fig. 2 more clearly shows this trend.

Comparisons with the SRD radiographic inspection report for this dome (Appendix B) show several damaged cords and plies along both the keel and bead bands that roughly correspond to the variations in deformation shown in Figs. 1 and 2. Such comparisons are complicated by the lack of an accurate field determination of the position of the bead band edges at the intersection with the keel bands. Nonetheless these results are encouraging since a clear variation in deformation is observed with an apparent correspondence in structural damage. An improved x ray determination of the band edge alignment and corresponding field load/indentation coordinates would improve such comparisons.

Any conclusions of potential damage based on the present deformation results alone are not yet possible. Further testing of this SRD on both the forward port and starboard sides is necessary as well as comparisons with other SRDs before a sufficient amount of information would allow such conclusions. By further investigating the deformation behavior of undamaged and damaged structures a measure of the sensitivity of this technique may be established. The results presented in this report would appear to warrant such further studies.

Profile changes and shape distortions under field load conditions have proved to be of interest during testing. At present these observations are both difficult to characterize and understand. Undoubtedly, the ply structure and layup, orientation of the plies, and overlap in splice regions and the resulting stiffness variations could result in markedly different

surface profiles under static loading. It is reasonable to expect that damage to the cords could therefore be detected some distance from the loading point as a change in the surface profile. During field tests on SRD S/N A008 several surface profile changes were noted, including apparent "crease lines" (lines where the indentation remained relatively flat), ply edges resulting in increased stiffness and reduced indentation away from the load point, and bulges or ripples due to possibly broken cords or damaged plys. For the present, due to the complexity of the effects capable of producing such profile changes, these variations should simply be noted where appropriate. Further testing of such structures may improve the ability to use such profile distortions as a contributory aid in SRD damage detection.

Several complications in SRD deformation testing and data interpretation and potential refinements in the test procedure and apparatus are identifiable. The effect of SRD construction, specifically the effect of ply layup and cord orientation, is difficult to separate from any effects due to damage. For this reason, a clearer picture of the relative influence of damage or absence of damage is very important. Secondly, an absolute measure of band edge positioning on the SRD also needs to be made to allow direct comparisons with radiographic information.

The use of a deformation reference based on the original surface profile, while simple in concept, has presented several complications in the field. The need is for a rigid profile reference that remains fixed as the SRD is deformed and yet is flexible to allow for measurements over a wide area. The wire system used for these preliminary studies was adequate but could undoubtedly be improved upon, thereby improving the speed and accuracy of field measurements. Such a system would also prove less useful in a pierside application. Finally, the alignment of the load device and SRD surface represents a variable that should be controlled for reproducible measurements. In these field trials the rod was positioned by eye so that it was nearly normal to the surface. The degree to which variations in the position of the rod affect the deformation is unknown.

Summary & Conclusions

Preliminary load/indentation results have been obtained for SRD S/N A008. The present results indicate a substantial variation in SRD stiffness exists in the region of the keel and bead band intersection. Several increases in indentation have been noted that appear to correspond to known damage sites as determined by radiographic inspection. The interdependent effect of SRD construction and damage in these regions upon the present results is unknown. Variations in the surface profile under static load have been identified as an area of potentially useful information indicating possible structural damage. Several improvements in test procedures and apparatus are necessary to alleviate field measurement problems and improve the speed with which measurements are made.

Recommendations

It is apparent from these investigations that several recommendations are warranted in the following areas:

Apparatus & Procedural Improvements — A continuing development of the testing procedure should be promoted to improve the efficiency and accuracy of load/deformation measurements. The need to rapidly move a load rod to a new position that is normal to the dome surface is apparent as is an absolute measure of the deformation of the surface from the original profile. Such improvements should also be easy to implement and not require continual adjustment in the field.

Program Development — A structured program should be developed to further determine the suitability of SRD deformation testing as a screening aid for x ray examinations. Such a program should encompass further testing of the starboard and port forward regions of SRD S/N A008 and testing of several undamaged and damaged SRDs. In conjunction with x ray examinations such tests could be completed quickly without major expense and with very little modification to the current device and test procedure. Further testing and device development should also lead to a simplified test procedure suitable for pierside application.

References

1. "Failure Analysis of the AN/SQS-56 Sonar Rubber Dome from USS *Rodney M. Davis*, FFG 60", C.D. Beachem, H.L. Schrader, and C.F. Poranski, Jr., NRL Memo Report 6263, Sept. 22, 1988.
2. "Failure Analysis of the AN/SQS-56 Sonar Rubber Dome (S/N A13) from USS *Lewis B. Puller*, FFG 23", C.D. Beachem, H.L. Schrader, and C.F. Poranski, Jr., NRL Memo Report 6451, Dec. 11, 1989.

APPENDIX A

SRD Load/Indentation Data for S/N A008 Removed From
the USS *Clark* (FFG 11)

(X,Y) POSITION (in., in.)	INDENTATION (in.) FOR LOAD (V)				NOTES
	-4.0	-5.0	-6.0	-6.0	
0,0	0.486	0.692	0.833	0.833	Point 0,0 is the edge of the 20" Keel band (Port side Forward) measured 24" from URL. X axis line through Y=0" is approx. 3" above line from 7/31/91. Y axis line through X=0" is within 1" of 7/31/91 location.
0,-2	0.533	0.694	0.841	0.841	
0,-4	0.558	0.716	0.889	0.889	
0,-6	0.560	0.697	0.891	0.891	
0,-8	0.574	0.725	0.896	0.896	
0,-10	0.492	0.651	0.806	0.806	
0,-12	0.445	0.582	0.725	0.725	
0,-14	0.416	0.552	0.644	0.644	
0,+2	0.459	0.559	0.651	0.651	
0,+4	0.413	0.521	0.624	0.624	
0,+6	0.400	0.471	0.553	0.553	
0,+8	0.315	0.385	0.455	0.455	
0,+10	0.194	0.254	0.316	0.316	
0,+12	0.196	0.233	0.298	0.298	
-2,+12	0.180	0.239	0.312	0.312	Point -2,0 is 2.0 in. forward of the 20" keel band edge (Port side Forward) measured along the surface of the SRD and 24" from URL.
-2,+10	0.175	0.218	0.268	0.268	
-2,+8	0.167	0.239	0.291	0.291	
-2,+6	0.197	0.275	0.358	0.358	
-2,+4	0.331	0.402	0.478	0.478	
-2,+2	0.324	0.429	0.534	0.534	
-2,0	0.343	0.442	0.576	0.576	
-2,-2	0.422	0.622	0.761	0.761	
-2,-4	0.503	0.633	0.764	0.764	
-2,-6	0.451	0.584	0.713	0.713	
-2,-8	0.470	0.614	0.750	0.750	
-2,-10	0.472	0.555	0.709	0.709	
-2,-12	0.396	0.509	0.621	0.621	

(X,Y) POSITION (in., in.)	LOAD (lb)	INDENTATION (in.)	INDENTATION DIAMETER (in.)		NOTES	
			POSITION			
			Top	Bottom		
0,0	3.03	24/64	2-13/16	3-12/16	Position (0,0) at the intersection of the 20" keel band and 24" bead band edges. Indentation measured from original surface profile using a 0.057" dia. wire formed to the original surface profile.	
	4.00	31/64				
	5.00	41/64	5-9/16	5-0/16		
	6.00	49/64	4-3/8	5-0/16		
0,+5.0	3.00	32/64	3-1/2	4-5/8	Actual indentation from original surface = measured indentation less the wire diameter.	
	4.00	40/64	3-13/16	4-15/16		
	5.11	49/64	5-1/2	8-1/4		
	6.04	58/64	6-0/16	na		
	7.00	1-6/64	5-5/8	na		
	8.01	1-16/64	5-1/2	na		
	9.10	1-43/64	na	na		
		3.00	24/64	3-1/4		3-1/4
		4.00	31/64	3-5/8		4-3/16
0,+9.0	5.20	39/64	4-3/16	4-1/4	Noticeable distortion in surface profile at 5-6 volts. Unable to measure Indentation diameter.	
	6.00	43/64	4-5/16	4-5/16		
	7.15	54/64	4-1/2	4-3/4		
	8.00	60/64	5-1/4	6-0/16		
	9.00	1-5/64	na	na		
		3.40	24/64	3-1/2		3-1/8
		4.20	28/64	3-1/2		3-1/2
		5.00	34/64	3-9/16		4-0/16
		6.00	40/64	4-0/16		5-1/16
		7.00	46/64	4-1/4		5-1/8
0,+12.5	8.00	51/64	4-9/16	5-1/4		
	9.00	56/64	4-3/4	5-3/4		
	10.00	60/64	4-7/8	5-9/16		
		3.00	8/64	2-0/16		3-1/8
		4.00	12/64	2-3/16		3-1/4
		5.00	15/64	2-3/8		3-1/2
		6.00	18/64	2-9/16		4-1/8
		7.00	22/64	3-1/8		4-3/16
		8.10	27/64	3-3/4		5
		9.00	31/64	4-1/2		5
	10.00	36/64	5	6		

APPENDIX B

**SRD Radiographic Inspection Report — Forward Exposures for
the USS *Clark* (FFG 11), Inspection Date: 6/11/90**

STARBOARD

PORT

FORWARD STARBOARD
EXPOSURES

FORWARD PORT
EXPOSURES

Keel bands

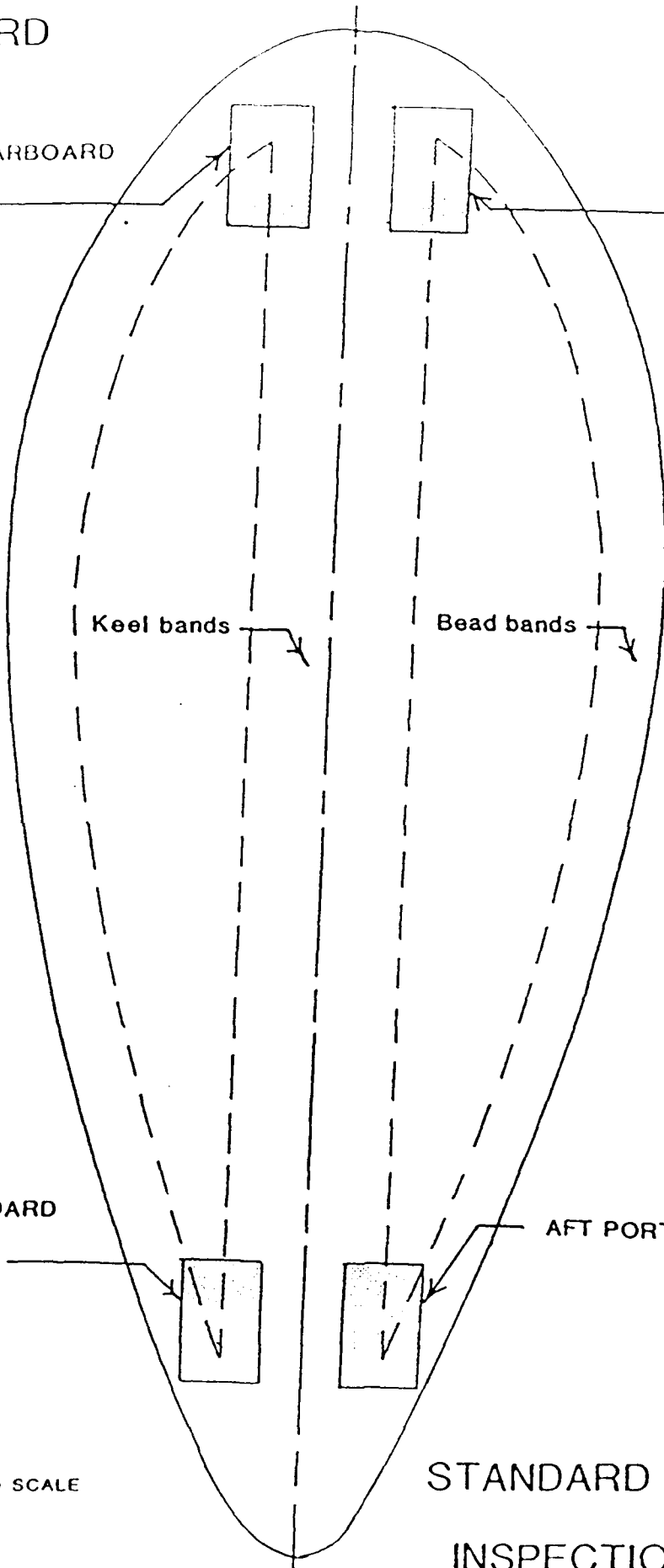
Bead bands

AFT STARBOARD
EXPOSURES

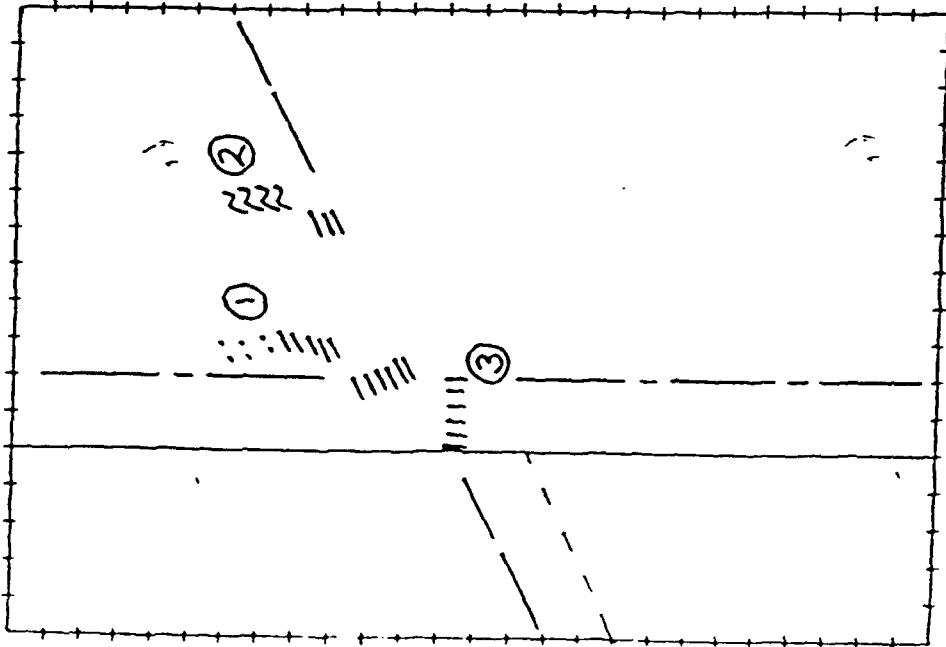
AFT PORT EXPOSURES

NOT TO SCALE

STANDARD KEEL DOME
INSPECTION AREAS

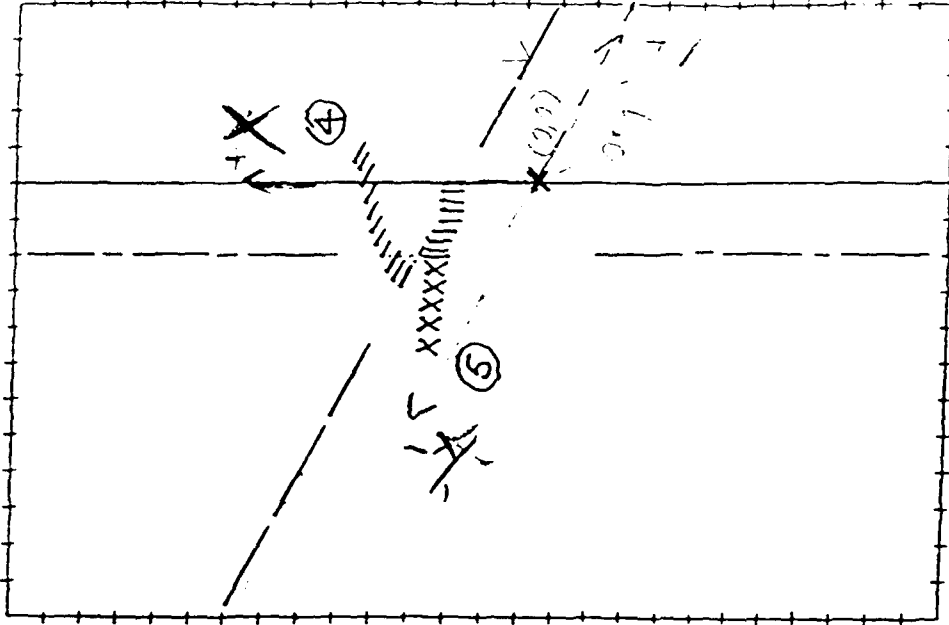


STARBOARD



FORWARD

PORT



INSPECTION DATE: 6-11-90 YARD: BOSTON

SHIP: CLARK HULL: FFG 11

S/N: A008 FWD/AFT DOME: KEEL

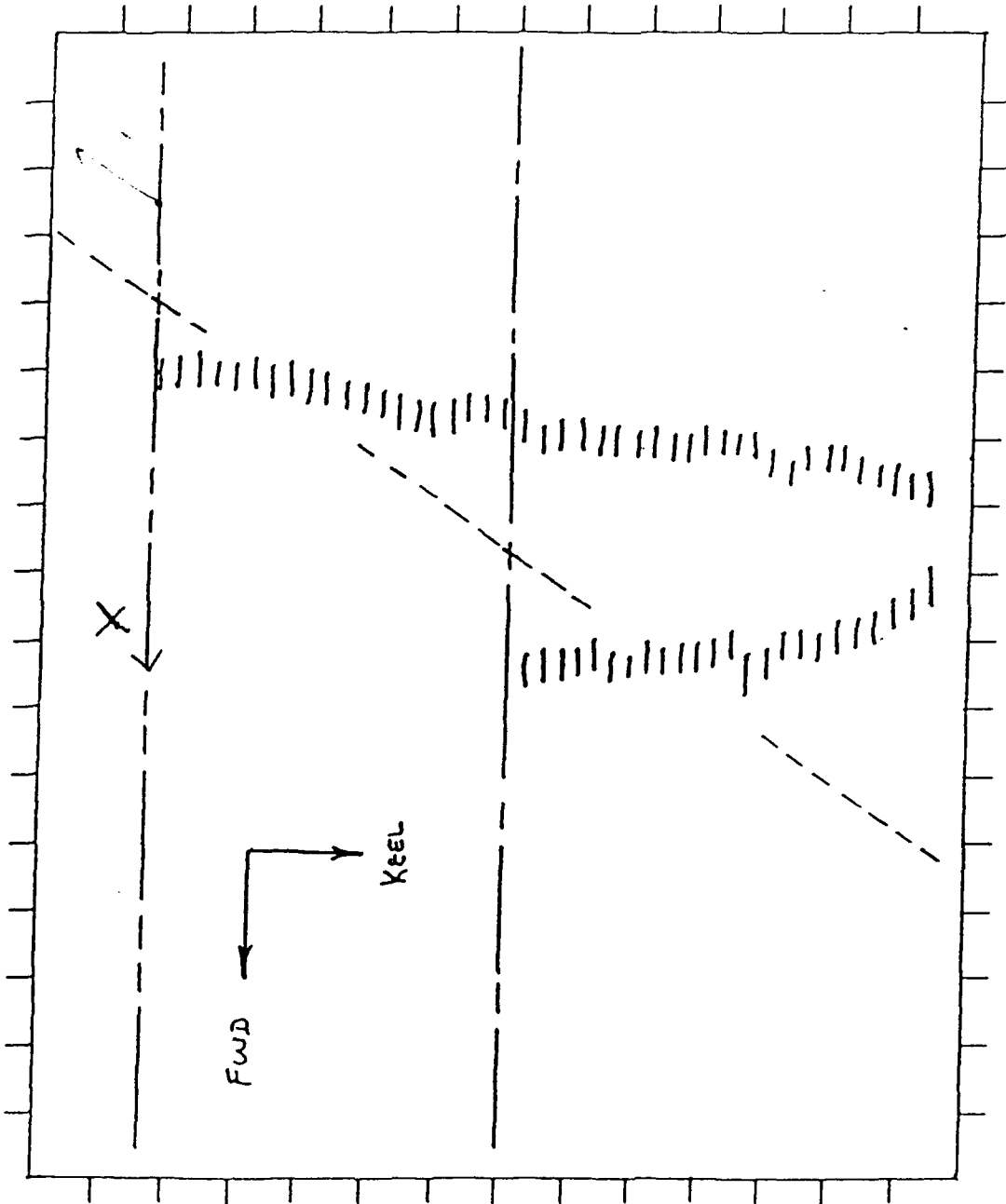
RADIOGRAPHIC INSPECTION DATA (FORWARD EXPOSURES)

Kinked cords ≈

LEGEND

- 20" keel band edge
- 24" keel band edge
- 1 ply damage
- 2 ply damage
- 1 div. = 1 inch
- 22" keel band edge
- 18" keel band edge

1287



Legend:

Damage 

20" keel band 

18" keel band 

22" bend band 

DETAIL of SITE #5

SCALE: FULL

SHIP TYPE SG NO. A008 SHIP CLARK

HULL NO. 7611

X-RAY DATE 6-11-90

LOC. BOSTON

APPENDIX F

**AN R:BASE DATABASE APPLICATION FOR AN OPTICAL DISK
DOCUMENT STORAGE AND RETRIEVAL (ODDSAR) SYSTEM**



GEO CENTERS, INC.

D - R - A - F - T

ODD

An R:BASE Database Application for an Optical Disk
Document Storage and Retrieval (ODDSAR) System

CONTENTS

1.0	INTRODUCTION	3
2.0	USER'S MANUAL	4
2.1	Database Description	4
2.2	Installation and Start-up	5
2.3	Updating the Database	6
2.4	Using the Database	7
3.0	TECHNICAL DOCUMENTATION	11
3.1	System Files	11
3.2	R:BASE Data Dictionary	12
3.3	R:BASE Form Layout	14
3.4	R:BASE Form Details	16
3.5	R:BASE Report Layout	27
3.6	R:BASE Report Details	29
3.7	R:BASE Call Tree	31
3.8	R:BASE File Cross Reference	31
3.9	R:BASE Object Cross-Reference	32
	Variables	32
	Reports	32
	Forms	32
3.10	Diagrammed Source Listing	33
3.11	Ancillary Programs	42

Appendices

- A - Index Record Report
- B - Master List Report

1.0 INTRODUCTION

This document describes an index search and query system developed to assist users of an archival optical disk document storage and retrieval system (ODDSAR). The ODDSAR system was developed by Advance Inc., a NAVSEA contractor. It is capable of scanning, storing, indexing, displaying and printing archived documents. Search capabilities, however are limited to known data field entries. Documents are retrieved by entering an identification number or other identifiers into an index form. Document index records with matching fields are then displayed. There is no subject keyword search capability. The system also is unable to generate summary reports or lists of its contents. To overcome these shortcomings, we have implemented an application of R:BASE entitled ODD. R:BASE is a relational database development system published by Microrim, Inc. Documents found using the R:BASE system can be easily retrieved by number on the ODDSAR system. In addition, listings of various index fields can be generated for all or for a subset of the archived documents.

This documentation consists of a user's manual and technical documentation. The user's manual contains a description of the ODD system and directions for installing, updating, and using it. Explanations and examples are also given for use of the basic R:BASE query commands. The user is referred to the R:BASE documentation for instruction regarding advanced use of the R:BASE command language. The user is also assumed to have a basic understanding of DOS commands. The technical documentation section includes a full description of the system files, R:BASE data structures, form and report designs, and programs.

While the ODD system is developed for use in conjunction with a specific archival data index, it can also serve as a prototype for any indexing system using an ASCII formatted data file.

2.0 USER'S MANUAL

In the following sections we will describe the ODD system and how to install and use it. We will use this convention when describing keyboard actions to be taken by the user:

Enter <ABC>

means that the user is to type the letters ABC and then press the Enter key. Do not type the < and > characters.

2.1 Database Description

ODD is an R:BASE database. The system is a collection of data files and application programs. The database files are named ODD1.RBF, ODD2.RBF, and ODD3.RBF. These three files contain the data structure or schema, the data, and pre-sorted indices to key fields, respectively. R:BASE data is organized into collections called tables. A table consists of columns and rows. The rows correspond to records and the columns are attributes or fields within each record. The ODD database contains three tables. Only one, named MASTER, contains document data. Each row in the MASTER table represents one document in the ODDSAR system and contains the indexing data transferred from that system. The other tables in ODD are named FORMS and REPORTS and contain formatting data used by R:BASE for displaying screens and printed reports. Figure 1 illustrates the database structure.

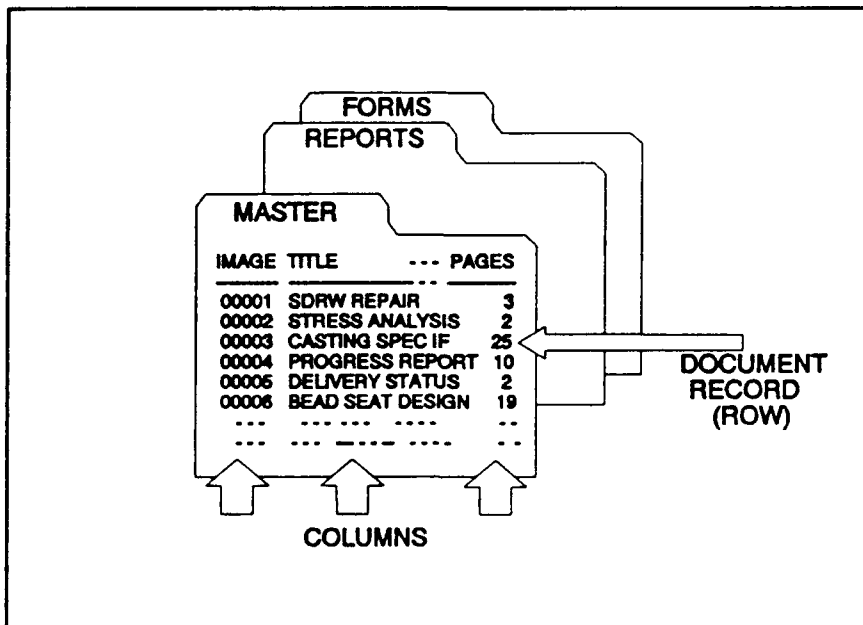


Figure 1. Database tables.

Columns in the MASTER table are named after the corresponding attributes in the ODDSAR system's database. A listing of the 30 columns is contained in section 3.1, the Data Dictionary. The meaning and significance of each column will not be discussed here, except to say that they are the same as specified in the ODDSAR system. A few key columns, however, are important to understanding and using the ODD system: The IMAGE column contains the unique document identification number. This is the most certain unique attribute to use for document retrieval. The PLATTER column contains the identification number of the optical disk which contains the document. This is useful because the ODDSAR system will search the default platter before determining that the file is not present. The TITLE is the document title, the best field to search for an indication of document content. The SORTDATE column is generated from the DOC_DATE column, when the system is updated. The difference is that SORTDATE is an R:BASE date data type. As such, it can be sorted as a date. DOC_DATE is the actual text entered into the field on the ODDSAR system index record. DOC_DATE is displayed or printed in forms and reports. SORTDATE should be used in commands requiring sorting on the date.

The R:BASE application program ODD.APX is automatically called by the startup file R:BASE.DAT when the R:BASE command is executed. This program provides a menu-based user interface. The most often needed operations are available via menu selections, although the full capability of the R:BASE language is available from the R:BASE command line prompt. In addition, for less frequent users, prompts for interactive execution of frequently used commands are available from the menu.

2.2 Installation and Start-up

The ODD database is designed to run on a Zenith Z-248 computer (PC-AT compatible) with a hard disk drive and Hewlett-Packard Laserjet Series II printer or equivalent. R:BASE for DOS system files must be installed as described in the R:BASE documentation. The directory containing the R:BASE files must be included in the DOS PATH, usually defined by a PATH statement in the AUTOEXEC.BAT file. A directory, C:\ODD, must also be created for the ODD files. As a minimum, 5 files must be present to run the system: The three database files, ODD1.RBF, ODD2.RBF, ODD3.RBF, the application program file ODD.APX, and startup file RBASE.DAT. Other files are necessary for full capability including updating the database and printing reports. See SYSTEM FILES, under the TECHNICAL DOCUMENTATION section for a complete list of the files.

After installing R:BASE for DOS and the ODD system files, change the default directory to C:\ODD and enter the command <R:BASE -R> to start the ODD system. (The -R parameter eliminates the R:BASE logo display.) The menu shown in Figure 2 will be displayed. From this menu, press the Esc key to exit the program and return control to the operating system. From sub-menus, press the Esc key to return to the Main menu. From an R> prompt within the ODD system, enter <EXIT> to return to the DOS operating system.

Figure 2. Main Menu

2.3 Updating the Database

Before using ODD, data must be transferred from the ODDSAR system. The vendor responsible for the ODDSAR system has provided a program, NAVCVT01, for writing all document index data into an ASCII formatted, comma delimited file, MAIN.ASC, which is readable by R:BASE. Since the ODDSAR system currently resides in a different host computer than the ODD database, it is necessary to transfer the data file between computers. A program, SQUEEZE.EXE, is provided to eliminate redundant quote and space characters in the MAIN.ASC file. This program greatly reduces the size of the data file making possible a transfer via floppy disk medium. In the process, the data file is renamed to MAIN.DAT (MAIN.ASC is left unchanged). Since the MAIN.DAT file is still too large for transfer, it must be further compressed using PKZIP, a file compression utility published by PKWare. The compressed file is named MAIN.ZIP. After copying the MAIN.ZIP file to the \ODD subdirectory it must be uncompressed by entering the command <PKUNZIP MAIN>.

Start ODD by entering the command <R:BASE -R>. Select number 7, "Update Data from Btrieve Files" from the menu (Btrieve is the name of the database file format used by the ODDSAR system, a concatenation of B-tree and retrieve.) The output of a directory command is displayed to verify the existence and date of the MAIN.DAT file on drive C, and the user is prompted to enter a Y to continue or an A or B to read MAIN.DAT from a floppy drive. (Enter any other key to abort the process.) The database is then cleared of all data and new data is read from the MAIN.DAT file. Presorted indexes are generated for key fields. This is a time consuming process. A long beep will signal the end of processing. Do not interrupt processing by re-booting or powering off which could result in damage to the database. If interruption occurs by pressing a key and responding to a prompt to abort, the database should be re-initialized by repeating the "Update Data ..." Menu selection. After successfully updating the database, the large MAIN.DAT file can be deleted to reclaim the disk space.

In summary, the steps to update the database are as follows:

- A. On the ODDSAR system host computer, in the directory containing ODDSAR Btrieve files:
Enter <NAVCVT01> to generate MAIN.ASC file.
Enter <SQUEEZE> to condense MAIN.ASC to MAIN.DAT
Enter <PKZIP -U MAIN MAIN.DAT> to update the MAIN.ZIP file
(If no MAIN.ZIP is present, use <PKZIP MAIN MAIN.DAT>)
Copy MAIN.ZIP to a floppy disk
- B. On the ODD database host computer:
Make \ODD the default directory.
Copy the MAIN.ZIP file from the floppy disk to \ODD.
Enter <PKUNZIP MAIN>
- C. Start the database by entering <R:BASE -R>.
Select "Update Data from Btrieve Files" from the menu.
Wait for a long beep to signal the end of processing.
Delete MAIN.ZIP and MAIN.DAT files if free space is needed.

2.4 Using the Database

The most frequently needed functions for routine database query are available from the menu shown in Figure 2. Descriptions of the use of each of the 8 selections follow:

(1) Title Keyword Search.

The user is prompted to enter a key word or phrase. A list is displayed of the image number and title of all records where the word or phrase is found in the document title. After each page, the user is prompted to press Esc to quit, any key to continue. After the last page the user is prompted to press a key and returned to the main menu. The full index record for a document may then be viewed or printed by selecting (3) or (4) respectively, and entering the image number.

(2) Display by Title Keyword.

The user is prompted to enter a key word or phrase. The full document index screen is displayed for the first record found in which the document title contains the word or phrase. Additional records satisfying the search criteria are displayed by selecting Next or Previous from a menu bar and pressing the enter key. Alternatively, the F8 and F7 keys can be used to view the Next or Previous records, respectively. If there are many matching records, it may be more useful to use selection (1) first for information to narrow the search.

(3) Display by Image Number.

The user is prompted for an image number. The document index screen is displayed.

Figure 3. Prompt Menu

(4) Print by Image Number.

Similar to (3), but the index information is printed. An Example is shown in Appendix A.

(5) R:BASE Prompts.

A menu of several R:BASE commands is displayed as shown in Figure 3. Selection of a command results in a series of screens which prompt the user in building up a command to query the database. The user is referred to the "Using R:BASE prompt by example" section in Chapter 1 of the R:BASE for DOS User's Manual and the R:BASE command dictionary for the individual command documentation. The frequent user will find it worthwhile to learn the use of these commands and enter them directly from the keyboard as in selection (8).

(6) Print Master List.

This option prints a listing of often needed fields of all records. An example of the output format is shown in Appendix B. A subset of the data may be printed in the same format using the R:BASE PRINT command. The report name is BIGLIST. Use the PRINT prompt under selection (5), or enter the PRINT command directly. See selection (8).

(7) Update Data from Btrieve Files.

This selection is used to initialize the database or to reload all the data. Because index data on the ODDSAR system can be changed, documents deleted, etc., an update consists of a complete replacement of the data rather than simply adding new records. This process is described in detail under the section "Updating the Database", above.

(8) R>

While the most frequent data query requirements can be anticipated and provided for in the application program, ad hoc inquiries often require a more flexible capability. The R:BASE command mode, indicated by an R> prompt, provides access to the extensive R:BASE command language. We refer the user to the R:BASE documentation for the use of this language. The following examples demonstrate how to use some of these commands within the context of

the ODD system. To return to the menu from the R> prompt, enter the command <RUN MENUS>.

Example 1.

Requirement: Create a list of all documents which have the ACTIVITY identified as "B.F. Goodrich", sorted by date.

Solution: This command will display the IMAGE, TITLE, and ACTIVITY fields from all records satisfying the search criteria:

```
SELECT IMAGE TITLE=50 ACTIVITY FROM MASTER SORTED BY SORTDATE WHERE ACTIVITY CONTAINS GOODRICH
```

Note that the CONTAINS operator is used in the WHERE clause. Because B.F. Goodrich can appear in the data as BF Goodrich, B F Goodrich, or BFGoodrich, the use of an equality to select the records would result in an incomplete list (with no warning). Note also that the records are sorted by SORTDATE and not DOC_DATE. DOC_DATE is the actual text data read in from the ascii file. SORTDATE is a date field created from DOC_DATE during the update process specifically for use in sorting by date. The -50 suffix to TITLE sets the display width for the field. The default width is only 15 characters.

To print a list of these records using the same fields and format as the Master List printout, use the following command sequence:

```
COPY 16CPIX8.LJ LPT1  
OUTPUT PRINTER  
PRINT BIGLIST SORTED BY SORTDATE WHERE ACTIVITY CONTAINS GOODRICH  
OUTPUT SCREEN  
COPY RESET.LJ LPT1
```

Example 2.

Requirement: Find documents referring to nut plate repairs.

Solution: Use this command:

```
SELECT IMAGE TITLE=60 FROM MASTER WHERE TITLE CONTAINS "NUT" AND TITLE CONTAINS "REPAIR"
```

Note that two keyword/phrases are used instead of one. This is a good example of the limitation of Menu selection (1). The documents entitled "REPAIR 20 INCHES OF DAMAGED NUTPLATES ON THE SDRW" and "SDRW NUT PLATE REPAIRS" can not be found using one keyword, unless a broader net is cast and which might include unwanted documents. Note also the two spellings of nut plates. Searching for NUT picks up both with little risk of bringing in many unwanted titles. Multiple search criteria are more time consuming but less vulnerable to typographical errors in the data. Should we also list titles such as "REPLACE NUT PLATES"? Although R:BASE is capable of complex logic in multiple search criteria, it is safer in this kind of search to make several

simpler searches. However, if a broad search yields a manageable list, this might be better than too narrow a search. The compute command can be used to find out how many records satisfy your search criteria:

```
COMPUTE COUNT IMAGE IN MASTER WHERE TITLE CONTAINS NUT
```

will return the number of documents where the title contains "NUT". If there are not too many, then listing them out and visually scanning the list might be easier than trying to narrow the search.

Example 3.

Requirement: List all Naval messages dated 1990.

Solution: Enter this command:

```
SELECT IMAGE ACTIVITY TITLE-50 FROM MASTER WHERE CODE = MSG AND SORTDATE >= 1/1/90 AND SORTDATE < 1/1/91
```

Note again the use of SORTDATE for the document date.

In these examples we have used the full spelling of R:BASE keywords. In most cases the first three letters are sufficient. Example 1 would then read:

```
SEL IMAGE TITLE-50 ACTIVITY FRO MASTER SOR BY SORTDATE WHE ACTIVITY CON GOODRICH
```

Note that text to be compared must be in quotes if it contains any spaces, for example:

```
...WHE ACTIVITY CON "B F GOODRICH"
```

3.0 TECHNICAL DOCUMENTATION

This section contains lists and descriptions of the ODD system files and the R:BASE data structures, which are of interest to the user, as well as form and report generation data and program source codes of interest to programmers.

3.1 System Files

File Name	Description
ODD1.RBF	R:BASE database schema.
ODD2.RBF	R:BASE data file.
ODD3.RBF	R:BASE index file.
RBASE.DAT	R:BASE startup file. Contains R:BASE command to run ODD.APX
ODD.APX	R:BASE application program. Manages menu selections.
ODD.APP	R:BASE source code for ODD.APX
NAVCVT01.EXE	Program on ODDSAR host to create MAIN.ASC from btrieve files
NAVCVT01.C	C source code for NAVCVT01.EXE
MAIN.ASC	ASCII file created by NAVCVT01.EXE containing all the data.
MAIN.DAT	Version of MAIN.ASC created by SQUEEZE.EXE - used to update ODD data.
MAIN.ZIP	Version of MAIN.DAT created by the PKZIP compression utility - needed to transfer the data file by floppy disk.
SQUEEZE.EXE	Creates MAIN.DAT from MAIN.ASC by removing redundant characters.
SQUEEZE.PAS	Pascal source code for SQUEEZE.EXE
16CPIX8.LJ	Laserjet printer command file - used for formatting Master List report.
RESET.LJ	Laserjet printer command file to reset the printer.

3.2 R:BASE Data Dictionary

Table: MASTER

Column definitions

#	Name	Type	Length	Key
1	SYSTEM	TEXT	21 characters	yes
2	CODE	TEXT	21 characters	
3	TOPIC	TEXT	21 characters	
4	NUMBER	TEXT	21 characters	
5	DTG	TEXT	21 characters	
6	DOC_DATE	TEXT	21 characters	
7	ACTIVITY	TEXT	21 characters	
8	AUTHOR	TEXT	21 characters	
9	SERIAL	TEXT	21 characters	
10	CTRACTOR	TEXT	21 characters	
11	YEAR	TEXT	9 characters	
12	DOCUMENT	TEXT	21 characters	
13	TYPE	TEXT	21 characters	
14	AMOUNT	TEXT	13 characters	
15	MODIF	TEXT	8 characters	
16	REF	TEXT	21 characters	
17	ORIG_COD	TEXT	11 characters	
18	ORIG_DAT	TEXT	9 characters	
19	REV	TEXT	21 characters	
20	PURPOSE	NOTE		
21	COMMENTS	NOTE		
22	TITLE	NOTE		
23	ACCESS	TEXT	2 characters	
24	SCANDATE	TEXT	9 characters	
25	CONTRACT	TEXT	21 characters	
26	DRAWINGS	TEXT	1 characters	
27	IMAGE	INTEGER		yes
28	PAGES	INTEGER		
29	SORTDATE	DATE		yes
30	PLATTER	TEXT	4 characters	

Current number of rows: (approximately 8000)

Table: FORMS

Column definitions

#	Name	Type	Length	Key
1	FNAME	TEXT	8 characters	yes
2	FDATA	TEXT	46 characters	

Current number of rows: 69

Table: REPORTS

Column definitions

#	Name	Type	Length	Key
1	RNAME	TEXT	8 characters	yes
2	RDATA	TEXT	80 characters	

Current number of rows: 95

3.3 R:BASE Form Layout

Note: Space occupied by data fields in form and report layouts is indicated by brackets containing periods. Ten, five, two, and one character fields, for example, are shown as

[.....], [...], [],],

respectively.

Form: master Tables: MASTER

<< IMAGE [.....] PLATTER [..] >>

[.....]
SYSTEM: CODE: TOPIC:
[.....] [.....] [.....]
NUMBER: DTG: DATE:
[.....] [.....] [.....]
ACTIVITY: AUTHOR: SERIAL NO:
[.....] [.....] [.....]

CONTRACT: [.....] CONTRACTOR: [.....] YEAR: [.....]
DOCUMENT: [.....] TYPE: [.....] AMOUNT: [.....]

DRAWINGS?(Y/N):] MOD: [.....] REF: [.....]
ORIG CODE: [.....] ORIG DATE: [.....] REV: [.....]

PURPOSE:
[.....]

COMMENTS:
[.....]

TITLE:
[.....]
]

ACCESS LEVEL: [] PAGES: [.....] SCAN DATE:[.....]

#	Name	Location	Type	Length
1:	MASTER			
1	SYSTEM	(7, 1 - 7,21)	TEXT	21
2	CODE	(7,24 - 7,44)	TEXT	21
3	TOPIC	(7,50 - 7,70)	TEXT	21
4	NUMBER	(9, 1 - 9,21)	TEXT	21
5	DTG	(9,24 - 9,44)	TEXT	21
6	DOC_DATE	(9,50 - 9,70)	TEXT	21
7	ACTIVITY	(11, 1 - 11,21)	TEXT	21
8	AUTHOR	(11,24 - 11,44)	TEXT	21
9	SERIAL	(11,50 - 11,70)	TEXT	21
10	CTRACTOR	(13,44 - 13,64)	TEXT	21
11	YEAR	(13,71 - 13,79)	TEXT	9

12	DOCUMENT	(14,11 - 14,31)	TEXT	21
13	TYPE	(14,37 - 14,57)	TEXT	21
14	AMOUNT	(14,67 - 14,79)	TEXT	13
15	MODIF	(16,40 - 16,47)	TEXT	8
16	REF	(16,56 - 16,76)	TEXT	21
17	ORIG_COD	(17,12 - 17,22)	TEXT	11
18	ORIG_DAT	(17,40 - 17,48)	TEXT	9
19	REV	(17,56 - 17,76)	TEXT	21
20	TITLE	(21, 1 - 21,79)	NOTE	79
21	ACCESS	(22,15 - 22,16)	TEXT	2
22	SCANDATE	(22,71 - 22,79)	TEXT	9
23	CONTRACT	(13,11 - 13,31)	TEXT	21
24	DRAWINGS	(16,17 - 16,17)	TEXT	1
25	IMAGE	(3,30 - 3,36)	INTEGER	7
26	PLATTER	(3,47 - 3,50)	TEXT	4
27	PAGES	(22,33 - 22,42)	INTEGER	10
28	PURPOSE	(18,11 - 18,79)	NOTE	69
29	COMMENTS	(19,11 - 19,79)	NOTE	69
30	TITLE	(5, 1 - 5,78)	NOTE	78

3.4 R:BASE Form Details

Form Characteristics

Primary Table Name : MASTER
Dependent Tables : NONE
Number of Screens : 1
Read Password : NONE
Modify Password : NONE
Clear Screen Before : YES
Clear Screen After : YES
Status Line : YES
Colors : DEFAULT
Use with ENTER : NO
ENTER Prompt Line : N/A
ENTER Options : N/A
Use with EDIT : YES
EDIT Prompt Line : Document Index Screen
EDIT Options : Next Previous Quit

Table Characteristics

Table Number : 1 of 1
Columns/Variables : 30
Expressions : 0
Add New Rows : NO
Replace Rows : NO
Automatic Replace : N/A
Delete Rows : NO
Restrict Delete : N/A
Many Side of 1:Many : N/A
Region Defined : NO

Field Characteristics for: SYSTEM

Location : (7, 1 - 7,21)
Length : 21
Lines : 1
Data Type : TEXT 21
Storage Type : COLUMN
Allow Enter : NO
Allow Edit : NO
Restrict Changes : N/A
Display Default : NO
Default Value : N/A
Colors : DEFAULT

Field Characteristics for: CODE

Location : (7,24 - 7,44)
Length : 21
Lines : 1
Data Type : TEXT 21
Storage Type : COLUMN
Allow Enter : NO
Allow Edit : NO
Restrict Changes : N/A
Display Default : NO
Default Value : N/A
Colors : DEFAULT

Field Characteristics for: TOPIC

Location : (7,50 - 7,70)
Length : 21
Lines : 1
Data Type : TEXT 21
Storage Type : COLUMN
Allow Enter : NO
Allow Edit : NO
Restrict Changes : N/A
Display Default : NO
Default Value : N/A
Colors : DEFAULT

Field Characteristics for: NUMBER

Location : (9, 1 - 9,21)
Length : 21
Lines : 1
Data Type : TEXT 21
Storage Type : COLUMN
Allow Enter : NO
Allow Edit : NO
Restrict Changes : N/A
Display Default : NO
Default Value : N/A
Colors : DEFAULT

Field Characteristics for: DTG

Location : (9,24 - 9,44)
Length : 21
Lines : 1
Data Type : TEXT 21
Storage Type : COLUMN
Allow Enter : NO
Allow Edit : NO
Restrict Changes : N/A
Display Default : NO
Default Value : N/A
Colors : DEFAULT

Field Characteristics for: DOC_DATE

Location : (9,50 - 9,70)
Length : 21
Lines : 1
Data Type : TEXT 21
Storage Type : COLUMN
Allow Enter : NO
Allow Edit : NO
Restrict Changes : N/A
Display Default : NO
Default Value : N/A
Colors : DEFAULT

Field Characteristics for: ACTIVITY

Location : (11, 1 - 11,21)
Length : 21
Lines : 1
Data Type : TEXT 21
Storage Type : COLUMN
Allow Enter : NO
Allow Edit : NO
Restrict Changes : N/A
Display Default : NO
Default Value : N/A
Colors : DEFAULT

Field Characteristics for: AUTHOR

Location : (11,24 - 11,44)
Length : 21
Lines : 1
Data Type : TEXT 21
Storage Type : COLUMN
Allow Enter : NO
Allow Edit : NO
Restrict Changes : N/A
Display Default : NO
Default Value : N/A
Colors : DEFAULT

Field Characteristics for: SERIAL

Location : (11,50 - 11,70)
Length : 21
Lines : 1
Data Type : TEXT 21
Storage Type : COLUMN
Allow Enter : NO
Allow Edit : NO
Restrict Changes : N/A
Display Default : NO
Default Value : N/A
Colors : DEFAULT

Field Characteristics for: CTRACTOR

Location : (13,44 - 13,64)
Length : 21
Lines : 1
Data Type : TEXT 21
Storage Type : COLUMN
Allow Enter : NO
Allow Edit : NO
Restrict Changes : N/A
Display Default : NO
Default Value : N/A
Colors : DEFAULT

Field Characteristics for: YEAR

Location : (13,71 - 13,79)
Length : 9
Lines : 1
Data Type : TEXT 9
Storage Type : COLUMN
Allow Enter : NO
Allow Edit : NO
Restrict Changes : N/A
Display Default : NO
Default Value : N/A
Colors : DEFAULT

Field Characteristics for: DOCUMENT

Location : (14,11 - 14,31)
Length : 21
Lines : 1
Data Type : TEXT 21
Storage Type : COLUMN
Allow Enter : NO
Allow Edit : NO
Restrict Changes : N/A
Display Default : NO
Default Value : N/A
Colors : DEFAULT

Field Characteristics for: TYPE

Location : (14,37 - 14,57)
Length : 21
Lines : 1
Data Type : TEXT 21
Storage Type : COLUMN
Allow Enter : NO
Allow Edit : NO
Restrict Changes : N/A
Display Default : NO
Default Value : N/A
Colors : DEFAULT

Field Characteristics for: AMOUNT

Location : (14,67 - 14,79)
Length : 13
Lines : 1
Data Type : TEXT 13
Storage Type : COLUMN
Allow Enter : NO
Allow Edit : NO
Restrict Changes : N/A
Display Default : NO
Default Value : N/A
Colors : DEFAULT

Field Characteristics for: MODIF

Location : (16,40 - 16,47)
Length : 8
Lines : 1
Data Type : TEXT 8
Storage Type : COLUMN
Allow Enter : NO
Allow Edit : NO
Restrict Changes : N/A
Display Default : NO
Default Value : N/A
Colors : DEFAULT

Field Characteristics for: REF

Location : (16,56 - 16,76)
Length : 21
Lines : 1
Data Type : TEXT 21
Storage Type : COLUMN
Allow Enter : NO
Allow Edit : NO
Restrict Changes : N/A
Display Default : NO
Default Value : N/A
Colors : DEFAULT

Field Characteristics for: ORIG_COD

Location : (17,12 - 17,22)
Length : 11
Lines : 1
Data Type : TEXT 11
Storage Type : COLUMN
Allow Enter : NO
Allow Edit : NO
Restrict Changes : N/A
Display Default : NO
Default Value : N/A
Colors : DEFAULT

Field Characteristics for: ORIG_DAT

Location : (17,40 - 17,48)
Length : 9
Lines : 1
Data Type : TEXT 9
Storage Type : COLUMN
Allow Enter : NO
Allow Edit : NO
Restrict Changes : N/A
Display Default : NO
Default Value : N/A
Colors : DEFAULT

Field Characteristics for: REV

Location : (17,56 - 17,76)
Length : 21
Lines : 1
Data Type : TEXT 21
Storage Type : COLUMN
Allow Enter : NO
Allow Edit : NO
Restrict Changes : N/A
Display Default : NO
Default Value : N/A
Colors : DEFAULT

Field Characteristics for: TITLE

Location : (21, 1 - 21,79)
Length : 79
Lines : 1
Data Type : NOTE
Storage Type : COLUMN
Allow Enter : NO
Allow Edit : NO
Restrict Changes : N/A
Display Default : NO
Default Value : N/A
Colors : DEFAULT

Field Characteristics for: ACCESS

Location : (22,15 - 22,16)
Length : 2
Lines : 1
Data Type : TEXT 2
Storage Type : COLUMN
Allow Enter : NO
Allow Edit : NO
Restrict Changes : N/A
Display Default : NO
Default Value : N/A
Colors : DEFAULT

Field Characteristics for: SCANDATE

Location : (22,71 - 22,79)
Length : 9
Lines : 1
Data Type : TEXT 9
Storage Type : COLUMN
Allow Enter : NO
Allow Edit : NO
Restrict Changes : N/A
Display Default : NO
Default Value : N/A
Colors : DEFAULT

Field Characteristics for: CONTRACT

Location : (13,11 - 13,31)
Length : 21
Lines : 1
Data Type : TEXT 21
Storage Type : COLUMN
Allow Enter : NO
Allow Edit : NO
Restrict Changes : N/A
Display Default : NO
Default Value : N/A
Colors : DEFAULT

Field Characteristics for: DRAWINGS

Location : (16,17 - 16,17)
Length : 1
Lines : 1
Data Type : TEXT 1
Storage Type : COLUMN
Allow Enter : NO
Allow Edit : NO
Restrict Changes : N/A
Display Default : NO
Default Value : N/A
Colors : DEFAULT

Field Characteristics for: IMAGE

Location : (3,30 - 3,36)
Length : 7
Lines : 1
Data Type : INTEGER
Storage Type : COLUMN
Allow Enter : NO
Allow Edit : NO
Restrict Changes : N/A
Display Default : NO
Default Value : N/A
Colors : BLACK on WHITE

Field Characteristics for: PLATTER

Location : (3,47 - 3,50)
Length : 4
Lines : 1
Data Type : TEXT 4
Storage Type : COLUMN
Allow Enter : NO
Allow Edit : NO
Restrict Changes : N/A
Display Default : NO
Default Value : N/A
Colors : BLACK on WHITE

Field Characteristics for: PAGES

Location : (22,33 - 22,42)
Length : 10
Lines : 1
Data Type : INTEGER
Storage Type : COLUMN
Allow Enter : YES
Allow Edit : YES
Restrict Changes : YES
Display Default : NO
Default Value : N/A
Colors : DEFAULT

Field Characteristics for: PURPOSE

Location : (18,11 - 18,79)
Length : 69
Lines : 1
Data Type : NOTE
Storage Type : COLUMN
Allow Enter : YES
Allow Edit : YES
Restrict Changes : YES
Display Default : NO
Default Value : N/A
Colors : DEFAULT

Field Characteristics for: COMMENTS

Location : (19,11 - 19,79)
Length : 69
Lines : 1
Data Type : NOTE
Storage Type : COLUMN
Allow Enter : YES
Allow Edit : YES
Restrict Changes : YES
Display Default : NO
Default Value : N/A
Colors : DEFAULT

Field Characteristics for: TITLE

Location : (5, 1 - 5,78)
Length : 78
Lines : 1
Data Type : NOTE
Storage Type : COLUMN
Allow Enter : NO
Allow Edit : NO
Restrict Changes : N/A
Display Default : NO
Default Value : N/A
Colors : BLACK on WHITE

5.5 R:BASE Report Layout

Report: IMAGE Table: MASTER

See Appendix A for visual layout - too wide for this format.

#	Name	Section	Location	Type	Length
1	IMAGE	D	(2, 15 - 2, 24)	INTEGER	10
2	PLATTER	D	(2, 41 - 2, 44)	TEXT	4
3	VDATE	D	(2, 62 - 2, 69)	DATE	8
4	TITLE	D	(3, 10 - 4, 77)	NOTE	2x68
5	SYSTEM	D	(7, 15 - 7, 35)	TEXT	21
6	CODE	D	(9, 15 - 9, 35)	TEXT	21
7	TOPIC	D	(11, 15 - 11, 35)	TEXT	21
8	NUMBER	D	(13, 15 - 13, 35)	TEXT	21
9	DTG	D	(15, 15 - 15, 35)	TEXT	21
10	DOC_DATE	D	(17, 15 - 17, 35)	TEXT	21
11	ACTIVITY	D	(19, 15 - 19, 35)	TEXT	21
12	AUTHOR	D	(21, 15 - 21, 35)	TEXT	21
13	SERIAL	D	(23, 15 - 23, 35)	TEXT	21
14	CONTRACT	D	(25, 15 - 25, 35)	TEXT	21
15	CTRACTOR	D	(27, 15 - 27, 35)	TEXT	21
16	YEAR	D	(29, 15 - 29, 23)	TEXT	9
17	DOCUMENT	D	(31, 15 - 31, 35)	TEXT	21
18	TYPE	D	(33, 15 - 33, 35)	TEXT	21
19	AMOUNT	D	(35, 15 - 35, 27)	TEXT	13
20	DRAWINGS	D	(37, 15 - 37, 15)	TEXT	1
21	MODIF	D	(39, 15 - 39, 22)	TEXT	8
22	REF	D	(41, 15 - 41, 35)	TEXT	21
23	ORIG_COD	D	(43, 15 - 43, 25)	TEXT	11
24	ORIG_DAT	D	(45, 15 - 45, 23)	TEXT	9
25	REV	D	(47, 15 - 47, 35)	TEXT	21
26	PURPOSE	D	(49, 12 - 50, 77)	NOTE	2x66
27	COMMENTS	D	(51, 13 - 52, 77)	NOTE	2x65
28	TITLE	D	(53, 10 - 54, 77)	NOTE	2x68
29	ACCESS	D	(55, 17 - 55, 18)	TEXT	2
30	IMAGE	D	(55, 31 - 55, 40)	INTEGER	10
31	SCANDATE	D	(55, 56 - 55, 64)	TEXT	9

Report: BIGLIST Table/View: MASTER

Note: See Appendix B for an example of this report. It is in a wide format for landscape printing.

#	Name	Section	Location	Type	Length
1	SYSTEM	D	(4, 4 - 4, 12)	TEXT	9
2	CODE	D	(4, 14 - *, 24)	TEXT	*x11
3	NUMBER	D	(4, 26 - *, 40)	TEXT	*x15
4	DOC_DATE	D	(4, 42 - 4, 49)	TEXT	8
5	ACTIVITY	D	(4, 51 - *, 62)	TEXT	*x12
6	TITLE	D	(4, 64 - *, 136)	NOTE	*x73
7	TOPIC	D	(4, 138 - *, 151)	TEXT	*x14
8	PLATTER	D	(4, 153 - 4, 156)	TEXT	4
9	IMAGE	D	(4, 158 - 4, 164)	INTEGER	7
10	PAGES	D	(4, 166 - 4, 170)	INTEGER	5
11	VDATE	PF	(5, 155 - 5, 162)	DATE	8
12	VPAGE	PF	(5, 170 - 5, 174)	INTEGER	5
13	VTOTAL	RF	(9, 161 - 9, 170)	INTEGER	10

3.6 R:BASE Report Details

Report: IMAGE Table/View: MASTER

Configuration	Form Feeds
-----	-----
Lines Per Page : 60	Before RH: NO
Remove Initial CR : NO	After RH : NO
Manual Break Reset : NO	Before RF: NO
Clear Vars After Printing: YES	After RF : YES
Page Footer Line Number : 0	

Located Fields (Columns and Variables):

Name	Section	Type	Var/Col	Location
-----	-----	-----	-----	-----
IMAGE	D	INTEGER	COLUMN	(2, 15 - 2, 24)
PLATTER	D	TEXT	COLUMN	(2, 41 - 2, 44)
VDATE	D	DATE	VARIABLE	(2, 62 - 2, 69)
TITLE	D	NOTE	COLUMN	(3, 10 - 4, 77)
SYSTEM	D	TEXT	COLUMN	(7, 15 - 7, 35)
CODE	D	TEXT	COLUMN	(9, 15 - 9, 35)
TOPIC	D	TEXT	COLUMN	(11, 15 - 11, 35)
NUMBER	D	TEXT	COLUMN	(13, 15 - 13, 35)
DTG	D	TEXT	COLUMN	(15, 15 - 15, 35)
DOC_DATE	D	TEXT	COLUMN	(17, 15 - 17, 35)
ACTIVITY	D	TEXT	COLUMN	(19, 15 - 19, 35)
AUTHOR	D	TEXT	COLUMN	(21, 15 - 21, 35)
SERIAL	D	TEXT	COLUMN	(23, 15 - 23, 35)
CONTRACT	D	TEXT	COLUMN	(25, 15 - 25, 35)
CTRACTOR	D	TEXT	COLUMN	(27, 15 - 27, 35)
YEAR	D	TEXT	COLUMN	(29, 15 - 29, 23)
DOCUMENT	D	TEXT	COLUMN	(31, 15 - 31, 35)
TYPE	D	TEXT	COLUMN	(33, 15 - 33, 35)
AMOUNT	D	TEXT	COLUMN	(35, 15 - 35, 27)
DRAWINGS	D	TEXT	COLUMN	(37, 15 - 37, 15)
MODIF	D	TEXT	COLUMN	(39, 15 - 39, 22)
REF	D	TEXT	COLUMN	(41, 15 - 41, 35)
ORIG_COD	D	TEXT	COLUMN	(43, 15 - 43, 25)
ORIG_DAT	D	TEXT	COLUMN	(45, 15 - 45, 23)
REV	D	TEXT	COLUMN	(47, 15 - 47, 35)
PURPOSE	D	NOTE	COLUMN	(49, 12 - 50, 77)
COMMENTS	D	NOTE	COLUMN	(51, 13 - 52, 77)
TITLE	D	NOTE	COLUMN	(53, 10 - 54, 77)
ACCESS	D	TEXT	COLUMN	(55, 17 - 55, 18)
IMAGE	D	INTEGER	COLUMN	(55, 31 - 55, 40)
SCANDATE	D	TEXT	COLUMN	(55, 56 - 55, 64)

Expressions:

Name	Type	Var/Col	Expression
-----	-----	-----	-----

VDATE DATE VARIABLE .#DATE

Report: BIGLIST Table/View: MASTER

Configuration		Form Feeds
Lines Per Page	: 59	Before RH: NO
Remove Initial CR	: YES	After RH : NO
Manual Break Reset	: NO	Before RF: NO
Clear Vars After Printing:	YES	After RF : NO
Page Footer Line Number	: 0	

Located Fields (Columns and Variables):

Name	Section	Type	Var/Col	Location
SYSTEM	D	TEXT	COLUMN	(4, 4 - 4, 12)
CODE	D	TEXT	COLUMN	(4, 14 - *, 24)
NUMBER	D	TEXT	COLUMN	(4, 26 - *, 40)
DOC_DATE	D	TEXT	COLUMN	(4, 42 - 4, 49)
ACTIVITY	D	TEXT	COLUMN	(4, 51 - *, 62)
TITLE	D	NOTE	COLUMN	(4, 64 - *,136)
TOPIC	D	TEXT	COLUMN	(4,138 - *,151)
PLATTER	D	TEXT	COLUMN	(4,153 - 4,156)
IMAGE	D	INTEGER	COLUMN	(4,158 - 4,164)
PAGES	D	INTEGER	COLUMN	(4,166 - 4,170)
VDATE	PF	DATE	VARIABLE	(5,155 - 5,162)
VPAGE	PF	INTEGER	VARIABLE	(5,170 - 5,174)
VTOTAL	RF	INTEGER	VARIABLE	(9,161 - 9,170)

Expressions:

Name	Type	Var/Col	Expression
VDATE	DATE	VARIABLE	.#DATE
VTIME	TIME	VARIABLE	.#TIME
VPAGE	INTEGER	VARIABLE	.#PAGE
VTOTAL	INTEGER	VARIABLE	SUM OF PAGES

3.7 R:BASE Call Tree

Calling

Line

Number Called File

```
-----  
  0      RUN ODD IN ODD.APX  
 30      RUN SELKEY  IN ODD.Apx  
 34      RUN FINDKEY  IN ODD.Apx  
 38      RUN FINDIMG  IN ODD.Apx  
 42      RUN PRINTIMG IN ODD.APX  
 84      RUN LONGLIST IN ODD.APX  
 87      RUN UPDATE   IN ODD.Apx  
200      RUN DEFTAB  IN ODD.APX  
 91      RUN CMDMODE  IN ODD.Apx  
 97      EXIT
```

3.8 R:BASE File Cross Reference

Called Block

or File Name

In File

Cmd

Calling File

Line Numbers

```
-----  
.VFILE          LOA  ODD.Apx      202  
16CPIX8.LJ     COP  ODD.APX      67 308  
CMDMODE        ODD.Apx  RUN  ODD.APX      91  
DEFTAB         ODD.APX  RUN  ODD.Apx     200  
FINDIMG        ODD.Apx  RUN  ODD.APX      38  
FINDKEY        ODD.Apx  RUN  ODD.APX      34  
LONGLIST       ODD.APX  RUN  ODD.APX      84  
LPT1           COP  ODD.APX     67 69 308 313  
Main           ODD.Apx  CHO  ODD.APX      25  
ODD            OPE  ODD.APX      16  
PRINTIMG       ODD.APX  RUN  ODD.APX     42  
PROMPT         ODD.Apx  CHO  ODD.APX      51  
RESET.LJ       COP  ODD.APX     69 313  
SELKEY         ODD.Apx  RUN  ODD.APX      30  
UPDATE         ODD.Apx  RUN  ODD.APX     87
```

3.9 R:BASE Object Cross-Reference

Variables

Name	Block	Line Numbers Where Referenced
EV	FINDIMG	151
EV	FINDKEY	125
EV	ODD	18
EV	PRINTIMG	166
EV	SELKEY	138
LEVEL2	ODD	47 48 49 79
PICK1	ODD	22 25 26 29 33 37 41 45 83 86 90 96
PICK2	ODD	46 51 52 55 59 64 65 74 80
Q	UPDATE	177 178 187 189 195 196. 219
VFILE	UPDATE	193 194 196 196. 202.
VIMG	FINDIMG	149 150. 155
VIMG	PRINTIMG	163 165. 172
VTAB	UPDATE	209
VWORD	FINDKEY	120 123 124.
VWORD	SELKEY	133 136 137.

Reports

Name	Block	Line Numbers Where Referenced
BIGLIST	LONGLIST	311
IMAGE	PRINTIMG	165

Forms

Name	Block	Line Numbers Where Referenced
MASTER	FINDIMG	150
MASTER	FINDKEY	124

3.10 Diagrammed Source Listing - ODD.APP

COMMAND: ODD

```
1  $COMMAND
2  ODD
3  SET QUOTES=NULL
4  SET QUOTES="
5  SET DELIMIT=NULL
6  SET DELIMIT=","
7  SET SEMI=NULL
8  SET SEMI=";"
9  SET PLUS=NULL
10 SET PLUS="+
11 SET SINGLE=NULL
12 SET SINGLE="?"
13 SET MANY=NULL
14 SET MANY="*"
15 SET MESSAGE OFF
16 OPEN ODD
17 SET ERROR MESSAGE OFF
18 SET ERR VAR EV
19 SET COLOR BACKGRND BLACK
20 SET COLOR FOREGRND WHITE
21 SET BELL OFF
22 SET VAR PICK1 INT
23 > LABEL STARTAPP
24 CLS
25 CHOOSE PICK1 FROM Main IN ODD.Apx
26 - IF PICK1 EQ 0 THEN
27 <   GOTO ENDAPP
28 - ENDIF
29 - IF PICK1 EQ 1 THEN
30 :   RUN SELKEY IN ODD.Apx
31 <   GOTO STARTAPP
32 - ENDIF
33 - IF PICK1 EQ 2 THEN
34 :   RUN FINDKEY IN ODD.Apx
35 <   GOTO STARTAPP
36 - ENDIF
37 - IF PICK1 EQ 3 THEN
38 :   RUN FINDIMG IN ODD.Apx
39 <   GOTO STARTAPP
40 - ENDIF
41 - IF PICK1 EQ 4 THEN
42 :   RUN PRINTIMG IN ODD.APX
43 <   GOTO STARTAPP
44 - ENDIF
45 - IF PICK1 EQ 5 THEN
46 :   SET VAR PICK2 TEXT
47 :   SET VAR LEVEL2 INT
```

```

48 :   SET VAR LEVEL2 TO 0
49 : - WHILE LEVEL2 EQ 0 THEN
50 : |   CLS
51 : |   CHOOSE PICK2 FROM PROMPT IN ODD.Apx
52 : | - IF PICK2 EQ "ESC" THEN
53 : # :   BREAK
54 : | - ENDIF
55 : | - IF PICK2 EQ "Edit" THEN
56 : | :   CLS
56 : | :   SET NULL " "
57 : | :   PROMPT EDIT
58 : | - ENDI
59 : | - IF PICK2 EQ "Select" THEN
60 : | :   CLS
60 : | :   SET NULL " "
61 : | :   PROMPT SELECT
62 : | :   WRI "Press a key.";
62 : | :   PAU
62 : | :   SET NULL -0-
63 : | - ENDIF
64 : | - IF PICK2 EQ "Browse" THEN
64 : | :   PROMPT BRO
64 : | - ENDI
65 : | - IF PICK2 EQ "Print" THEN
66 : | :   SET NULL " "
67 : | :   COPY 16CPIX8.LJ LPT1
68 : | :   PROMPT PRINT
69 : | :   COPY RESET.LJ LPT1
70 : | :   SET NULL -0-
71 : | :   BEEP
72 : | :   BEEP
73 : | - ENDI
74 : | - IF PICK2 EQ "Other" THEN
75 : | :   PROMPT
76 : | :   WRI "Press a key.";
76 : | :   PAU
77 : | - ENDI
78 : - ENDWHILE
79 :   CLEAR LEVEL2
80 :   CLEAR PICK2
81 < GOTO STARTAPP
82 - ENDIF
83 - IF PICK1 EQ 6 THEN
84 :   RUN LONGLIST IN ODD.APX
85 - ENDIF
86 - IF PICK1 EQ 7 THEN
87 :   RUN update   IN ODD.Apx
88 < GOTO STARTAPP
89 - ENDIF
90 - IF PICK1 EQ 8 THEN
91 :   RUN CMDMODE  IN ODD.Apx
92 < GOTO STARTAPP

```

```
93 - ENDIF
94 < GOTO STARTAPP
95 > LABEL ENDAPP
96 CLEAR PICK1
97 ^ EXIT
98
```

MENU: Main

99 \$MENU
100 Main
101 COLUMN Document Index Database
102 Title Keyword Search
103 Display by Title Keyword
104 Display by Image Number
105 Print by Image Number
106 R:BASE Prompts
107 Print Master List
108 Update Data from Btrieve Files
109 R>

MENU: Prompt

110 \$MENU
111 Prompt
112 ROW Rbase Command Prompts
113 Edit
114 Select
115 Print
116 Browse
117 Other

COMMAND: FINDKEY

118 \$COMMAND
119 FINDKEY
120 SET V VWORD TEXT
121 CLS
122 SET NULL " "
123 FILL VWORD USI "Key word or phrase: "
124 EDIT USI MASTER WHE TITLE CON .VWORD
125 - IF EV NE 0 THEN
126 : WRI "No match found. Press a key."
127 : PAU
128 - ENDI
129 SET NULL -0-
130

COMMAND: SELKEY

```
131 $COMMAND
132 SELKEY
133 SET V VWORD TEXT
134 CLS
135 SET NULL " "
136 FILL VWORD USI "Key word or phrase: "
137 SEL IMAGE TITLE=65 FRO MASTER WHE TITLE CON .VWORD ORD BY IMAGE
138 - IF EV NE 0 THEN
139 :   WRI "No match found."
140 - ENDI
141 WRI "Press a key.";
141 PAU
142 SET NULL -0-
143
```

COMMAND: FINDIMG

```
144 $COMMAND
145 FINDIMG
146 SET VIMG INT
147 SET NULL " "
148 CLS
149 FILL VIMG USI "Image number: "
150 EDI USI MASTER WHE IMAGE - .VIMG
151 - IF EV NE 0 THEN
152 :   WRI "Not found. Press a key."
153 :   PAU
154 - ENDI
155 CLE VIMG
156 SET NULL -0-
157
```

COMMAND: PRINTIMG

```
158 $COMMAND
159 PRINTIMG
160 SET VIMG INT
161 SET NULL " "
162 CLS
163 FILL VIMG USI "Image number: "
164 OUT PRI
165 PRINT IMAGE WHE IMAGE - .VIMG
166 - IF EV NE 0 THEN
167 :   OUT SCR
168 :   WRI "Not found. Press a key."
169 :   PAU
170 - ENDI
171 OUT SCR
172 CLE VIMG
```

```
173 SET NULL -0-
174
```

```
-----
| COMMAND: UPDATE |
-----
```

```
175 $COMMAND
176 UPDATE
177 CLE Q
178 SET V Q TEXT
179 CLS
180 WRI " "
181 WRI "This selection deletes all data and loads update
182 WRI "from a disk file named MAIN.DAT."
183 WRI "An updated MAIN.DAT file must be present."
184 WRI " "
185 WRI "Checking..."
186 DIR MAIN.DAT
187 FIL Q=0 USI +
188 "Enter Y to continue, N to cancel, or drive letter for MAIN.DAT: "
189 - IF Q = "Y" OR Q = "A" OR Q = "B" THEN
190 : CLS
191 : SET MESS ON
192 : SET ERR MESS ON
193 : SET V VFILE TEXT
194 : SET V VFILE = "MAIN.DAT"
195 : - IF Q EQ "A" OR Q EQ "B" THEN
196 : : SET V VFILE = (.Q + ":\\" + .VFILE)
197 : - ENDI
198 : REM TAB MASTER
199 : PACK
200 : RUN DEFTAB IN ODD.APX
201 : SET QUOTES-^
202 : LOAD MASTER FROM .VFILE AS ASCII
203 : SET QUOTES-"
204 : RED SORTDATE TO DATE IN MASTER
205 : BUI KEY FOR SYSTEM IN MASTER
206 : BUI KEY FOR IMAGE IN MASTER
207 : BUI KEY FOR SORTDATE IN MASTER
208 : LIST TAB
209 : CLE VTAB
210 : BEEP
211 : BEEP
212 : BEEP
213 : BEEP
214 : WRI "Finished. Press a key."
215 + ELSE
216 : WRI "Cancelled. Press a key."
217 - ENDI
218 PAU
219 CLE Q
220 SET MESS OFF
221 SET ERR MESS OFF
```

COMMAND: DEFTAB

223	\$COMMAND		
224	DEFTAB		
225	DEFINE		
226	COLUMNS		
227	SYSTEM	TEXT	21
228	CODE	TEXT	21
229	TOPIC	TEXT	21
230	NUMBER	TEXT	21
231	DTG	TEXT	21
232	DOC_DATE	TEXT	21
233	ACTIVITY	TEXT	21
234	AUTHOR	TEXT	21
235	SERIAL	TEXT	21
236	CTRACTOR	TEXT	21
237	YEAR	TEXT	9
238	DOCUMENT	TEXT	21
239	TYPE	TEXT	21
240	AMOUNT	TEXT	13
241	MODIF	TEXT	8
242	REF	TEXT	21
243	ORIG_COD	TEXT	11
244	ORIG_DAT	TEXT	9
245	REV	TEXT	21
246	PURPOSE	NOTE	
247	COMMENTS	NOTE	
248	TITLE	NOTE	
249	ACCESS	TEXT	2
250	SCANDATE	TEXT	9
251	CONTRACT	TEXT	21
252	DRAWINGS	TEXT	1
253	PLATTER	TEXT	4
254	IMAGE	INTEGER	
255	PAGES	INTEGER	
256	SORTDATE	- (SGET('DOC_DATE',8,1))	TEXT
257	TABLES		
258	MASTER	WITH +	
259	SYSTEM	+	
260	CODE	+	
261	TOPIC	+	
262	NUMBER	+	
263	DTG	+	
264	DOC_DATE	+	
265	ACTIVITY	+	
266	AUTHOR	+	
267	SERIAL	+	
268	CTRACTOR	+	
269	YEAR	+	
270	DOCUMENT	+	

271 TYPE +
272 AMOUNT +
273 MODIF +
274 REF +
275 ORIG_COD +
276 ORIG_DAT +
277 REV +
278 PURPOSE +
279 COMMENTS +
280 TITLE +
281 ACCESS +
282 SCANDATE +
283 CONTRACT +
284 DRAWINGS +
285 PLATTER +
286 IMAGE +
287 PAGES +
288 SORTDATE
289 PASSWORDS
290 RPW FOR MASTER IS NONE
291 MPW FOR MASTER IS NONE
292 END
293

COMMAND: CMDMODE

294 \$COMMAND
295 CMDMODE
296 CLS
297 SET NULL -0-
298 SET QUOTES=" "
299 SET MESS ON
300 SET ERR MESS ON
301 INPUT TERM
302

COMMAND: LONGLIST

```
303 $COMMAND
304 LONGLIST
305 CLS
306 WRI "Very long list. Fill Laserjet paper tray."
307 WRI "Press a key when ready. ";
307 PAU
308 COPY 16CPIX8.LJ LPT1
309 SET NULL " "
310 OUT PRI
311 PRINT BIGLIST SOR BY SYSTEM SORTDATE
312 OUT SCR
313 COPY RESET.LJ LPT1
314 SET NULL -0-
315 BEEP
316 BEEP
317 BEEP
318 BEEP
319 WRI "Finished. Press a key."
320 PAU
```

3.11 Ancillary Programs

File: SQUEEZE.PAS

Language: Turbo Pascal Ver. 6.0

Purpose: Removes leading and trailing blanks from text fields. Removes text delimiters (^) from empty text fields, leaving the field delimiters (,).

Input file: MAIN.ASC

Output file: MAIN.DAT

```
-----  
PROGRAM Squeeze;  
Uses CRT;  
  
VAR  
  InFile, OutFile : Text;  
  InCount, OutCount: longint;  
  InQuotes, IOok: boolean;  
  ch, prevch: char;  
  j, perct, SpaceCt, CharCount: integer;  
  
PROCEDURE Init; (Initialize variables, open files)  
BEGIN  
  Textcolor(White);  
  InCount := 0;  
  OutCount := 0;  
  CharCount := 0;  
  SpaceCt := 0;  
  InQuotes := false;  
  IOok := true;  
  {$I-}  
  Assign(InFile, 'MAIN.ASC');  
  Reset(InFile);  
  IF IOResult <> 0 THEN  
  BEGIN  
    Writeln('ERROR - MAIN.ASC file not found.');    IOok := false;  
    Exit;  
  END;  
  Assign(OutFile, 'MAIN.DAT');  
  Rewrite(OutFile);  
  IF IOResult <> 0 THEN  
  BEGIN  
    Writeln('ERROR opening MAIN.DAT for output.');    Close(InFile);  
    IOok := false;  
    Exit;  
  END;  
END;
```

```

($I+)
END;

PROCEDURE ProcessFiles; (read input file 1 char at a time,)
BEGIN
    Textcolor(White);
    WHILE NOT EOF(Infile) DO
        BEGIN
            Read(Infile, ch);
            Inc(InCount);
            IF InQuotes THEN Inc(CharCount);
            CASE ch OF
                '^': BEGIN
                    IF InQuotes THEN
                        BEGIN
                            InQuotes := false;
                            IF CharCount < (SpaceCt+1) THEN
                                BEGIN
                                    Write(OutFile, '^');
                                    Inc(OutCount);
                                END;
                            END
                        ELSE
                            BEGIN
                                InQuotes := true;
                                CharCount := 0;
                            END;
                            SpaceCt := 0;
                        END;
                    ' ' : Inc(SpaceCt);
                ELSE
                    BEGIN
                        IF InQuotes THEN
                            BEGIN
                                IF CharCount = SpaceCt + 1 THEN
                                    BEGIN
                                        Write(OutFile, '^');
                                        Inc(OutCount);
                                    END;
                                END;
                                IF SpaceCt > 0 THEN
                                    BEGIN
                                        FOR j := 1 TO SpaceCt DO
                                            BEGIN
                                                Write(Outfile, ' ');
                                                Inc(OutCount);
                                            END;
                                        SpaceCt := 0;
                                    END;
                                END;
                            Write(OutFile, ch);
                            Inc(OutCount);
                        END;
                    END;
                END;
            END;
        END;
    END;

```

```
        END; (CASE)
    END;
END;

BEGIN (Main program)
    ClrScr;
    Writeln;
    Init;
    IF Iook THEN
    BEGIN
        ProcessFiles;
        Close(OutFile);
        Close(InFile);
        Writeln(InCount, ' bytes read. ');
        Writeln(OutCount, ' bytes written. ');
        IF InCount > 0 THEN
        BEGIN
            Perct := Round(100*(1 - OutCount/InCount));
            Writeln(Perct, ' % reduction. ');
        END;
    END;
END.
```


File: RESET.LJ

Language: Hewlett-Packard Laserjet Command Language

Purpose: Reset the HP Laserjet printer to its default configuration (ejects last page if still in printer memory).

Note: Code (not shown) simply consists of an escape (ASCII 027) character followed by the letter E.

SYSTEM	CODE	NUMBER	DATE	ACTIVITY	TITLE	TOPIC	PLAT IMAGE	PAGES
CG27	TESR		05/06/80	BF GOODRICH	INSPECT QUESTIONABLE FAIRNESS AREAS ON THE SDRW OF THE DANIELS	REPAIR	0002	17970
CG27	LETTER		04/16/83	NAVSEA	CG27, X-RAY REPORT 04/16/83	X-RAY	0002	17960
CG27	LETTER		12/21/85	NAVSEA	CG27, X-RAY REPORT 12/21/85	X-RAY	0002	17957
CG27	LETTER		09/29/89	NAVSEA	CG27, X-RAY REPORT 09/18/89	X-RAY	0002	17954
CG27	LETTER		06/14/90	NAVSEA	CG27, X-RAY REPORT 06/14/90	X-RAY	0002	17945
CG27	TESR		07/23/91	BF GOODRICH	TO INSPECT THE CONDITION OF THE SDRW ON THE USS DANIELS REPORT FINDINGS	TEST	0004	67277
CG27	LETTER		08/01/91	NAVSEA	X-RAY INSPECTION (CG27) 07/25/91	X-RAY	0004	66774
CG27	MSG		08/12/91	NAVSURFLANT NORFOLK	REF A REQUESTED A WAIVER TO USE EPOXY FILLER TO RETURN DOME FAIRNESS	REPAIR	0004	66810
CG27	TESR		08/16/91	BF GOODRICH	TO ACCOMPLISH GENERAL REPAIRS AND APPLY EPOXY TO THE CLOSURE PLATE AREA	REPAIR	0004	69317
CG27	MSG			NAVSURFLANT	REF A REQUESTED GUIDANCE FOR REPAIRS TO USS JOSEPHUS DANIELS	REPAIR	0002	17962
CG27	MSG			NAVSEA	SOMAR DOME RUBBER WINDOW CERTIFICATION DLG-27	CERTIFICATION	0002	17961
CG27	MSG			NAVSURFLANT	SOMAR DOME STRUCTURE TECH ASSIST VISIT REPORT	REPORT	0002	17963
CG27	MSG			USS JOSEPHUS DANIELS	APPROX ELEVEN FEET OF RUBBER WINDOW CLOSURE PLATE SEPARATED FROM HULL	PRODUCT	0103	51287
CG27	MSG			USS JOSEPHUS DANIELS	REPAIRS TO BE COMPLETED DURING REGULAR OVERHAUL SCHEDULED	REPAIR	0103	54535
CG27	MEMO			NAVSEA	REF A REQUESTED A WAIVER TO USE EPOXY FILLER TO RETURN DOME FAIRNESS	REPAIR	0004	68982
CG27	MSG			NAVSURFLANT NORFOLK	REF A REQUESTED WAIVER OF REF B PARA 8-3.7.6.11 NOTE RELATING TO EPOXY	REPAIR	0004	66812
CG28	TESR		03/07/78	BFGOODRICH	INSPECTION	REPAIR	0002	17994
CG28	TESR		04/17/78	BFGOODRICH	REPAIRS CLOSURE	REPAIR	0002	17991
CG28	TESR		05/15/78	BFGOODRICH	FINAL FINISH AFTER CLOSURE PLATE REPLACEMENT ON THE USS MAINWRIGHT	REPAIR	0002	17985
CG28	TESR		03/26/83	BFGOODRICH	REPLACE DAMAGED HUT PLATE SECTION AND INSTRUCT PERSONNEL IN MISC REPAIRS	REPAIR	0002	17984
CG28	LETTER		12/01/86	NAVSEA	CG28, X-RAY REPORT 12/01/86	X-RAY	0002	18019
CG28	LETTER		06/06/89	NAVSEA	SOMAR DOME RUBBER WINDOW (SDRW) DOME ENTRY CRITERIA	PRODUCT	0103	51789
CG28	TESR		10/02/90	BFGOODRICH	INSPECTION EXTERIOR CONDITION OF THE SDRW	REPAIR	0002	18010
CG28	LETTER		10/05/90	NAVSEA	CG28, X-RAY REPORT 10/01/90	X-RAY	0002	18022
CG28	LETTER		10/25/90	NAVSEA	CG28, X-RAY REPORT 10/25/90	X-RAY	0002	18015
CG28	INFORMATION		10/29/90	BFGOODRICH	CG28 REPAIR FOR FAIRING	REPAIR	0001	7127
CG28	INFORMATION		11/05/90	BFGOODRICH	CG26 NUTPLATE REPAIR	REPAIR	0001	7123
CG28	TESR		12/04/90	BFGOODRICH	INSPECTION AND PAIR A MINDOR SDRW MARRIAGE LINE FLAW	REPAIR	0002	18013
CG29	TESR		06/16/80	BFGOODRICH	WITNESS THE INITIAL SHIPBOARD HARDWARE CHECK	REPAIR	0002	18068
CG29	TESR		07/01/80	BFGOODRICH	WITNESS THE FINAL CHECK OF THE BEADSEAT HARDWARE OFFSETS	REPAIR	0002	18064
CG29	TESR		08/05/80	BFGOODRICH	WITNESS THE DOME INSTALLATION	REPAIR	0002	18061
CG29	TESR		08/21/80	BFGOODRICH	FINAL FINISH AND FAIRNESS REWORK ON THE SDRW	REPAIR	0002	18060
CG29	TESR		12/03/82	BFGOODRICH	REPLACE A DAMAGED SDRW	REPAIR	0002	18048
CG29	TESR		12/03/82	BFGOODRICH	TECHNICAL ASSISTANCE TO SRF	REPAIR	0002	18040
CG29	TESR		12/03/82	BFGOODRICH	FINISH WORK TO THE USS JOUETT'S SDRW	REPAIR	0002	18049
CG29	TESR		12/03/82	BFGOODRICH	FINISH WORK TO THE USS JOUETT'S SDRW	REPAIR	0002	18042
CG29	TESR		04/16/83	BFGOODRICH	FINISH WORK TO THE USS JOUETT'S SDRW	REPAIR	0002	18051
CG29	TESR		04/16/83	BFGOODRICH	REPLACE DAMAGED SDRW	REPAIR	0002	18057
CG29	LETTER		05/06/83	NAVSEA	CG29, X-RAY REPORT 04/27/88	X-RAY	0002	18073
CG29	LETTER		03/14/85	NAVSEA	CG29, X-RAY REPORT 03/14/85	X-RAY	0002	18076
CG29	MSG			USS JOUETT	SDRW PRESSURIZATION SYSTEM	PRESSURIZATION	0002	18079
CG29	MSG			NAVSURFLANT	SPEED IS RESTRICTED TO 13 KTS MAX TO AVOID DAMAGE TO TRANSDUCER ELEMENTS	REPAIR	0103	51291
CG29	MSG			USS JOUETT	THERE IS NO EFFECTIVE METHOD FOR TEMPORARY REPAIRS TO THE SUBJ SDRW	REPAIR	0103	51290
CG29	MSG			USS JOUETT	A DEPRESSED AREA 1 1/2 IN. DEEP AND 12 IN. DIAM MIDWAY UP THE DOME	PRODUCT	0103	51293
CG30	TESR		09/30/76	BFGOODRICH	BFG REPRESENTATIVE REQUESTED TO WITNESS INITIAL SHOP HARDWARE ALIGNMENT	PRODUCT	0002	18124
CG30	TESR		09/30/76	BFGOODRICH	BFG REP. REQUESTED TO WITNESS INITIAL SHOP HARDWARE ALIGNMENT CHECK	PRODUCT	0002	18101
CG30	TESR		09/30/76	BFGOODRICH	BFG REP. REQUESTED TO WITNESS INITIAL SHOP HARDWARE ALIGNMENT CHECK	INSPECTION	0002	18100
CG30	TESR		10/30/76	BFGOODRICH	BFG REPRESENTATIVE TO WITNESS INITIAL SHOP HARDWARE ALIGNMENT CHECK	PRODUCT	0002	18105
CG30	TESR		12/01/76	BFGOODRICH	INSPECT BEAD SEAT ASSEMBLY TACK WELDED TO THE SHIP	PRODUCT	0002	18121
CG30	TESR		12/13/76	BFGOODRICH	WITNESS FINAL HARDWARE ALIGNMENT CHECK USS HORNE	HARDWARE ALIGNMENT	0002	18117

SYSTEM	CODE	NUMBER	DATE	ACTIVITY	TITLE	TOPIC	PLAT	IMAGE	PAGES
CG30	TESR		01/03/77	BFGOODRICH	SDRW-2 WAS INSTALLED ON THE SHIP	REPAIR	0002	18126	1
CG30	TESR		07/27/77	BFGOODRICH	SUPERVISE THE APPLICATION OF HP-2 ELASTOLOCK TO THE UPPER BOW AREA	REPAIR	0002	18125	1
CG30	TESR		05/03/84	BFGOODRICH	INSPECTION	REPAIR	0002	18111	3
CG30	LETTER		07/02/84	NAVSEA	CG30, X-RAY REPORT 07/02/84	X-RAY	0002	18090	2
CG30	TESR		07/09/84	BFGOODRICH	EVALUATE BEAD SEAT OFFSETS AND INSTALL SDRW-2	REPAIR	0002	18108	2
CG30	LETTER		07/17/84	NAVSEA	CG30, X-RAY REPORT 07/17/84	X-RAY	0002	18088	2
CG30	LETTER		08/10/84	NAVSEA	CG30, X-RAY REPORT 08/10/84	X-RAY	0002	18086	6
CG30	LETTER		11/06/84	PEARL HARBOR	INVESTIGATION CIRCUMSTANCES CONNECTED RIPTURED SDRW ON BOARD USS HORNE	PRODUCT	0002	19675	1
CG30	OTHER		03/10/86	BFGOODRICH	CG30, X-RAY REPORT 03/10/86	X-RAY	0002	18099	4
CG30	LETTER		11/23/88	NAVSEA	CG30, X-RAY REPORT 11/09/88	X-RAY	0002	18095	5
CG30	MSG			NAVSEA	SONAR DOME RUBBER WINDOW CERTIFICATION	CERTIFICATION	0002	18267	1
CG30	MSG			CINCPACFLT	USS HORNE FY84 SRA SCHEDULE REVISION	PRODUCT	0002	18080	1
CG30	MSG			NAVSEA	REF A ADVISED SUPSHIP SAN DIEGO ASSIGNED SDRW REPLACEMENT	PRODUCT	0103	51295	2
CG30	MSG			USS CAPE COD	USS CAPE COD DIVING TEAM INSPECTED SONAR DOME AM 18 MAY.	PRODUCT	0103	51298	2
CG30	MSG			NAVSHIPREPFA	SONAR DOME RUBBER WINDOW CASUALTY ANALYSIS	PRODUCT	0103	51296	1
CG31	TESR		08/06/79	BFGOODRICH	INSPECT THE BEAD SEAT HARDWARE	PRODUCT	0002	18205	4
CG31	TESR		10/09/79	BFGOODRICH	INITIAL HARDWARE OFFSET CHECK	REPAIR	0002	18201	2
CG31	TESR		10/19/79	BFGOODRICH	FINAL HARDWARE OFFSET INSPECTION	REPAIR	0002	18199	3
CG31	TESR		10/26/79	BFGOODRICH	FINAL HARDWARE OFFSET INSPECTION	REPAIR	0002	18196	6
CG31	TESR		11/13/79	BFGOODRICH	BOW DOME WAS NOT READY FOR SDRW INSTALLATION	REPAIR	0002	18190	10
CG31	TESR		12/07/79	BFGOODRICH	BOW DOME WAS NOT READY FOR SDRW INSTALLATION	REPAIR	0002	18180	1
CG31	TESR		12/07/79	BFGOODRICH	FINAL FINISH AND FAIRNESS REMORK ON THE SDRW	REPAIR	0002	18179	4
CG31	LETTER		07/15/83	NEWPORT	CG31, X-RAY REPORT 07/15/83	X-RAY	0002	18161	6
				RHODE ISLAND					
CG31	TESR		12/20/83	BFGOODRICH	INSPECT AND REPAIR DAMAGED AREAS ON THE SDRW	REPAIR	0002	18175	4
CG31	LETTER		12/28/83	NAVSEA	CG31, X-RAY REPORT 12/28/83	X-RAY	0002	18150	3
CG31	LETTER		01/31/84	NAVSEA	CG31, X-RAY REPORT 01/31/84	X-RAY	0002	18147	1
CG31	LETTER		11/27/84	NRL	CG31, X-RAY REPORT 05/15/84	X-RAY	0002	18165	4
CG31	LETTER		12/13/84	NAVSEA	CG31, X-RAY REPORT 12/13/84	X-RAY	0002	18129	3
CG31	LETTER		01/20/85	NAVSEA	CG31, X-RAY REPORT 01/20/85	X-RAY	0002	18146	7
CG31	LETTER		01/29/85	NAVSEA	CG31, X-RAY REPORT 01/29/85	X-RAY	0002	18139	1
CG31	LETTER		09/20/85	NAVSEA	CG31, X-RAY REPORT 09/20/85	X-RAY	0002	18138	4
CG31	LETTER		11/20/85	NAVSEA	CG31, X-RAY REPORT 11/20/85	X-RAY	0002	18134	5
CG31	TESR		12/12/85	BFGOODRICH	SDRW HAD BEEN EXPERIENCING BREAKS	REPAIR	0002	18220	8
CG31	TESR		07/01/86	BFGOODRICH	DETERMINE IF THE BEAD SEAT HARDWARE WAS DAMAGED.	REPAIR	0002	18212	7
CG31	LETTER		06/23/88	NAVSEA	CG31, X-RAY REPORT 06/06/88	X-RAY	0002	18155	5
CG31	MSG		09/07/91	USS STERETT	SUPSHIP OBTAIN ASSIST FROM IIT BARTON GAGE COMPANY FOR REPLACEMENT	PRODUCT	0004	69328	1
CG31	TESR		09/15/91	BFGOODRICH	INSPECTION AND REPAIR, DOME LEAK, AND ADDENDUM	REPAIR	0004	69609	5
CG31	TESR		09/15/91	BFGOODRICH	C31 INSPECTION AND REPAIR RUBBER	REPAIR	0004	69602	3
CG31	LETTER		10/01/91	NAVSEA	CG31 X-RAY REPORT, NO DAMAGE	X-RAY	0004	69594	2
CG31	TESR		11/06/91	BFGOODRICH	RUBBER REPAIR TO CG31	REPAIR	0004	70648	3
CG31	MSG			NAVSHIPREPFA	SDRW REPLACEMENT AND REPAIRS	REPAIR	0002	18169	2
				C					
CG31	MSG			NAVSHIPYD	SDRW INSTALLATION	INSTALLATION	0002	18167	2
CG31	MSG			NAVSHIPREPFA	SDRW REPLACEMENT AND REPAIRS	REPAIR	0002	18171	2
				C					
CG31	MSG			NAVSESSE	DISCREPANCY CONCERNING MAXIMUM PRESSURE TO BE MAINTAINED INSIDE SD	SAFETY	0103	52572	4
CG31	MSG			USS STERETT	NAVSEACENPAC, SAN DIEGO TECH ASSIST INSPECTION & REPAIR OF SDRW RUPTURE	REPAIR	0004	68953	1
CG32	TESR		02/03/75	BFGOODRICH	DISCUSSIONS ON REPAIRING THE DAMAGED AREA	REPAIR	0002	18240	2
CG32	TESR		02/12/75	BFGOODRICH	REPAIR 8FT X 8IN AREA ON PORT UPPER NUT PLATE	REPAIR	0002	18238	8
CG32	TESR		06/03/76	BFGOODRICH	INSPECTION AND RECOMMEND REPAIR	REPAIR	0002	18230	4
CG32	LETTER		03/04/77	CHARLESTON	USS STANDLEY (CG 32); APPLICATION OF UNDERWATER PAINT	INSTALLATION	0002	18282	2
				S.C.					
CG32	TESR		02/01/78	BFGOODRICH	INSPECT SDRW DRYDOCKED	REPAIR	0012	18226	2
CG32	TESR		04/16/78	BFGOODRICH	REPAIR DAMAGE AND IMPROVE FAIRNESS	REPAIR	0002	18224	4

SYSTEM	CODE	NUMBER	DATE	ACTIVITY	TITLE	TOPIC	PLAT IMAGE	PAGES
AN/SQY-1	LETTER		06/18/91	NAVSEA	NEW DOME DESIGN REQUIREMENTS		0004	70078
AN/SQY-1	LETTER		06/19/91	NAVSEA	NEW DOME DEVELOPMENT FOR INSTALLATION AFT OF SDRV	NEW MATERIAL	0004	70068
BUDGET	FUNDING		08/07/91	NAVSEA	SCN TO NAVSSES 78,000	SCN	0004	69684
BUDGET	FUNDING		08/07/91	NAVSEA	SCN TO NAVSSES 442,800	SCN	0004	69685
BUDGET	FUNDING		08/13/91	NAVSEA	OPN FOR NAVSSES 153,390	OPN	0004	69681
BUDGET	FUNDING		08/13/91	NAVSEA	OPN TO NAVSSES 110,846	OPN	0004	69683
BUDGET	FUNDING		09/10/91	NAVSEA	OM&N FOR CRANE 21,000	OM&N	0004	69677
BUDGET	MEMO	N0002492MR01089	09/13/91	NAVSEA	DDG51 CLASS ASPD DDG 68/69/70/71/72	SCN	0004	69922
BUDGET	FUNDING		10/01/91	NAVSEA	OM&N \$5,000 TO CHEATHAM	OM&N	0004	69801
BUDGET	FUNDING	N0002492MR01086	10/29/91	NAVSEA	41K, OM&N, FOR NAVSSES	OM&N	0004	70394
BUDGET	FUNDING		03/28/90	NAVSEA	FUNDING FOR DAVID TAYLOR, FAIRING DEVELOPMENT PROGRAM	SCN	0004	70528
BUDGET	FUNDING	N0002491MR20266	09/16/91	CRANE	89 SCN FOR CRANE FOR DDG54-58	SCN	0004	69604
CASTING	CONTRACT		09/02/87	BF GOODRICH	BASIC CONTRACT FOR CASTINGS FROM BFG	PRODUCT	0103	55876
CASTING	INFORMATION 1		04/07/89	DAVIE	MARCH 89 PROGRESS REPORT CASTINGS	PRODUCT	0103	50963
CASTING	INFORMATION 2		04/27/89	DAVIE	APRIL 89 PROGRESS REPORT CASTINGS	PRODUCT	0103	50962
CASTING	INFORMATION 22		05/13/91	DAVIE	APRIL 91 PROGRESS REPORT CASTINGS	PRODUCT	0103	52468
CASTING	OTHER	MIL0038	09/19/91	DAVIES	DD250 FOR CASTING 13AB	DD250	0004	69647
CASTING	CONTRACT	MIL0041	11/22/91	DAVIE	ITEM 0014AA 2ND SET CASTINGS	DD250	0004	70649
CASTING	CONTRACT	P00009	12/06/91	NAVSEA	P00009 MOD TO PAY FOR ITEM 18 ESCALATION	PRODUCT	0004	70745
CASTINGS	STUDY		11/12/68	BF GOODRICH	ATTACHMENT HARDWARE STRESS ANALYSIS FOR SDRV, NOV 68, BEAD SEAT CASTING	PRODUCT	0001	4653
CASTINGS	ESHM	82-095	07/14/70	BF GOODRICH	CASTINGS, BEAD SEAT AND CLAMP	PRODUCT	0002	25895
CASTINGS	ESHM	82-096	05/27/71	BF GOODRICH	CASTINGS, WELD ASSEMBLY AND MACHINING	PRODUCT	0002	25903
CASTINGS	STUDY	73-14-040	06/01/73	BF GOODRICH	STRESS ANALYSIS COMPARISON OF CAST BEAD CLAMPS TO FORGED BEAD CLAMPS	OFFSETS	0002	24842
CASTINGS	ECP	ECP 42, VECF 4	01/21/74	BF GOODRICH	USE OF FORGED CLAMPS	PRODUCT	0001	2900
CASTINGS	ESHM	82-143-R3	07/15/74	NAVSEA	SPEC 82-143-R3, BEAD CLAMP FORGING SPECIFICATION	PRODUCT	0001	8197
CASTINGS	ESHM	ESMM-S-60-R2	02/15/80	BF GOODRICH	CASTING SPECIFICATION BEAD SEAT & BEAD CLAMPS PRRSD - KEEL DOME	OFFSETS	0002	25398
CASTINGS	ESHM	ESMM-S-83-R1	05/11/80	NAVSEA	CASTING SPECIFICATION: BEAD SEAT AND BEAD CLAMP	PRODUCT	0002	23406
CASTINGS	ECP	K-16	03/25/81	BF GOODRICH	MODIFY PRESSURE PLATE/BEAD SEAT CASTINGS	OFFSETS	0002	24211
CASTINGS	ECP	ECP 120	07/24/81	BF GOODRICH	BEAD SEAT TAIL SECTION ASSEMBLY CHANGE	PRESSURIZATION	0002	28994
CASTINGS	TESR		02/13/82	BIW	INSPECT & REPAIR QUESTIONABLE LOOSE RUBBER AREAS OF BEAD CASTINGS	PRODUCT	0001	2881
CASTINGS	ECP	WAIVER F-2	06/22/82	BF GOODRICH	BEAD SEAT CASTINGS - HIGH CHROMIUM LEVEL	REPAIR	0004	67542
CASTINGS	ECP	K-28	10/29/82	BF GOODRICH	CASTING SPECIFICATION - HEAT TREAT RECORD CHANGE	PRODUCT	0004	67385
CASTINGS	ESHM	ESMM-S-60-R5	12/21/82	BF GOODRICH	CASTING SPECIFICATION BEAD SEAT & BEAD CLAMPS	PRODUCT	0002	29071
CASTINGS	ECP	K-33	04/06/83	BF GOODRICH	CASTING WELDING INSPECTION - CHANGE SPECIFICATION	PRODUCT	0002	25960
CASTINGS	ESHM	ESMM-S-83-R2	04/29/83	BF GOODRICH	CASTING SPECIFICATION: BEAD SEAT AND BEAD CLAMP	REPAIR	0002	29103
CASTINGS	ECP	K-37	05/17/83	BF GOODRICH	BEAD SEAT CASTINGS - MINOR CORRECTIONS	OFFSETS	0002	24245
CASTINGS	ESHM	ESMM-P-41	04/08/85	BF GOODRICH	BEAD SEAT HARDWARE ANALYSIS	REPAIR	0002	29134
CASTINGS	ESHM	ESMM-S-242	09/30/85	BF GOODRICH	BEAD SEAT ANALYSIS PART II CASTING INSPECTION CG 57	TOOLING	0001	6734
CASTINGS	LETTER		11/06/85	BF GOODRICH	CONTOUR ANALYSIS PART II CASTING INSPECTION CG 57	TOOLING	0001	3682
CASTINGS	STUDY		11/12/85	BF GOODRICH	BEAD SEAT DESIGN RESULTS FOR CG47 CLASS	PRODUCT	0002	27937
CASTINGS	ESHM		12/03/85	BF GOODRICH	CONTOUR ANALYSIS PART II CASTING INSPECTION CG-57	TOOLING	0001	8123
CASTINGS	ESHM		12/03/85	BF GOODRICH	CONTOUR ANALYSIS PART II CASTING INSPECTION CG-57	OFFSETS	0002	23489
CASTINGS	ESHM		12/03/85	BF GOODRICH	POTENTIAL FOR REFURBISHMENT OF SONAR DOME BEAD SEAT CASTINGS	OFFSETS	0002	24598
CASTINGS	LETTER		12/18/85	NAVSEA	SDRV-1 1A LOFT SUPPLEMENTAL COORDINATE DATA CL TRANSDUCER X=12.125FT	REFERB	0002	28286
CASTINGS	ESHM	ESMM-S-271	05/08/86	BF GOODRICH	CASTING SPECIFICATION: BEAD SEAT, SDRV, 5/86	OFFSETS	0002	24122
CASTINGS	ESHM	ESMM-S-274	05/17/86	BF GOODRICH	SDRV-1A LOFT COORDINATE DATA CL TRANSDUCER X = 0.00	PRODUCT	0001	4936
CASTINGS	ESHM	EMM-S-270-R1	07/02/86	BF GOODRICH	SDRV-1A LOFT COORDINATE DATA CL TRANSDUCER X = 0.00	OFFSETS	0002	24149
CASTINGS	ESHM	ESMM-S-270-R1	07/02/86	BF GOODRICH	CASTING SPECIFICATION BEAD SEAT, ESMM-S-274-R2	PRODUCT	0002	32537
CASTINGS	ESHM	ESMM-S-274-R2	07/30/86	BF GOODRICH	CASTING SPECIFICATION BEAD SEAT SDRV-1 BOW DOMES	TOOLING	0001	6727
CASTINGS	ESHM	ESMM-S-274-R1	07/30/86	BF GOODRICH	CASTING SPECIFICATION BEAD SEAT SDRV-1 BOW DOMES	TOOLING	0001	6727
CASTINGS	LETTER		08/05/86	BF GOODRICH	BEAD SEAT HARDWARE, SYMMETRIC TO LOFT DESIGN, ECP 192	TOOLING	0002	23669
CASTINGS	LETTER		08/05/86	BF GOODRICH	STRESS ANALYSIS, BEAD SEAT MATERIAL, AUG 86	PRODUCT	0001	5359
CASTINGS	LETTER		08/05/86	BF GOODRICH	STRESS ANALYSIS, BEAD SEAT MATERIAL, AUG 86	PRODUCT	0001	5357
CASTINGS	ECP	192	08/19/86	BF GOODRICH	BEAD SEAT CASTING REDESIGN	PRODUCT	0001	5360
CASTINGS	ESHM	ESMM-S-327	10/08/87	BF GOODRICH	SDRV-1A LOFT COORDINATE DATA CL TRANSDUCER X = 12.125 FT ON SHIP'S FRAM	PRODUCT	0002	29690
CASTINGS	ESHM				SDRV-1A LOFT COORDINATE DATA CL TRANSDUCER X=12.125FT	OFFSETS	0002	23566

SYSTEM	CODE	NUMBER	DATE	ACTIVITY	TITLE	TOPIC	PLAT IMAGE	PAGES
CG32	LETTER		03/21/86	NAVSEA	CG32, X-RAY REPORT 03/13/86	X-RAY	0002	18280
CG32	LETTER		03/09/88	NAVSEA	CG32, X-RAY REPORT 02/26/88	X-RAY	0002	18276
CG32	TESR		07/23/90	BFGOODRICH	EXTERNAL INSPECTION	REPAIR	0002	18250
CG32	LETTER		07/27/90	NAVSEA	CG32, X-RAY REPORT 07/22/90	X-RAY	0002	18268
CG32	TESR		08/27/90	BFGOODRICH	REPAIR TEN FEET OF DAMAGED NUTPLATES	REPAIR	0002	18245
CG32	TESR		09/20/90	BFGOODRICH	REPAIR 20 INCHES OF DAMAGED NUTPLATES ON THE SDRW	REPAIR	0002	18255
CG32	MSG			NAVSHIPYD	SDRW INSPECTION	INSPECTED	0002	18266
CG32	MSG			NAVSEA	SDRW REPLACEMENT	REPAIR	0002	18259
CG32	MSG			NAVSURFPAC	RESTRICTED AVAIL USS STANLEY	REPAIR	0002	18261
CG32	MSG			SUPSHIP	SDRW REPAIRS	REPAIR	0002	18256
CG32	MSG			NAVSURFAC	SDRW REPLACEMENT	REPAIR	0002	18260
CG32	MSG			NAVSEA	SDRW REPAIR RECOMMENDATIONS	REPAIR	0002	18264
CG32	MSG			USS STANLEY	SDRW REPAIRS	REPAIR	0002	18277
CG32	MSG			USS WILLIAM STANLEY	AIR FILLER ELEMENT, ACCESS PLATE CLAMPS, OVHD VENTILATION DUCTING DAMAGED	SAFETY	0103	52622
CG32	MSG			USS WILLIAM STANLEY	AIR FILLER ELEMENT, ACCESS PLATE CLAMPS, OVHD VENTILATION DUCTING DAMAGED	SAFETY	0103	52620
CG33	TESR		10/18/78	BFGOODRICH	INVESTIGATE DAMAGE AND SUPERVISE REPAIRS SDRW-2	REPAIR	0002	18361
CG33	TESR		10/18/78	BFGOODRICH	INSPECT SDRW AND PURPOSE METHODS OF REPAIR	REPAIR	0002	18358
CG33	TESR		01/07/79	BFGOODRICH	REPLACEMENT OF 42 INCH SECTION OF NUT PLATES	REPAIR	0002	18356
CG33	LETTER		04/05/83	NAVSEA	CG33, X-RAY REPORT 04/05/83	X-RAY	0002	18303
CG33	TESR		04/06/83	BFGOODRICH	INSPECTION OF SDRW-2	REPAIR	0002	18350
CG33	TESR		05/26/83	BFGOODRICH	SUPERVISE AND ASSIST THE SHIPYARD PERSONNEL IN REPAIRING THE SDRW-2 S/N6	REPAIR	0002	18346
CG33	TESR		02/24/86	BFGOODRICH	SDRW INSPECTION	REPAIR	0002	18342
CG33	LETTER		02/25/86	NAVSEA	CG33, X-RAY REPORT 02/25/86	X-RAY	0002	18295
CG33	TESR		03/03/86	BFGOODRICH	OBTAIN BEAD SEAT HARDWARE OFFSET DATA	REPAIR	0002	18334
CG33	LETTER		03/05/86	NAVSEA	CG33, X-RAY REPORT 02/25/86	X-RAY	0002	18292
CG33	TESR		03/13/86	BFGOODRICH	TECHNICAL ASSISTANCE TO SOUTHWEST MARINE	REPAIR	0002	18325
CG33	TESR		03/23/86	BFGOODRICH	INSTALL SDRW-2 (S/N23, BFG LAYUP #24)	REPAIR	0002	18329
CG33	TESR		04/04/86	BFGOODRICH	COMPLETE THE FINAL FINISH WORK ON THE SDRW	REPAIR	0002	18321
CG33	LETTER		03/18/88	NAVSEA	CG33, X-RAY REPORT 03/18/88	X-RAY	0002	18291
CG33	TESR		11/14/89	BFGOODRICH	INSPECT THE SDRW-2 (S/N 23)	REPAIR	0002	18315
CG33	LETTER		11/20/89	NAVSEA	CG33, X-RAY REPORT 11/20/89	X-RAY	0002	18287
CG33	LETTER		12/05/89	NAVSEA	CG33, X-RAY REPORT 11/20/89	X-RAY	0002	18283
CG33	TESR		01/15/90	BFGOODRICH	GENERAL REPAIRS AND INSTALL MISSING DEGREE TILES TO THE SDRW	REPAIR	0002	18311
CG33	MSG			NAVSEA	EVALUATION OF THE SDRW	PRODUCT	0002	18305
CG33	MSG			NAVSEA	SDRW BEAD SEAT CASTING MEASUREMENT COMPLETED	REPAIR	0002	18308
CG33	MSG			NAVSEA	DELIVERY AND REPLACEMENT OF USS FOX	REPAIR	0002	18307
CG34	TESR		10/15/79	BFGOODRICH	TO WITNESS THE SHOP CHECK OF THE HARDWARE OFFSETS	REPAIR	0002	18390
CG34	TESR		12/26/79	BFGOODRICH	TO WITNESS THE INITIAL SHIPBOARD CHECK OF THE HARDWARE OFFSETS	REPAIR	0002	18364
CG34	TESR		01/20/80	BFGOODRICH	TO WITNESS THE FINAL HARDWARE CHECK OF THE HARDWARE OFFSETS	REPAIR	0002	18384
CG34	TESR		03/23/80	BFGOODRICH	FAIRNESS REMARK ON SDRW AFTER NEW INSTALLATION	REPAIR	0002	18380
CG34	TESR		04/11/80	BFGOODRICH	FINAL FINISH OF RUBBER/STEEL MARRIAGE LINE ON BOTH SDRW INSTALLATIONS	REPAIR	0002	18378
CG34	LETTER		06/18/81	NAVSEA	USS BIDDLE (CG 34) AN/SOS-268X SDRW CERTIFICATION TEST; REPORT OF	TEST	0002	18408
CG34	LETTER		07/19/85	NAVSEA	CG34, X-RAY REPORT 07/19/85	X-RAY	0002	18398
CG34	LETTER		07/23/85	NAVSEA	CG34, X-RAY REPORT 07/19/85	X-RAY	0002	18407
CG34	TESR		07/30/85	GEO-CENTERS	OBSERVE THE RADIOGRAPHIC INSPECTION PERFORMED ON THE USS BIDDLE SDRW	REPAIR	0002	18371
CG34	LETTER		08/13/86	NAVSEA	CG34, X-RAY REPORT 08/09/86	X-RAY	0002	18395
CG34	LETTER		08/19/86	BFGOODRICH	INSPECT SDRW-2 (S/N 13, BFG LAYUP #14)	REPAIR	0002	18368
CG34	TESR		05/03/89	NAVSEA	CG34, X-RAY REPORT 05/03/89	X-RAY	0002	18406
CG34	LETTER		05/15/89	NAVSEA	CG34, X-RAY REPORT 05/03/89	X-RAY	0002	18402
CG34	LETTER		05/03/90	NAVSEA	CG34, X-RAY REPORT 04/27/90	X-RAY	0002	18401
CG34	LETTER		05/06/91	NAVSEA	CG34, X-RAY REPORT 04/30/91	X-RAY	0103	50072
CG35	LETTER		10/22/85	NAVSEA	CG35, X-RAY REPORT 10/15/85	X-RAY	0002	18417
CG35	LETTER		01/23/89	NAVSEA	CG35, X-RAY REPORT 01/13/89	X-RAY	0002	18413

APPENDIX G

**ON-SITE INSPECTION OF THE BEAD NECK REGIONS OF THE
AN/SQQ 23 SONAR RUBBER DOMES (SRDS) INSTALLED ON THE
USS DAHLGREN, DDG-43, NORFOLK, VA
21 DECEMBER 1990**



GEO-CENTERS, INC.

Subj: ON-SITE INSPECTION OF THE BEAD NECK REGIONS OF THE AN/SQQ
23 SONAR RUBBER DOMES (SRDS) INSTALLED ON THE USS
DAHLGREN, DDG-43, NORFOLK, VA, 21 DECEMBER 1990

Ref: (a) BFGoodrich TESR #1 (USS DAHLGREN) dated
11-12 December 1990

(b) "Initial Findings of Failure Analysis on Sonar Rubber
Dome (SRD) S/N B022, ex-USS PRATT, Aft Dome," NRL
Letter Report 6120-609 of 30 September 1988

(c) "Trim Mold Fill Plates on Molds S/N 80S1486, 79S1445
and 81S1714," BFGoodrich ECP 6037-31, dated 6 October
1989

1. On 19 December 1990, NAVSEA Code 06U1D asked NRL to carry out the subject inspection to clarify the bead neck damage reported in Ref. (a). The inspection was conducted by C. Beachem on 21 December 1990.

2. There are two AN/SQQ 23 SRDs installed on the USS DAHLGREN. SRD S/N A066 is the forward one and SRD S/N A058 is the aft SRD. Both domes were installed in March 1978 and by December 1990 have seen 153 months of service. They received the standard x-ray inspection in December 1990. SRD A066 has two forward and two aft damage sites, while SRD A058 has one forward and two aft damage sites. The x-ray report is attached as Appendix A.

3. The BFGoodrich report stated that cracks were present along the bead necks of both domes (Ref. (a)). We confirmed the findings of that report. We also found bead neck cracks in the area behind the baffles. While we found exposed wire cords along most cracks, we could find no broken cords. Figure 1 shows a typical crack in the forward dome. The bead neck of the aft dome had been repaired at some time in the past; in this inspection we observed cracks through the repairs, as shown by Figures 2a and 2b.

4. Catastrophic failure through the bead neck can occur with little or no indications. The area has received little attention until recently, when NRL became concerned after the failure of the SRD on the USS PRATT (Ref. (b)). Since our work on the SRD from the USS PRATT, the manufacturer has found and corrected a problem in the manufacturing procedure (Ref. (c)). NRL is focussing attention on the bead neck area, not only because domes can fail there, but also because cracking in these areas may be an entry point for water into the main SRD structure, leading to corrosion weakening of the structural wires in the forward and aft quadrants of SRDs where most of the structural damage occurs.

5. We recommend that both SRDs be replaced, since we do not have the ability now to predict their lifetimes. Repair of the bead neck of these domes, which exhibit advanced bead neck damage, will likely have little or no effect in prolonging the service life of these domes. The presence of structural cord damage should also be considered in making decisions about these two SRDs

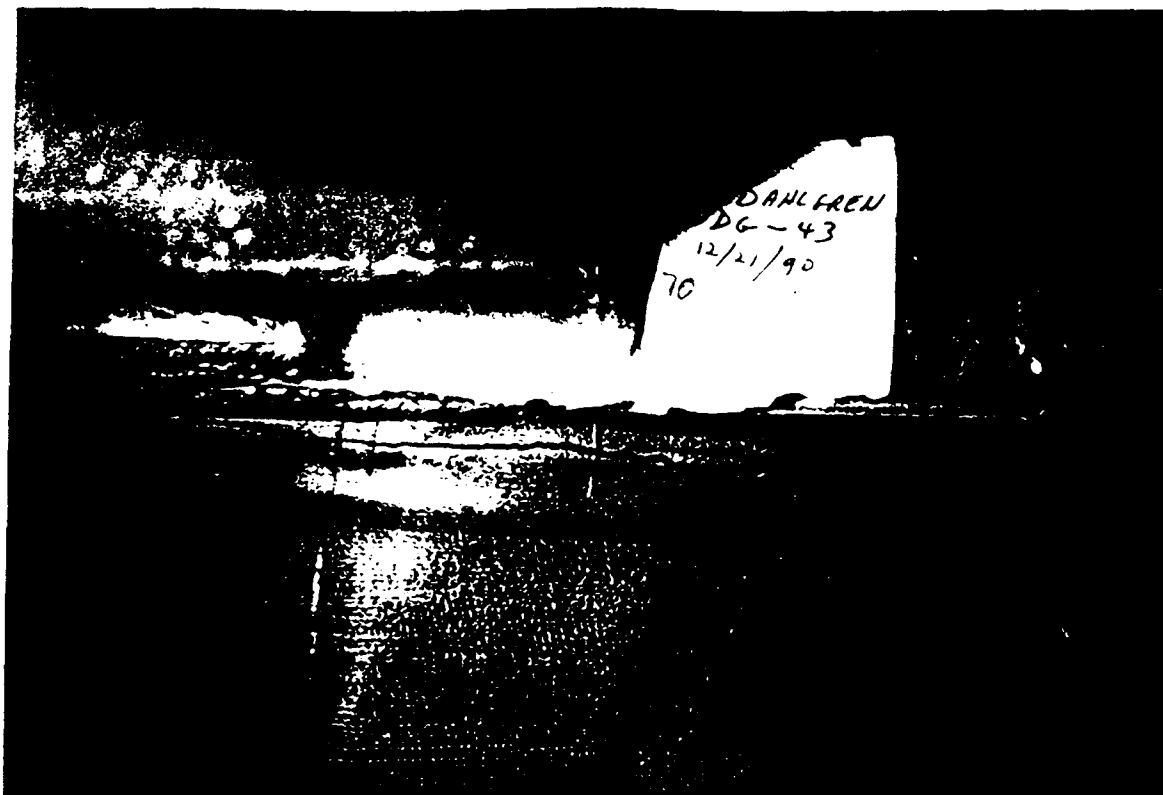


Figure 1
Bead neck crack, typical, at 70" Starboard on fwd dome.



Figure 2a
Close up of damage through the repair area, on ait dome.

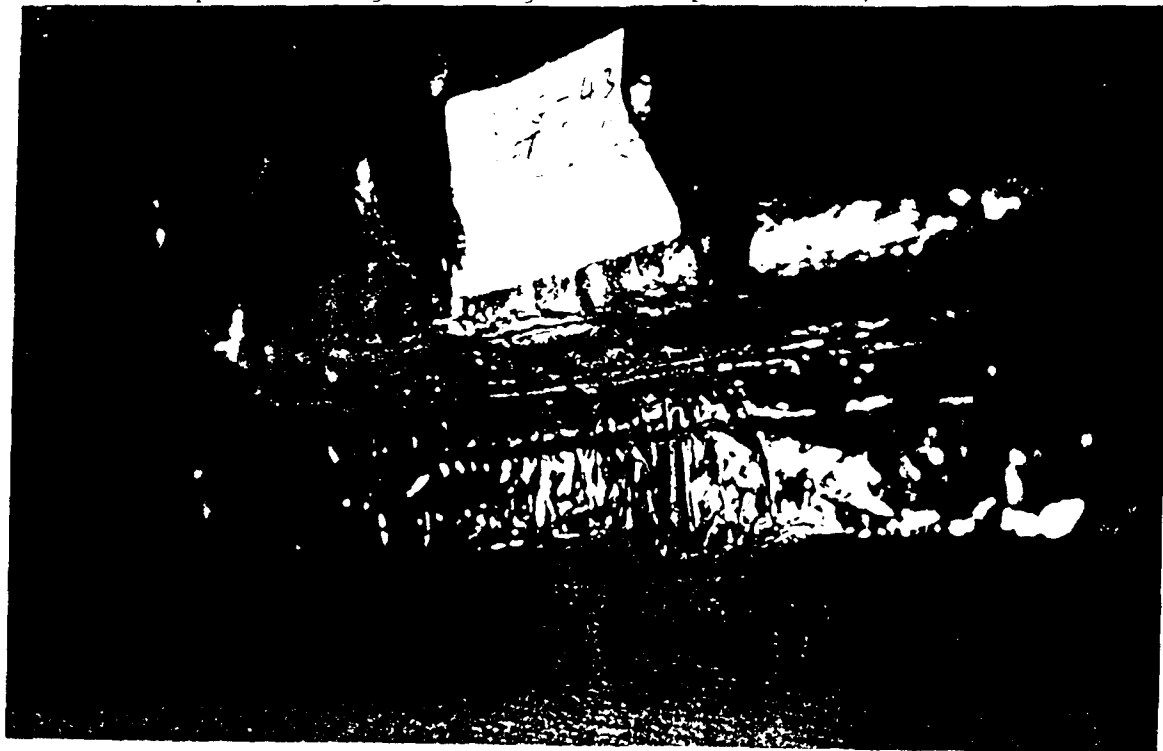


Figure 2b
Close up of damage through the repair area, on ait dome.

APPENDIX H

**RADIOGRAPHIC INSPECTION AND SUBSEQUENT EVALUATION OF
THE DAMAGED BEAD NECK REGION ON THE A063 KEEL DOME,
FORMERLY INSTALLED ON THE USS SIMPSON**



GEO-CENTERS, INC.

MEMORANDUM

May 14, 1991

From: James B. Nagode
To: Chester F. Poranski, Jr.

Subj: RADIOGRAPHIC INSPECTION AND SUBSEQUENT EVALUATION OF THE DAMAGED BEAD NECK REGION ON THE A063 KEEL DOME, FORMERLY INSTALLED ON THE USS SIMPSON.

Ref: (a) USS SIMPSON SRD INSPECTION TRIP, NRL Ltr 6120-03, 15 January 1991.

(b) BEAD NECK DAMAGE IN AN/SQS 56 SRD S/N A063: EX-USS SIMPSON SRD - INSPECTION TRIP #2: (AT BFGOODRICH, JACKSONVILLE, FL, 30 JANUARY 1991), NRL Ltr 6120-59, 1 March 1991.

REVIEW

The keel dome removed from the USS Simpson experienced two prior inspections where the following discoveries were made:

TRIP #1 (Ref a): The AS-1 filler appeared to be spongy and inhomogeneous in the area of the bead coinciding with water leakage. Further probing of this area met with little or no resistance. Voids were present running parallel to the bead neck, containing rust and mineral deposits.

TRIP #2 (Ref b): With bead clamps removed, kinked and broken bead wrap cords were seen along the bead neck. The bead neck itself appeared compressed, allowing a channel to form. A water entry point was established on the inside of the SRD.

RADIOGRAPHY

1. At least two bead wrap plies are affected directly. The two outer-most plies are kinked along the port side of the SRD.

2. At least one bead wrap ply (outer-most) is broken for an undetermined length, and possibly in multiple locations.

3. Excessive rust is present in the bead neck, at the very least the port side is affected. The potential is high that the entire bead neck has been contaminated with sea water (in view of the leak).

4. From a standard radiographic inspection (10/90), moderate structural damage is known to exist in the 22" bead band, and 20" keel band, both port and starboard.

DISCUSSION

Since structural damage exists in the bead neck region, it is difficult to believe that anything but a structural repair will yield acceptable results. In addition, sea water contamination has already predicted a shorter lifetime for this SRD. Even if a structural repair is implemented, the SRD's service life would be further limited by the onset of corrosion fatigue.

On the other hand, a structural repair presents some unique problems in the bead neck region. The first problem to note should be one of attachment and adhesion of ply. The curved and channelled profile of the bead neck would require specialized hardware and tooling to force the structural ply to conform. Once in place, it is doubtful that the ply would not delaminate over time. Since adhesion is paramount for the repair to be successful, a lack thereof would preclude any load transfer. Even if an effective structural repair could be made, the forces of the bead clamps against the repair ply, combined with mechanical flexure in the bead neck region, would likely cause a delamination to occur.

BF Goodrich engineers have expressed their doubts in being able to complete a successful structural repair of the bead neck region. In light of these data provided, we would not recommend that the A063 SRD be retained for service.

APPENDIX I

**PROPOSED CHANGES TO SONAR DOME RUBBER WINDOW (SDRW)
INSPECTION INTERVALS**



GEO-CENTERS, INC.

Ser 6120-164A
6 May 1992

Subj: PROPOSED CHANGES TO SONAR DOME RUBBER WINDOW (SDRW)
INSPECTION INTERVALS

- Ref: (a) "SDRW Radiograph Evaluation and Recommendations," NRL
Ltr 6120-120, Feb 20, 1986.
- (b) "Revised NRL Recommendations for Repaired Sonar Dome
Rubber Windows (SDRW)," NRL Ltr 6120-53, Feb 11, 1987.
- (c) "Revisions to NRL Technical Data Requirements for the
Radiographic Inspection of Sonar Dome Rubber Windows
(SDRW)," NRL Ltr 6120-2, Jan 1990.
- (d) "Assessment of Sonar Dome Rubber Window (SDRW)
Corrective Actions," NRL Ltr 6120-238, Jun 6, 1989.

- Appendix (1) Atlantic Fleet SDRW Inspection Schedule
(2) Pacific Fleet SDRW Inspection Schedule

1. Summary.

The purpose of this report is to propose an increase in the interval between radiographic inspections of 6-ply SDRWs, which are a significant sub-set of the SDRWs in service. The proposed change will result in cost savings due to the decreased inspection frequency. Additionally, it will be possible to meet the inspection requirement coincident with scheduled ship overhauls (ROH), eliminating the need for more costly waterborne (pierside) inspection methods. Such a liberalization is justified by a statistical analysis of cumulative inspection results.

2. Current inspection intervals.

The current radiographic inspection intervals are 12 months for SDRWs with known splice damage and 24 months for all others. In References (a) and (b) we recommended these intervals and set forth criteria for determining actions to be taken in response to inspection results. According to our scheme, each SDRW has a current "recommendation" based upon our most recent damage assessment. The recommendation attribute is maintained in our SDRW database along with a "status" attribute. The values of these attributes are used to provide an inspection due date for planning purposes and to flag ships which are overdue. Periodic reports are provided to the Fleet commands from this database to

Encl (1) to NRL Ltr Ser 6120-164
NRL Prob 61-1549

advise them of SDRW status, inspection due dates, and inspection priorities.

3. Drydock vs. pierside inspection.

Radiographic SDRW inspections can be accomplished using either drydock or pierside methods. Initially, standard radiography techniques were implemented in the drydock setting only. As the extent of the SDRW failure crisis became apparent, NRL developed a waterborne method to enable us to monitor those domes which could not be replaced for mission or logistic reasons. Also, we needed to assess the entire SDRW equipped fleet to identify all the damaged domes and accumulate data for failure analysis.

Pierside inspection capability has been important in the management of the SDRW failure problem. But the method is expensive. Divers are required to place film on the outside surface of the SDRW. Time limits apply to the divers and also to x-ray technicians working in the pressurized dome. The radiographic data is also inferior to that obtained in drydock, due to the less optimal inspection geometry. Poor quality data can also result from difficulties maintaining close film contact and preventing film movement underwater.

In Reference (c), we provided revised inspection coverage requirements for pierside inspections to lower the cost. Based upon an analysis of inspection data, coverage of areas with low damage probability was eliminated. But costs remain higher than drydock inspections and compliance with recommended schedules continues to be less than desired.

4. Improved SDRWs.

A number of engineering changes have been implemented in response to the SDRW failure problem. The changes seek to block the entry and migration of seawater to the SDRW splice, to strengthen the splice, and to redistribute the stress gradients present at splice edges. Table 1 chronicles milestones in the implementation of these improvements. Table 2 lists the current distribution of splice improvements in the fleet.

In Reference (c) we considered the question of how long inspection data must be accumulated before it can be shown that SDRW design changes are effective. A statistical procedure was selected for detecting a significant difference between two populations. The procedure was used to analyze the performance of the various improved sub-populations of SDRWs. We found that the best division between improved and unimproved SDRWs was based on the change from 5-ply to 6-ply construction. Although no 6-ply SDRWs had sustained any damage, operating times and numbers of inspections were too low at the time to satisfy the test for

significance. We recommended that the question be revisited after accumulating more data.

We have updated our statistical analysis of cumulative inspection results based upon data as of December 1991. In spite of one occurrence of damage in an improved SDRW (USS Cushing), the conditions to demonstrate lower risk of damage in improved SDRWs have now been satisfied.

5. Proposed inspection intervals.

We propose that undamaged 6-ply SDRWs be inspected during regular overhaul (ROH) availabilities. We understand that this interval is currently in the vicinity of 42 months for DD963 class destroyers. We propose that a limit of 48 months be used for due date purposes. The pierside inspection option should be used as necessary to prevent exceeding the 48 month limit. 5-ply SDRWs and damaged 6-ply SDRWs should continue to be inspected on 24 month and 12 month schedules, as in paragraph 2. Appendices 1 and 2 provide inspection schedules based upon the proposed intervals for the Atlantic and Pacific fleets, respectively.

6. Recommendations.

We recommend the following:

- (a) NAVSEA adopt the SDRW inspection intervals proposed in paragraph 5.
- (b) NRL incorporate the proposed intervals into the SDRW database system, making the necessary changes to data, structure, and program codes.
- (c) NRL provide a more detailed version of this report, containing an explanation of the statistical method and data used for our determination.


C. F. Poranski
Materials Chemistry Branch
Code 6120
Chemistry Division

APPENDIX J

**MECHANICAL, PHYSICAL, AND THERMAL PROPERTIES OF AN
ELECTRICALLY CONDUCTIVE HEAT RESISTANT POLYMER**



GEO CENTERS, INC.

MECHANICAL, PHYSICAL, AND THERMAL PROPERTIES OF AN
ELECTRICALLY CONDUCTIVE HEAT RESISTANT POLYMER

M. L. Warzel*, T. R. Walton, and C. M. Roland,

Naval Research Laboratory,

Washington, DC 20375-5000

*Geo-Centers, Inc., Ft. Washington, MD 20744

Synopsis

The mechanical, physical, and thermal properties of an electrically conductive, heat resistant polymer prepared by thermal cure of a completely conjugated acetylene-terminated resin, N,N'-(1,3-phenylenedimethylidene)bis(3-ethynylaniline), are reported. Properties of the isomer N,N'-(1,4-phenylenedimethylidene)bis(3-ethynylaniline) are also reported. The precursors are processed into materials with conductivities ranging from insulating to 10^{+2} S/cm. Materials processed from 150 °C to 400 °C in an oxygen-free environment show similar mechanical properties with tensile strengths of approximately 45 MPa, tensile moduli near 5 GPa, and strain to break values near 1.0 %. These materials all have conductivities below 10^{-9} S/cm. Materials processed above 400 °C show substantial improvements in electrical conductivity and mechanical properties. Specimens processed 100 hours at 800 °C in an oxygen-free environment, for example, have a room temperature electrical conductivity in excess of 10^{+2} S/cm, a tensile strength as high as 120 MPa, a tensile modulus of approximately 30 GPa, and a strain to break of 0.4 %. These materials are both thermally and oxidatively stable. A material with an initial conductivity of $3 \times 10^{+1}$ S/cm, for example, has an onset of oxidative degradation at 525 °C and only an 18 % weight loss at 900 °C in an inert atmosphere. Due to their high temperature and oxidative stability in aggressive environments these polymers should find applications as stable electrically conductive materials as well as heat resistant resins for carbon-carbon and carbon-glass composites.

INTRODUCTION

Our approach to the development of electrically conducting organic materials that have high stability in aggressive environments is based on the synthesis of polymers with extended π -electron delocalization. The precursors are soluble and meltable, and completely conjugated with reactive end groups that are capable of being polymerized into conjugated/aromatic linking groups to form the polymer structure. Although detailed structural information is difficult to obtain, ideally, the resultant structure is expected to be a completely conjugated polymer network. Due to the extended conjugation, these materials are intrinsically conducting without the necessity of adding reactive dopants that would render the material sensitive to oxygen, water, and/or heat. With our approach, highly stable conductivity has been achieved. For example, a material with a conductivity of 3 S/cm has shown no change in conductivity after

1000 hours in boiling water. Similarly, exposure of the material to 500 °C for 500 hours in an oxygen-free atmosphere gave no change in the room temperature conductivity.

Earlier papers have described the synthesis, characterization, and polymerization of acetylene-terminated and ortho-dinitrile terminated precursors, as well as their conversion into environmentally stable conductive polymers⁽¹⁻³⁾. In general, the precursors, are thermally polymerized as a melt at 120-300 °C for a few hours and then postcured in an air environment at 300 °C for 50 hours. Actually, this is a much longer cure time than required; for example, the acetylene groups are completely reacted after a few hours at 250-300 °C. Other polymerizable groups under investigation, however, are much less reactive and longer cures are required. For comparative purposes, all the materials have been cured under identical conditions. Following the 300 °C cure, the polymers are insulators ($< 10^{-12}$ S/cm); conductivity develops on further processing at higher temperatures in an inert atmosphere. Although extended processing conditions have been used as a means of standardizing the treatment of these materials, it is important to emphasize that these conditions are not necessarily optimal. Long processing times are used to minimize the effects of heating and cooling cycles relative to the isothermal stage, to establish thermal equilibrium in the furnace, to help define thermal stability, and to minimize small time/temperature errors. Faster processing is possible.

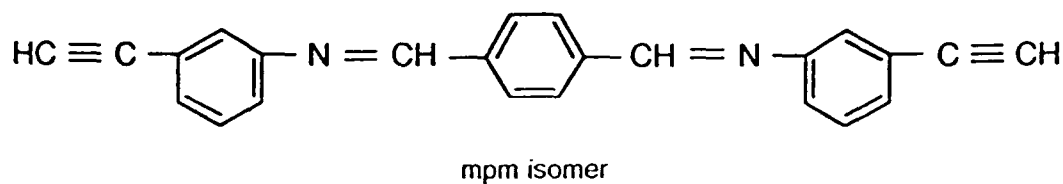
Interest in acetylene-terminated resins (ATR) and precursors is high and a large number of systems have been synthesized and studied by the Air Force, NASA, Hughes, Gulf Research, National Starch, and others. Several reviews are available in this area⁽⁴⁻⁶⁾. However, with the exception of some work by Rossi et al.⁽⁷⁻⁹⁾, in which the structure of the central aromatic ring was extensively varied and the interior conjugation extended in the precursor, this is the only ATR system that has been successfully processed at high temperatures into conductive polymers.

The present report details the mechanical, physical, and thermal properties of a conductive polymer prepared from an all-meta acetylene-terminated resin precursor. The processibility of this isomer is excellent⁽³⁾, allowing for easy preparation of mechanical test specimens with minimal or no damage encountered as specimens are processed at higher temperatures. Additional property data are also presented for polymers prepared from the meta-para-meta isomer of this precursor.

EXPERIMENTAL

Processing

The synthesis and characterization of the all-meta (mmm) acetylene-terminated resin, N,N'-(1,3-phenylenedimethylidene)bis(3-ethynylaniline), and the meta-para-meta (mpm) isomer, N,N'-(1,4-phenylenedimethylidene)bis(3-ethynylaniline), have been previously described⁽¹⁻³⁾.



Unless otherwise noted, the mmm precursor was thermally cured in an air environment for 2 hours at 120 °C, 1 hour at 145 °C, 2 hours at 150 °C, 1 hour at 200 °C, 1 hour at 250 °C, and 50 hours at 300 °C. Physical and mechanical test specimens were cured for 24 hours at 155 °C in silicone molds. Specimens cured above 155 °C were free-standing. The mpm precursor was thermally cured in an air environment for 2 hours at 150 °C, 1 hour at 200 °C, 1 hour at 250 °C, and 50 hours at 300 °C.

A standardized heating procedure was used to process the samples into conductive polymers. Following the 300 °C cure in air, samples were successively heated in an argon atmosphere to 400 °C for 100 hours, 500 °C for 100 hours, and so on in 100 °C increments to 800 °C. Property measurements were obtained following each 100 hour period. Heating and cooling rates were 0.5 °C/min.

Mechanical Measurements

Tensile measurements at room temperature were carried out with an Instron 4206 instrument at a crosshead speed of 0.508 mm/min. Tensile strength measurements were made with a minimum of three ASTM D638 type V specimens at a grip separation of 1.0 in. Tensile moduli were obtained on rectangular or dogbone shaped specimens with a clip-on strain gage mounted at a gage length of 1.0 in. The end tabs for all specimens were potted in Epon 828/Versamid 140 (1:1 by weight) to allow firm gripping without

any premature fracture in the grips. Strain values were calculated from tensile strength and modulus data assuming completely brittle failure.

Dynamic mechanical measurements were obtained with a Dupont 982/1090 system at a heating rate of 2 °C/min and nitrogen flow rate of 100 ml/min. A length correction of 1.00 was measured for a sample processed to 300 °C, and 1.50 for a sample processed to 600 °C. Oscillation amplitude was set at 0.05 mm, and a value of 0.33 was assumed for Poisson's ratio. Dynamic property measurements were also obtained with an Imass Dynastat Mark II instrument.

Thermogravimetric and Thermomechanical Analysis

Thermogravimetric analysis (TGA) was performed on approximately 4 mg samples with a Perkin-Elmer TGA 7 instrument at a heating rate of 10 °C/min. Thermal stability was determined in an argon atmosphere and oxidative stability in an air environment at purge flow rates of 100 ml/min. Powdered samples were used to standardize the level of oxidation during heating.

Thermal expansion measurements were performed on cylindrical specimens 3-6 mm in diameter and 6-12 mm in height with a Perkin-Elmer TMA 7 instrument using a quartz expansion probe. Measurements were made over the temperature range 45-55 °C at a heating/cooling rate of 1 °C/min and an applied force of 1 mN.

Density Measurements

Bulk density measurements were performed by immersion of specimens in vacuum degassed, deionized water at 24.0 °C using a 25 ml pycnometer. A minimum of five measurements were recorded for each sample cure temperature with several specimens having weights ranging from 0.3 to 0.7 g.

RESULTS AND DISCUSSION

Mechanical Properties

Tensile measurements for the mmm ATR materials are shown in Figure 1 for specimens processed at temperatures up to 800 °C. The high process temperatures used to increase electrical conductivity results in a significant increase in tensile strength and modulus. Two distinct property regimes are evident. Below 400-500 °C, mechanical properties are relatively insensitive to the process temperature. Tensile strengths of approximately 45 MPa, tensile moduli of 4-5 GPa, and strain to break values near

1.0% are obtained. Processing above 400 °C, however, markedly changes the mechanical properties. For example, following 100 hours at 800 °C, a tensile strength as high as 120 MPa, a tensile modulus of approximately 30 GPa, and a strain to break near 0.4% are obtained. These results, along with others to be discussed later, indicate that the polymer network is being extended and further crosslinked during exposure to high process temperatures. As less stable bonds are broken more stable bonds are formed, extending the conjugated network and π -band delocalization that are accompanied by improved mechanical properties and, presumably, increased electrical conductivity.

The precision in the tensile strength data, represented by one standard deviation in Figure 1, clearly indicates that improvement in the structural properties is occurring during high temperature processing. Similar error bars for tensile moduli measurements are not shown due to the improved repeatability of these measurements for individual specimens as well as the limited number of samples tested. Failure strain values were not directly measured but instead were calculated from tensile strength and modulus data assuming completely brittle failure in the type V specimens.

Preliminary studies of the influence of uniaxial stress on electrical conductivity have also been undertaken. Results for two specimens with conductivities of 1.1 S/cm and 1.1×10^{-2} S/cm, respectively, have indicated that the conductivity remains constant up to the point of failure with no influence of repeated stress cycling. Provided the electrical conductivity is intrinsically associated with the network, conceivably the distortion of bond lengths and angles accompanying deformation would influence the electrical behavior. Indeed, one might expect an increase or decrease in conductivity depending on whether strain improved or distorted the π -bond alignment. The observed insensitivity of conductivity to strain may simply be due to the small magnitude of the strain in these highly crosslinked, rigid materials.

Dynamic moduli for the mmm ATR materials are shown in Figure 2. The mechanical response was measured for a sample processed at 300 °C for 50 hours followed by processing to 600 °C for 60 hours. The relative stability of the modulus at high temperatures is evident following each processing period. Although a few apparent transitions are shown following processing at 600 °C, a detailed analysis of this behavior has not been made.

Similar measurements on the mpm ATR materials have also been performed. Figure 3 shows data from several preparations and repeated runs of the mpm materials processed at 300 °C for 50 hours and 600 °C for 60 hours. The reproducibility shown is very good and the results indicate that a significant retention of the modulus is obtained at high temperatures for both ATR materials.

Although the dynamic mechanical response is quite similar for both isomers after the initial 300 °C cure, processing the materials to 600 °C results in significant differences in this behavior. The mmm isomer shows a higher room temperature modulus than the mpm isomer (17 vs 14 GPa) that decreases more rapidly at higher temperatures (8.5 vs 10.5 GPa at 500 °C, for example). At present the reasons for these differences are unknown; further work in this area is necessary before any substantive arguments concerning this behavior can be presented.

It should be emphasized that data collected with the DuPont 982 instrument is based on the natural resonance frequency of the sample, which changes with temperature. In these studies, the frequency varied from 32 Hz at room temperature to 14 Hz at 500 °C. In order to assess how these frequency changes might affect the modulus measurements, a Dynastat Mark II instrument was used to measure the dynamic properties of mmm ATR materials. These experiments were performed on a sample processed to 400 °C for 100 hours over a range of frequencies and amplitudes at temperatures up to 200 °C (Table 1). Only a modest frequency dependence of the dynamic modulus is observed, consistent with an absence of significant viscoelastic motions in these highly crosslinked materials (the loss tangent is typically less than 0.01). The variation in frequency associated with the dynamic mechanical results should therefore exert a negligible effect on the measured moduli.

Comparisons of dynamic modulus data obtained with both instruments for the mmm ATR materials and tensile moduli data previously discussed show similar values. At room temperature, the storage modulus measured by DMA and the Dynastat are about the same, approximately 4 GPa. Tensile modulus measurements, as previously mentioned, are within the 4-6 GPa range for materials processed up to 400 °C. For samples processed to 600 °C for 60 hours, the dynamic modulus is near 14 GPa, while tensile moduli for samples processed to 600 °C for 100 hours are 18-19 GPa.

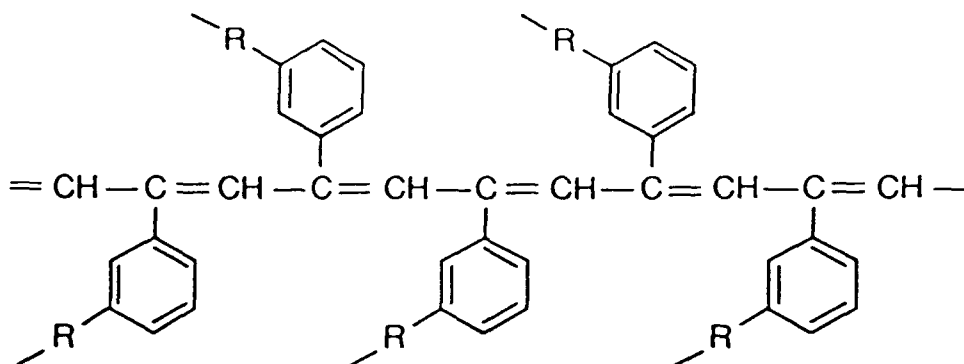
Thermal and Oxidative Stability

Thermal stability of the mmm ATR material in an inert atmosphere is illustrated in Figure 4. Both weight loss (Figure 4) and electrical conductivity (Figure 5) increase asymptotically with higher processing temperatures, reaching values of 13.3 % and 113 S/cm at 800 °C, respectively. A corresponding increase in linear shrinkage is associated with this weight loss⁽²⁾. Samples processed at these temperatures have shown excellent integrity with no cracking or failure observed during processing.

Figures 6 and 7 show TGA oxidative and thermal stability of mmm ATR materials (powdered) in air and nitrogen environments, respectively. The samples for this study were cured to 250 °C in air for 2 hours rather than only 1 hour. One sample was removed and the remaining samples were then transferred to an furnace for oxygen-free processing to 300 °C for 50 hours, 400 °C for 100 hours, 500 °C for 100 hours, 600 °C for 100 hours, and 700 °C for 100 hours. After each 100 °C interval the samples were cooled to room temperature, and one specimen was removed for TGA analysis.

In an oxidative environment very little difference in the weight stability is observed for samples initially cured at 250 °C and further processed up to 500 °C. At processing temperatures above 500 °C, however, a continuing improvement in the oxidative stability is seen (curves 1 and 2 in Figure 6). The temperature at which complete degradation occurs in an air environment is also higher than for samples processed up to 500 °C.

A slight weight increase in air is noted between 275-400 °C for samples processed at 250 °C, 300 °C, and 400 °C. Final catastrophic degradation occurs at approximately 525 °C. This weight increase is due to the formation of oxidation products in the polymer. Infra-red studies have indicated the formation of carbonyl groups under these conditions. This is believed to occur in the conjugated polyene structure that forms during the initial thermal polymerization of all acetylene-terminated resins⁽¹⁰⁾:



Such an unsaturated polyene is expected to be sensitive to oxidation. For samples processed at higher temperatures (> 400 °C), these structures are converted into aromatic or condensed aromatic ring structures that are not readily oxidized. Thus, samples processed at temperatures of 500 °C and above do not exhibit any weight gain.

It is apparent from these observations that the bulk, solid polymer may react with oxygen in a diffusion controlled process, even though no weight loss occurs for extended cures in air at 300 °C. Although any oxygen uptake may be expected to increase moisture absorption, no differences in electrical conductivity were observed between samples cured in air and samples cured in an air-free environment.

Infra-red studies for specimens cured at 150 °C have shown the presence of unreacted terminal acetylene groups, indicating an incomplete cure in these materials⁽³⁾. After 50 hours at 300 °C, the acetylene C-H absorption can no longer be observed by FTIR, indicating substantially complete reaction. Actually, infra-red absorptions by terminal acetylenic groups are absent from the FTIR spectrum after a few hours at 300 °C, but all samples were processed for 50 hours at this temperature as a means of standardizing the process conditions.

The thermal stability in a nitrogen environment (Figure 7) shows a similar improvement as samples are processed at higher temperatures. The fact that the 250 °C and 300 °C processed samples exhibit some weight gain in the 300-400 °C region indicates a trace amount of oxygen in the nitrogen carrier gas. The gradual weight loss, approximately 2.5%, from 30-450 °C is primarily absorbed water⁽²⁾.

The lower weight loss observed in TGA samples processed at higher temperatures can, in part, be attributed to prior weight loss during processing. The extended controlled processing may actually

increase the thermal and oxidative stability thereby contributing to the observed lower weight loss. For example, the difference in weight loss between a sample processed at 600 °C for 100 hours followed by 700 °C for 100 hours (Figure 6) is only approximately 0.4%. TGA weight loss data, by comparison, shows a difference of approximately 2.5% between the two samples at 700 °C and 7% at 900 °C rather than the 0.4% that might be expected if the improvement were due totally to additional weight loss during the 700 °C processing. Since the TGA experiment involves a more aggressive thermal treatment (continuous heating to 900 °C at 10 °C/min) compared to the processing conditions (heating rates of 0.5 °C/min and long isothermal times of 100 hours before processing to the next higher temperature), the stable structures that develop during processing may not have time to form at the higher temperatures in the TGA before decomposition begins. Polyene structures formed in the initial polymerization, for example, are much less stable than the condensed aromatic ring structures that form at higher temperatures. Since the solid state multimolecular reactions that are occurring at these higher temperatures are relatively slow processes, a too rapid heating schedule can fragment the polyenes, forming volatile species, before they have condensed into aromatic structures.

Physical Properties

Thermal expansion and density were measured to determine the influence of process conditions on the bulk structural properties of mmm ATR materials. In addition, these properties are important for materials intended for applications in high temperature composites. Table 2 summarizes the thermal expansion coefficients of mmm ATR materials measured at 50 °C. Linear expansion coefficients vary by an order of magnitude for samples cured below 400 °C as compared with samples cured to 800 °C. Following the 300 °C cure, for example, the coefficient is $4.3 \times 10^{-5}/^{\circ}\text{C}$; after processing for 100 hours at 700 °C the coefficient is reduced to $0.4 \times 10^{-5}/^{\circ}\text{C}$. As with the mechanical properties, it appears that most of the variation in the expansion coefficient occurs during processing at temperatures where the electrical conductivity increases most rapidly (400-600 °C). In comparison with crosslinked epoxy resins exhibiting coefficients near $50 \times 10^{-6}/^{\circ}\text{C}$, the mmm ATR material cured at 700 °C is a much closer match to the thermal expansion coefficients of typical composite fibers such as graphite (parallel: $-0.75 \times 10^{-6}/^{\circ}\text{C}$; radial: $10 \times 10^{-6}/^{\circ}\text{C}$) and E glass ($4.9 \times 10^{-6}/^{\circ}\text{C}$) and thus may reduce the thermal stress between fiber and

polymer during heating and cooling. It is expected that dimensional changes in structural components would also be reduced for these materials.

A continued increase in density for mmm ATR materials processed at higher temperatures is evident with most of the increase again occurring over the 400-600 °C range (Figure 8). Interestingly, a nearly constant density is observed for materials processed above 700 °C, accompanied by slight increases in the weight loss and linear shrinkage⁽²⁾. While experimental error may account for some small differences in the values between 700-800 °C, it is important to note that significant improvements in electrical conductivity and mechanical properties are realized by processing at these temperatures.

SUMMARY AND CONCLUSIONS

Earlier papers have demonstrated that acetylene-terminated resin systems yield materials with stable conductivities when exposed to aggressive environments. The present report demonstrates that the mechanical, physical, and thermal properties of a polymer prepared by thermal cure of a completely conjugated acetylene-terminated resin, N,N'-(1,3-phenylenedimethylidene)bis(3-ethynylaniline), are significantly improved during processing at the high temperatures used to increase conductivity. Both tensile modulus and strength significantly increase when inert processing is extended to 800 °C. Two distinct regimes for materials processed below and above 400 °C are also evident. Materials processed from 150 °C to 400 °C in an oxygen-free environment show relatively invariant mechanical properties: tensile strengths are near 45 MPa, tensile moduli near 5 GPa, and strain to break values near 1.0 %. These materials all have conductivities below 10^{-9} S/cm. Materials processed above 400 °C show increased electrical conductivity and mechanical properties. Specimens processed 100 hours at 800 °C in an oxygen-free environment, for example, have a room temperature electrical conductivity in excess of 10^{+2} S/cm, a tensile strength as high as 120 MPa, a tensile modulus of approximately 30 GPa, and a strain to break of 0.4 %. These materials also retain their dynamic properties at elevated temperatures, with moduli of 14 GPa at room temperature and 10 GPa at 500 °C for the mpm isomer, and 17 GPa and 8.5 GPa, respectively, for the mmm isomer. The high oxidative and thermal stability has also been demonstrated, with a 5% weight loss at 575 °C in air and 625 °C in argon for samples processed to 700 °C; at 900 °C in argon the weight loss is only 17.5%. Although the high crosslink density of these polymers

results in a relatively brittle material, the resulting low coefficient of thermal expansion ($4 \times 10^{-5}/^{\circ}\text{C}$ to $4 \times 10^{-6}/^{\circ}\text{C}$ at 50°C) should help to minimize thermal stresses. Finally, although our initial interest in the development and application of these materials was due to their conductivity, the demonstrated high temperature stability and mechanical properties suggests potential applications in heat resistant composites, and carbon-carbon and carbon-glass composites.

ACKNOWLEDGEMENT

This research was partially funded by the Naval Air Development Center, Warminster, PA under their 6.2 Airborne Materials Block Program and we specifically thank Mr. Irv Shaffer and Dr. Leonard Buckley of that Laboratory for this support.

REFERENCES

1. Walton, T.R., Griffith, J.R., and Reardon, J.P., *J. Appl. Polym. Sci.*, **30**, 2939, (1985).
2. Walton, T.R., *J. Appl. Polym. Sci.*, **33**, 971, (1987).
3. Walton, T.R., *J. Appl. Polym. Sci.*, **37**, 1921, (1989).
4. Denny, L.R., Goldfarb, I.J., and Lee, C.Y-C, Int'l SAMPE Symposium, "Materials Science for the Future", 153, Apr. 7-10, 1986.
5. Hergenrother, P.M., *J. Macromol. Sci. Rev. Macromol. Chem.*, C19 (1), 1, (1980).
6. Hedberg, F.L., Kovar, R.F., and Arnold, F.E., "Acetylene Containing Heterocyclic Polymers", *Contemporary Topics in Polymer Science*, Eli Pearce, Ed., vol. 2, Plenum Publishing Corp., NY (1977).
7. Rossi, R.D., Capo, D.J., Fenelli, S.R., and Machiesky, P., 18th Int'l. SAMPE Technical Conf., Seattle, WA, 959, Oct. 7-9, 1986.
8. Rossi, R.D., et al., U.S. Pat. 4,730,032, Mar. 8, 1988.
9. Rossi, R.D., Fenelli, S.R., and Hartman, E., "New Processable Acetylene Functional Schiff's Base Monomers and Oligomers. Study of Their Thermal and Electrical Properties", SPE, Atlanta, Apr. 18, 1988.
10. Koenig, J.L., and Shields, C.M., *J. Polym. Sci. Polym. Phys. Ed.*, **23**, 845, (1985).

TABLE 1
TEMPERATURE AND FREQUENCY DEPENDENCE OF THE
STORAGE MODULUS FOR mmm ATR MATERIALS CURED AT 400 °C

TEMPERATURE (°C)	STORAGE MODULUS (GPa)			
	0.01 Hz	0.1 Hz	1.0 Hz	10.0 Hz
40.0	3.82	3.84	3.89	3.97
79.7	3.71	3.85	3.91	3.95
128.0	3.71	3.75	3.82	3.87
163.8	3.53	3.66	3.74	3.79
199.4	3.51	3.63	3.70	3.74

TABLE 2
THERMAL EXPANSION COEFFICIENTS AT 50 °C FOR mm ATR
MATERIALS PROCESSED AT ELEVATED TEMPERATURES

PROCESS TEMPERATURE (°C)	THERMAL EXPANSION COEFFICIENT (°C ⁻¹ x 10 ⁺⁵)
155	3.9
300	4.3
400	3.0
500	1.1
600	0.6
700	0.4

FIGURE CAPTIONS

Fig. 1. Room temperature tensile strength, tensile modulus, and failure strain of the mmm ATR polymer processed at elevated temperature. Measurements were made at 0.508 mm/min. Ordinate error bars are for 1 standard deviation in the sample. Two regimes are clearly indicated for materials processed below and above 400 °C; at higher process temperatures, increases in conductivity are accompanied by improved mechanical properties.

Fig. 2. Dynamic mechanical spectra under inert environment for an mmm ATR sample processed at 300 °C for 50 hours, followed by processing up to 600 °C for 60 hours.

Fig. 3. Dynamic mechanical spectra under inert environment for an mpm ATR sample processed at 300 °C for 50 hours, followed by processing up to 600 °C for 60 hours. Numbered curves indicate successive experiments under conditions detailed in the text.

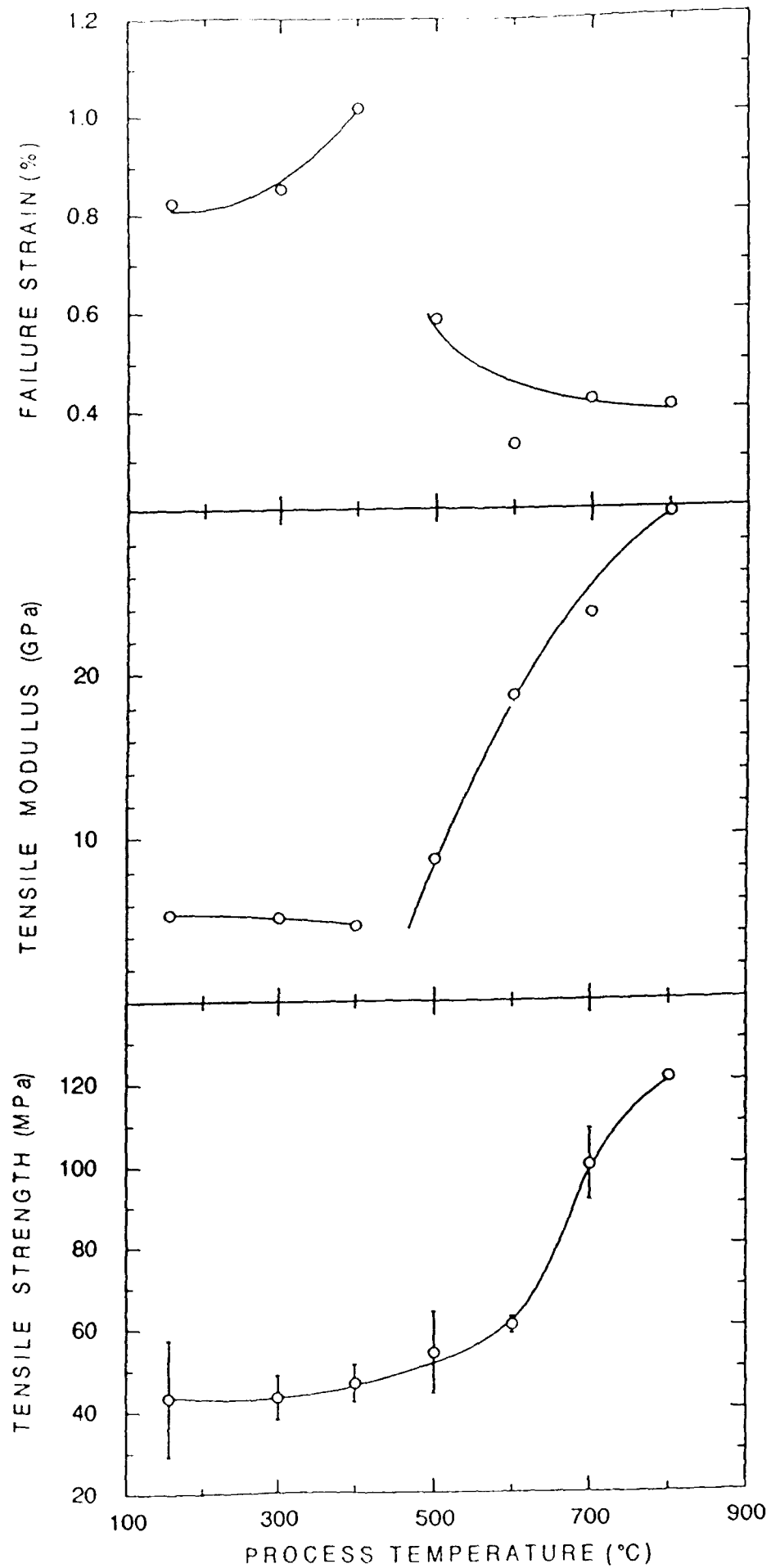
Fig. 4. Cumulative weight loss for the mmm ATR polymer processed at elevated temperature.

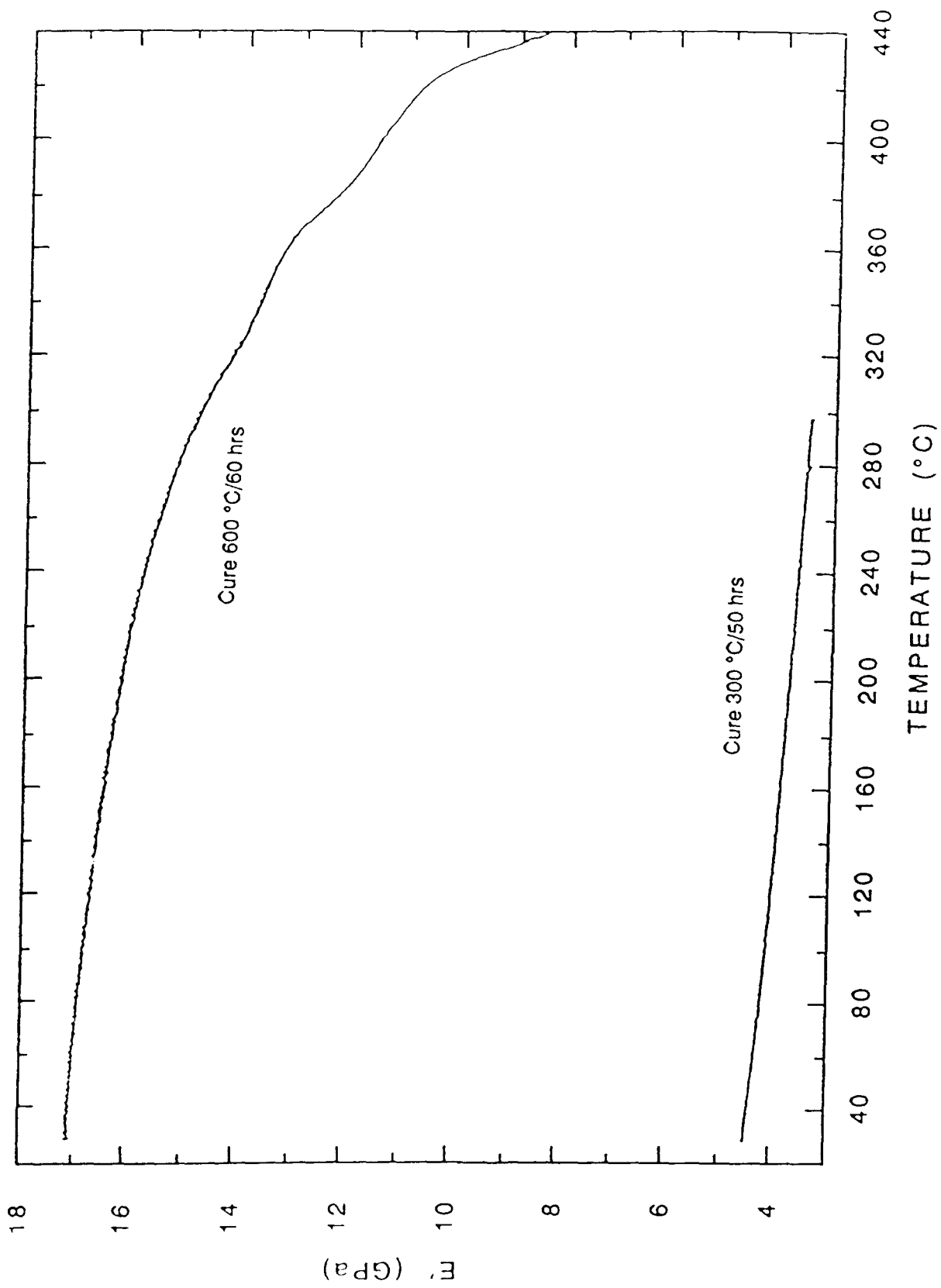
Fig. 5. Room temperature electrical conductivity of the mmm ATR polymer processed at elevated temperature as measured by the four-point probe technique⁽²⁾.

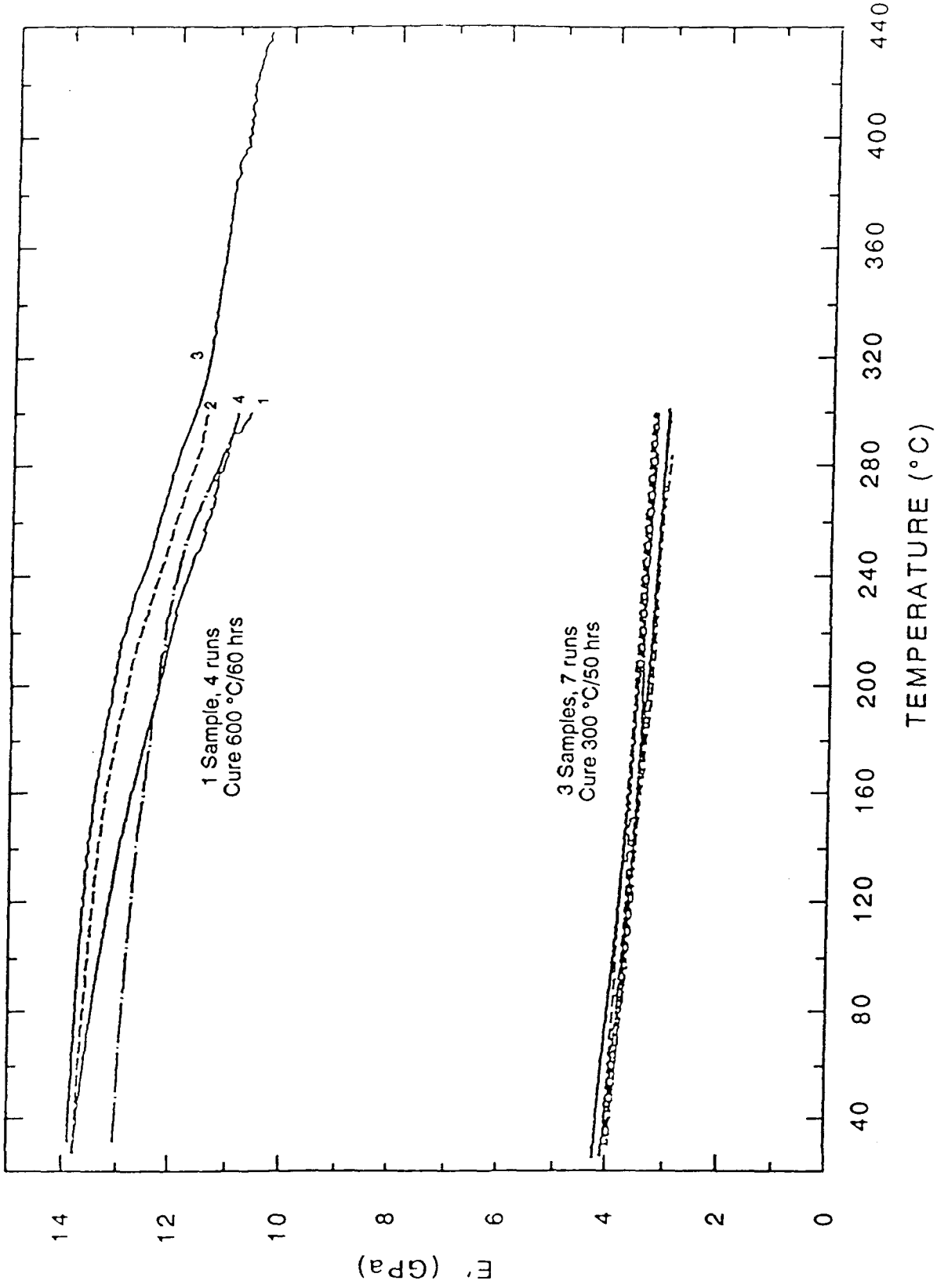
Fig. 6. Oxidative stability of mmm ATR polymer powders processed at elevated temperature as measured by TGA in air. A continuing improvement in the oxidative stability is indicated for materials processed above 500 °C.

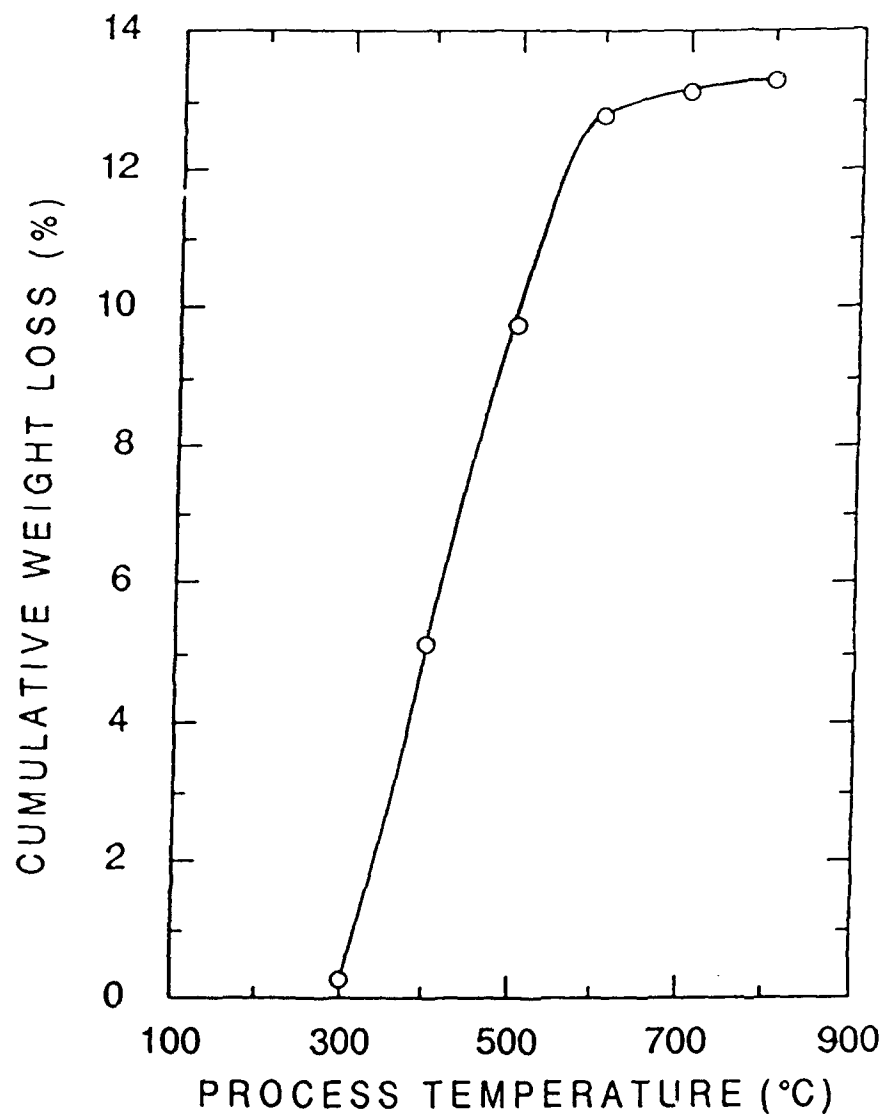
Fig. 7. Thermal stability of mmm ATR polymer powders processed at elevated temperature as measured by TGA in nitrogen. A continuing improvement in the thermal stability is observed for materials processed at higher temperatures.

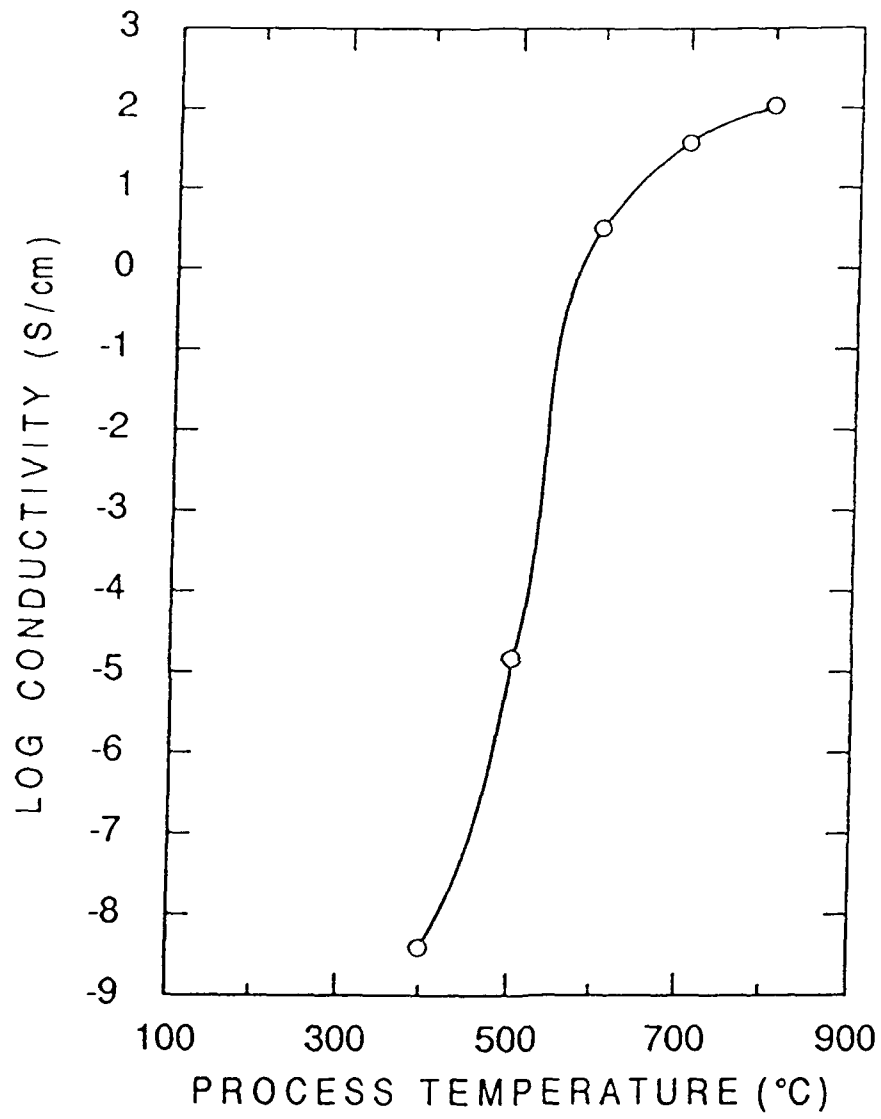
Fig. 8. Bulk density of the mmm ATR materials measured at 24.0 °C by immersion in distilled water. Increases in density parallel the increase in structural development above 300 °C with a plateau at 700 °C and above. Ordinate error bars are for 1 standard deviation in the sample.

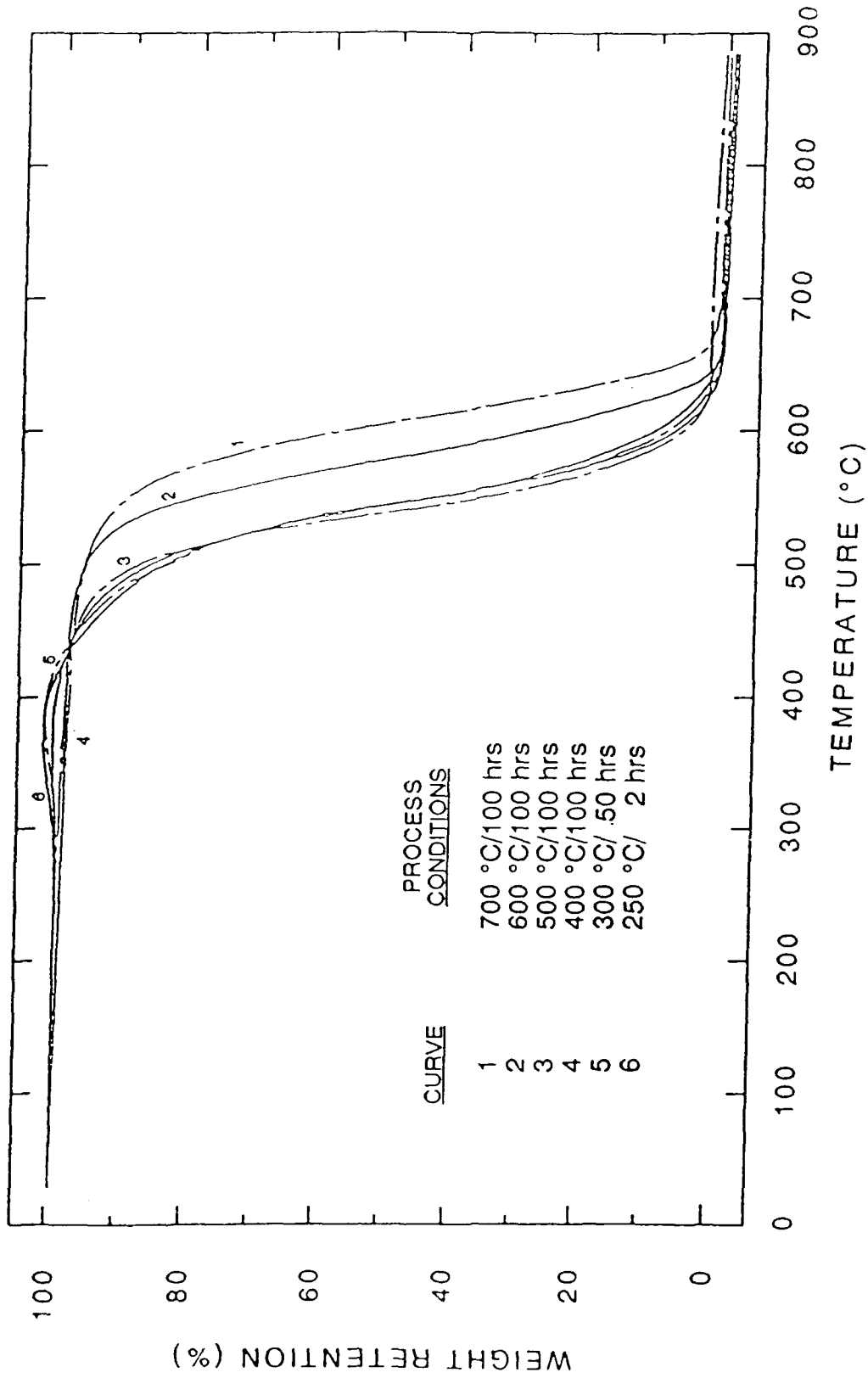


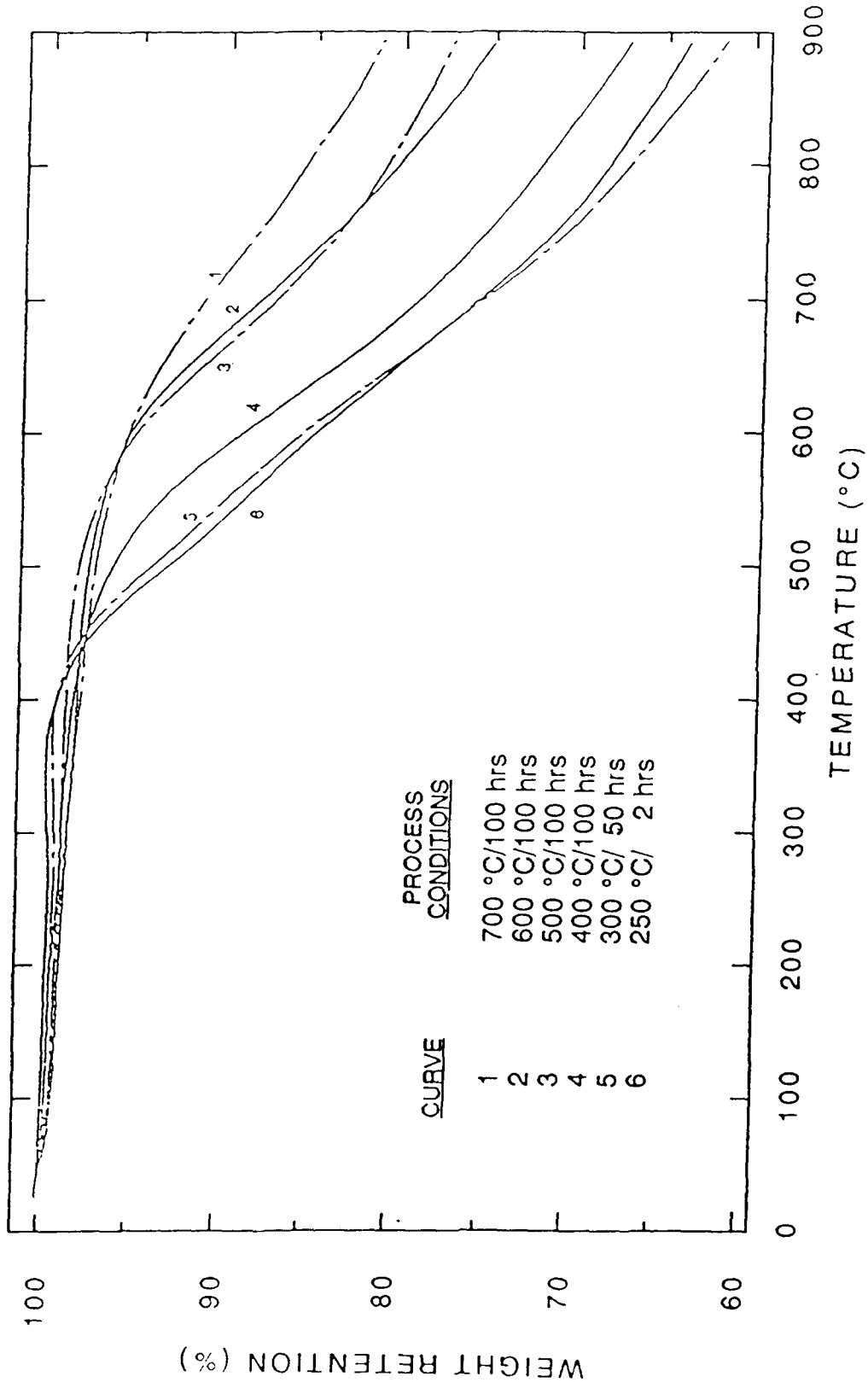


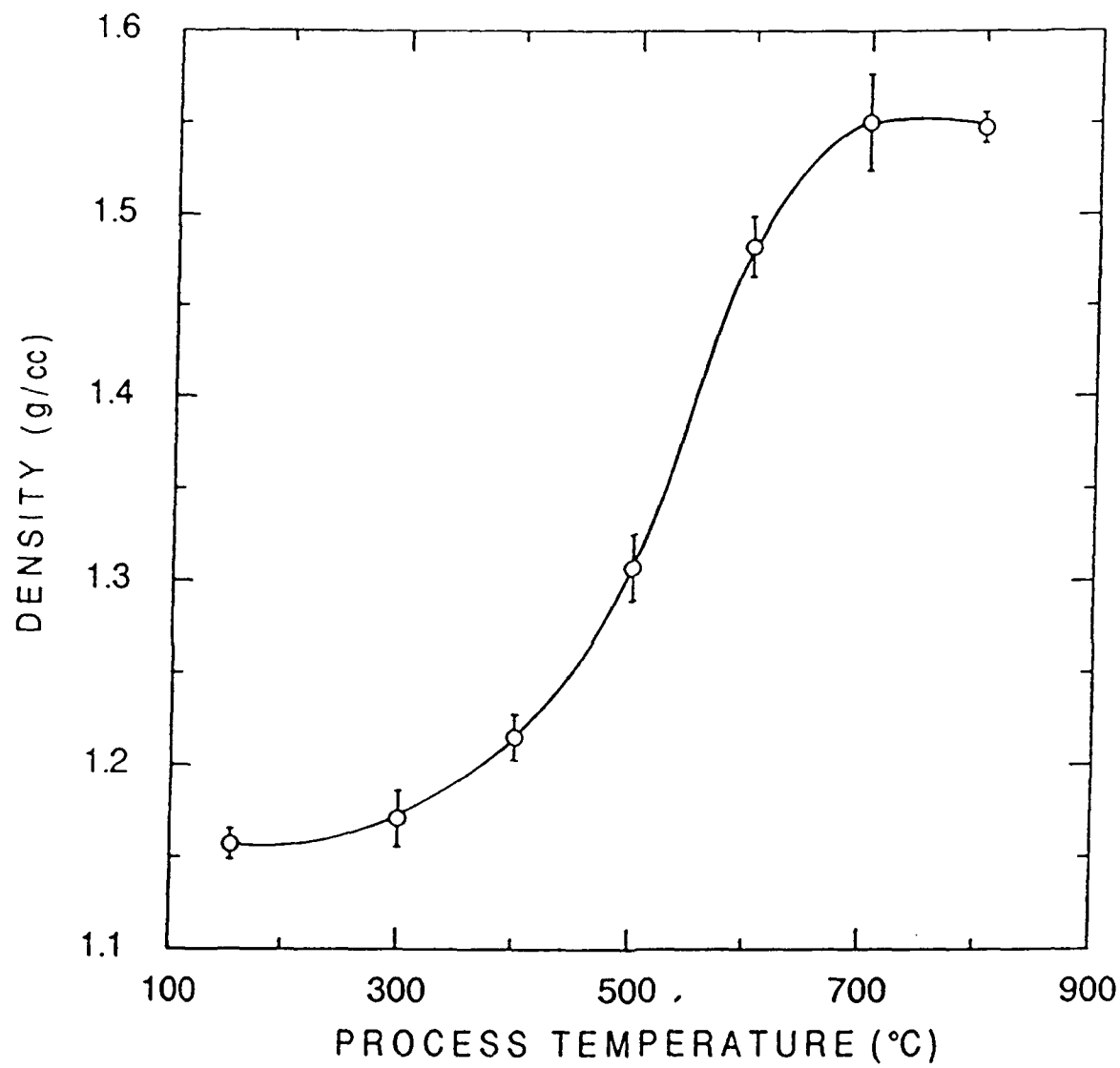


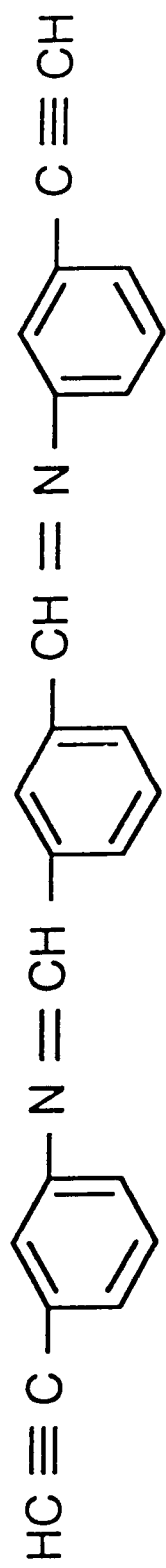


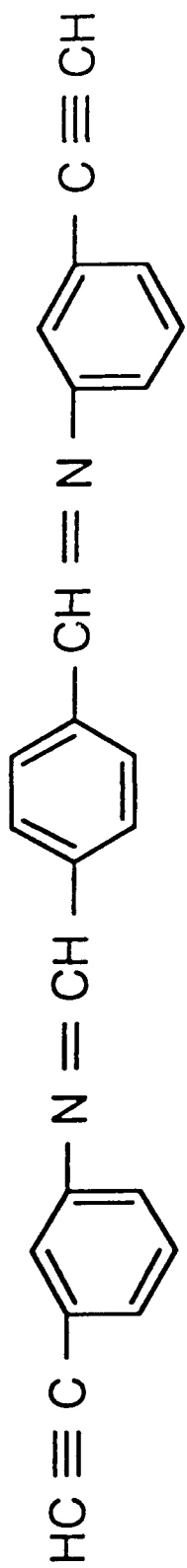


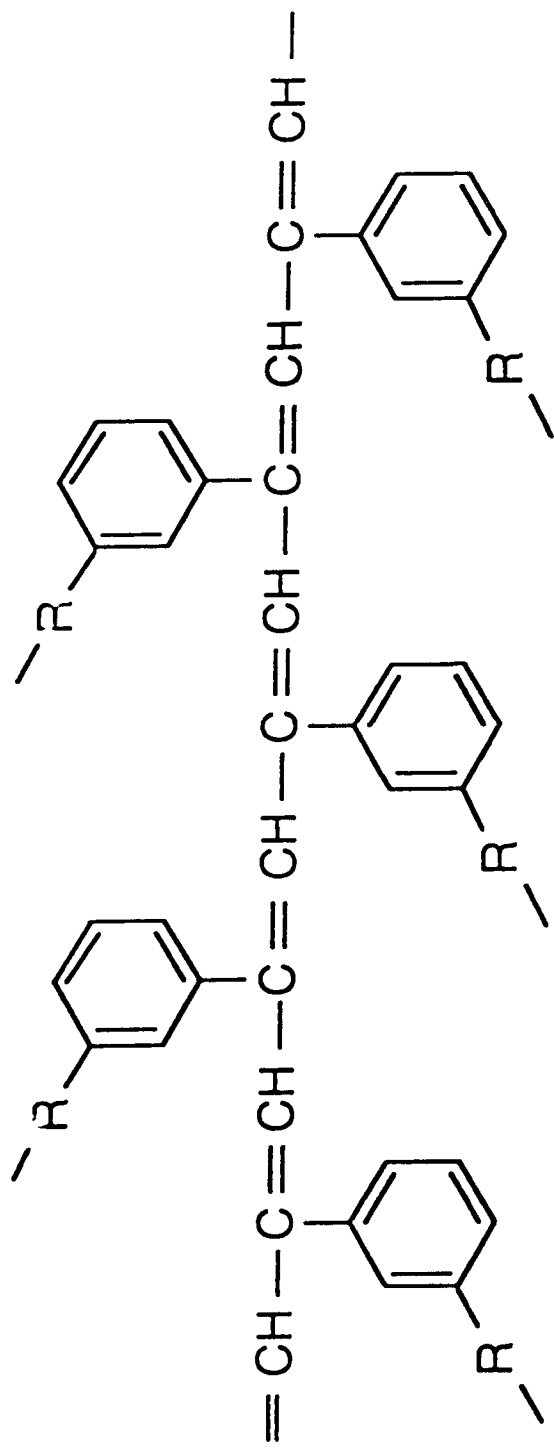












APPENDIX K
**TENSILE AND FRACTURE PROPERTIES OF A PHTHALONITRILE
POLYMER**



GEO-CENTERS, INC.

TENSILE AND FRACTURE PROPERTIES OF A PHTHALONITRILE POLYMER

M. L. Warzel* and T. M. Keller†

Materials Chemistry Branch

Chemistry Division, Code 6120

Naval Research Laboratory,

Washington, DC 20375-5000, USA

*Geo-Centers, Inc., Ft. Washington, MD 20744, USA

†To whom correspondence should be addressed

Synopsis

The properties of a polymer prepared from an aromatic diether-linked phthalonitrile resin, 4,4'-bis(3,4-dicyanophenoxy)biphenyl, and cured with 1,3-bis(3-amino phenoxy)benzene are reported. The resin is easily processed from the melt of the monomer in a controlled manner as a function of the amine content and processing conditions. The resulting polymers show an excellent retention of mechanical properties following inert atmosphere postcure to 375°C and oxidative aging at 315°C for 100 h. Results are reported for the effects of cure, postcure, and aging conditions on the tensile and fracture properties of these polymers.

(Keywords: phthalonitrile; mechanical properties; fracture toughness; double torsion; elevated temperature; thermal stability)

Introduction

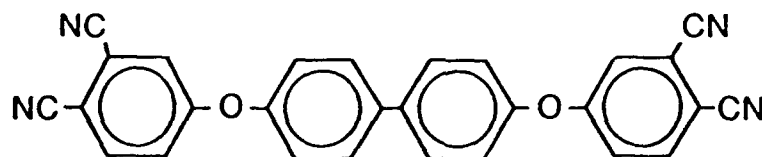
Organic polymers that are both thermally and oxidatively stable above 315°C (600°F) are in demand as matrix materials for advanced composite applications, as adhesives for high temperature materials, and as weight-reducing replacement materials for metals. A new class of phthalonitrile-based polymers¹⁻³ with excellent thermoxidative properties has been under investigation for application in these areas. The phthalonitrile monomers are readily converted to crosslinked thermosetting polymers in the presence of thermally stable aromatic diamines⁶. The polymerization reaction occurs through the terminal phthalonitrile units which are interconnected by aromatic dioxy linkages, yielding heterocyclic crosslinked materials. Shaped components are easily processed by heating the polymerization mixture above its melting point or glass transition until gelation occurs. The prepolymers formed from these monomers are soluble in common solvents and indefinitely stable at room temperature.

Previous investigations of the properties of these materials have shown a high retention of weight and mechanical properties following exposure to elevated temperatures and oxidative conditions. Keller et. al. have reported the dynamic mechanical behavior^{1,2,5,7}, the thermal and oxidative weight loss for various cure and aging conditions^{1-3,5-8}, the network characteristics and

glass transition behavior^{1,2}, and the conductivity behavior of phthalonitrile-based materials³. However, little information exists concerning the failure properties of these materials or the influence of postcure and aging conditions on these properties. The present work details the tensile failure and fracture properties of the phthalonitrile polymer following exposure to elevated temperature and oxidative conditions.

Experimental

Synthesis and Polymerization — The synthesis and characterization of the monomer has been previously described^{1,4,6-8}. The phthalonitrile resin was synthesized by the nucleophilic displacement of a nitro substituent from 4-nitrophthalonitrile by the dialkali salt of 4,4'-biphenyldiol in dry dimethyl sulfoxide. The phthalonitrile monomer (I) was melted at 240°C, cooled to 220-230°C, and 1,3-bis(3-aminophenoxy)benzene (APB, 1.5% by weight) was added with vigorous stirring. The resulting mixture was poured into aluminum or brass moulds



4,4'-bis(3,4-dicyanophenoxy)biphenyl (I)

and cured successively in air at 240°C for 6 h, 280°C for 16 h, and 315°C for 24 h. Free-standing samples were successively postcured in an argon atmosphere at 350°C for 12 h and 375°C for 12 h. Samples previously postcured at 375°C were oxidatively aged in an air-recirculating oven at 315°C for 100 h.

Mechanical Measurements — Tensile strength measurements were made on a minimum of five dogbone-shaped specimens for each cure, postcure, and aging condition. Specimen dimensions, chosen to minimize material requirements, were 50 mm long overall with a gage region of approximately 16 mm (L) x 3 mm (W) x 2 mm (T). All tensile strength specimens were abrasively ground and polished to final dimensions. Tensile modulus measurements were obtained on rectangular or dogbone-shaped specimens with a clip-on strain gage mounted at a gage length of

25.4 mm. The end tabs for all specimens were potted in Epon 828/Versamid 140 (1:1 by weight) to allow firm gripping without premature fracture in the grips.

Tensile measurements at room temperature ($22 \pm 2^\circ\text{C}$) were carried out using an Instron 4206 instrument at a crosshead speed of $0.508 \text{ mm min}^{-1}$. A grip separation of 25.4 mm was used for the tensile strength specimens, producing an initial strain rate of $5.3 \times 10^{-4} \text{ sec}^{-1}$ in the gage region. The stress-strain response was recorded with a computer data collection and instrument control system which allowed for calculation of the tensile modulus.

Fracture Measurements — The concepts of linear elastic fracture mechanics, often applied to crack growth in brittle polymeric materials, have been extensively developed, both theoretically and experimentally⁹⁻¹⁴. The double-torsion technique (DT)⁹⁻¹⁴ was used for these studies due to the relative simplicity of specimen geometry and preparation, the stability of the crack growth, and the potential for studying variations in material and test conditions. The relation between the stress intensity factor in mode I fracture⁹, K_I , specimen geometry, and load, P , for a DT specimen in plane-strain is given by⁹⁻¹⁴,

$$K_I = P W_m \left[\frac{(1 + \nu)}{W t^3 t_n k_1} \right]^{1/2} \quad (1)$$

where, W_m = moment arm (9.525 mm), W = specimen width, t = specimen thickness, t_n = web thickness (specimen thickness less the depth of the V-groove), ν = Poisson's ratio, P = applied load, K_I = stress intensity factor or fracture toughness, and k_1 = correction factor constant for finite specimen width¹⁰.

The strain-energy release rate, or fracture energy, for a given crack velocity, G_{II} , is given by¹⁰,

$$G_{II} = \frac{1}{2} \frac{P_i^2}{t_n} \frac{dC}{da} \quad (2)$$

where, P_i = load at a given crack velocity, and dC/da = derivative of the experimentally determined compliance, C , which varies with crack length, a . Alternatively, the critical strain-energy release rate, G_{Ic} , may be determined from¹⁰,

$$G_{Ic} = \frac{K_{Ic}^2}{E} (1 - \nu^2) \quad (3)$$

where E is Young's modulus.

The average crack speed, \dot{a} , for a crosshead rate, \dot{x} , is given by¹²,

$$\dot{a} = \frac{\dot{x}}{P(dC/da)} \quad (4)$$

Double torsion specimens were prepared from moulded 10 cm x 10 cm plates. Specimen dimensions, selected in accordance with generally accepted dimensional ratios^{10,14}, were approximately 100 mm (L) x 38 mm (W) x 6 mm (T). All samples were abrasively ground, giving uniform dimensions and parallel faces. A grooving/scoring technique was used for the tensile face as an aide in specimen alignment and in control of the crack growth profile. A centered V-shaped groove was produced along the length of the specimen by using a 90° high-speed spiral fluted bit, held inverted to produce successively deeper cuts as the sample was passed over the cutter. The sample was held at an angle of 45° to the axis of the bit rotation by the use of a plexiglas jig. A final groove depth of 2.0 mm was produced by this method. The center of the groove was then lightly scored with a razor blade along the length of the specimen, in the direction of crack growth, to a depth of 0.1 mm. A stress-relieved cut-crack was made by drilling a 0.6 mm hole perpendicular to the center of the V-groove at various lengths along the sample. The cut-crack was completed by using a 0.3 mm saw to cut the sample from the centerline of the V-groove at the loading end of the specimen to the drilled hole. The cut was ground to remove score marks and a razor blade was used to introduce a pre-crack along the centerline of the V-groove. By following this procedure, any overloading due to an initially blunt crack tip was minimized.

Fracture tests at room temperature ($22 \pm 2^\circ\text{C}$) were performed on an Instron 4206 at a displacement rate of $0.508 \text{ mm min}^{-1}$. A fracture test fixture was used to apply the load to the specimen, thereby propagating the crack in a stable and controlled manner. Test specimens were used to determine both the steady crack propagation load, P_c , and the compliance response at various initial crack lengths. A computer data collection and instrument control system was used to record the load-crosshead displacement response and calculate the compliance for each initial crack

length. Specimens used to determine the compliance were successively cut to various lengths along the V-groove and pre-cracked as described above prior to testing.

Results and Discussion

Mechanical Properties — Tensile strength values for the phthalonitrile polymer at room temperature are summarized in Table 1 for various cure, postcure, and oxidative aging conditions. These properties indicate a high retention of mechanical performance with only a small decrease following oxidative aging for 100 h at 315 °C. Compared with other state-of-the-art thermosetting materials, the neat phthalonitrile resin exhibits an excellent, if not superior, retention of mechanical strength. PMR resins, by comparison, have tensile strengths of 48-83 MPa¹⁵ at room temperature. Other thermosetting polyimides exhibit similar or higher mechanical property values but, in certain cases, do not maintain the same degree of thermal and oxidative stability as is shown by phthalonitrile-based materials¹⁵. Materials formed from acetylene-terminated resin (ATR) precursors have also been shown to exhibit superior mechanical and thermoxidative properties¹⁶. The very brittle nature of ATR materials, however, limits their potential applications.

Preliminary tensile stress-strain measurements at room temperature indicate that the phthalonitrile polymers behave as brittle materials for cure/postcure conditions at 315°C or above. Tensile moduli range from 3.6 GPa to 2.4 GPa for specimens cured at 315°C and 375°C, respectively. Previous results¹ have shown similar dynamic storage moduli with evidence of viscoelastic transitions to the rubbery state between 200-360°C for materials cured at 350°C or below. Phthalonitrile polymers postcured at 375°C, as well as those aged at elevated temperatures following postcure at 375°C, do not show any evidence of glass/rubber transitions up to 375°C. The maximum in the loss tangent also shifts to higher temperatures for cure temperatures below 375°C; glass transition maxima are observed at 290°C and 332°C following cure for 16-24 h at 315°C and postcure for 4 h at 350°C, respectively¹.

Fracture Behavior — The room temperature fracture behavior of phthalonitrile materials cured at 315°C for 24 h has been studied. Stable crack growth was achieved under specimen and test

conditions previously described which allowed for a determination of crack propagation loads and specimen/test fixture compliance. As shown in Figure 1, for each cut-crack length a near linear load-displacement response was obtained until an initiated crack profile developed. At this point the load became nearly constant with the crack propagating at a steady rate along the length of the specimen. Occasionally, a slight overloading was observed prior to steady state crack growth (Figure 1, curve c); however, the overloading was apparently not sufficiently great enough to cause complete and unsteady failure in the specimens. The relatively small crack arresting potential of these specimens compared with thicker materials generally resulted in unstable crack growth for specimens with initial cut-cracks greater than 50 mm. For this reason, compliance calibrations were restricted to a cut-crack length of 10-50 mm. Since the stress intensity is generally constant over the length of the specimen, with the exception of the initial and final 15-20 percent¹⁰, a determination of the compliance in this region allowed for calculation of the fracture energy. Figure 2 shows a linear variation of the compliance with initial cut-crack length as is expected for brittle materials.

The fracture toughness and energy of the phthalonitrile materials were calculated using equations (1) and (2), respectively. Test results on five samples yield a fracture toughness of 0.61-0.63 $\text{MNm}^{-3/2}$, and a fracture energy of 120-130 Jm^{-2} . The corresponding crack speeds were 70-80 mm/min. Tests on similar poly(methyl methacrylate) (PMMA) specimens, performed as a means of comparison with published results, yielded K_{Ic} values of 1.2-1.3 $\text{MNm}^{-3/2}$. By comparison, values between 1.1-1.3 $\text{MNm}^{-3/2}$ are cited for the room temperature fracture toughness of PMMA at similar crack speeds¹². A comparison of the fracture properties of phthalonitrile polymers with other thermosetting materials shows that the phthalonitrile materials are typical of highly crosslinked brittle resins at room temperature test conditions. Representative fracture toughness values for unmodified epoxy resins^{9,13,17}, for example, range from 0.5-0.8 $\text{MNm}^{-3/2}$.

Preliminary results obtained to verify the requirements of plane-strain conditions due to specimen thickness have also been made. Plate specimens, prepared without V-grooves, with thicknesses ranging from 4.0 to 6.0 mm have been tested, yielding K_{Ic} values between 0.60-65

MNm^{3/2}, and fracture energy values comparable to the grooved specimens. Limited testing was performed with ungrooved specimens, however, due to the difficulty in specimen alignment in the fracture jig, and the increased potential for crack wandering. According to ASTM E399-83, the minimum thickness required for plane-strain conditions is at least $2.5(K_{Ic}/\sigma_y)^2$, where σ_y is the tensile yield stress. Using a value of 94 MPa for σ_y , the required minimum thickness is approximately 0.1 mm. The observed insensitivity of the fracture toughness results to specimen thickness and groove geometry are therefore consistent with the existence of plane-strain conditions in these specimens.

Summary and Conclusions

Phthalonitrile-based polymers prepared from 4,4'-bis(3,4-dicyanophenoxy)biphenyl, cured in the presence of a diamine, and exposed to elevated postcure and aging conditions, have been shown to exhibit a high retention of mechanical strength. The thermoxidative properties of these polymers are excellent with very low weight loss and good mechanical properties obtained for cure conditions to 315°C, inert atmosphere postcure to 375°C, and oxidative aging at 315°C. The plane strain fracture behavior of the phthalonitrile polymers shows properties similar to unmodified epoxies, with brittle failure at room temperature observed. Due to the ease of processing and excellent mechanical properties evidenced by these materials it is anticipated that potential applications will include fabricated composites and structures subjected to elevated temperature and oxidative environments.

Acknowledgements

Partial funding support from the Office of Naval Research is gratefully acknowledged.

Table 1 Effect of Cure Conditions on the Room Temperature Tensile Strength of Biphenyldiol-Based Phthalonitrile Polymers

Cure/Postcure ^a (°C)	Conditions		Tensile Strength at Break (MPa)
	(hrs)	Atmosphere	
315	24	Air	94 ± 17
350	12	Argon	94 ± 21
375	12	Argon	80 ± 7
315	100	Air	72 ± 5

^aAll materials were initially cured at 240°C for 6 h and 280°C for 16 h. Tabulated conditions are successive thermal and oxidative treatments.

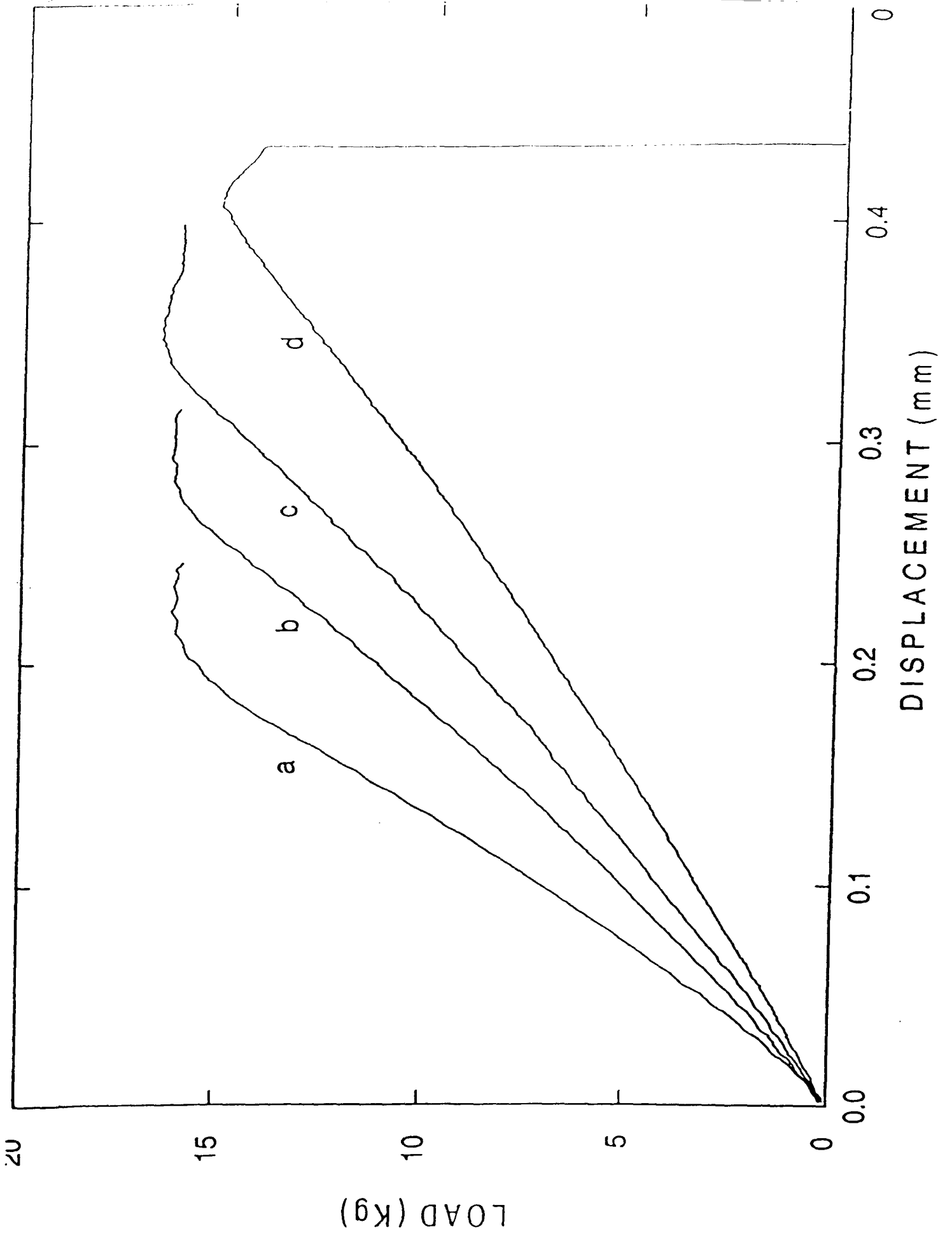
References

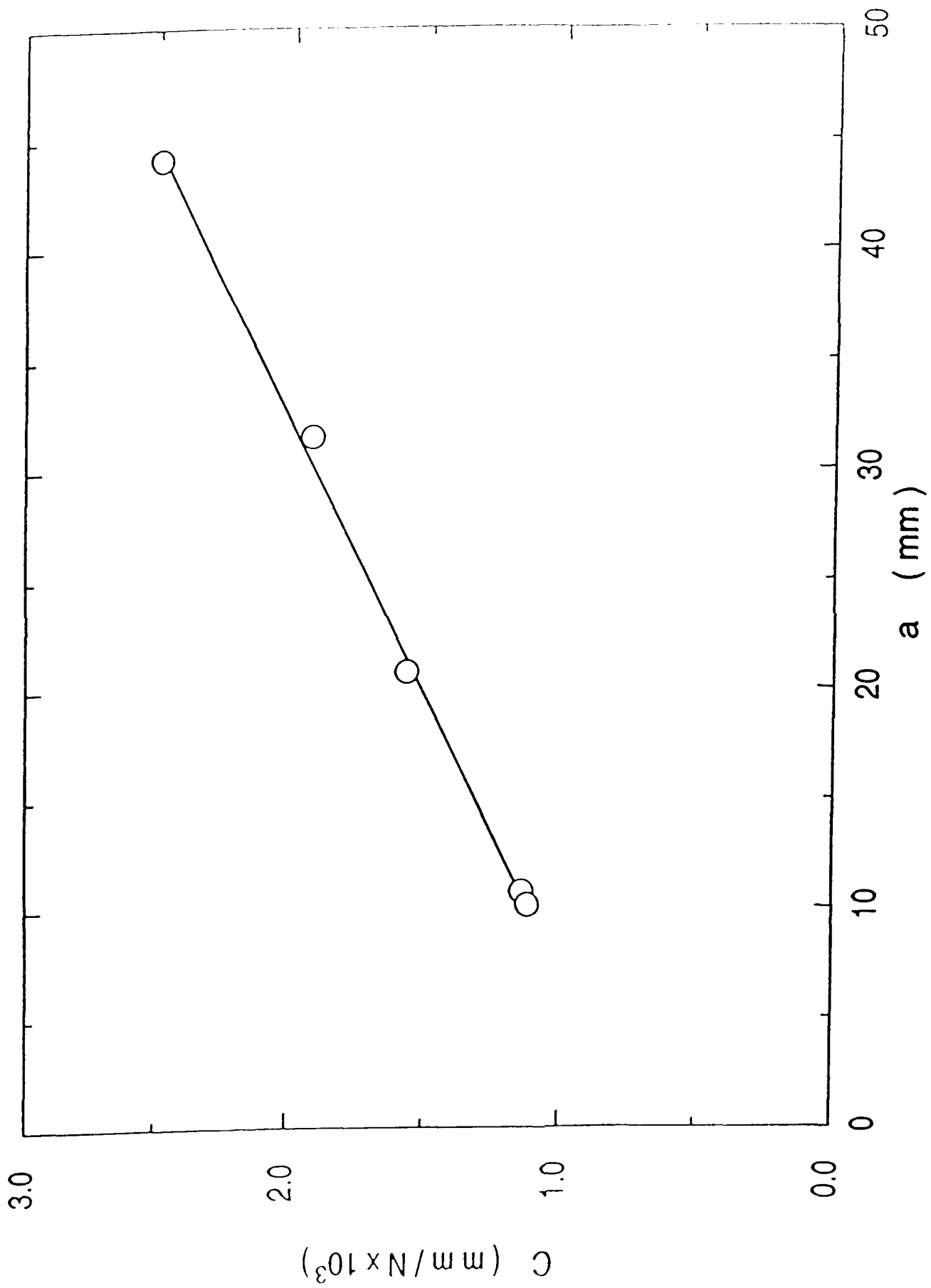
1. Keller, T. M. *J. Polym. Sci.: Part A: Polym. Chem.* 1988, **26**, 3199
2. Keller, T. M. *Polym. Prep.* 1987, **28**(1), 37
3. Keller, T. M. *J. Polym. Sci., Polym. Chem. Ed.* 1987, **25**, 2569
4. Keller, T. M. *J. Polym. Sci., Polym. Lett. Ed.* 1986, **24**, 211
5. Hinkley, J. A. *J. Appl. Polym. Sci.* 1984, **29**, 3339
6. Keller, T. M. and Price, T. R. *J. Macromol. Sci. Chem.* 1982, **A18**(6), 931
7. R. Y. Ting, Keller, T. M., Price, T. R. and Poranski, C. F., Jr. *Cyclopolymerization and Polymers with Chain-Ring Structures, Am. Chem. Soc. Symp. Ser.* 1982, **195**, 337
8. Keller, T. M. and Griffith, J. R. *Resins for Aerospace, Am. Chem. Soc. Symp. Ser.* 1980, **132**, 25
9. Kinloch, A. J. and Young, R. J. 'Fracture Behaviour of Polymers', Elsevier Applied Science, London, 1983, ch. 3
10. Tait, R. B., Fry, P. R. and Garrett, G. G. *Experimental Mechanics* Mar. 1987, 14
11. Young, R. J. and Beaumont, P. W. R. *J. Mater. Sci.* 1975, **10**, 1343
12. Marshall, G. P., Coutts, L. H. and Williams, J. G. *J. Mater. Sci.* 1974, **9**, 1409
13. Truong, V.-T. *Polymer* 1990, **31**, 1669
14. Kinloch, A. J., Maxwell, D. L. and Young, R. J. *J. Mater. Sci.* 1985, **20**, 4169
15. Critchley, J. P., Knight, G. J. and Wright, W. W. in 'Heat Resistant Polymers', Plenum Press, New York, 1983, Table 5.31
16. Warzel, M. L., Walton, T. R. and Roland, C. M. submitted to *J. Appl. Polym. Sci.*
17. Kinloch, A. J., Shaw, S. J., Tod, D. A. and Hunston, D. L. *Polymer* 1983, **24**, 1341

Figure Captions

Fig. 1. Load-displacement response at 22°C for the phthalonitrile polymer cured at 315°C for 24 h. The curves represent the compliance response for various initial cut-crack lengths: (a) 10.1 mm, (b) 20.7 mm, (c) 31.4 mm, and (d) 44.0 mm.

Fig. 2. Compliance calibration at 22°C for the phthalonitrile polymer showing the linearity of specimen compliance variation with crack length.





APPENDIX L

**OBSERVATION OF SPINOIDAL DECOMPOSITION AND POLYMER
DIFFUSION VIA ^{129}Xe NMR**



GEO-CENTERS, INC.

Observation of Spinoidal Decomposition and Polymer Diffusion Via ^{129}Xe NMR

J. H. Walton, J. B. Miller, C. M. Roland, and J. B. Nagode*

Chemistry Division, Code 6120

Naval Research Laboratory

Washington, D.C. 20375-5000

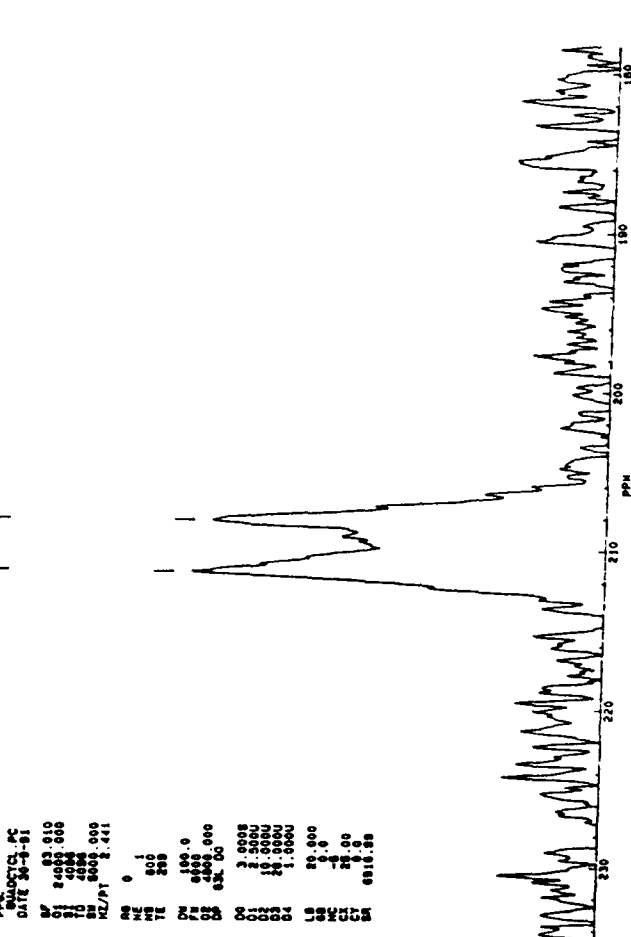
We present ^{129}Xe NMR results on Xe dissolved in a blend of 34 % *cis*-1,4-polyisoprene ($M_w = 115,000$) and 66 % 1,4-polybutadiene ($M_w = 23,600$). This blend is known to have an LCST¹ at approximately 97 C. Annealing at 103 C induces spinoidal decomposition and rapid quenching to room temperature produces a metastable phase separation. The ^{129}Xe NMR lineshape is used to follow the mutual diffusion of the two constituent polymers back to miscibility.

¹ C. A. Trask and C. M. Roland, *Poly. Comm.*, **29**, 332 (1988).

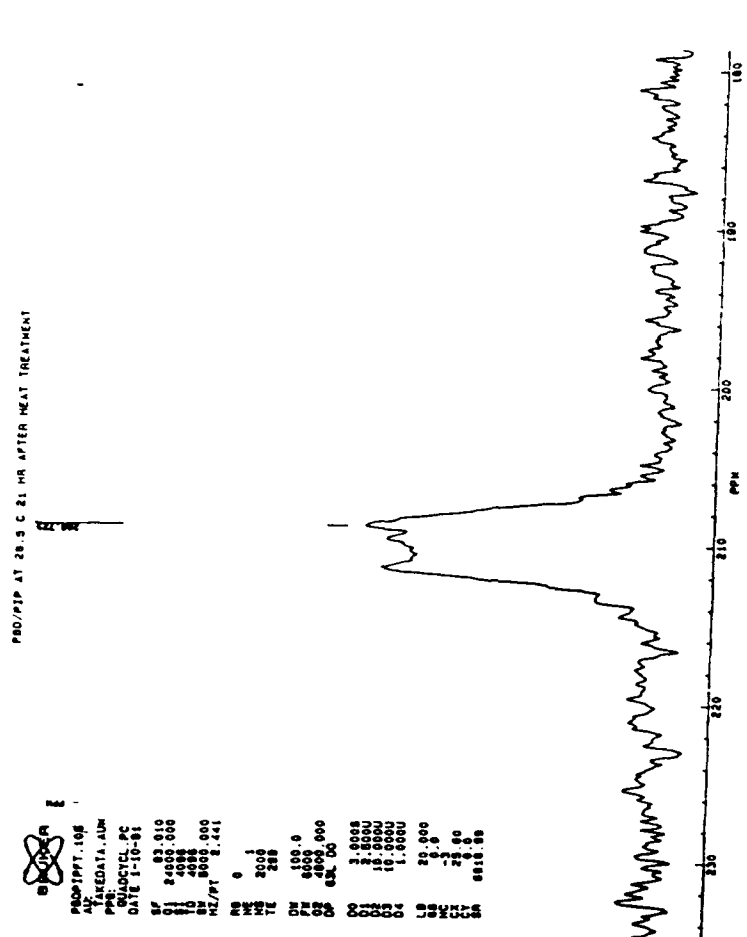
U/DIR

150-M* 000
 PPS
 QUA/CTCL PC
 DATE 1-10-81
 SF 83 010
 SI 1000 000
 SD 4088
 SW 25000 000
 SZ 10
 ME 1 11
 WE 300
 PW 3200 0
 Q2 1800 000
 Q3 831 DO
 Q4 3 0003
 Q5 2 000
 Q6 10 000
 Q7 1 0000
 Q8 83 000
 Q9 0 0
 Q10 1 0
 Q11 75 00
 Q12 5318 59

PRO/PT 102
 ALI
 TAKE DATA ALM
 PPS
 QUA/CTCL PC
 DATE 1-10-81
 SF 83 010
 SI 1000 000
 SD 4088
 SW 25000 000
 SZ 10
 ME 1 11
 WE 300
 PW 3200 0
 Q2 1800 000
 Q3 831 DO
 Q4 3 0003
 Q5 2 000
 Q6 10 000
 Q7 1 0000
 Q8 83 000
 Q9 0 0
 Q10 1 0
 Q11 75 00
 Q12 5318 59



POS/PIP AT 87.9 C 4 HR AFTER HEAT TREATMENT
 U/DIR
 PRO/PT 105
 ALI
 TAKE DATA ALM
 PPS
 QUA/CTCL PC
 DATE 1-10-81
 SF 83 010
 SI 1000 000
 SD 4088
 SW 25000 000
 SZ 10
 ME 1 11
 WE 300
 PW 3200 0
 Q2 1800 000
 Q3 831 DO
 Q4 3 0003
 Q5 2 000
 Q6 10 000
 Q7 1 0000
 Q8 83 000
 Q9 0 0
 Q10 1 0
 Q11 75 00
 Q12 5318 59



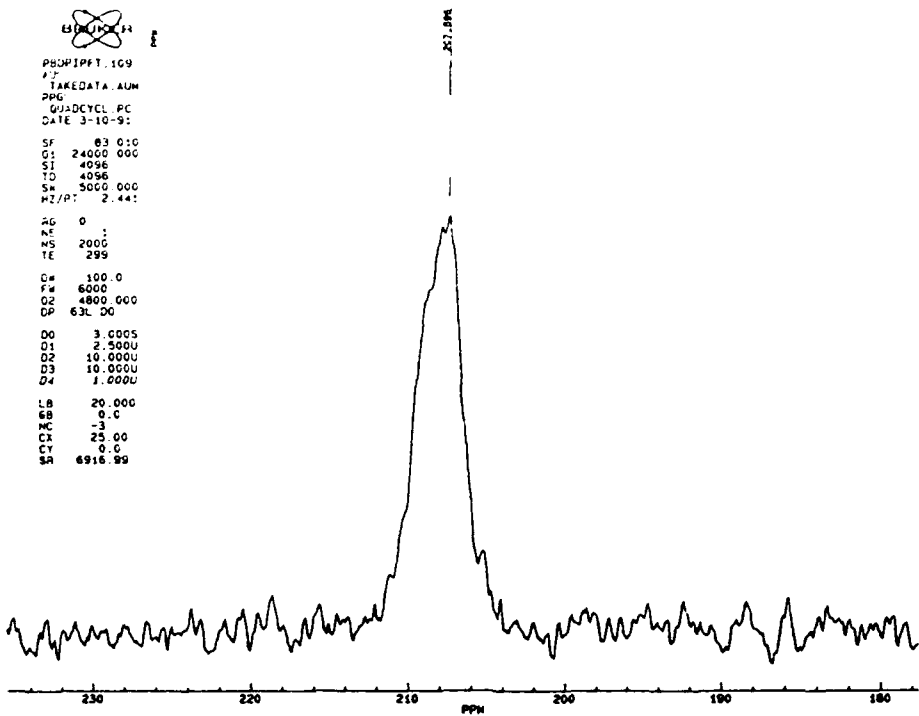
POS/PIP AT 28.5 C 21 HR AFTER HEAT TREATMENT
 U/DIR
 PRO/PT 106
 ALI
 TAKE DATA ALM
 PPS
 QUA/CTCL PC
 DATE 1-10-81
 SF 83 010
 SI 1000 000
 SD 4088
 SW 25000 000
 SZ 10
 ME 1 11
 WE 300
 PW 3200 0
 Q2 1800 000
 Q3 831 DO
 Q4 3 0003
 Q5 2 000
 Q6 10 000
 Q7 1 0000
 Q8 83 000
 Q9 0 0
 Q10 1 0
 Q11 75 00
 Q12 5318 59



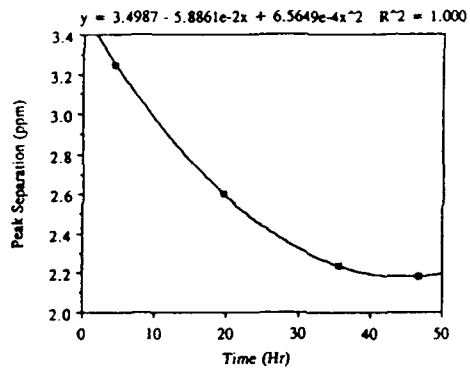


```

PBD/PIPT.109
#3
TAKEDATA.AUM
PPG
QJADCYCL.PC
DATE 3-10-91
SF 03 0:00
G1 24000 000
S1 4096
TD 4096
SM 5000 000
M2/P1 2.441
RG 0
RF :
NS 2000
TE 299
CW 100.0
FW 6000
DZ 4800 000
DP 63L 00
D0 3.0005
D1 2.5000
D2 10.0000
D3 10.0000
D4 1.0000
LB 20.000
GB -3
MC -3
CX 25.00
CY 0.0
SA 6916.99
    
```



PBD/PIP Data



Figures - preceding page - clockwise from top left: Polyisoprene/Polybutadiene blends at 1. 26°C prior to annealing; 2. immediately after annealing; 3. 4 hours after annealing; 4. 21 hours after.

Figures - this page top: PIP/PBD blend 67 hours after annealing; bottom: NMR peak separation as a function of time, showing a return to single phase in the blend.

APPENDIX M

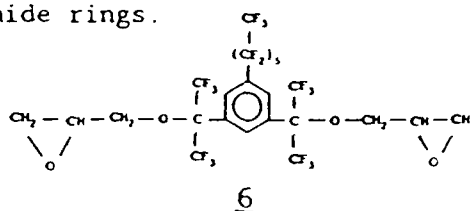
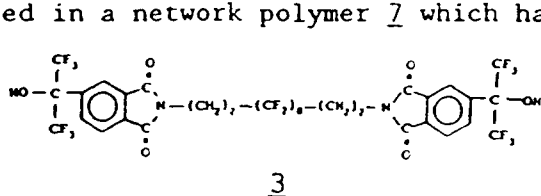
**A NOVEL ROUTE TO TWO HEAVILY FLUORINATED EPOXY
RESINS FROM A FLUORODIIMIDEDIOL**



GEO-CENTERS, INC.

A NOVEL ROUTE TO TWO HEAVILY FLUORINATED EPOXY RESINS FROM A
 FLUORODIIMIDEDIOL. Henry S-W. Hu, Geo-Centers, Inc., Fort
 Washington, MD 20744 and James R. Griffith, Naval Research Laboratory,
 Washington, D.C. 20375

Two synthetic methodologies leading to heavily fluorinated epoxy resins are reported. The title compound 3, a fluorodiimidediol, was prepared through the condensation of the corresponding anhydride 1 and diamine 2. The conversion of 3 into diepoxy via dichlorohydrin 4 resulted in the formation of a network polymer 5 in which the imide structure has disappeared to yield amide components. On the other hand, the curing of a fluorodiepoxy 6 with equivalent 3 in the catalytic presence of tetramethylammonium bromide resulted in a network polymer 7 which has intact imide rings.



A Novel Route to Two Heavily Fluorinated Epoxy
Resins from a Fluorodiimidediol

by

Henry S-W. Hu
Geo-Centers, Inc., Fort Washington, MD 20744

and

James R. Griffith
Naval Research Laboratory, Washington, D.C. 20375

INTRODUCTION

Fluorinated epoxy resins are the key intermediates for new types of practical organic coatings and plastics which have fluorocarbon properties and convenient characteristics such as hydrophobicity, oleophobicity, light stability, low friction and possibly high thermal stability in some cases.

A series of studies have been carried out in our laboratory to design and synthesize new fluorinated epoxy and acrylic resins for many applications because of their unique properties.^{1,2,3}

In this paper we report two specific synthetic methodologies by using a fluorodiimidediol 3 to prepare the heavily fluorinated epoxy resins as shown in Scheme 1 and Scheme 2.

EXPERIMENTAL

Materials and Methods

4-(2-Hydroxyhexafluoro-2-propyl)phthalic anhydride 1 was prepared by a multistep route according to the procedure of Griffith, O'Rear and Reardon.⁴ Hexadecafluoro-1,12-decanediamine 2 was obtained from Fluorochem, Inc., (680 Ayon Ave., Azusa, CA 91702). The diglycidyl ether 6 of 1,3-bis-(2-hydroxyhexafluoro-2-propyl)-5-tridecafluorohexyl-benzene was prepared by a multistep route according to the general procedure of Griffith and O'Rear.^{5,6} IR spectra were recorded on a Perkin-Elmer 1800 Fourier Transform Infrared Spectrophotometer. ¹H-NMR spectra were recorded on a 90 MHz Varian EM390 Spectrometer.

Preparation of diimidediol 3

Anhydride 1 (41g, 0.130mole) and diamine 2 (25g, 0.051mole) in 300 mL of toluene were heated to reflux for 20h under a Dean Stark trap. Upon cooling in an ice bath, a red oil settled to the bottom. It was separated and solidified. This crude product was stirred as a suspension in water at 50°C until the water became neutral. It was filtered and dried in vacuo to give a white powder 18.8g, yield 34%, recrystallization from hexanes/THF (10:1) with 90% recovery, mp 145-148°C. One spot in TLC (Silica gel, CH₂Cl₂ 1.5mL/ acetone 3 drops), rf = 0.27. IR(KBr pellet) 3415 (OH), 1780 and 1720 (imide), 1450, 1388, 1300-1100 (F), 980, 970, 750, 722 cm⁻¹. NMR(CDCl₃/TMS)δ 8.38 (m, 1H), 8.3-7.8 (m, 2H), 4.07 (m, 2H, N-CH₂-), 2.9-2.2 (m, 2H, -CH₂-CF₂-).

Preparation of 5 from 3 via 4

A mixture of 3 (0.2g, 0.186mmole), epichlorohydrin (1.74g, 18.80mmole) and tetramethylammonium bromide (0.030g, 0.195mmole) was stirred and maintained at 90°C for 70h. Evaporation at 90°C/20mm left a viscous liquid 0.36g of dichlorohydrin 4. IR(neat film) 3480, and 3300 (OH), 3070, 3006, 2960, 1781 and 1720 (imide), 1485, 1450, 1385, 1300-1050 (F), 1015, 982, 945, 915, 858, 750, 726, 708 cm⁻¹. NMR(CDCl₃/TMS)δ showed only 8.3-7.9 in the aromatic region indicated no 3 present, but additional integration in 4.3-2.2 indicated there was some epichlorohydrin left.

Dehydrochlorination of 4 was accomplished by first mixing it with toluene (5g) and ethanol (1.7g) under nitrogen and stirring in an ice bath; a 18% sodium hydroxide solution (4g) was then added dropwise during 10 min. After stirring at room temperature overnight and then at 55°C for 1h, a yellow oil stayed between the top organic layer and bottom aqueous layer. Tetrahydrofuran (2mL) was added and the mixture was stirred at room temperature for 10 min during which the yellow oil dropped to the bottom. It was separated and dried in vacuo at room temperature for 2h to a semisolid which became a white solid 5 on standing. 0.161g, yield 78%, no mp observed but there was softening and color change. IR(KBr pellet) 3400 (OH), 3080, 2980, 2890, 1655, 1625, 1600, 1570, 1390, 1300-1100 (F), 1020, 995, 970, 840, 735, 715, 700, 543 cm⁻¹.

Preparation of 7 from 3 and 6

Diepoxy 6 (0.84g, 0.001mole) and diimidediol 3 (1.07g, 0.001mole) were mixed well and the mixture heated at 110°C overnight during which no change

took place. Tetramethylammonium bromide in catalytic amount was added, mixed well and heated at 110°C. After one day a brittle transparent solid was obtained. During two more days it became a very hard solid 7. IR(KBr pellet) 3480 (OH), 1785 and 1730 (imide), 1452, 1388, 1300-1100 (F), 1050, 1018, 983, 750, 730, 716, 708 cm⁻¹.

RESULTS AND DISCUSSION

The absence of an infrared absorption peak around 913 cm⁻¹ (10.95μ) for both 5 and 7 indicates that the glycidyl rings are mostly converted into resins through cross-linking.⁷ Heavily fluorinated compounds, 5 and 7, have very strong infrared absorption in the region of 1300-1100 cm⁻¹.

Upon the formation of 5, the absence of 1780 and 1720 cm⁻¹ peaks for an imide ring and the appearance of an amide peak at 1655 cm⁻¹ as well as a carboxylate salt peak at 1570 cm⁻¹ strongly indicated that the imide ring reacted with the glycidyl ring. Since amides are curing reagents for epoxies,⁸ the imide ring may be partially hydrolyzed into secondary amide and carboxylate salt under the basic conditions with the presence of tetramethylammonium bromide as catalyst; it may have further reacted with epoxy to form tertiary amide as shown in Scheme 3.

For the formation of 7 from equivalent amounts of 3 and 6, reaction took place only in the presence of tetramethylammonium bromide catalyst. In contrast to the behavior of 5, the imide ring structure remained but with a shift in infrared absorption from 1780 and 1720 cm⁻¹ to 1785 and 1730cm⁻¹. One might expect the product generated from 3 and 6 to have less intermolecular hydrogen bonding. Therefore, the classical reaction⁸ between epoxy and alcohol is suggested as shown in Scheme 4 to produce less acidic alcohol. The fluorodiepoxy 6 has been reported recently in curing with SA type silicone diamine to form a network polymer,⁹ while in our study a catalyst such as tetramethylammonium bromide is required for the reaction of 6 with 3.

Acknowledgement

Partial funding support from the Office of Naval Research is gratefully acknowledged.

References

1. J. R. Griffith and R. F. Brady, Jr., CHEMTECH,

19(6), 370-373 (1989).

2. J. R. Griffith, CHEMTECH, 12(5), 290-293 (1982).

3. J. R. Griffith, J. G. O'Rear and S. A. Reines, CHEMTECH, 2(5), 311-316 (1972).

4. J. R. Griffith, J. G. O'Rear and J. P. Reardon, Adhesion Science and Technology, vol. 9A, L. -H. Lee, Ed., Plenum, New York, N. Y., 429-435 (1975).

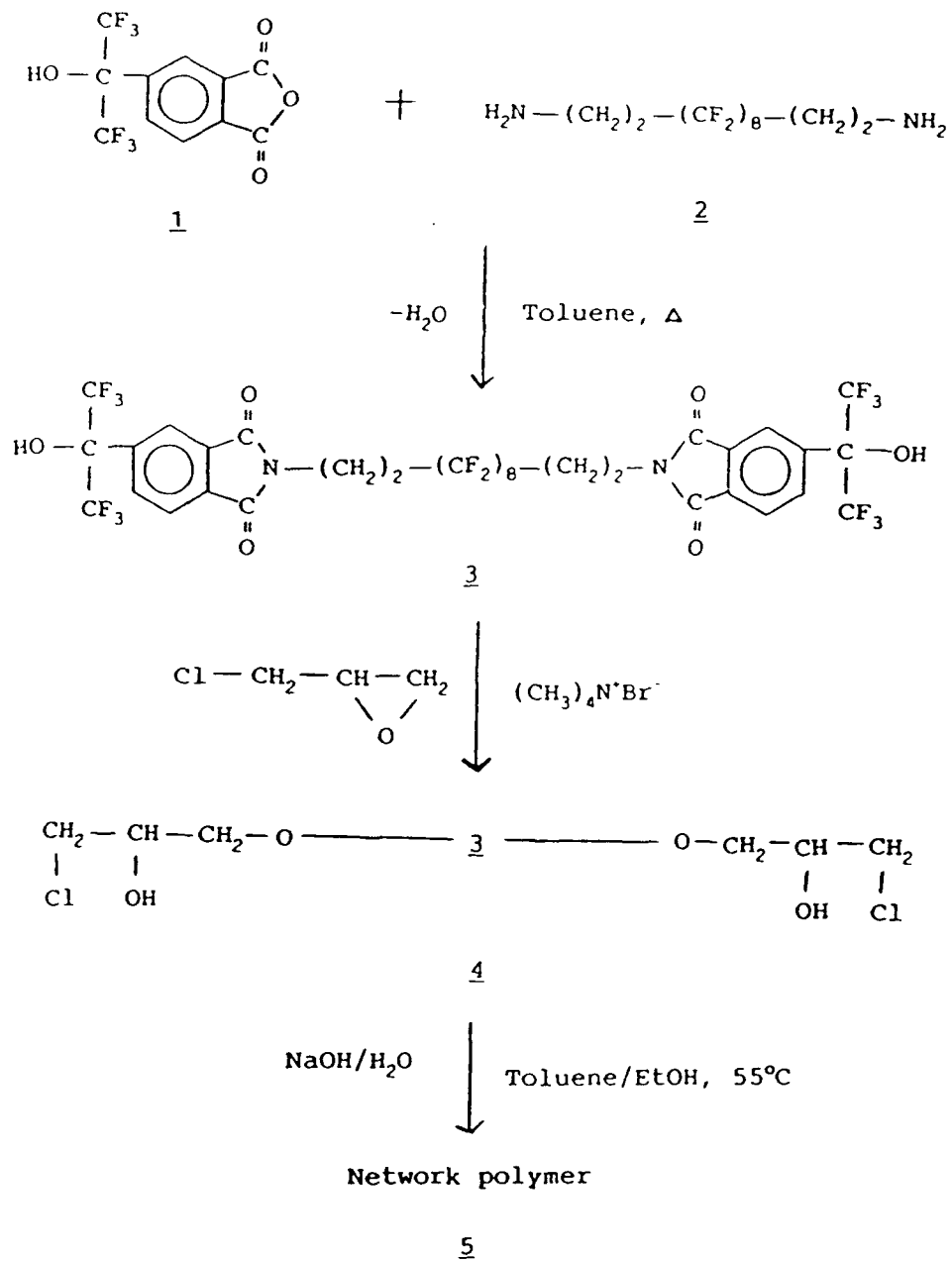
5. J. G. O'Rear and J. R. Griffith, Org. Coatings and Plastics Chem., 33, 657-662 (1973).

6. J. R. Griffith and J. G. O'Rear, Synthesis, 493 (1974).

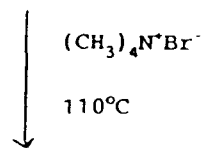
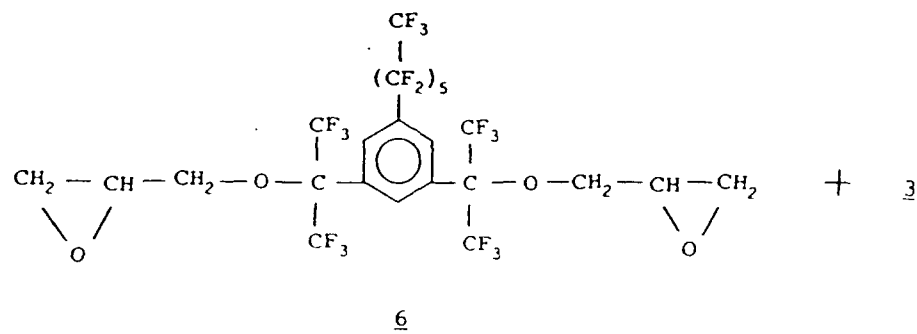
7. H. Lee and K. Neville, Handbook of Epoxy Resins, McGraw-Hill, New York, N. Y., (1967). see Appendix 4-1: IR Spectra of Uncured Epoxy Resins.

8. ref. 7, see [7] and [10] in Appendix 5-1: Reaction of Epoxides.

9. T. E. Twardowski and P. H. Geil, J. Appl. Polym. Sci., 41, 1047-1054 (1990).



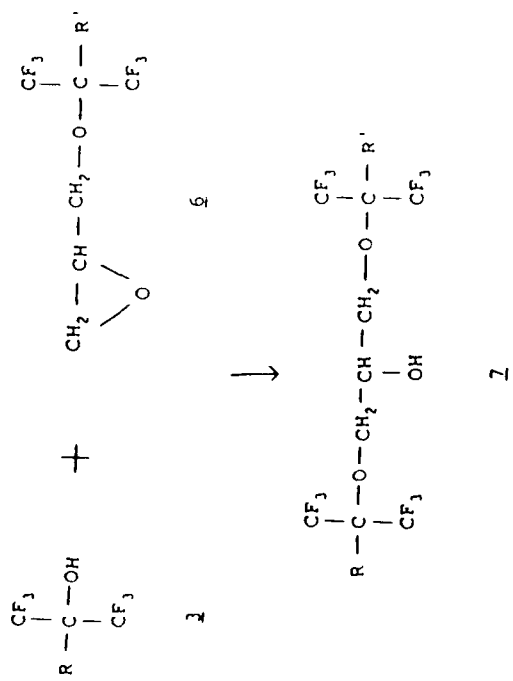
Scheme 1



Network polymer

7

Scheme 2



Scheme 4

APPENDIX N

**PROCESSABLE HEAVILY FLUORINATED ACRYLIC RESINS WITH
LOW DIELECTRIC CONSTANTS**



GEO CENTERS, INC.

PROCESSABLE HEAVILY FLUORINATED ACRYLIC RESINS
WITH LOW DIELECTRIC CONSTANTS

Henry S.-W. Hu
Geo-Centers, Inc., Fort Washington, MD 20744
and
James R. Griffith
Naval Research Laboratory, Washington, D.C. 20375

INTRODUCTION

Materials exhibiting dielectric constants below 3 are in increasing demand in the aerospace and electronic circuit industries. Present computer operations are limited by the coupling capacitance between circuit paths and integrated circuits on multilayer boards, since the computing speed between integrated circuits is reduced by this capacitance and the power required to operate is increased. The maximum frequency of operation of the field-effect transistor can be given by the frequency corresponding to the dielectric constant in the reverse proportion.

Reductions in such parasitic capacitance can be achieved in a number of ways through proper selection of materials and the design of circuit geometry. In 1988 St. Clair *et al.* reported a reduction of dielectric constant down to 2.39 by chemically altering the composition of a polyimide backbone to reduce the interactions between linear polyimide chains and by the incorporation of fluorine atoms.

A series of studies have been carried out in our laboratory to design and synthesize new fluorinated epoxy and acrylic resins. These materials have many applications because of their unique properties.

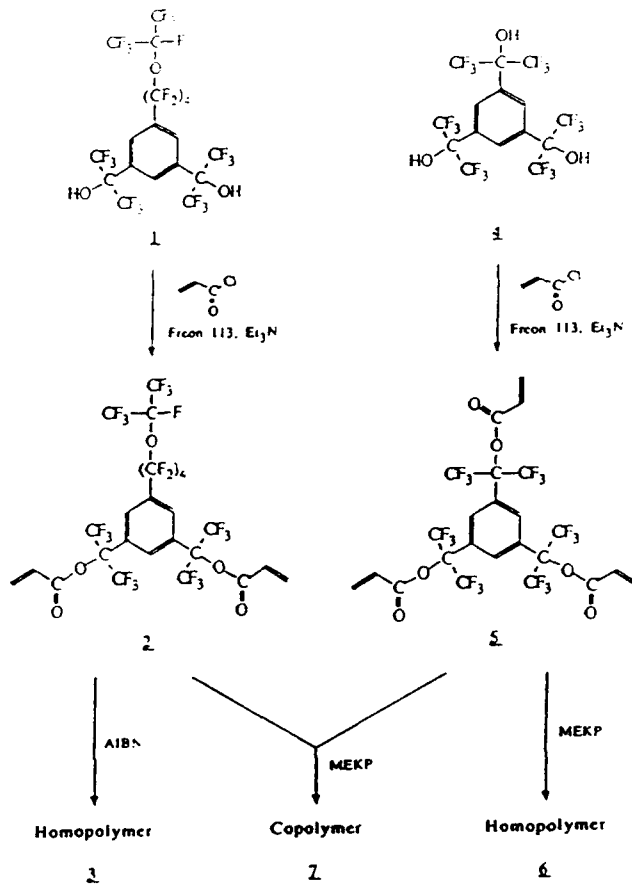
In this paper we report the preparation of a series of new processable heavily fluorinated acrylic resins which exhibit dielectric constants as low as 2.10, very close to the known minimum values, 2.0-2.08 for poly(tetrafluoroethylene) (PTFE),⁶ and 1.89-1.93 for copolymers of 2,2-bis(trifluoromethyl)-4,5-difluoro-1,3-dioxole and tetrafluoroethylene.

EXPERIMENTAL

The synthetic routes used to obtain the monomers and polymers are outlined in Scheme I. Details of the synthesis will be reported elsewhere.

Dielectric constant (DE) measurements

Dielectric constant values are reported as "Permittivity" with symbol ϵ or K_e . The polymer donuts were used for the measurement of DE on a Hewlett Packard 8510 Automated Network Analyzer over a frequency band of 500 MHz to 18.5 GHz. Samples stood at room temperature in air prior to testing; measurements were run at room temperature and approximately 25% RH. A virgin Teflon (PTFE) sheet (MMS-636-2) was obtained from Gilbert Plastics & Supply Co. and cut into the same donut size. The result for PTFE reported here is the average of DE values measured for three samples.



Scheme I

Table I

Summary of Data for Dielectric Constant Measurements^a

samples	frequency (GHz)			
	0	3.5	9.5	15.5
3	2.11	2.10	2.12	2.13
6	2.23	2.23	2.23	2.22
7	2.22	2.23	2.24	2.22
PTFE ^b	1.96	1.98	1.99	—

^aSee Experimental Section for detail.

^bPoly(tetrafluoroethylene).

RESULTS AND DISCUSSION

Monomers: The preparation of etherdiol **1** and triol **4** was carried out in multistep routes according to the reported procedures.^{8,10} As summarized in Scheme I, the synthesis of acrylic esters, **2** and **5**, was carried out in a fluorocarbon solvent such as Freon 113 by the reaction of alcohols, **1** and **4**, with acryloyl chloride and an amine acid acceptor such as triethylamine. Other attempts to esterify the fluoroalcohols directly with acrylic acid or acrylic anhydride were not successful. Product purification by distillation was not feasible because of the temperature required, but purification by percolation of fluorocarbon solutions through neutral alumina resulted in products, **2** and **5**, of good purity identified by TLC, NMR and IR.

The stability of the monomers **2** and **5** is good at room temperature, and it is found that no change can be detected by use of IR and NMR after storing in air for three months.

Polymerization: Due to their liquid or semisolid nature, monomers **2** and **5** are easy to process into polymers. For radical polymerization the use of solid AIBN for liquid **2** at room temperature and liquid MEKP for semisolid **5** or a mixture of **2** and **5** with some heating is convenient.

During the course of curing at 85-100°C the problem of surface inhibition of free radicals by oxygen of air can be avoided by inert gas blanketing.

Dielectric constant (DE): In order to validate the accuracy of our measurements, three samples of virgin Teflon (PTFE) in the same donut size were measured and found to have average DE values around 1.96-1.99, which are close to the reported values 2.0-2.08.⁶ Summarized results of the DE measurement on the polymer donuts **3**, **6**, **7**, and PTFE are shown in Table I. All the new polymers exhibit unusually low DEs around 2.10-2.24 over a wide frequency region of 500 MHz to 18.5 GHz; the variation of DE values over the measured frequency region is within 0.03 for each polymer. The 50/50 (w/w) copolymer **7**, having a molar ratio 45/55 of **2** and **5**, showed DE of 2.22 which is close to that of **6**; this indicates that the copolymer **7** was not completely homogeneous and compatible.

The wide range frequency independence of these low DEs and the processability of these monomers suggests many potential applications. In particular, it is known that the addition of a fluorine-containing group to the polymer backbone will reduce the polymer chain-chain electronic interactions, resulting in a reduction of DE as reported by St. Clair *et al.*,⁴ but the DEs for **3** (fluorine content 57%) are at most 0.13 below those for **6** (fluorine content 46%), which may indicate that a minimum value might have been nearly reached regarding the structure/property relationship.

In 1990 Resnick⁷ reported that the lowest dielectric constant (1.89-1.93) of any polymer thus far was obtained from copolymers of 2,2-bis(trifluoromethyl)-4,5-difluoro-1,3-dioxole **8** and tetrafluoroethylene **9** with structures shown in Scheme II. In addition to the effect of the fluorine content, the existence of similar perfluoroalkyl ether linkage on the double bonds in both monomers **8** and **2** seems to play a very important role in further reducing the dielectric constant values.



Scheme II

St. Clair *et al.*⁴ also observed that the low dielectric constant polyimides containing the -CF₃ group show excellent resistance to moisture, exhibiting almost PTFE-like behavior. Since PTFE contains 76% fluorine, it appears that the DE values for the heavily fluorinated **3**, **6** and **7** with fluorine content around 46-57% will be humidity-independent. It is known that water has a very high DE of 79.45. The low DE values for **3**, **6** and **7** suggest a very low water content after polymerization of the hydrated monomers.

ACKNOWLEDGEMENT

We are indebted to Mr. Jonas K. Lodge of SFA, Inc. for the dielectric constant measurements. Partial funding support from the Office of Naval Research is gratefully acknowledged.

REFERENCES

1. W. E. Dorogy, Jr. and A. K. St. Clair, *Polym. Mater. Sci. Eng.*, **64**, 379-380 (1991).
2. J. J. Licari and L. A. Hughes, *Handbook of Polymer Coating for Electronics*, Noyes Publications, Park Ridge, N. J., (1990). see p. 114. The relationship of capacitance C with dielectric constant K_s can be expressed as $C = AK_s\epsilon_0/d$ where A is area, d is distance, and $\epsilon_0 = 8.85418 \times 10^{-12}$ F/cm.
3. A. S. Grove, *Physics and Technology of Semiconductor Devices*, John Wiley & Sons, New York, N. Y. (1967). see pp. 254-255 for detail. K_s represents the dielectric constant in equation 8.22 with $K_s = \epsilon_s/\epsilon_0$.
4. A. K. St. Clair, T. L. St. Clair and W. P. Winfree, *Polym. Mater. Sci. Eng.*, **59**, 28-32 (1988).
5. (a) J. R. Griffith and R. F. Brady, Jr., *CHEMTECH*, **19**(6), 370-373 (1989). (b) H. S.-W. Hu and J. R. Griffith, *Polym. Prepr.*, **32**(3), 216-217 (1991).
6. Ref. 2, see p. 378-379, Table A-13: Dielectric Constants for Polymer Coatings (at 25°C).
7. P. R. Resnick, *Polym. Prepr.*, **31**(1), 312-313 (1990).
8. J. R. Griffith and J. G. O'Rear, *Polym. Mater. Sci. Eng.*, **53**, 766-769 (1985).
9. J. R. Griffith and J. G. O'Rear in "Biomedical and Dental Applications of Polymers", C. G. Gebelein and F. F. Koblitz, eds., Plenum, New York, N. Y., 373-377 (1981).
10. R. L. Soulen and J. R. Griffith, *J. Fluorine Chem.*, **44**, 203-210 (1989).

APPENDIX O

**PROCESSABLE HEAVILY FLUORINATED ACRYLIC RESINS WITH
LOW DIELECTRIC CONSTANTS**



Geo CENTERS, INC.

PROCESSABLE HEAVILY FLUORINATED ACRYLIC RESINS WITH
LOW DIELECTRIC CONSTANTS

Henry S.-W. Hu*

Geo-Centers, Inc., Fort Washington, MD 20744

and

James R. Griffith*

Naval Research Laboratory, Washington, D.C. 20375

ABSTRACT: The preparation of a new class of processable heavily fluorinated acrylic resins with very low dielectric constants is reported. The title compounds 2 and 5 were prepared through the condensation of the respective alcohols 1 and 4 with acryloyl chloride. Unlike tetrafluoroethylene, monomers 2 and 5 are easy to process into polymers under normal conditions due to their liquid or semisolid nature. Radical polymerization of the title compounds with a trace amount of azobisisobutyronitrile or methyl ethyl ketone peroxide at 85-100°C leads to homopolymers 3 and 6 and copolymer 7. All polymers exhibit dielectric constants around 2.10-2.24 over a frequency region of 500 MHz to 18.5 GHz; the variation of dielectric constant values over the measured frequency region is within 0.03 for each polymer. These values are very

close to the known minimum dielectric constants of 2.0-2.08 for poly(tetrafluoroethylene) and 1.89-1.93 for a terpolymer of 2,2-bis-(trifluoromethyl)-4,5-difluoro-1,3-dioxole 8, perfluoropropylene and tetrafluoroethylene 9. The dielectric constants for poly(tetrafluoroethylene) measured with the same method are observed to be around 1.96-1.99 in order to validate the accuracy of our measurement.

Introduction

Materials exhibiting dielectric constants below 3 are in increasing demand in the aerospace and electronic circuit industries.¹ Dielectric constant is defined as a measure of the ability of a dielectric to store an electric charge. A dielectric is a nonconducting substance or an insulator. Dielectric constant is directly proportional to the capacitance of a material, which means that the capacitance is reduced if the dielectric constant of a material is reduced. For high-frequency, high-speed digital circuits, the capacitances of substrates and coatings are critical to the reliable functioning of the circuits. Present computer operations are limited by the coupling capacitance between circuit paths and integrated circuits on multilayer boards since the computing speed between integrated circuits is reduced by this capacitance and the power required to operate is increased.² The maximum frequency of operation of the field-effect transistor can be given by the frequency corresponding to the dielectric constant in the reverse proportion.³

With recent trends toward microminiaturization and utilization of very thin conductor lines, close spacings, and very thin insulation of 5 mils or less, greater demands are being placed on the insulating layer. Insulating materials must possess very low dielectric constants and at the same time must retain other required engineering and manufacturing properties. For high frequency linear circuits, such as those used in radar assemblies, the dielectric constant of insulators again becomes important, especially since it may vary with changes in frequency.

Reductions in such parasitic capacitance can be achieved in a number of ways through the proper selection of materials and the design of circuit geometry. In 1988 St. Clair *et al.* reported a reduction of dielectric constant to 2.39 by chemically altering the composition of a polyimide backbone to reduce the interactions between linear polyimide chains and by the incorporation of fluorine atoms.⁴

Poly(tetrafluoroethylene) (PTFE), which is a solid at room temperature, has a dielectric constant⁵ in the range of 2.00-2.08 while its monomer, tetrafluoroethylene, is a gas at room temperature. Poly(tetrafluoroethylene) is exceptionally chemically inert, has excellent electrical properties, has outstanding stability, and retains mechanical properties at high temperatures. The problem with poly(tetrafluoroethylene) is that it is not processable. A commercial material believed to be a terpolymer of tetrafluoroethylene 9, perfluoropropylene and 2,2-bis(trifluoromethyl)-4,5-difluoro-1,3-dioxole 8 (a derivative of

hexafluoroacetone) is reported to have a dielectric constant in the range of 1.89-1.93. It is reported to be more processable than poly(tetrafluoroethylene).⁶

A series of studies have been carried out in our laboratory to design and synthesize new fluorinated epoxy and acrylic resins. These materials have many applications because of their unique properties.⁷ In this paper we report the preparation of a series of new processable heavily fluorinated acrylic resins which exhibit dielectric constants as low as 2.10, very close to the known minimum values.

Experimental Section

Materials. Triethylamine was fractionally distilled from lithium aluminum hydride under nitrogen and acryloyl chloride was distilled under nitrogen. 1,1,2-Trichlorotrifluoroethane (Freon 113) was distilled from phosphorus pentoxide under nitrogen. Azobisisobutyronitrile (AIBN) was used as received. Methyl ethyl ketone peroxide (MEKP) (9% A.O. Max., Organic Peroxide VN 2550) was obtained from Witco. Alumina (neutral, Brockman activity 1, 80-200 mesh) was obtained from Fisher Scientific Co. All other reagents were used as received or purified by standard procedures.

Techniques. Infrared spectra were obtained with a Perkin-Elmer 1800 Fourier Transform Infrared Spectrophotometer and the absorption frequencies are reported in wavenumbers (cm^{-1}). Proton-1 NMR spectra were obtained with a 300 MHz BZH-300 Bruker FT NMR spectrometer. Chloroform-d was used as solvent, and chemical

shifts are reported in ppm downfield from tetramethylsilane for δ . Rf values were obtained from silica gel thin layer chromatography developed with a mixture of methylene chloride 1.5 mL and acetone 3 drops. The number of hydrate water molecules was calculated from the integration of proton-1 NMR spectra.

Preparation of etherdiacrylate 2 from 1. 1,3-Bis-(2-hydroxy-hexafluoro-2-propyl)-5-(4-heptafluoro-isopropoxy-1,1,2,2,3,3,4,4-octafluoro-1-butyl)benzene 1, bp 95°C/1.0mm, was prepared by the multistep route reported by Griffith and O'Rear⁸. Elemental analysis showed it to be anhydrous, but after long storage it had 0.5 H₂O as water of hydration. Rf 0.36; ¹H NMR δ 8.35 (s, 1H, 2-ArH), 8.09 (s, 2H, 4,6-ArH), 4.14 (s, 2H, -OH), 2.13 (s, 1H, H₂O); IR(neat) 3620 and 3515 br (OH), 3125, 1618, 1468, 1365, 1350-1100(CF), 1005, 992, 980, 948, 938, 900, 872, 841, 800, 775, 768, 758, 738, 728, 707, 690, 668, 621 cm⁻¹.

The etherdiacrylate 2 was prepared by a modification of the procedure of Griffith and O'Rear.⁹ To a solution of 1 (3 g, 3.78 mmol) in Freon 113 (10 mL) in an ice-water bath under nitrogen, triethylamine (0.791 g, 7.81 mmol) in Freon 113 (5 mL) was added dropwise in 10 min. After 10 more min, acryloyl chloride (0.707 g, 7.81 mmol) in Freon 113 (5 mL) was added dropwise in 20 min; a precipitate formed immediately. After stirring 2 hr at room temperature, filtration through Celite to remove the solid, followed by evaporation at room temperature *in vacuo*, 3.02 g of a viscous liquid was obtained.

The liquid was dissolved in a mixture of methylene chloride (20

mL) and Freon 113 (10 mL); filtration through neutral alumina (1 g) gave a clear filtrate. It was cooled in an ice bath, washed twice with 1.3N sodium hydroxide 10 mL, washed with water 10 mL, dried over anhydrous sodium sulfate, percolated and washed through a column of neutral alumina (3 g) twice, and evaporated *in vacuo* at room temperature for 3 hr to give a colorless viscous liquid 2 1.38 g, yield 40%. Rf 0.92; IR(neat) 3118, 1772, 1637, 1468, 1410, 1365, 1350-1100(CF), 1055, 1040, 992, 900, 878, 848, 800, 770, 759, 740, 728, 718, 670 cm^{-1} ; $^1\text{H NMR}$ δ 7.68 (s, 2H, 4,6-ArH), 7.63 (s, 1H, 2-ArH), 6.61 (d, J=17 Hz, 2H), 6.29 (d, d, J=17, 10 Hz, 2H), 6.13 (d, J=10 Hz, 2H), 1.57 (s, 2H, H_2O) indicated 1.0 H_2O as water of hydration.

Preparation of triacrylate 5 from 4. 1,3,5-Tris(2-hydroxyhexafluoro-2-propyl)benzene 4 was prepared by a multistep route according to the procedure of Soulen and Griffith.¹⁰ This compound was hygroscopic as also observed by Griffith and O'Rear.⁸ Rf 0.15; IR(KBr pellet) 3660, 3618, 3590 and 3513 (OH), 3125, 1465, 1300-1100(CF), 1026, 1013, 980, 891, 775, 730, 709, 693 cm^{-1} ; $^1\text{H NMR}$ δ 8.25 (s, 1H, ArH), 4.44 (s, 1H, -OH), 2.11 (s, 1.5H, H_2O) indicated 2.25 H_2O as water of hydration.

The triacrylate 5 was prepared by a procedure similar to that described for the synthesis of 2. Triol 4 (2.176 g, 3.78 mmol), triethylamine (1.517 g, 15.0 mmol) and acryloyl chloride (1.358 g, 15.0 mmol) were used. After filtration and evaporation, 1.82 g of a viscous liquid was obtained. It was dissolved in a mixture of methylene chloride (20 mL) and Freon 113 (20 mL), and a gelatinous

solid was removed by filtration through neutral alumina (1 g). The filtrate was purified by percolation and washing through a column of neutral alumina (3 g) twice. Evaporation at room temperature *in vacuo* 3 hr gave 1.12 g (40% yield) of 5 as a very viscous colorless liquid, which upon standing at -13°C became a semisolid. $^1\text{H NMR } \delta$ 7.53 (s, 3H), 6.57 (d, $J=17$ Hz, 3H), 6.24 (d, d, $J=17, 10$ Hz, 3H), 6.06 (d, $J=10$ Hz, 3H) indicated no water of hydration present. This semisolid is, however, hygroscopic. R_f 0.85; IR(KBr pellet) 3515, 3130, 2920, 2850, 1770, 1635, 1630, 1412, 1350-1100(CF), 1090, 1055, 995, 940, 900, 802, 750, 740, 725, 715, 689, 669 cm^{-1} ; $^1\text{H NMR } \delta$ 7.51 (s, 3H), 6.60 (d, $J=17$ Hz, 3H), 6.28 (d, d, $J=17, 10$ Hz, 3H), 6.11 (d, $J=10$ Hz, 3H), 1.56 (s, 3H, H_2O) indicated 1.5 H_2O as water of hydration.

Preparation of polymer "cylindrical donuts" from monomers. In order to prepare the samples for dielectric constant measurements, etherdiacrylate 2 was mixed with a trace amount of AIBN at room temperature in a cylindrical donut mold made from General Electric RTV 11 silicon molding compound. Donuts had an outer diameter of 7.0 mm, inner diameter of 3.0 mm and a thickness of 3.0 mm; the semisolid triacrylate 5 was mixed with a trace amount of liquid methyl ethyl ketone peroxide (MEKP) with some heating to obtain a clear liquid; equal masses of 2 and 5 were also mixed with MEKP with some heating.

For polymerization the filled donut molds were kept under an inert atmosphere, the temperature was raised to 85°C over 2 hr, then kept at $85-100^{\circ}\text{C}$ for 20 hr. Two homopolymers 3 (from 2) and

6 (from 5), and one copolymer 50/50 (w/w) 7 were obtained.

Dielectric constant (DE) measurements. Dielectric constant values are reported as "Permittivity" with the symbol ϵ or K_s . The polymer cylindrical donuts were used for the measurement of DE on a Hewlett Packard 8510 Automated Network Analyzer. The analyzer is capable of measuring 401 data points over a frequency band of 500 MHz to 18.5 GHz. Typically S11 and S21 values, which correspond to reflection and transmission respectively, are measured and then these values are used to calculate the permittivity and permeability.

Samples stood at room temperature in air prior to testing; measurements were run at room temperature and approximately 25% RH. A virgin PTFE sheet (MMS-636-2) was obtained from Gilbert Plastics & Supply Co. and cut into the same cylindrical donut size. The result for PTFE reported here is the average of DE values measured for three samples.

Results and Discussion

Monomers. The preparation of etherdiol 1 and triol 4 was carried out in multistep routes according to the reported procedures.^{8,10} As summarized in Scheme I, the synthesis of acrylic esters, 2 and 5, was carried out in a fluorocarbon solvent such as Freon 113 by the reaction of alcohols, 1 and 4, with acryloyl chloride and an amine acid acceptor such as triethylamine. Other attempts to esterify the fluoroalcohols directly with acrylic acid or acrylic anhydride were not successful.⁹ Product purification by

distillation was not feasible because of the temperature required, but purification by percolation of fluorocarbon solutions through neutral alumina resulted in products, 2 and 5, of good purity identified by TLC, proton-1 NMR and IR.

In proton-1 NMR spectra, both 2 and 5 showed a characteristic ABX pattern for acrylate in the region of δ 6.8-6.0 with a pair of doublet couplings for each vinyl proton as shown in Figure II and Figure III; the products purified by percolation over alumina contained no detectable hydrate water or polymerized impurities. After standing in air at room temperature, both alcohols 1, 4 and acrylates 2, 5 are found to contain hydrate water as shown in Table II with the chemical shifts and integral ratios. Only the alcohol 4 was reported^{8,10} to be a hygroscopic solid but gave anhydrous product by distillation or sublimation. It is interesting to note that the etherdiacrylate 2 contained twice the amount of hydrate as the etherdiol 1, while the triacrylate 5 contained only two-thirds the amount of hydrate as the triol 4 because in the case of the acrylates, there are equivalent hydrates for both 2 and 5.

The monomers 2 and 5 are stable at room temperature, and no change can be detected by use of IR and NMR after storing in air for three months.

Polymerization. Due to their liquid or semisolid nature, monomers 2 and 5 are easy to process into polymers. For radical polymerization the use of solid azobisisobutyronitrile (AIBN) for liquid 2 at room temperature and liquid MEKP for semisolid 5 or a mixture of 2 and 5 with some heating is convenient. During the

course of curing at 85-100°C the problem of surface inhibition of free radicals by oxygen of air can be avoided by inert gas blanketing.

Since each acrylate group is difunctional, the etherdiacrylate 2 is tetrafunctional while the triacrylate 5 is hexafunctional. For polymerization of the polyfunctional monomers at sufficiently high degrees of conversion, the branching must result in the formation of cross-links to give a three dimensional network. As expected, the homopolymers 3, 6 and the 50/50 (w/w) copolymer 7 are semitransparent, hard solids.

The degree of polymerization or conversion of 2 or 5 can be easily monitored with fourier transform infrared spectrophotometer, for example, by examining the intensity of the absorption frequencies at 1635 and 1410 cm^{-1} which are assigned to the acrylate functional groups as shown in Figure IV.

Dielectric constant (DE). In order to validate the accuracy of our measurements, three samples of virgin PTFE in the same cylindrical donut size were measured and found to have average DE values around 1.96-1.99, which are close to the reported values 2.0-2.08.⁵ Summarized results of the DE measurement on the polymer donuts 3, 6, 7, and PTFE are shown in Table I, while the observed measurement curves are shown in Figure I. All the new polymers exhibit unusually low DEs around 2.10-2.24 over a wide frequency region of 500 MHz to 18.5 GHz; the variation of DE values over the measured frequency region is within 0.03 for each polymer. The 50/50 (w/w) copolymer 7, having a molar ratio 45/55 of 2 and 5,

showed DE of 2.22 which is close to that of 6; this indicates that the copolymer 7 was not completely homogeneous and compatible.

The wide range frequency independence of these low DEs and the processability of these monomers suggest many potential applications. In particular, it is known that the addition of a fluorine-containing group to the polymer backbone will reduce the polymer chain-chain electronic interactions, resulting in a reduction of DE as reported by St. Clair *et al.*⁴, but the DEs for 3 (fluorine content 57%) are at most 0.13 below those for 6 (fluorine content 46%), which may indicate that a minimum value might have been nearly reached regarding the structure/property relationship.

In 1990 Resnick⁶ reported that the lowest dielectric constant (1.89-1.93) of any polymer thus far was obtained from copolymers of 2,2-bis(trifluoromethyl)-4,5-difluoro-1,3-dioxole 8 and tetrafluoroethylene 9 with structures shown in Scheme II. In addition to the effect of the fluorine content, the existence of similar perfluoroalkyl ether linkage on the double bonds in both monomers 8 and 2 seems to play an important role in further reducing the dielectric constant values.

It has been reported¹¹ that in the preparation of polyimides the more flexible *meta*-linked diamine systematically gave lower DE values than the corresponding *para*-linked system and that this may be related to free volume in the polymer since the *meta*-substituted systems should have a higher degree of entropy. This *meta* effect may be somewhat responsible for the low DE values for the fully

1,3,5-substituted 3, 6 and 7.

St. Clair *et al.*⁴ also observed that the low dielectric constant polyimides containing the $-CF_3$ group show excellent resistance to moisture, exhibiting almost PTFE-like behavior. Since PTFE contains 76% fluorine, it appears that the DE values for the heavily fluorinated 3, 6 and 7 with fluorine content around 46-57% will be humidity-independent. It is known that water has a very high DE of 79.45. The low DE values for 3, 6 and 7 suggest a very low water content after polymerization of the hydrated monomers.

Processibility and Applications. The liquid or low melting solid monomers 2 and 5 can be cured to the solid state by incorporating therein a curing catalyst and heating the mixtures below the decomposition temperature thereof. Moreover the cured solids 3, 6, and 7 are transparent and hard polymers formed of three dimensional networks and reasonable thermostability.

In the course of curing, the viscosity varies from thin to syrupy liquids which is favorable for use to impregnate reinforcing materials, such as fiber glass scrim, used in making wiring boards or circuit boards or other electronic components used in electric or electronic applications.

Dielectric constants of these materials can be further lowered by known means such as by incorporating air bubbles in the materials or by mixing glass therewith. A difference of a couple of hundredths in the dielectric constant value may be important when one is at the low extremes thereof.

A compound containing two or three unsaturated groups would be

expected to polymerize to a crosslinked, solid, and non-linear thermosetting polymer. Fluorinated compounds which have one unsaturated group can be used in a mixture with 2 or 5 to polymerize to a solid polymer of a thermoset nature.

Conclusions

In this work we have demonstrated that a new class of heavily fluorinated acrylic resins can be efficiently synthesized and then cured to solid form with a catalyst at elevated temperatures. These cured resins were found to have unusually low dielectric constants, which are close to the known minimum values for PTFE and its terpolymers. In contrast to tetrafluoroethylene, our monomeric fluorinated aromatic acrylates are processable under normal conditions due to the fact that they are liquids or low melting solids, and moreover are soluble in common organic solvents. A practical manipulation in making network polymers is also established. We foresee many applications of these new fluoropolymers in aerospace and electronic circuit industries.

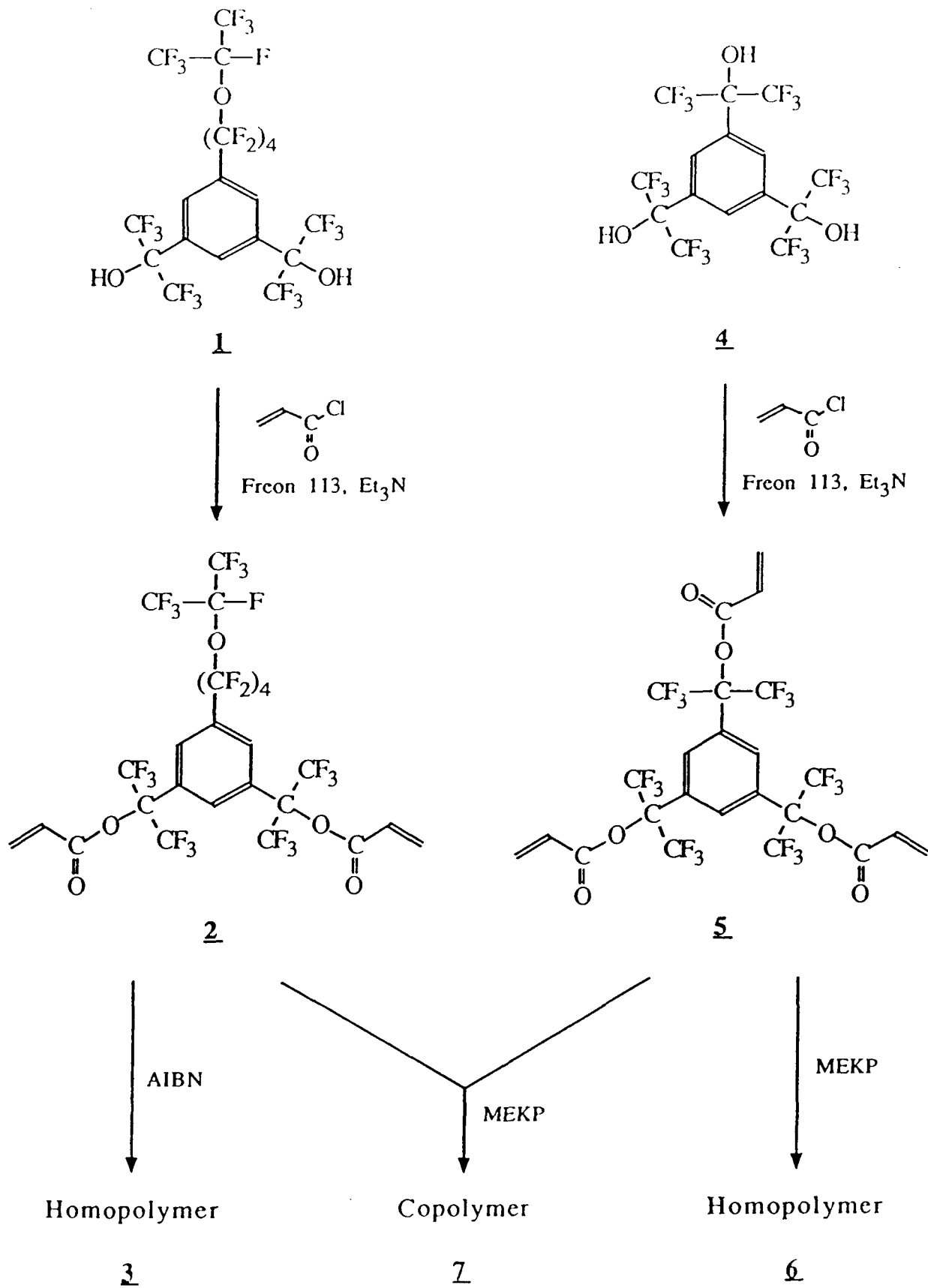
Acknowledgement. We are indebted to Mr. Jonas K. Lodge of SFA, Inc. for the dielectric constant measurements. Partial funding support from the Office of Naval Research is gratefully acknowledged.

References and Notes

- (1) Dorogy, W. E. Jr.; St. Clair, A. K. *Polym. Mater. Sci. Eng.*

- 1991, 64, 379.
- (2) Licari, J. J.; Hughes, L. A. *Handbook of Polymer Coating for Electronics*; Noyes Publications: Park Ridge, NJ, 1990; p 114. The relationship of capacitance C with dielectric constant K_S can be expressed as $C = AK_S\epsilon_0/d$ where A is area, d is distance, and $\epsilon_0 = 8.85418 \times 10^{-14}$ F/cm.
- (3) Grove, A. S. *Physics and Technology of Semiconductor Devices*; John Wiley & Sons: New York, NY, 1967; pp 254-255. K_S represents the dielectric constant in equation 8.22 with $K_S = \epsilon_S/\epsilon_0$.
- (4) St. Clair, A. K.; St. Clair, T. L.; Winfree, W. P. *Polym. Mater. Sci. Eng.* 1988, 59, 28.
- (5) see Ref. (2), pp 378-379, Table A-13: Dielectric Constants for Polymer Coatings (at 25°C).
- (6) Resnick, P. R. *Polym. Prepr.* 1990, 31(1), 312.
- (7) (a) Griffith, J. R.; Brady, R. F. Jr. *CHEMTECH*, 1989, 19(6), 370. (b) Hu, H. S.-W.; Griffith, J. R. *Polym. Prepr.* 1991, 32(3), 216.
- (8) Griffith, J. R.; O'Rear, J. G. *Polym. Mater. Sci. Eng.* 1985, 53, 766.
- (9) Griffith, J. R.; O'Rear, J. G. In *Biomedical and Dental Applications of Polymers*; Gebelein, C. G., Koblitz, F. F., Eds.; Plenum: New York, NY, 1981; pp 373-377.
- (10) Soulen, R. L.; Griffith, J. R. *J. Fluorine Chem.* 1989, 44, 210.
- (11) St. Clair, T. L. In *Polyimides*, ... D.; Stenzenberger,

H. D., Hergenrother, P. M., Eds.; Blackie: Glasgow, U.K.,
1990; pp 58-78. see p 74.



Scheme 1

Table I

Summary of Data for Dielectric Constant Measurements^a

samples	frequency (GHz)			
	0	3.5	9.5	15.5
<u>3</u>	2.11	2.10	2.12	2.13
<u>6</u>	2.23	2.23	2.23	2.22
<u>7</u>	2.22	2.23	2.24	2.22
PTFE ^b	1.96	1.98	1.99

^aSee Experimental Section for detail.

^bPoly(tetrafluoroethylene).

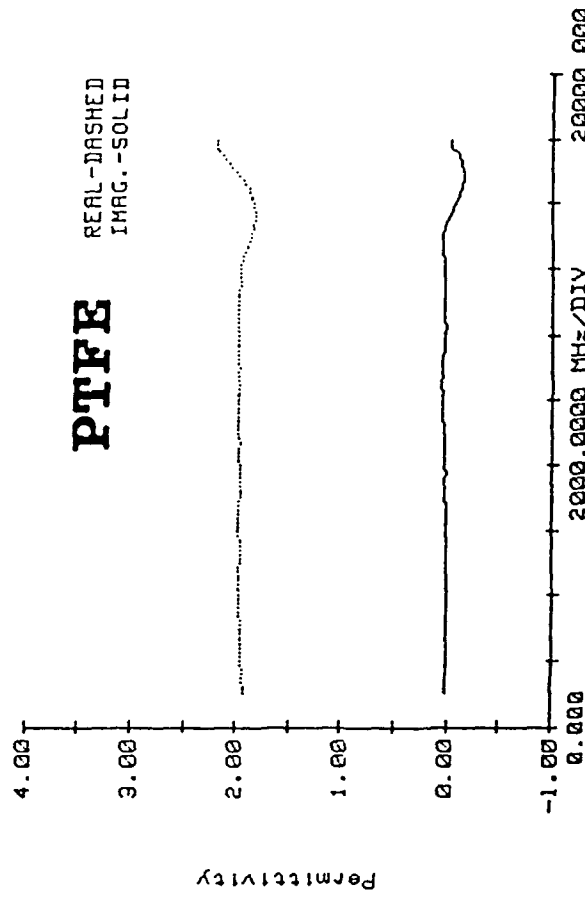
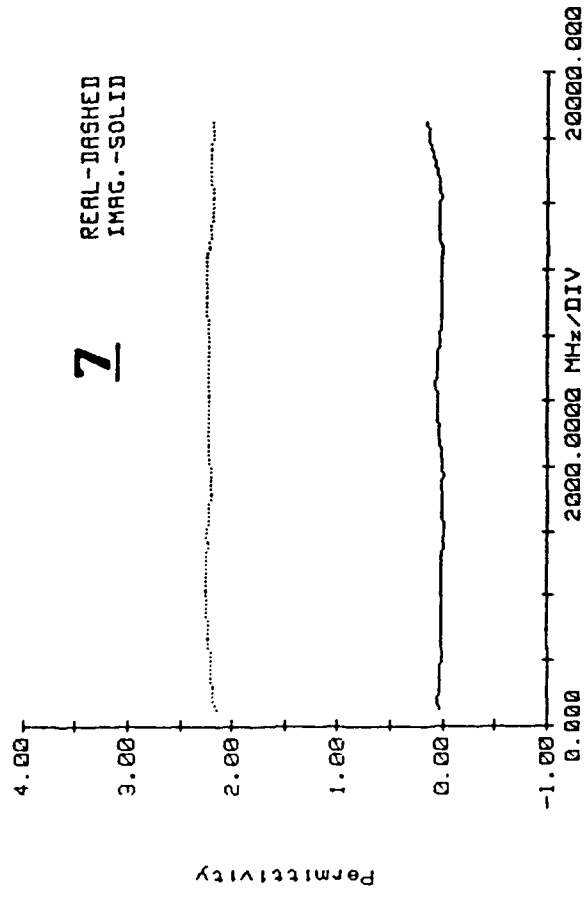
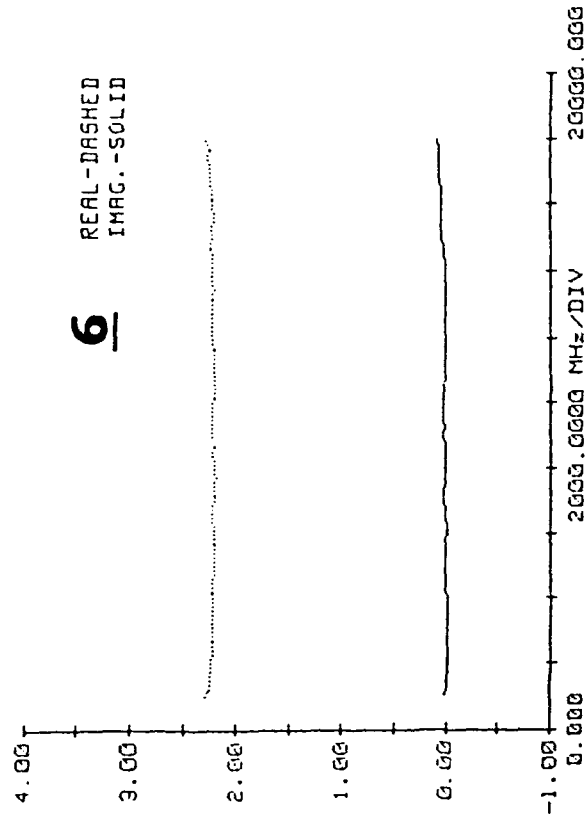
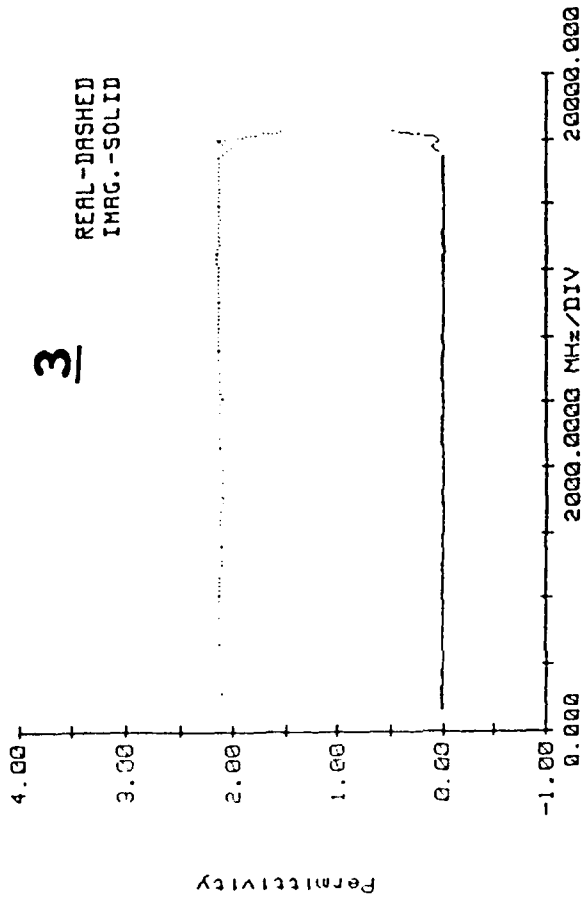


Figure 1 Observed curves of dielectric constant measurement for 3, 6, 7 and Teflon.

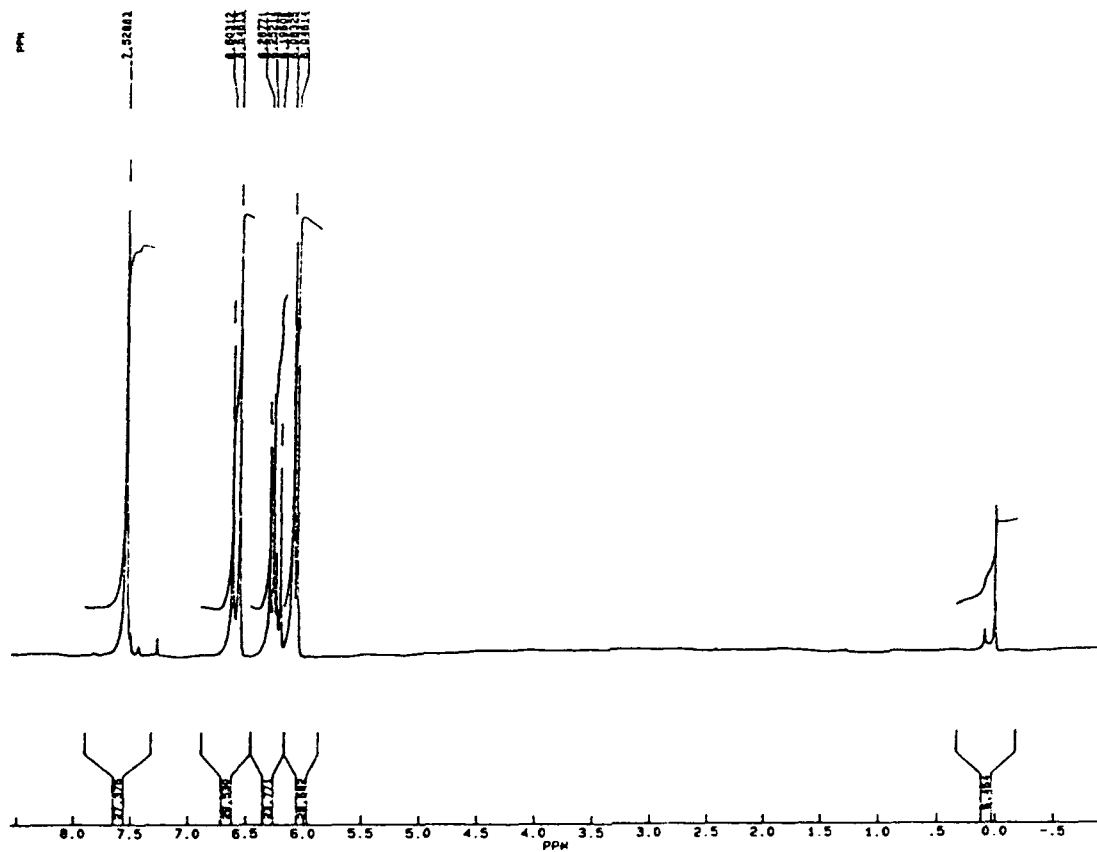


Figure II 300 MHz ^1H NMR spectrum of anhydrous **5** in CDCl_3 .

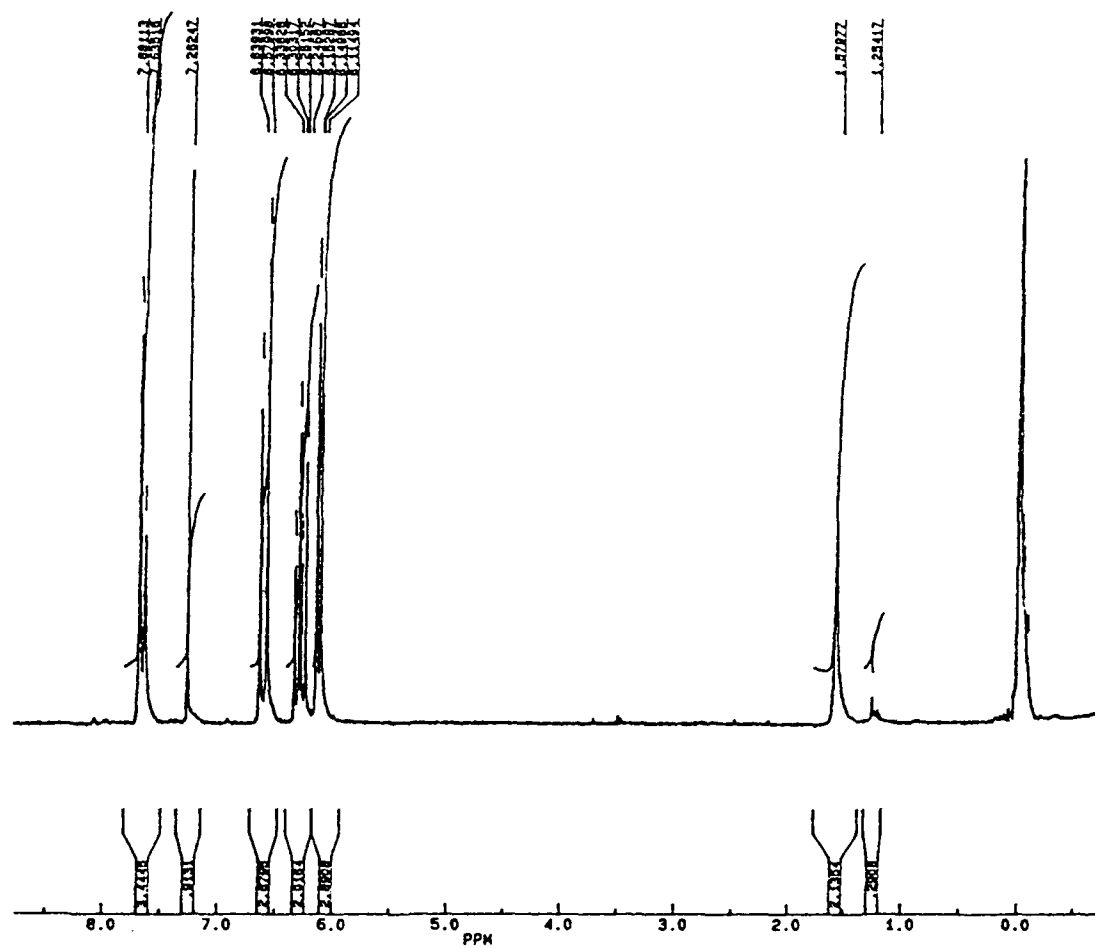


Figure III 300 MHz ^1H NMR spectrum of hydrated 2 in CDCl_3 .

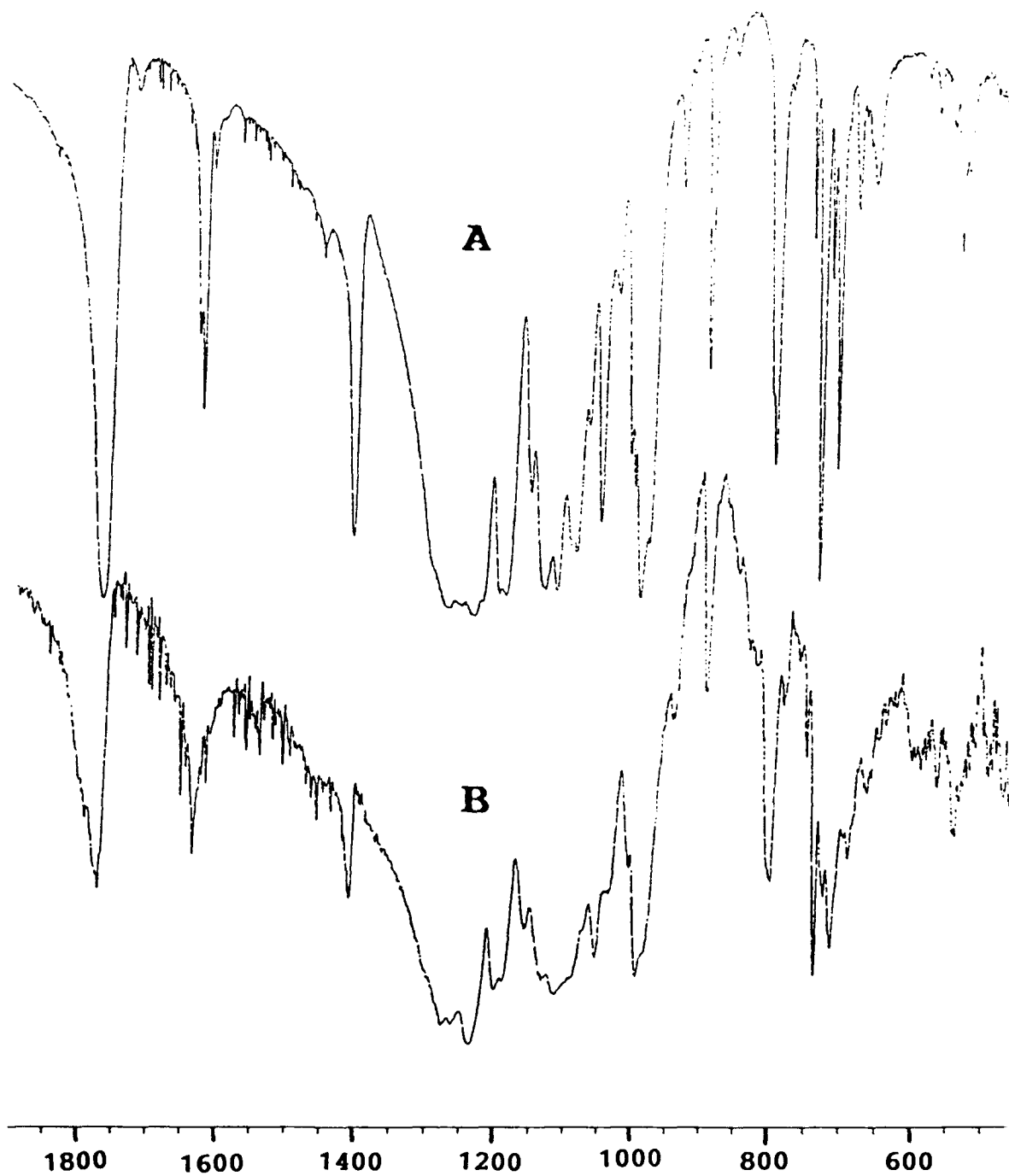
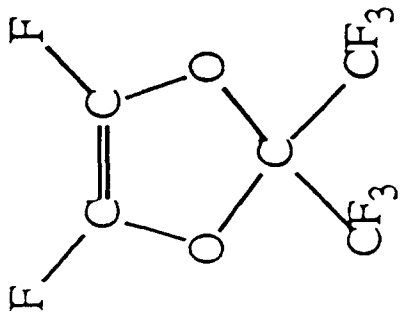


Figure IV FT-IR (KBr pellet) spectra of (A) anhydrous 5 and (B) its curing with AIBN at 100°C for 18 hr.

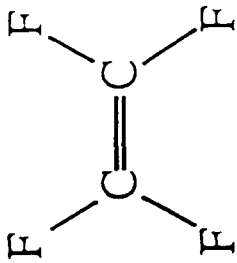
Table II

Summary of Data for Hydrate Water Relationship

samples	^1H NMR δ (CDCl_3/TMS)		$(\text{H}_2\text{O})_n$ n	functionality ratio vinyl or -OH vs $(\text{H}_2\text{O})_n$
	-OH	$(\text{H}_2\text{O})_n$		
<u>1</u>	4.14	2.13	0.5	2 : 1
<u>2</u>		1.57	1.0	4 : 2
<u>4</u>	4.44	2.11	2.25	3 : 4.5
<u>5</u>		1.56	1.5	6 : 3



8



9

Scheme II

APPENDIX P
L-PROLINE MODIFIED NYLONS



GEO-CENTERS, INC.

H. S-W. Hu^a, J. R. Campbell^b and J. R. Griffith^b
^aGeo-Centers, Inc., Fort Washington, Maryland 20744
^bNaval Research Laboratory, Washington, D.C. 20375

INTRODUCTION

The conformational constraints that L-proline imposes upon natural polypeptides has been recognized as the most significant factor in the occurrence of β bends and pleats^{1, 2, 3}. The amino group of this most unusual natural amino acid is secondary and contained in a five-membered ring structure, and as one consequence of this, the peptide linkage formed with the amine group lacks an available hydrogen atom for hydrogen bonding. The implications for the materials properties, as opposed to the biological properties, of natural and synthetic polyamides containing L-proline are most interesting. Thus we have begun a synthetic effort with a first objective of defining the minimal structure of synthetic polymer for which L-proline will control the elastic properties.

A most effective synthesis of regularly ordered copolyamides, which could properly be called the Bailey Synthesis^{4, 5}, has produced a number of unique products of this type. This is the first application of this general synthetic procedure to a proline-containing copolyamide. The 11-carbon moiety was selected as the reactant to complement proline for several reasons. First, proline compounds are frequently oils, which are difficult to crystallize and purify. This problem, however, is offset by the relative ease with which long chain aliphatic amides can be crystallized. Second, in the polymers that contain proline, there should be a length of inert chain between the beta type bends, and the straight-chain 11-carbon aliphatic structure is a good substitute for the hydrophobic amino acid residues often found in natural chains. Last, the 11-aminoundecanoic acid 1 is a readily available, long-chain amino acid reactant.

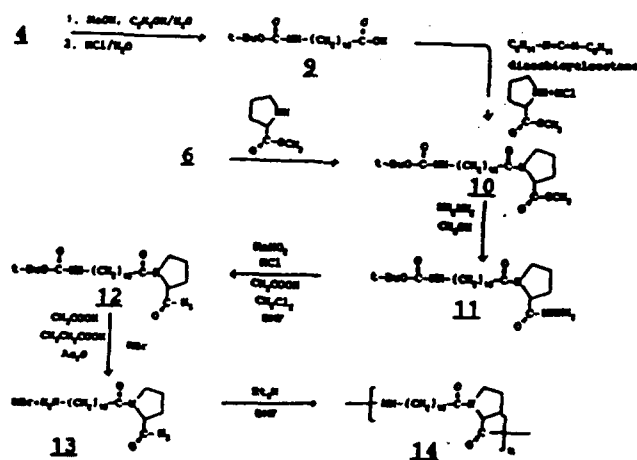
EXPERIMENTAL

As illustrated in Scheme 1, the polyamide of 11-aminoundecanoic acid (Nylon 11) 8 was synthesized by a seven-step procedure. 11-Aminoundecanoic acid 1 was first converted to its ethyl ester amine hydrochloride 2 (mp 140-143°C, lit⁶. 143°C) with hydrogen chloride in anhydrous ethanol. Refluxing 2 with phosgene in toluene to emit hydrogen chloride, ethyl 11-isocyanatoundecanoate 3 (bp 150°C/2.0 mm, lit⁶. 149°C/2.0 mm) was obtained through distillation in quantitative yield. Addition of t-butanol to 3 at 60°C with di(n-butyl)tin diacetate catalyst gave a nearly quantitative yield of semisolid ethyl 11-t-butyloxycarbonylamino-undecanoate 4 (mp \approx 25°C). This gave the crystalline solid 11-t-butyloxycarbonylaminoundecanoyl hydrazide 5 (mp 93-94°C) upon treatment with methanolic hydrazine at 40°C. This was converted to solid 11-t-butyloxycarbonylamino-undecanoyl azide 6 in 93% yield with addition of aqueous sodium nitrite at -10°C into a mixture of dimethylformamide (DMF), dichloromethane, acetic acid and hydrochloric acid. Compound 6 was then deblocked at -20°C with hydrogen bromide in acetic acid, propionic acid and acetic anhydride. The mixture was then added to cooled dry ether (-40°C) to precipitate a very hygroscopic crystalline solid 11-amino-undecanoyl azide hydrobromide 7 in 60% yield. Finally, a very slow addition of

triethylamine to the DMF solution of 7 at -20°C followed by standing for 3 days at -15°C yielded DMF-insoluble and DMF-soluble polymers. The former 8 was filtered off, and the latter was obtained by precipitation with water.



Scheme 1



Scheme 2

Copolyamide 14 of 1 and L-proline was synthesized in Scheme 2 from 4 and 6. The preparation of methyl 11-t-butyloxycarbonylaminoundecanoyl-L-prolinate 10 (mp 43.5-45°C) has been carried out in two steps. Hydrolysis of ethanolic 4 with the addition of aqueous sodium hydroxide and acidification gave 11-t-butyloxycarbonylamino-undecanoic acid 9 (mp 67.5-68.5°C) in 91% yield, which was then coupled with methyl L-prolinate hydrochloride in 78% yield by using dicyclohexylcarbodiimide and 1,4-diazabicyclo[2,2,2]octane in dry methylene chloride. The condensation of 9 with methyl L-prolinate in ethyl acetate at 5°C resulted in an oil in 29% yield, which showed a similar infrared spectra to that of 10. It is acceptable for practical use although it can not be crystallized.

Compound 10 was converted into crystalline 11-t-butyloxycarbonylaminoundecanoyl-L-prolyl hydrazide 11 (mp 58-61°C) with methanolic hydrazine at 40°C in a quantitative yield. Solid 11-t-butyloxycarbonylaminoundecanoyl-L-prolyl azide 12 was obtained in 80% yield with the same method described above. Deblocking of 12 at -20°C with hydrogen bromide in acetic acid, propionic acid and acetic anhydride yielded a semisolid 11-aminoundecanoyl-L-prolyl azide hydrobromide 13 in 90% yield. A very slow addition of triethylamine to the DMF solution of 13 at -20°C followed by standing for 3 days at -15°C resulted in DMF-insoluble polymers 14.

RESULTS AND DISCUSSION

Our study of the preparation of polypeptides through the polymerization of the amino acid azide hydrobromides basically followed Bailey's general method^{4,5} with modifications. The key to the success of Bailey's method is the isolation and purification of crystalline amino acid or peptide azide hydrobromides. Thus, the synthesis of a regular alternating copolyamide of 11-aminoundecanoic acid and L-proline was accomplished by the condensation of 11-aminoundecanoyl-L-prolyl azide hydrobromide 13. Similarly, the homopolyamide of 11-aminoundecanoic acid was obtained through the condensation of 11-aminoundecanoyl azide hydrobromide 7.

Compound 3 is a colorless liquid obtained from distillation; all others are isolated as solids. Due to thermal decomposition to emit nitrogen gas, compounds 6, 7, 12 and 13 containing the acyl azide group should be always kept around -15°C. Melting points can not be obtained. Compounds 6 and 12 are resistant to water while the corresponding amine hydrobromide salts 7 and 13 are extremely hygroscopic and must be always kept under dry nitrogen. The characteristic infrared absorptions can be easily used to demonstrate the reaction pathway.

We note that the infrared spectra of 14 did not show the typical absorption bands of 960 and 1355 cm⁻¹ characteristic for poly-L-proline Form I in which all the peptide bonds are in the cis conformation⁶. It is obvious that the steric restraint to rotation about the carbonyl carbon-carbon bond and the carbonyl carbon-nitrogen (proline) is lower than that of poly-L-proline.

It was shown that a regularly alternating copolyamide in which one of the comonomers was an α -amino acid was biodegradable⁹. For example, the alternating copolyamide of glycine and 6-aminocaproic acid is readily broken down in several weeks and utilized as food by a number of bacteria and fungi. In contrast, polyglycine and Nylon 6 are both relatively inert under the same condition. We have observed that 14, but not 8, decomposed at elevated temperature while poly-L-proline and Nylon 11 are both stable.

In differential scanning calorimetry measurements compound 8 showed T_g at 50°C and T_m at 158°C which remained unchanged even after several hours heating. The commercial Nylon 11 produced from 11-aminoundecanoic acid at 200-220°C has T_m at 185°C. The decrease of T_m in 8 may reflect a lower molecular weight produced by the method of polymerization. Compound 14 showed a decomposition starting from 125°C and finishing at 188°C. The presence of L-proline in 14 may cause the decomposition at elevated temperature.

We have observed that 13 decomposed at room temperature rapidly into a white solid with melting point around 130-140°C. Infrared absorption spectra showed strong peaks at 1607 and 1659 cm⁻¹ indicating a copolyamideurea may be obtained.

REFERENCES

1. H.N. Rydon and P.W.G. Smith, *J. Chem. Sci.*, 3642 (1957).
2. J.T. Edsall, *J. Polym. Sci.*, 12, 253 (1954).
3. D.W. Urry, *Research and Development*, August, 57 (1988).
4. W.J. Bailey and R.C. Capozza, *Polym. Prep.*, 9(2), 61 (1968).
5. W.J. Bailey and Y. Okamoto, *Polym. Prep.*, 12(1), 177 (1971).
6. W.J. Humphlett and C.V. Wilson, *J. Org. Chem.*, 26, 2507 (1961).
7. W.L. Mattice and L. Mandelkern, *J. Am. Chem. Sci.*, 93, 1769 (1971).
8. H.D. Kim, C.H. Jang, and T. Ree, *J. Polym. Sci., Polym. Chem. Ed.*, 28, 1273 (1990).
9. W.J. Bailey, Y. Okamoto, W-C. Kuo, and T. Narita, *Proceedings of the Third International Biodegradation Symposium* (J.M. Sharpley and A.M. Kaplan, Ed., Applied Science Publishers Ltd., London, 1976) Kingston, R.I., Aug. 17-23, 1975, p. 765.

APPENDIX Q

L-PROLINE MODIFIED NYLONS

1. THE ALTERNATING COPOLYAMIDE OF L-PROLINE AND 11-AMINOUNDECANOIC ACID



GEO-CENTERS, INC.

L-Proline-Modified Nylons. 1. The Alternating Copolyamide of
L-Proline and 11-Aminoundecanoic Acid

Henry S-W. Hu,^a James R. Campbell^b and James R. Griffith^b

^aGeo-Centers, Inc., Fort Washington, Maryland 20744

^bNaval Research Laboratory, Washington, D.C. 20375

L-Proline is a principal amino acid in the resilient natural proteins, such as elastin. The unique elastic properties of elastin may arise from the cyclic secondary amine structure without hydrogen-bonding capacity found at a proline peptide linkage. The synthesis of an alternating copolyamide of L-proline and 11-aminoundecanoic acid as well as a homopolyamide of 11-aminoundecanoic acid involving the tertiary butoxycarbonyl group (t-BOC) and the azide functionality is reported here. This copolyamide is one in a series of nylon-type synthetic polymers which promise exceptionally tough and resilient materials.

INTRODUCTION

The conformational constraints that L-proline imposes upon natural polypeptides has been recognized as the most significant factor in the occurrence of β bends and pleats^{1, 2, 3}. The amino group of this most unusual natural α -amino acid is secondary and contained in a five-membered ring structure, and as one consequence of this, the peptide linkage formed with the amine group lacks an available hydrogen atom for hydrogen bonding. The implications for

the materials properties, as opposed to the biological properties, of natural and synthetic polyamides containing L-proline are most interesting. Thus we have begun a synthetic effort with a first objective of defining the role of L-proline in the control of elastic properties of synthetic copolyamides.

A most effective synthesis of regularly ordered copolyamides, which could properly be called the Bailey Synthesis^{4, 5}, has produced a number of unique products of this type. This is the first application of this general synthetic procedure to a L-proline-containing copolyamide. The readily-available 11-carbon moiety was selected as the reactant to complement proline for several reasons. First, proline derivatives are frequently oils, which are difficult to crystallize and purify. This problem, however, is offset by the relative ease with which long chain aliphatic amides can be crystallized. Second, in the polymers that contain proline, there should be a length of inert chain in order to achieve the β -type bends; the straight-chain 11-carbon aliphatic structure is a good substitute for the hydrophobic amino acid residues often found in natural chains.

EXPERIMENTAL

As illustrated in Scheme 1, the polyamide 8 (Nylon 11) of 11-aminoundecanoic acid was synthesized by a seven-step procedure. 11-Aminoundecanoic acid 1 (300g) in 1.5L of anhydrous ethanol was first converted to its ethyl ester amine hydrochloride 2 in 96% yield with the addition of hydrogen chloride (131g) at room temperature. Refluxing 2 (186g) in 0.5L of toluene with the

addition of phosgene (90g) to emit hydrogen chloride, ethyl 11-isocyanatoundecanoate 3 was obtained through distillation in 98% yield. Addition of t-butanol (10.6g) to 30g of 3 at 60°C with di(n-butyl)tin diacetate catalyst (12 drops) gave a 95% yield of semisolid ethyl 11-t-butoxycarbonylaminoundecanoate 4. This gave the crystalline solid 11-t-butoxycarbonylaminoundecanoyl hydrazide 5 in 72% yield upon treatment with anhydrous methanolic hydrazine at 40°C. Solid 11-t-butoxycarbonylaminoundecanoyl azide 6 was obtained in 93% yield with addition of aqueous sodium nitrite at -10°C into a solution of 5 in a mixture (8/2/2.5/5 by volume) of dimethylformamide (DMF), dichloromethane, acetic acid and 1N hydrochloric acid. The butoxycarbonyl group of 6 in ether was then removed at -20°C with hydrogen bromide in acetic acid, propionic acid and acetic anhydride. The mixture was then added to a cooled dry ether (-40°C) to precipitate a very hygroscopic crystalline solid 11-amino-undecanoyl azide hydrobromide 7 in 60% yield. Finally, a very slow addition of triethylamine (1.0g) to the DMF (12ml) solution of 7 (0.8g) at -20°C followed by standing for 3 days at -15°C yielded DMF-insoluble and DMF-soluble polymers. The former 8 in 57% yield was filtered off, and the latter was obtained by precipitation with water. The overall yield of 1 → 8 is 20%.

Copolyamide 14 of 1 and L-proline was synthesized as shown in Scheme 2. The preparation of methyl 11-t-butoxycarbonylamino-undecanoyl-L-prolinate 10 has been carried out in two ways. Hydrolysis of 20 ml ethanolic 4 (5g) with the addition of 10ml aqueous sodium hydroxide (0.75g) and acidification gave 11-t-butoxycarbonylaminoundecanoic acid 9 in 91% yield, which was then

coupled with methyl L-prolinate hydrochloride (2.75g from Aldrich Co.) in 78% yield by using dicyclohexylcarbodiimide (3.3g) and 1,4-diazabicyclo[2,2,2]octane (1.5g) in 100ml of dry methylene chloride. On the other hand, methyl L-prolinate hydrochloride (0.25g) in water was neutralized with 5% aqueous sodium hydroxide, its ethyl acetate extract was then condensed with 6 (0.50g) at 5⁰C resulted in an oil in 29% yield, which showed a similar infrared spectra to that of 10. This oil is acceptable for practical use although it can not be crystallized. Compound 10 was converted into crystalline 11-t-butoxycarbonylaminoundecanoyl-L-prolyl hydrazide 11 with methanolic hydrazine at 40⁰C in 99% yield. Solid 11-t-butoxycarbonylaminoundecanoyl-L-prolyl azide 12 was obtained in 80% yield with the same method described above for 6. Deblocking of 12 at -20⁰C with hydrogen bromide in acetic acid, propionic acid and acetic anhydride yielded a semisolid 11-aminoundecanoyl-L-prolyl azide hydrobromide 13 in 90% yield. A very slow addition of triethylamine to the DMF solution of 13 at -20⁰C followed by standing for 3 days at -15⁰C resulted in a DMF-insoluble polymer 14. The overall yield of 1 → 4 → 9 → 14 is 16%.

Properties: mp, bp, T_g, and T_m in ⁰C, recrystallization solvent, yield, infrared absorption frequencies in cm⁻¹ and NMR chemical shift δ(CDCl₃/TMS) with assignments are reported. 2. 140-143 (lit⁶. 143), (EtOAc), 96%. 3. bp 150/2.0 mm (lit⁶. 149/2.0 mm), 98%, 2265 OCN, 1733 COO. 4.14 (q, J = 7 Hz, 2H, COOCH₂), 3.29 (t, J = 7 Hz, 2H, OCNCH₂), 2.29 (t, J = 7 Hz, 2H, CH₂COO), 1.7-1.2 (m, 19H, CH₂ and CH₃). 4. ≈25 (Hexane), 95%, 3380 NH, 1736 COO, 1719 OCON.

4.6 (br, 1H, NH), 4.14 (q, J = 7 Hz, 2H, OCH₂), 3.10 (2t, J = 7 Hz, 2H, NCH₂), 2.30 (t, J = 7 Hz, 2H, CH₂COO), 1.7-1.2 (m, 28H, CH₂ and CH₃). 5. 93-94 (EtOAc), 72%, 3355 and 3305 NH, 1688 OCON, 1660 1638 CON. 7.25 (br, 1H, NH), 4.63 (br, 1H, NH), 3.85 (br, 2H, NH₂), 3.09 (2t, J = 7 Hz, 2H, NCH₂), 2.16 (t, J = 7 Hz, 2H, CH₂COO), 1.7-1.2 (m, 25H, CH₂ and CH₃). 6. no mp (decomposed), (ppt from water), 93%, 3395 NH, 2138 NNN, 1718 CONNN, 1690 OCON. 7. no mp (decomposed), (ppt from ether), 60%, 3370 NH, 2138 NNN, 1700 CONNN. 8. DMF-insoluble: Tg 50, Tm 158, 57%, 3310 NH, 1640 CON. 9. 67.5-68.5 (EtOAc/petroleum ether, 1:1), 91%, 3370 NH and OH, 1700 COO, 1690 OCON. 9.04 (br, 1H), 3.10 (2t, J = 7 Hz, 2H, NCH₂), 2.34 (t, J = 7 Hz, 2H, CH₂COO), 1.7-1.2 (m, 25H, CH₂ and CH₃). 10. 43.5-45 (EtOAc/petroleum ether, 1:10), 78%, 3395 NH, 1745 COO, 1693 OCON, 1640 CON. 4.53 (m, 1H, CHCOO), 3.73 (s, 3H, OCH₃), 3.58 (m, 2H, NCH₂), 3.11 (2t, J = 7 Hz, 2H, NHCH₂), 2.31 (t, J = 7 Hz, 2H, CH₂COO), 2.05 (m, 4H, 3,4-CH₂), 1.5-1.1 (m, 28H, CH₂ and CH₃). 11. 58-61 (EtOAc/petroleum ether, 1:1), 99%, 3385, 3340 NH, 1688 OCON, 1657 CONH, 1637 CON. 4.55 (m, 1H, CHCOO), 3.54 (m, 2H, NCH₂), 3.11 (2t, J = 7 Hz, 2H, NHCH₂), 2.31 (t, J = 7 Hz, 2H, CH₂COO), 1.98 (m, 4H, 3,4-CH₂), 1.5-1.1 (m, 25H, CH₂ and CH₃). 12. no mp (decomposed), (ppt from water), 80%, 3395 NH, 2155 NNN, 1725 CONNN, 1695 OCON, 1642 CON. 13. no mp (decomposed), (ppt from ether), 90%, 3370 NH, 2155 NNN, 1720 CONNN, 1645 CON. 14. DMF-insoluble: decomposed from 125 to 188⁰C, 35%, 3300 NH, 1650 CONH, 1640 CON.

RESULTS AND DISCUSSION

Our study of the preparation of polyamides through the polymerization of the amino acid azide hydrobromides basically followed Bailey's general method^{4, 5} with modifications. The key to the success of Bailey's method is the isolation and purification of crystalline amino acid or peptide azide hydrobromides. Thus, the synthesis of an alternating copolyamide of 11-amino-undecanoic acid and L-proline was accomplished by the condensation of 11-aminoundecanoyl-L-prolyl azide hydrobromide 13. Similarly, the homopolyamide of 11-aminoundecanoic acid was obtained through the condensation of 11-aminoundecanoyl azide hydrobromide 7.

Compound 3 is a colorless liquid obtained from distillation; all others are isolated as solids. Due to thermal decomposition to emit nitrogen gas, compounds 6, 7, 12 and 13 containing the acyl azide group should be always kept around -15°C. Melting points can not be obtained. Compounds 6 and 12 are resistant to water while the corresponding amine hydrobromide salts 7 and 13 are extremely hygroscopic and must be always kept under dry nitrogen. The characteristic infrared absorptions can be easily used to demonstrate the reaction pathways. The spectra (Fig. 1 and 2) indicate 6 → 7 → 8 and 12 → 13 → 14.

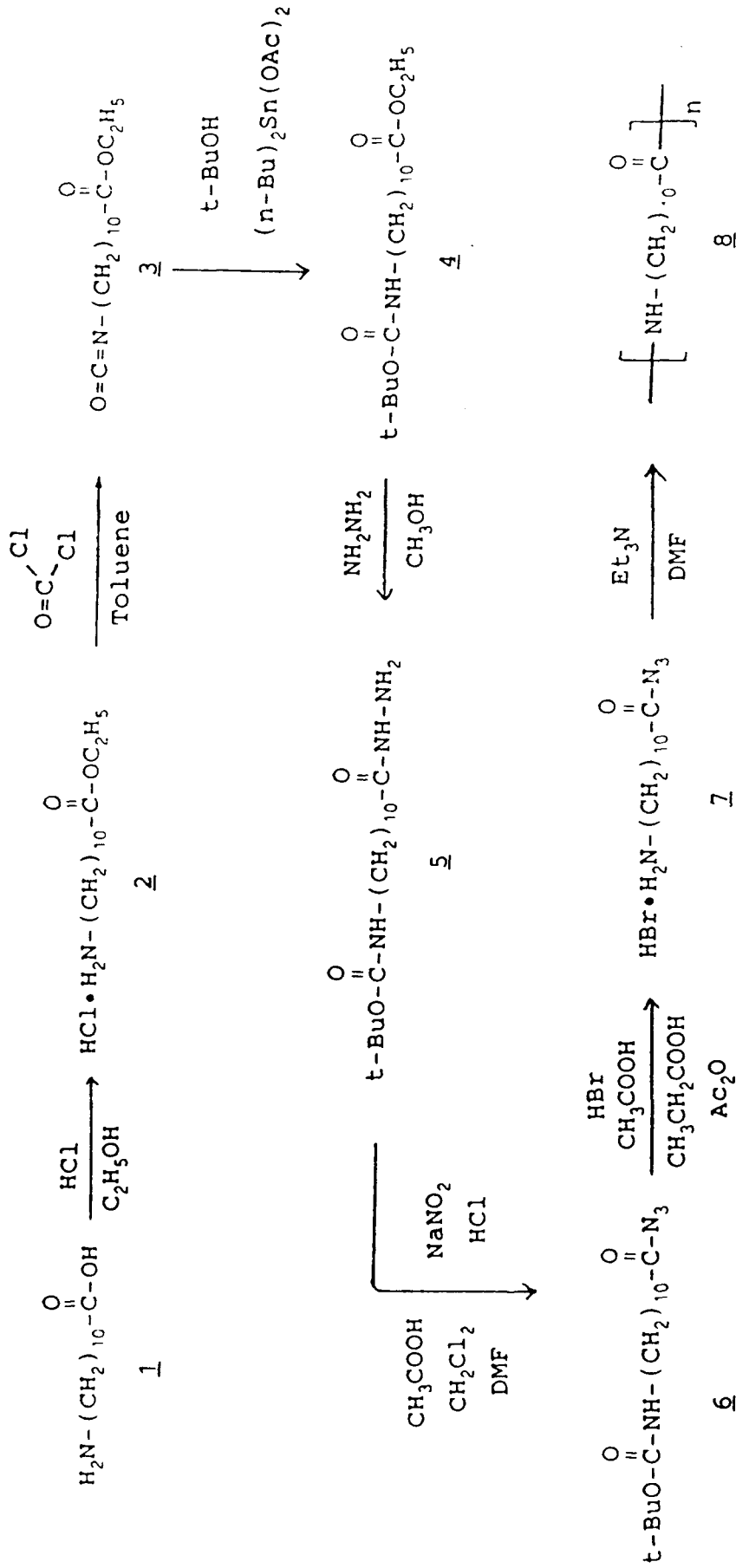
We note that the infrared spectra of 14 did not show the typical absorption bands of 960 and 1355 cm⁻¹ characteristic for poly-L-proline Form I in which all the peptide bonds are in the cis conformation^{7, 8}. It is obvious that the steric restraint to rotation about the carbonyl carbon-α carbon bond and the carbonyl carbon-nitrogen (proline) is lower than that of poly-L-proline.

It has been shown⁹ that a regularly alternating copolyamide in

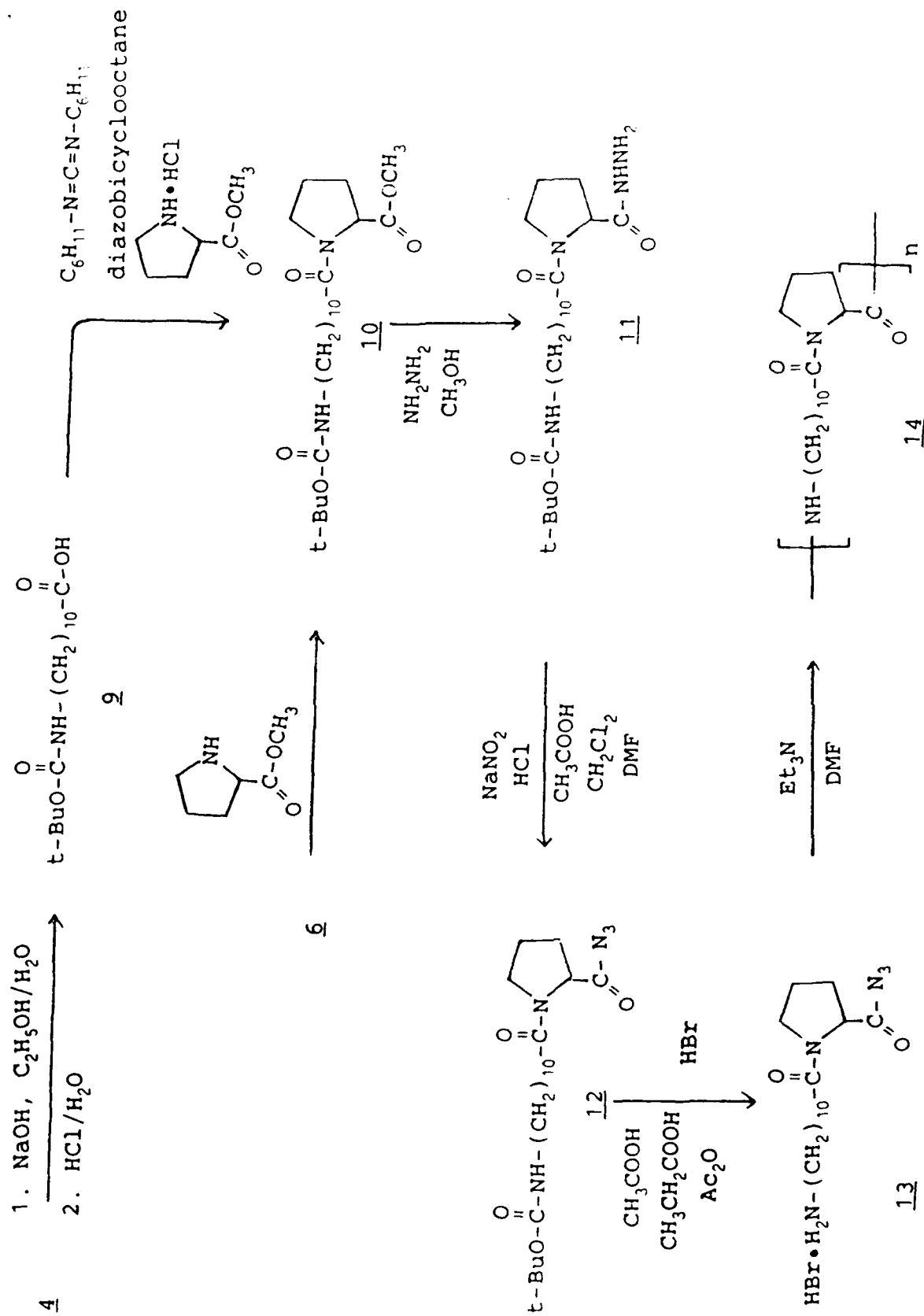
which one of the comonomers was an α -aminoacid was biodegradable. For example, the alternating copolyamide of glycine and 6-aminocaproic acid is readily broken down in several weeks and utilized as food by a number of bacteria and fungi. In contrast, polyglycine and Nylon 6 are both relatively inert under the same conditions. In differential scanning calorimetry measurements compound 8 showed T_g at 50°C and T_m at 158°C which remained unchanged even after several hours heating. The commercial Nylon 11 produced from 11-aminoundecanoic acid at $200\text{-}220^{\circ}\text{C}$ has T_m at 185°C and an infrared spectrum¹⁰ similar to that of 8. The decrease of T_m in 8 may reflect product variations produced by the method of polymerization; for example, the IR peak at 2040 cm^{-1} in 8 and 14 data doesn't appear in commercial Nylon 11. Compound 14 showed a decomposition starting from 125°C and finishing at 188°C . The presence of L-proline in 14 may cause the decomposition at elevated temperature.

References

1. H.N. Rydon and P.W.G. Smith, *J. Chem. Sci.*, 3642 (1957).
2. J.T. Edsall, *J. Polym. Sci.*, 12, 253 (1954).
3. D.W. Urry, *Research and Development*, August, 57 (1988).
4. W.J. Bailey and R.C. Capozza, *Polym. Prep.*, 9(2), 1261 (1968).
5. W.J. Bailey and Y. Okamoto, *Polym. Prep.*, 12(1), 177 (1971).
6. W.J. Humphlett and C.V. Wilson, *J. Org. Chem.*, 26, 2507 (1961).
7. W.L. Mattice and L. Mandelkern, *J. Am. Chem. Sci.*, 93, 1769 (1971).
8. H.D. Kim, C.H. Jang, and T. Ree, *J. Polym. Sci., Polym. Chem. Ed.*, 28, 1273 (1990).
9. W.J. Bailey, Y. Okamoto, W-C. Kuo, and T. Narita, *Proceedings of the Third International Biodegradation Symposium* (J.M. Sharpley and A.M. Kaplan, Ed., Applied Science Publishers Ltd., London, 1976) Kingston, R.I., Aug. 17-23, 1975. p. 765.
10. C.J. Pouchert, *The Aldrich Library of Infrared Spectra*, 2nd Ed., Aldrich Chemical Co. Inc., 1975, p. 1354B.



Scheme 1



Scheme 2

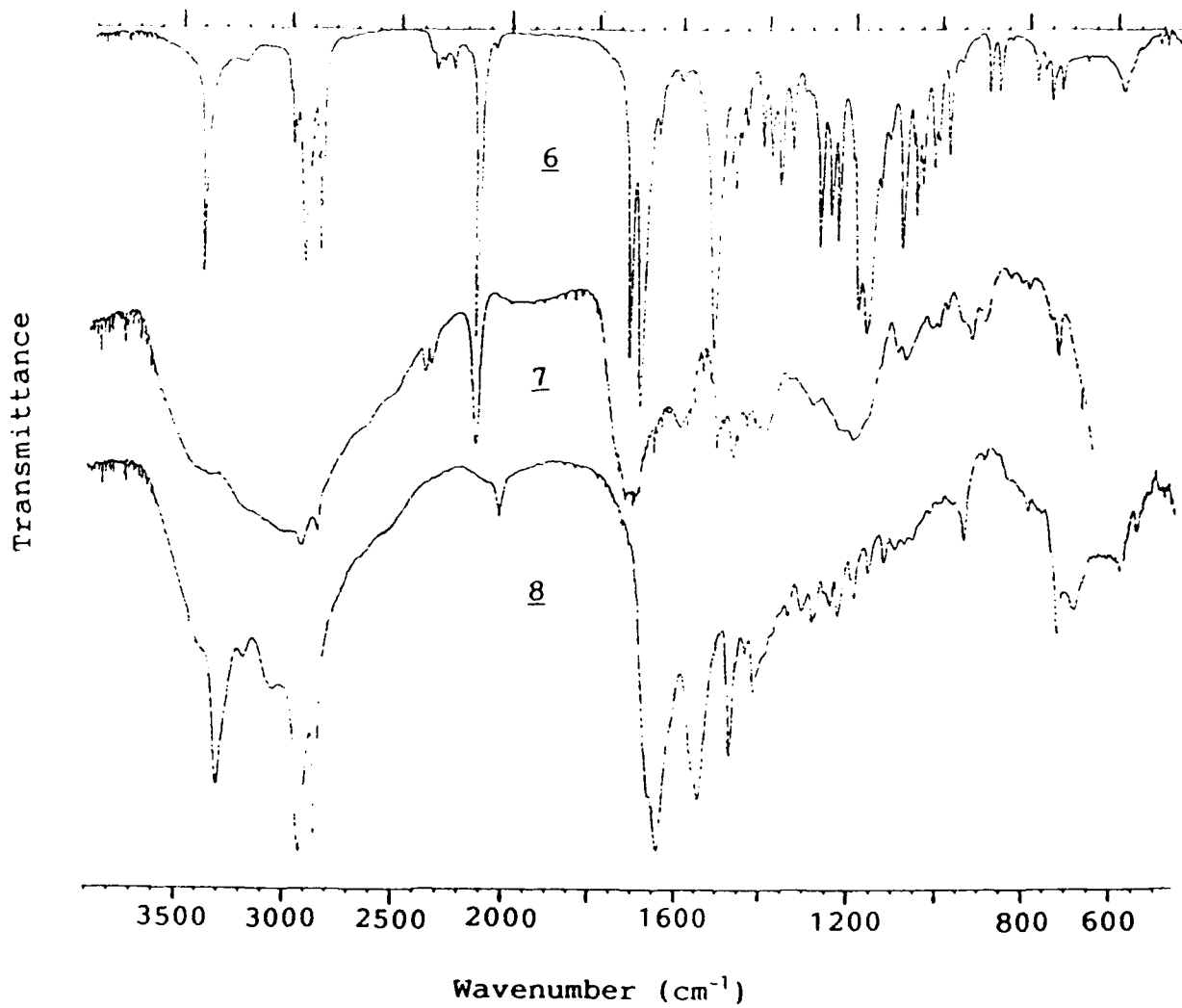


Figure 1: Infrared spectra of 6, 7 and 8.

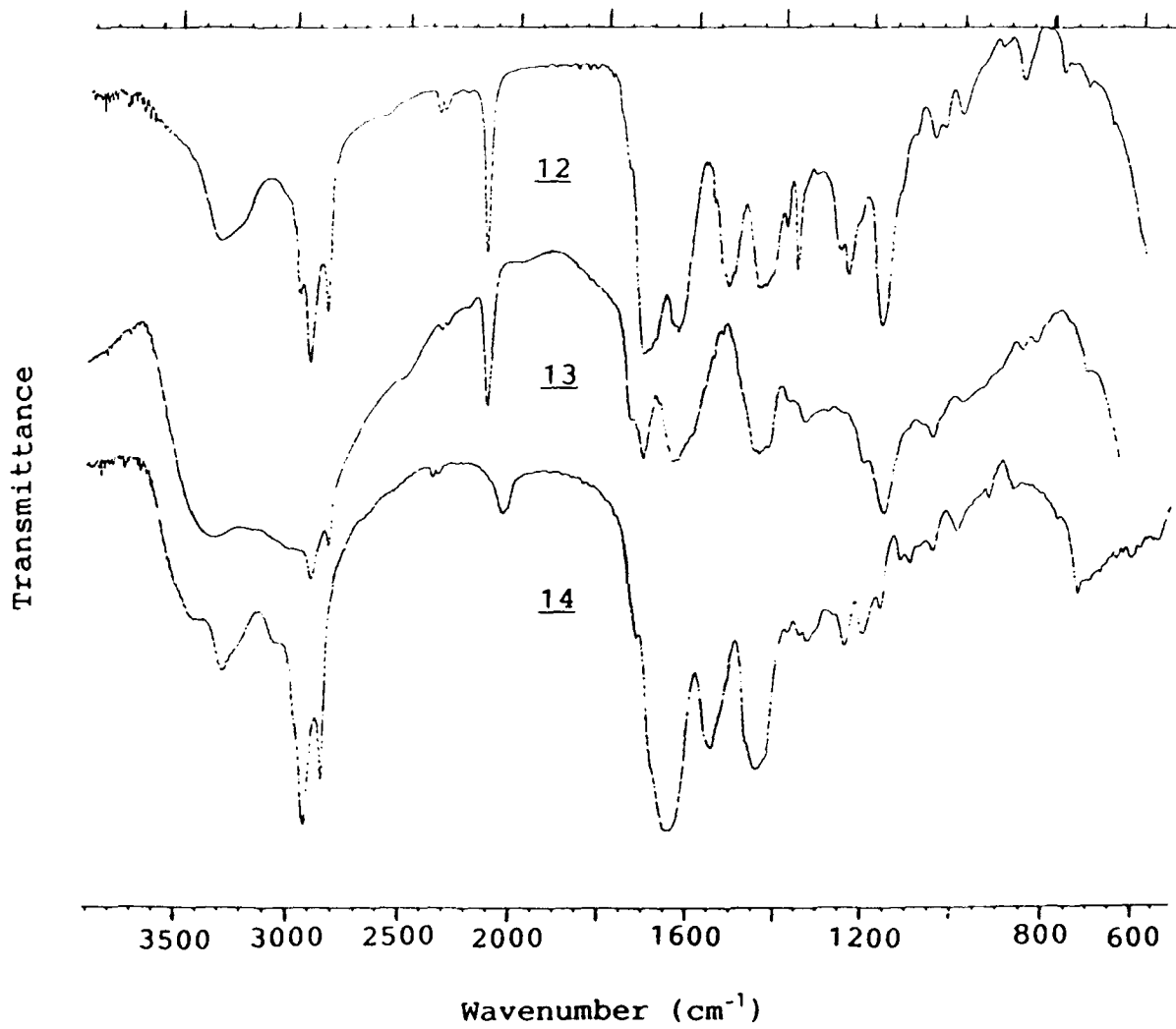


Figure 2: Infrared spectra of 12, 13 and 14.

APPENDIX R
NYLON 6 VS NYLON 66 SHOCK LOADING



GEO-CENTERS, INC.

February 7, 1992

Nylon 6 vs Nylon 66 Shock Loading

Distribution

Summary

Previous work on the relative performance of nylon 6 vs. nylon 66 in airdrop applications by D. C. Prevorsek et al. suggested nylon 6 webbings had some property advantages over similar webbings based on commercially available nylon 66. It was unclear whether this performance enhancement was inherent to nylon 6 or was influenced by the different fabric stress-strain behavior. To further substantiate these results and define the inherent benefit due to nylon 6, we have performed similar shock loading experiments at the Naval Research Laboratory (NRL) in Washington D.C. The original test was slightly modified to achieve higher loading rates (Figure 1) to address our concerns about viscoelastic effects and any potential heat generation during this cyclic fatigue test. This modification allowed us to achieve a minimum loading rate of 10,000 lbs/sec as measured via chart recorder (Figure 2) with oscilloscope estimation suggesting a much higher rate (circa 20,000 lbs/sec).

Two different sets of nylon 6 (N6) and nylon 66 (N66) webbings were tested at this higher loading rate, the original Murdock webbings and a new set of webbings produced by Elizabeth. These webbing sets differed in stress-strain and shock loading behavior. The N6 and N66 webs produced by Murdock were very different (Figure 3), while the Elizabeth webs had very similar properties (Figure 4). The webbing properties after shock loading are shown in Figures 5-7 and are summarized in Table 1.

Web temperature was measured on the Elizabeth webs one inch from the 90° steel abrasion point (Figure 8) and found to be insignificant (1°C) over 30 cycles as shown in Figure 9.

Based on these shock loading experiments we believe the initial webbing stress-strain behavior dictates the energy absorption characteristics of the web after shock loading. Therefore, N6 and N66 should perform equally in airdrop applications if they are processed such that the final web properties are similar. However, if the Murdock webs are more representative of the current military webbings, than the higher energy absorption characteristic of N6 could yield superior performance in this application. Further work is suggested to confirm these results on fabrics made from N6/N66 yarns with similar properties and to jointly develop this end-use testing procedure with the Army.

Table 1*

<u>Sample</u>	<u>Breaking Strength</u>	<u>Ultimate Elongation</u>	<u>Energy To Break</u>
	LBS	%	Joules
Elizabeth Webs			
<u>Nylon 6</u>			
Control	15934	30.5	380
Fatigued 10X	16128 (101)*	24.1 (79)	357 (94)
Fatigued 30X	15595 (98)	22.5 (74)	298 (78)
<u>Nylon 66</u>			
Control	16435	28.1	380
Fatigued 10X	16801 (102)	22.8 (81)	351 (92)
Fatigued 30X	16935 (103)	19.8 (70)	301 (79)
Murdock Webs			
<u>Nylon 6</u>			
Control	15026	34.5	392
Fatigued 10X	15487 (103)	25.9 (75)	377 (96)
<u>Nylon 66</u>			
Control	15412	24.5	320
Fatigued 10X	16688 (108)	17.4 (71)	293 (92)

* All properties represent one good Instron tensile test. Further testing for statistical averaging was not performed since these results suggested further test method development must be undertaken and there was a limited quantity of these webs available.

** Represents percent property retained

Experimental

The web stress-strain behavior was obtained using a computer controlled Instron 4206 equipped with a Wallace optical extensometer. A crosshead speed of 2"/minute was employed with grip center-to-center distance of circa 8 inches. Each sample was preloaded to 50 Kg at which time the webbing was marked with lines 50mm apart to allow tracking of the actual web strain with the optical extensometer. A "good" Instron break is defined as one which occurs by web failure outside the gripping region.

A MTS 810 testing frame with an Instron hydraulic system equipped with a wave generator was operated under load control to perform these fatigue experiments. The shock loading procedure was performed as described below using the apparatus shown in Figure 8. The slack in the system was removed by slowly loading the web until the system could sustain a 5000 lb. load for one minute at a distance below the crossheads' maximum travel. At this time the load was reduced to 3000 lbs. and the sample was cycled between 3000 and 5000 lbs. at 0.5 Hz for 10 or 30 cycles. Upon completion of this procedure the webbing was removed and immediately tested on the Instron. Temperature measurements were made by placing a small thermocouple in the middle of the loose web at the 90° steel abrasion point. Upon tensioning the web to 3000-5000 lbs., the thermocouple moved to a point 1-2 inches from the actual abrasion point.

Discussion

Test Method

The actual load profile during deployment is shown in Figure 1 along with the profiles selected for simulation purposes. It is apparent from this Figure that neither procedure duplicates the real life situation. The original Albany test went from 0 to 5000 lbs. compared to the 3000 to 5000 lb. cycle used at NRL. The smaller cycle amplitude used at NRL allowed attainment of higher stress rates more indicative of parachute deployment. The cycling frequency used in the Albany test is not obvious from the original report while 0.5 cycles/second was used at NRL. Therefore, the Albany test with lower cycling frequencies, from 0 minimum load to 5000 lbs. (approximately 30% of the nominal breaking load), compared to the NRL test with high cycling frequencies from 3000 to 5000 lbs. (18 to 30% of the nominal breaking load) are both extreme cases. The former simulates ten initial deployments of the parachute, and the latter, the sinusoidal fluctuations of several deployments. If the purpose of the test is to simulate a worst case load profile during 10 different deployments of the airdrop sling, a lower frequency should be chosen or the web should be loaded and then relaxed several hours and loaded again. If we are trying to simulate the actual stress scheme, 0.5 Hz would be the correct frequency and four sinusoidal load peaks should be used as one deployment simulation. Relaxing the web after this test and repeating this scheme x times would probably be the best duplication of multiple deployments. During the testing at NRL, a square wave profile was selected because it offers the fastest possible loading response. Further discussion with R&T and the end-user should be undertaken to arrive at the best loading scheme. This analysis suggests neither of

the shock loading experiments duplicate the real airdrop deployment, but both assess the relative fatigue resistance of these webbings under dynamic loading over a steel edge.

Heat generation was measured during both loading profiles and found to be trivial relative to the melting point of these fibers. As mentioned above, these test do not reflect the measured response which shows four load peaks, and these simulation tests were run at higher loads for 10-30 cycles.

In conclusion we believe the tests developed thus far demonstrate the relative performance of N6 and N66 under cyclic loading over a steel edge. However, further test refinement is required to yield a procedure which more accurately reflects the actual measured response.

NRL Results

Table 1 and Figures 3-6 summarize the results obtained at NRL and suggest the following trends.

- 1) Strength loss was rarely observed after this cyclic loading procedure.
- 2) Intermediate modulus of the web always increased after shock loading.
- 3) Ultimate elongation always decreased after dynamic loading.
- 4) Energy to break was always reduced after tension fatigue.
- 5) Except for the 30 cycle fatigue samples web failure did not occur in the abraded area.
- 6) There was no significant relative change difference (in contrast to absolute values) for N6 and N66 for any of these properties

Points 1-5 indicate this was not a very severe test and the higher modulus, UE/energy-to-break decrease, are most likely due to cycling the web and packing the constituent strands into jamming positions during testing, rather than actual fiber property reduction due to fatigue.

Under the higher loading rate conditions employed at NRL, N6 and N66 webs exhibit equal performance under cyclic loading if adjusted to similar stress-strain response.

Albany International Testing

The test results obtained at Albany International are summarized below in Table 2.

Table 2

<u>Sample</u>	<u>Breaking Strength</u> LBS	<u>Ultimate Elongation</u> %	<u>Energy To Break</u> IN-LBS/IN
Murdock Webs			
<u>Nylon 6</u>			
Control	15500	35.5	2310
Fatigued 10X	13600 (88)	25.3 (71)	1140 (49)
<u>Nylon 66</u>			
Control	17900	28.0	1710
Fatigued 10X	12900 (72)	19.5 (70)	730 (43)

These results indicate a significant strength loss after shock loading due to localized abrasion at the 90° steel edge. However, percentage elongation and energy-to-break changes were similar for both materials. This behavior indicates the Albany test imparted much greater abrasion to the web than did the NRL test. There could be several origins for this higher abrasion compared to the NRL test, such as the greater load change, and differences in the experimental setup (e.g., type of steel, its roughness and the angle of the abrading edge).

This data indicates N6 has better strength retention than N66 after shock loading yet this might be expected from a web with higher initial toughness. Since strength retention is a major issue, inherent abrasion resistance becomes important as pointed out in the original report. Therefore, we should also consider finish and weave differences since these are known to affect abrasion. Energy-to-break retention was 6% greater for N6 but the significance of this could be questioned in light of the radically different web starting properties.

Conclusions/Recommendations:

- 1) The current shock loading fatigue procedures do not properly simulate the measured airdrop sling load profile and need to be improved towards this end. It is recommended that a new test be developed jointly with R&T and the Army.
- 2) Loading rate does not appear to be an important factor in temperature rise or property retention over the experimentally covered range.
- 3) Initial web properties dictate the performance of these materials under these cyclic fatigue tests. N6 and N66 web designed to yield like stress-strain properties exhibit similar behavior under these conditions.
- 4) Abrasion resistance is a very important factor in determining the performance of the web in these tests and therefore, fabric finish and construction should be carefully controlled.
- 5) The best fundamental comparison between these materials could probably be achieved by comparing web produced from fiber of similar initial properties.

C.A. Trask

L.T. Heirigs

W.G. Mordecai

Distribution:

C.J. Nelson
H.H. Rowan
D.D. Wheeler
J.C. Fegley
I.H. Brisson
E.J. Corrigan
B.M. Mago
D.C. Prevorsek
E.W. Pulver
C.M. Roland
J.B. Nagode

Figure 1

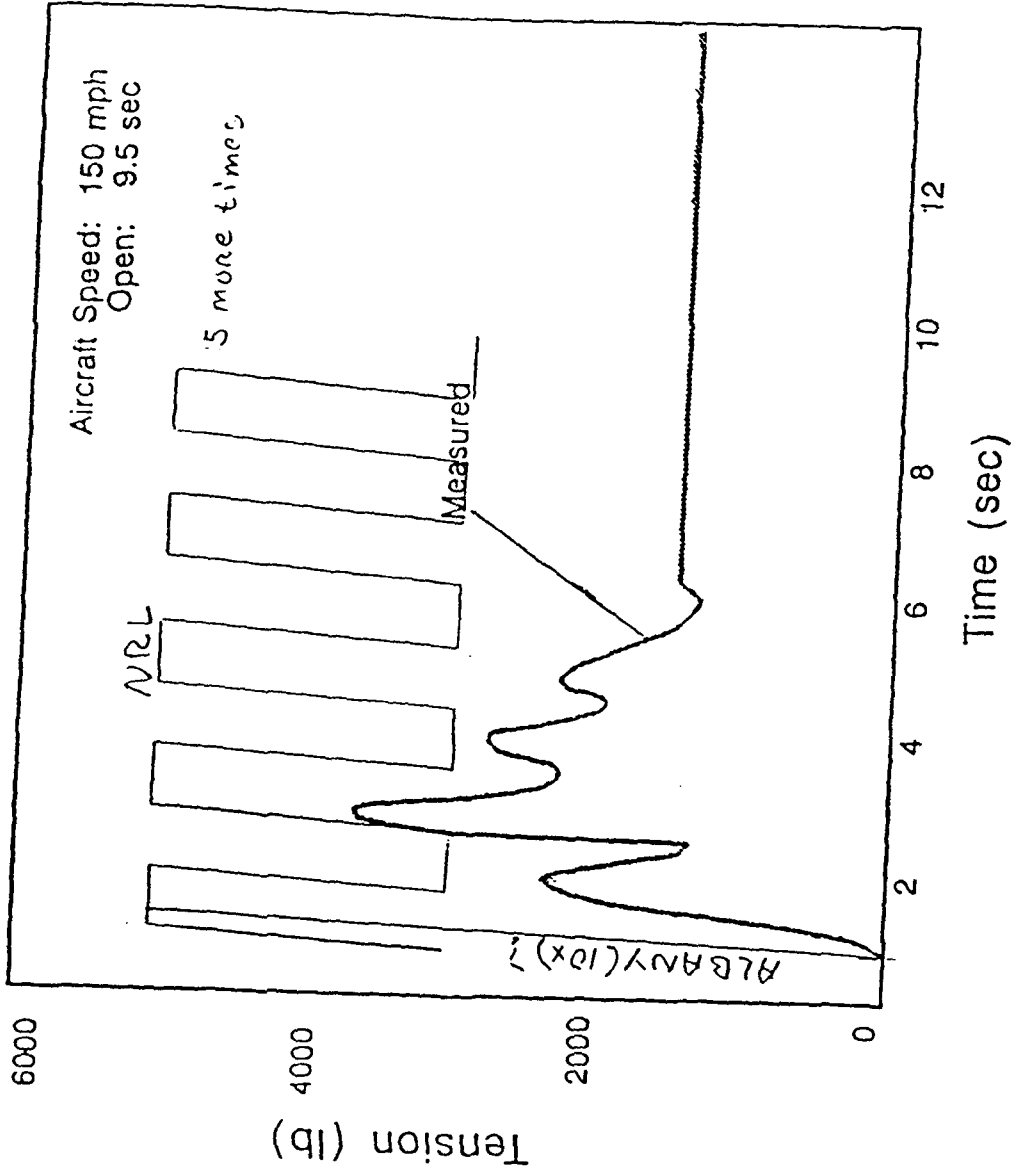


Figure 2

500 0003

3000 105

0.5 sec

1.0 sec

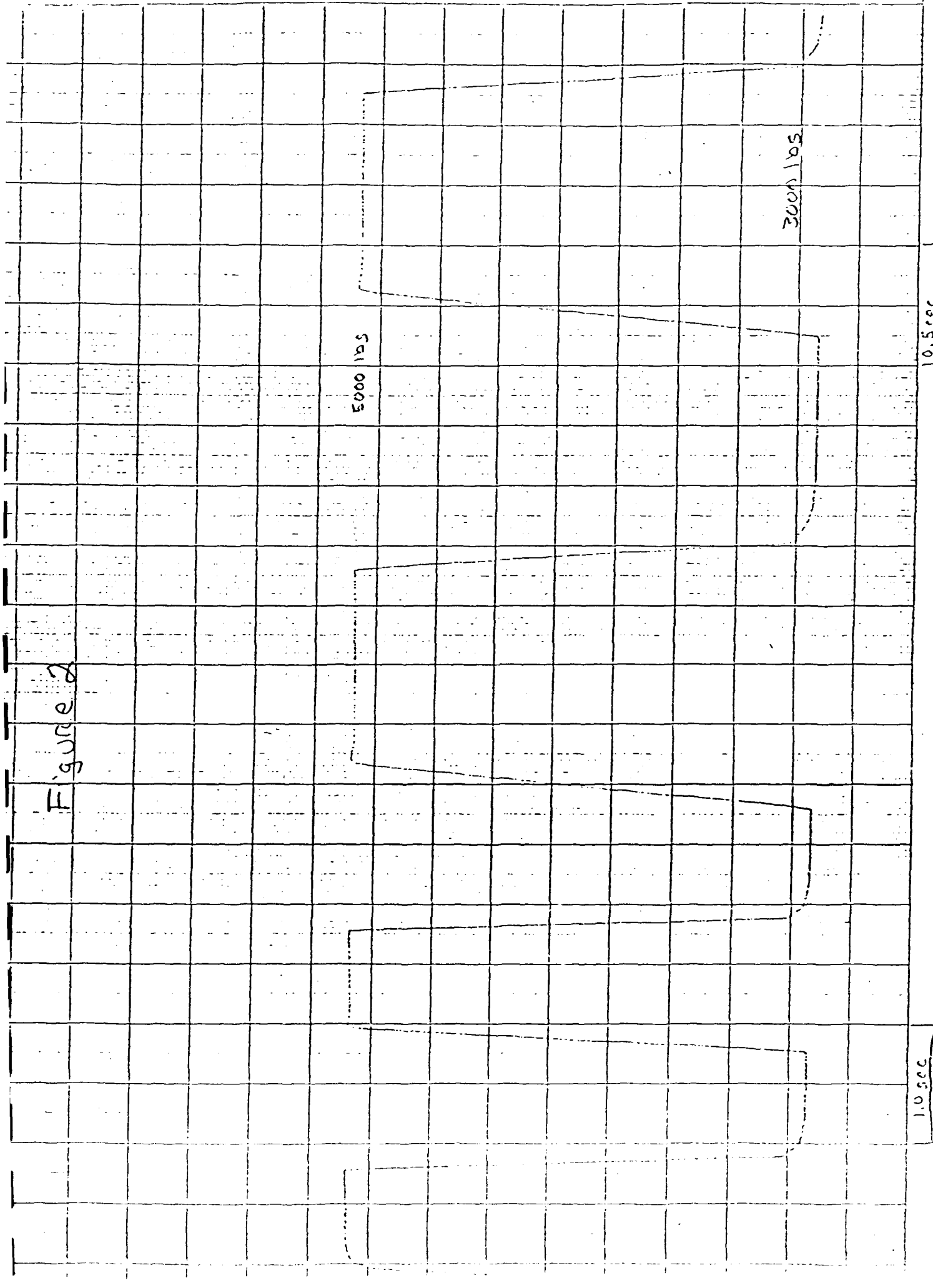


Figure 5

MURDOCK CONTROL WEBS

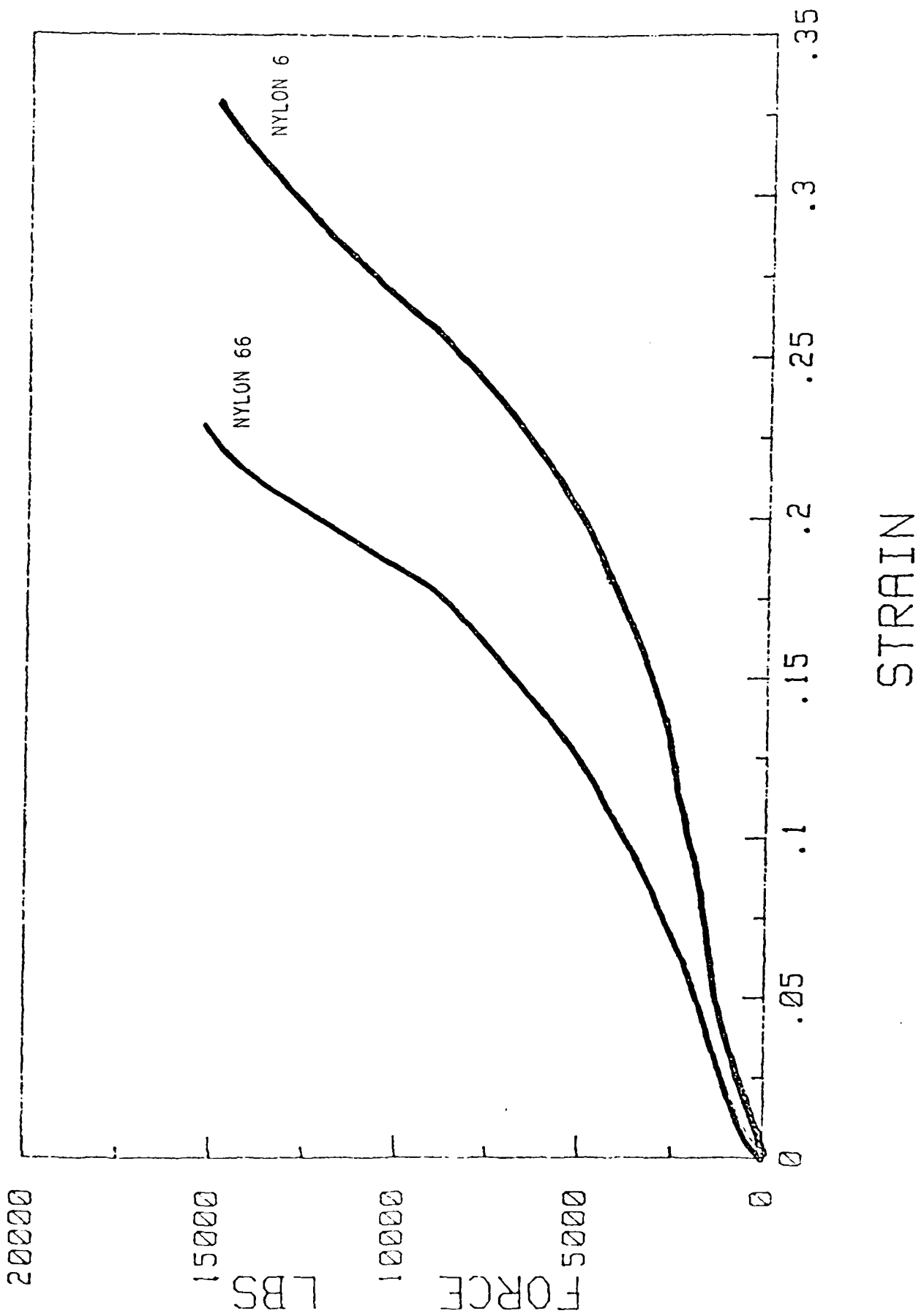


Figure 4

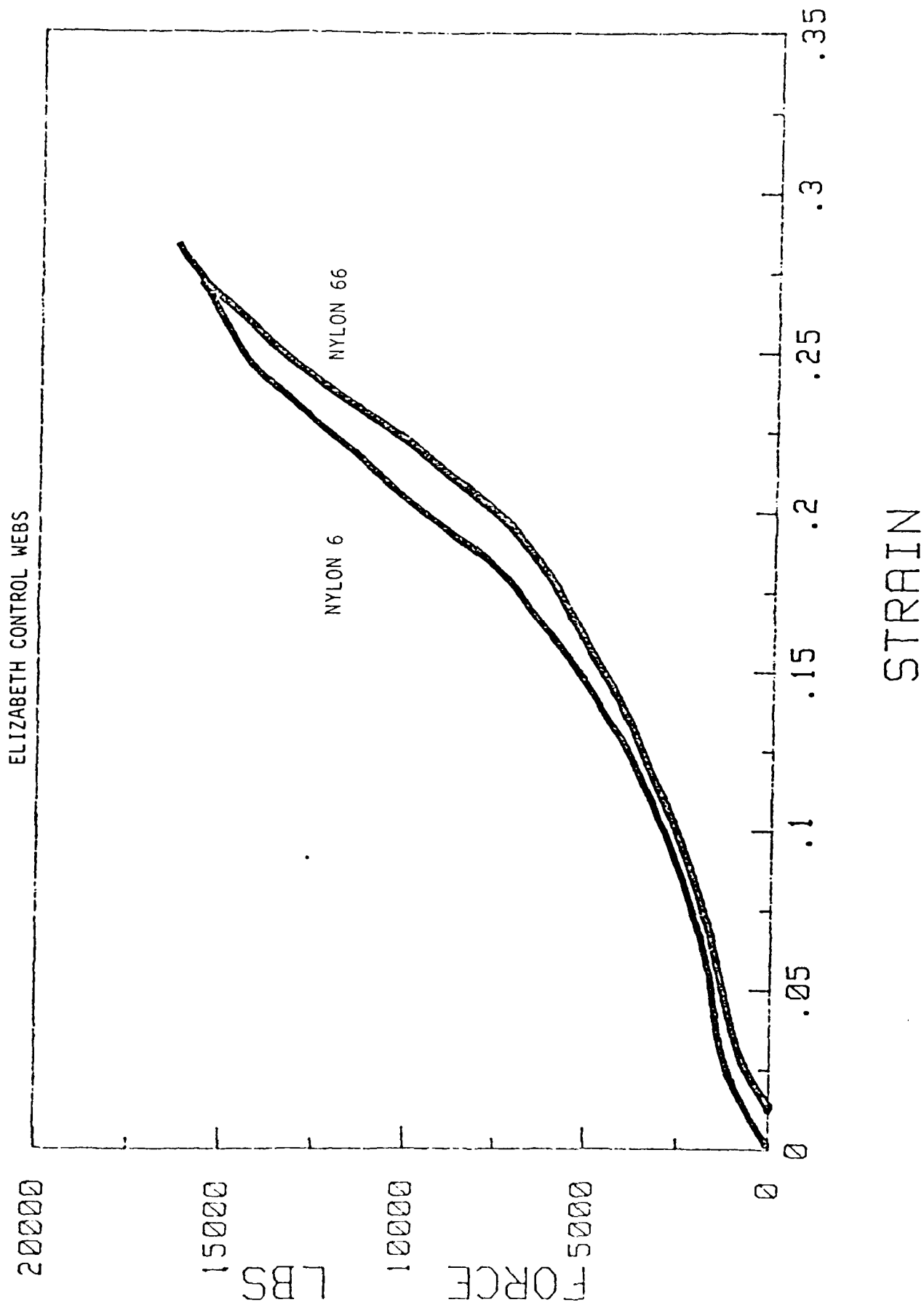


Figure 5

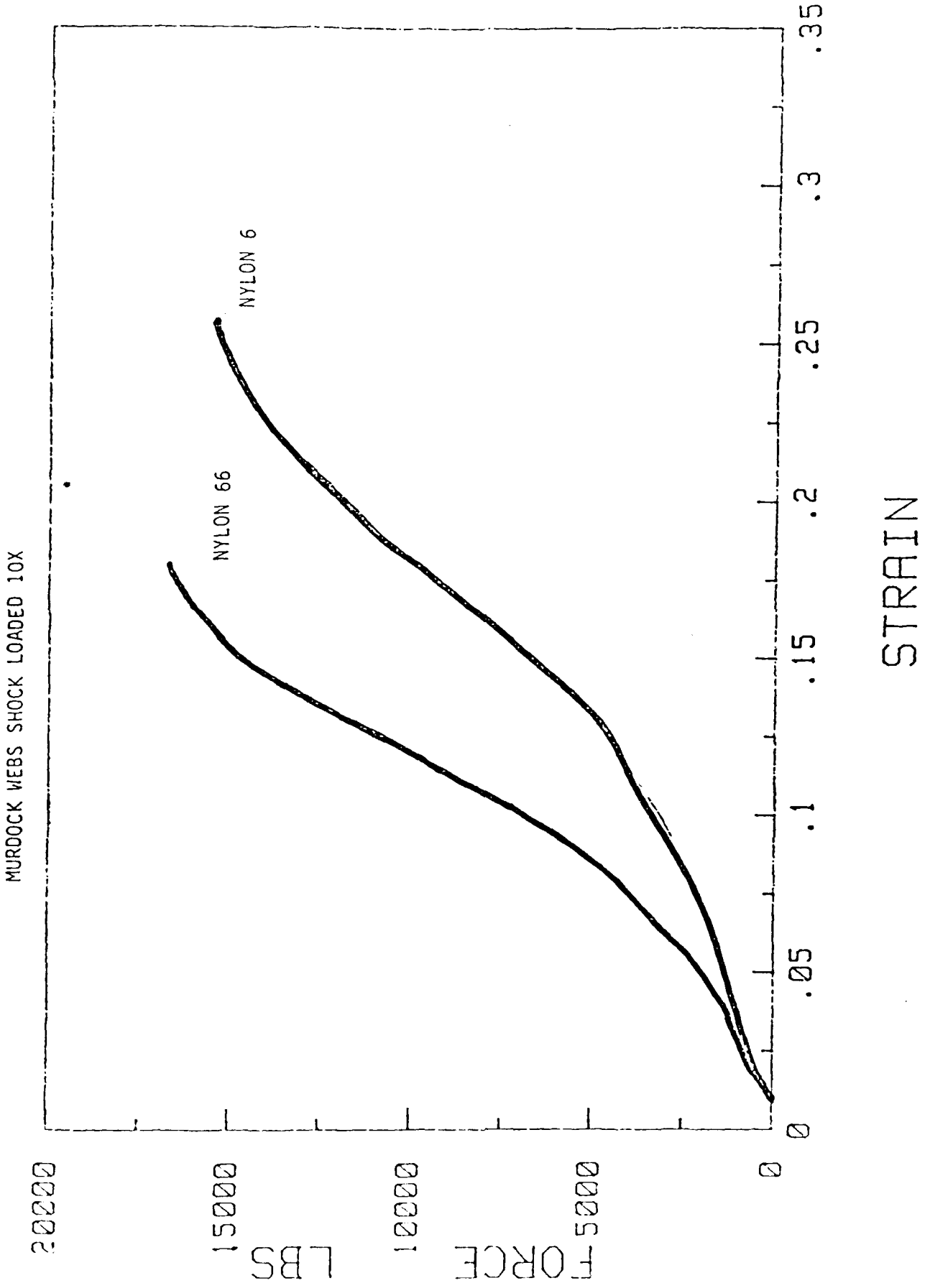


Figure 6

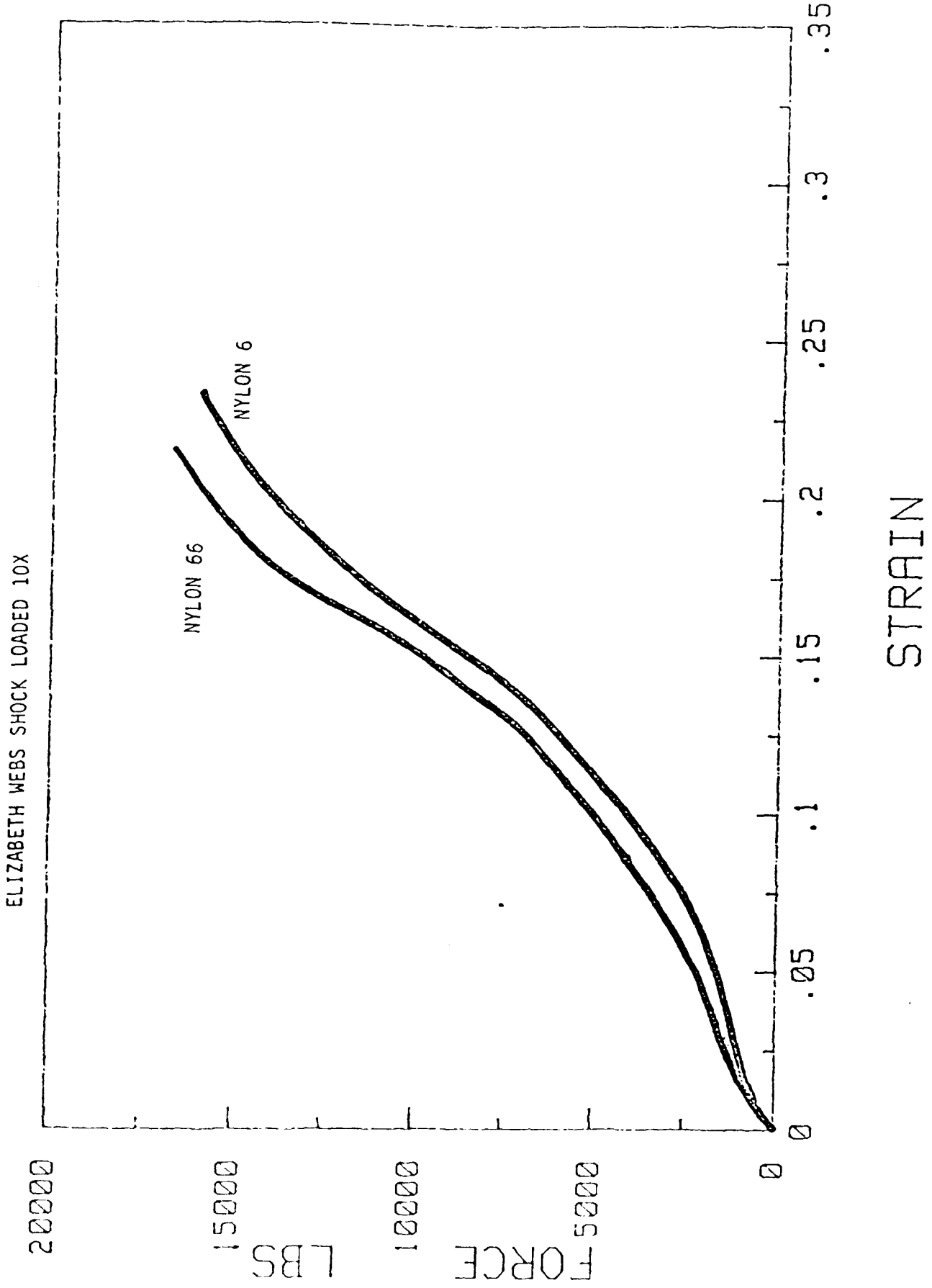


Figure 7

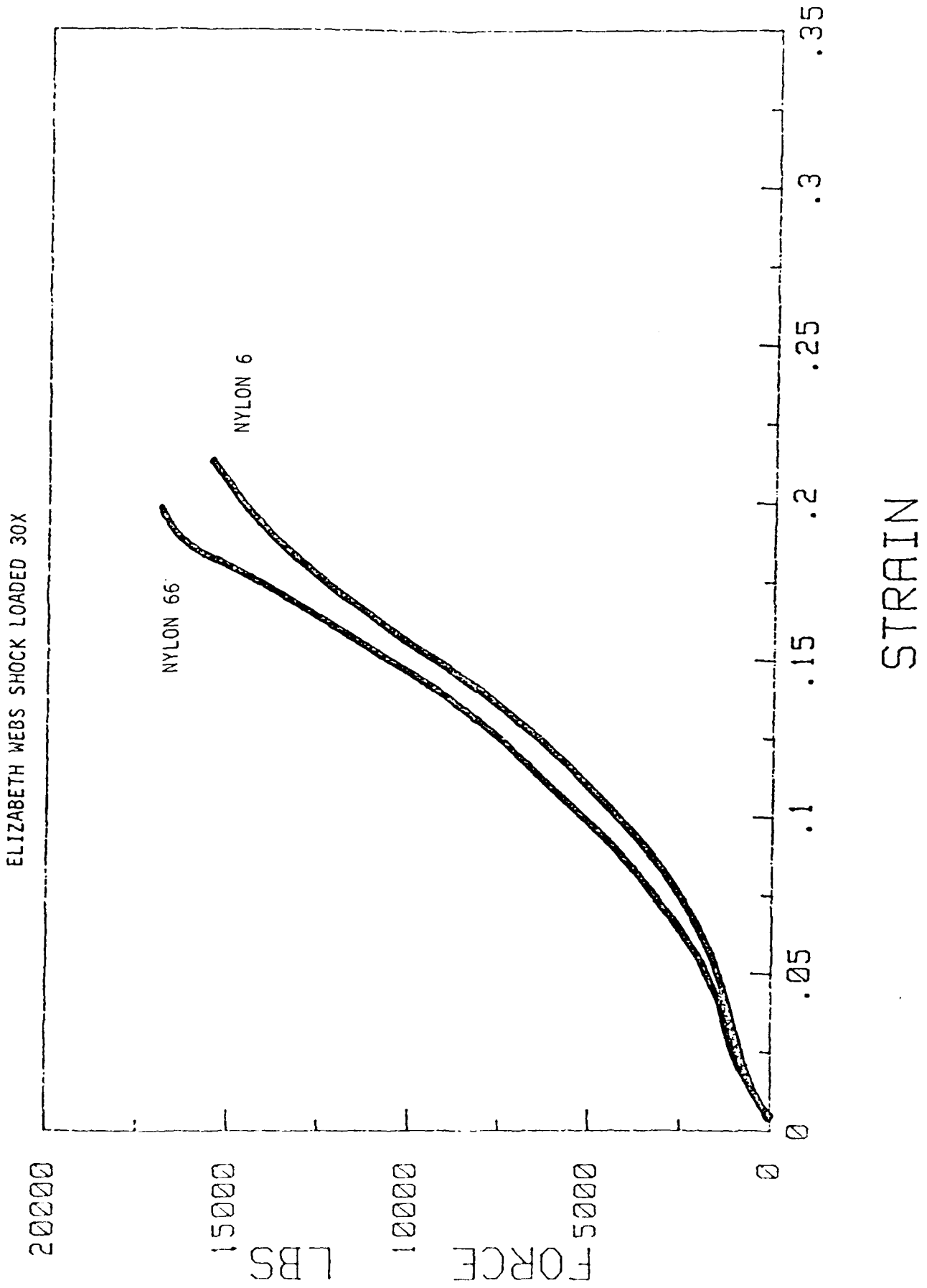
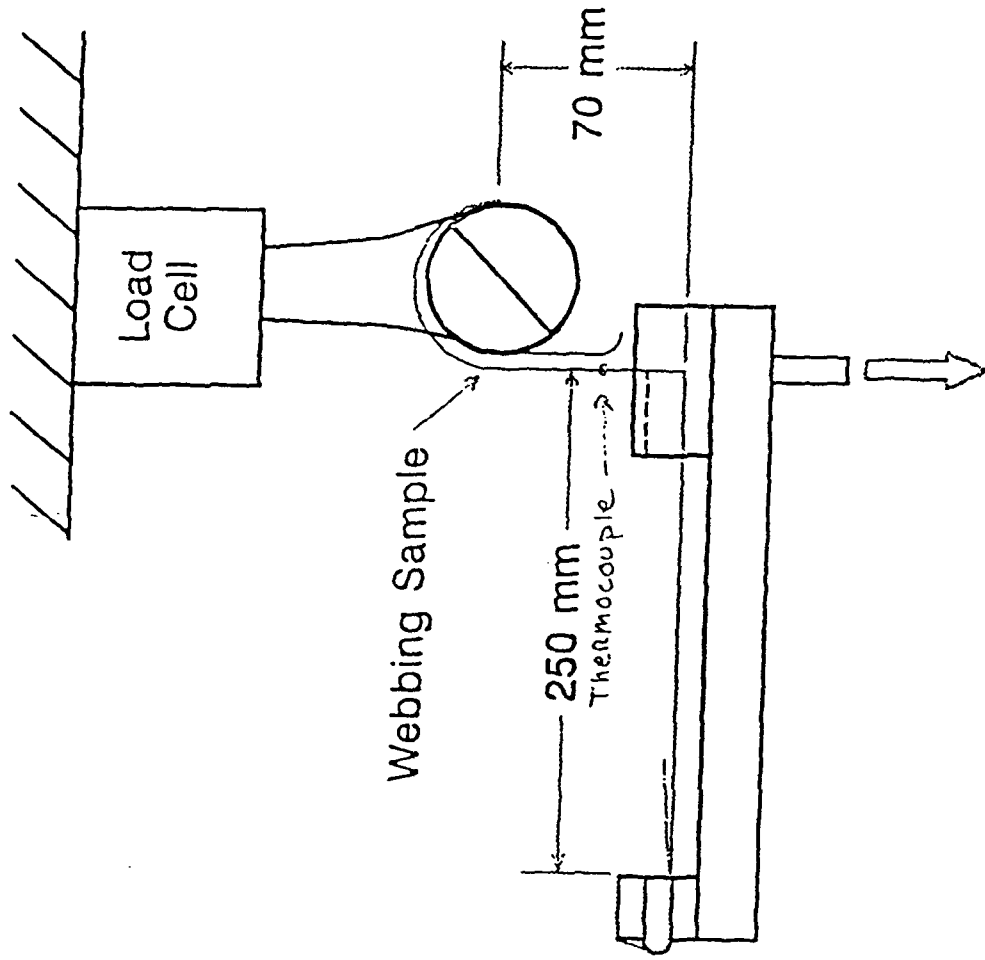


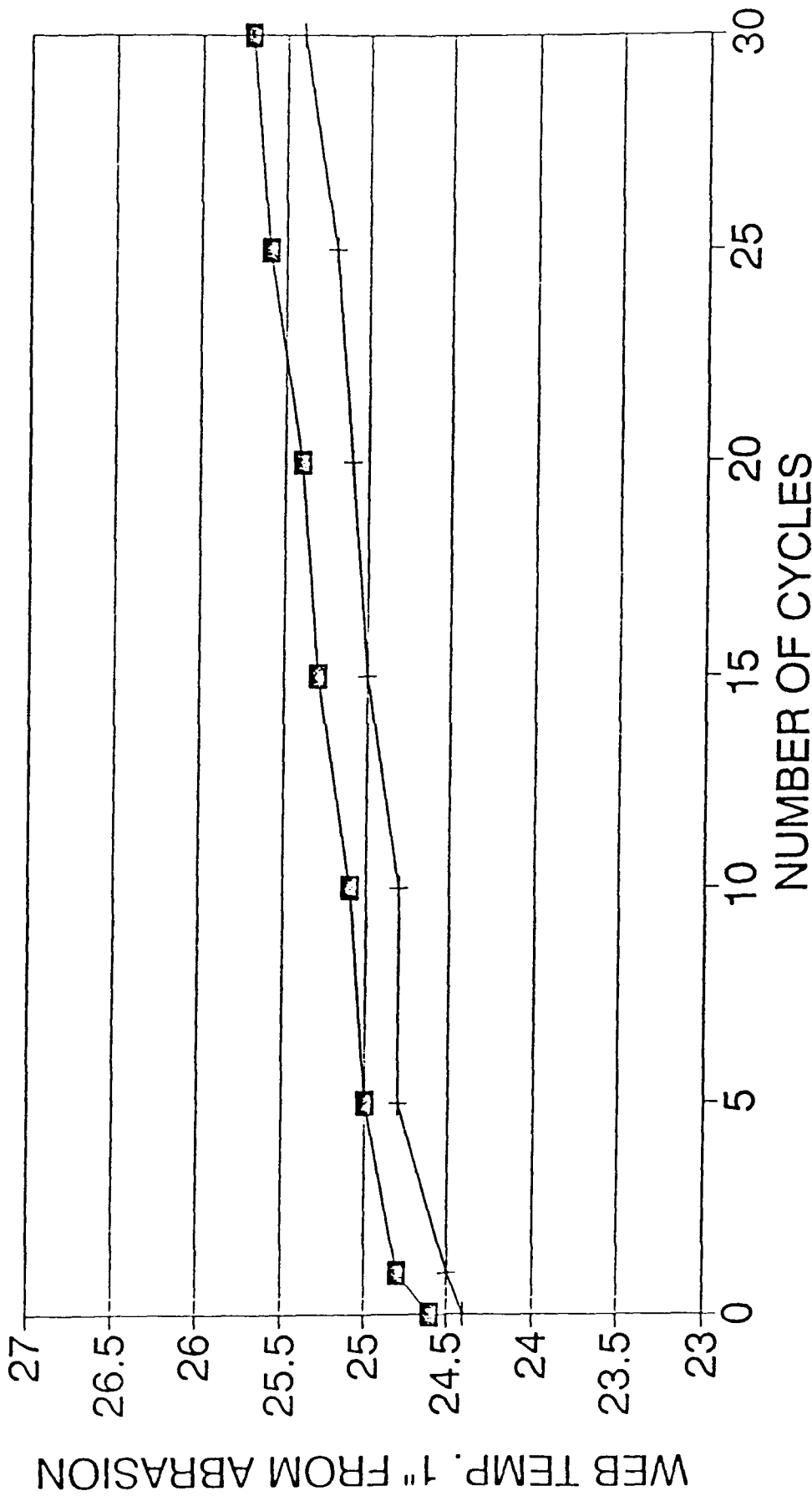
Figure 8

Web Impact Test



WEB TEMPERATURE RISE

0.5 CYCLES/SEC 3000-5000 LBS



—■— NYLON 6 —+— NYLON 66